Министерство здравоохранения Республики Беларусь
Учреждение образования
«Гомельский государственный медицинский университет»

Кафедра лучевой диагностики, лучевой терапии с курсом ФПКиП

Н. М. ЕРМОЛИЦКИЙ

ЛУЧЕВАЯ ДИАГНОСТИКА И ЛУЧЕВАЯ ТЕРАПИЯ

Допущено Министерством образования Республики Беларусь в качестве учебного пособия для иностранных студентов учреждений высшего образования, обучающихся по специальности «Лечебное дело»

В двух частях

Часть 2
Клиническая радиология и радиотерапия

RADIOLOGY

Teaching guide

In two parts

Part 2
Clinical radiology and radiotherapy

Гомель
ГомГМУ
2022

УДК 616-073.75+615.849(075.8)=111
ББК 53.6я73=432.1
Е 74

Рецензенты:
кандидат медицинских наук,
доцент кафедры онкологии с курсом ФПКиПК
Витебского государственного ордена Дружбы народов
медицинского университета
Г. И. Гренков;
кандидат медицинских наук,
заведующий кафедрой лучевой диагностики и лучевой терапии
Гродненского государственного медицинского университета
А. С. Александрович

Ермолицкий, Н. М.
Е 74 Лучевая диагностика и лучевая терапия : учебное пособие : в 2 ч. Ч. 2. Клиническая радиология и радиотерапия = Radiology : Teaching guide : in 2 pt. Part 2. Clinical radiology and radiotherapy / Н. М. Ермолицкий. — Гомель : ГомГМУ, 2022. — 156 с.
ISBN 978-985-588-258-0

Учебное пособие на английском языке подготовлено в соответствии с типовой программой по специальности «Лечебное дело», содержит необходимые для усвоения основные разделы по лучевой диагностике пищеварительной, мочевыделительной, репродуктивной и эндокринной систем, а также по лучевой терапии и введение в радиобиологию, представлены наиболее частые случаи.

Материалы изложены в удобной форме для изучения в VI семестре и адаптированы к программе лучевой диагностики и лучевой терапии с учетом объема часов преподавания, представлена аутентичная английская терминология к описанию специфики предмета. Пособие предназначено для иностранных студентов 3 курса медицинских вузов.

Учебное пособие может быть полезным иностранным студентам старших курсов при изучении терапевтических и хирургических дисциплин, а также клиническим ординаторам радиологии.

УДК 616-073.75+615.849(075.8)=111
ББК 53.6я73=432.1

ISBN 978-985-588-256-6
ISBN 978-985-588-258-0 (Ч. 2)

CONTENTS

I. GASTROINTESTINAL IMAGING

The esophagus, stomach, and small intestine are not well seen on plain x-ray films. In order to examine these organs well, it is necessary to swallow a barium fluid that can be seen on a fluoroscope screen and on the x-ray films. The classical radiological imaging methods such as upper gastrointestinal (GI) examination still play an important role whenever physiological motion plays a role (swallowing, peristalsis of the esophagus, gastric motility, etc.) and in postoperative patients, e.g., when the evaluation of an anastomosis has been requested. The oral administration of contrast is obligatory in these cases.

We are privileged to practise radiology and abdominal imaging in an era that includes classic radiologic techniques — such as radiography, fluoroscopy, and nuclear medicine — as well as modern state-of the-art high-resolution ultrasound, multidetector computed tomography, magnetic resonance imaging, positron emission tomography computed tomography, and the advanced postprocessing techniques that can be applied to these imaging data. The combination of these diagnostic radiologic and imaging modalities makes it possible to provide the most accurate and comprehensive diagnostic information to patients and their physicians in a manner that allows for the optimal treatment and management of gastrointestinal diseases.

Examination techniques of gastrointestinal tract

Plain film radiography

There is no routine use of plain radiography in the assessment of oesophageal disease, with the exceptions of suspected perforation or radio-opaque foreign bodies, when a preliminary chest radiograph is indicated. However, in general, plain radiographs add little useful information. With the proliferation over the past two decades of imaging techniques, such as CT and ultrasound (US), and other modalities, such as endoscopy, the role of plain abdominal radiography has decreased. The abdomen X-ray (AXR) is still a quite usually primary investigation in the patient with acute abdomen. A number of less-common indications will be encountered such as swallowed (or inserted) foreign body.

Luminal contrast barium studies

Principle: water suspension barium sulfate contrast is instilled into the organ that is being studied and x-rays are then taken.

Luminal contrast examinations of the gastrointestinal tract can be performed with a variety of contrast materials. Barium sulfate suspensions are the preferred material for most examinations. A variety of barium products are available commercially, and many are formulated for specific examinations depending on their density and viscosity. Water-soluble contrast agents, which contain organically bound iodine, are used less often, primarily to demonstrate perforation of a hollow viscus or to evaluate the status of a surgical anastomosis in the gastrointestinal tract.

These are simple to perform, inexpensive and have high sensitivity. Ideally, as in the rest of the alimentary tract, the best results are obtained with double-contrast studies, although these may be difficult to achieve because of the transient nature of oesophageal dilatation during swallowing. Good fluoroscopy is essential, aided by digital imaging for spot radiographs.

A single-contrast study of a GI structure means that one contrast agent is used, such as a suspension of barium sulfate, an ionic water-soluble contrast agent such as diatrizoate meglumine (gastroview/gastrografin), or a nonionic water-soluble contrast agent such as iohexol (omnipaque).

In a double-contrast study, a radiologist uses two contrast agents to examine the organs in question. A double-contrast upper GI series uses an effervescent agent that creates carbon dioxide to distend the luminal organs and high-density barium to "scrub and paint" the mucosa.

Patient preparation included: nil by mouth for a couple of hours. Contraindications of examination: bowel obstruction. A good examination requires an empty stomach and therefore you will not be able to have any food or fluids by mouth l0–l2 hours before your exam. Chewing gum or other material or smo-king will also create saliva to swallow which will make extra fluid in the stomach and must be avoided.

Computed tomography

The major role of computed tomography (CT) in the assessment of oesophageal disease is mainly confined to the staging of oesophageal cancer. It performs two functions here: (A) the assessment of local spread of tumour; and (B) the assessment of a metastatic disease, particularly to the liver and gastric lymph nodes. Thus, the whole of the thorax and upper abdomen should be examined.

CT imaging of the abdomen can portray the various hollow organs of the gastrointestinal tract. Mucosal disease, such as ulcers, and small neoplasms will not be shown with this imaging modality. Larger gastrointestinal neoplasms, thickening of the walls of the hollow organs, and extrinsic processes can be easily detected. Also, with the use of luminal distention and intravenous contrast material, a variety of gastrointestinal disorders are more readily evaluated.

Abdominal ultrasound

Abdominal ultrasound has had an increasing impact on evaluation of the hollow organs of the gastrointestinal tract. The location of the hollow organs and the presence of gas interference remain technical problems; however, inflammatory disorders can be evaluated, such as acute appendicitis, especially in pediatric patients. Endoluminal ultrasound using blind probes or those attached to an endoscope has been used in the upper gastrointestinal tract to detect and stage malignancy; other indications include fine-needle aspiration (FNA) through the gastrointestinal wall.

Endoscopic ultrasound

The limitations of CT in assessing the oesophageal wall can be overcome by the use of endoscopic ultrasound. This technique utilizes an US probe that is mounted at the end of an endoscope and, depending on the manufacturer, is either of linear array or a radial sector arrangement. The endoscope itself may be forward-viewing or oblique-viewing so that a lesion can be observed and then the probe applied to it. The probe frequencies are in the range of 7 – 12 MHz and this is high enough to delineate the five layers of the oesophageal wall: mucosa, muscularis mucosa, submucosa, muscularis propria and adventitia. These are demonstrated as alternating layers of reflectivity. In addition, small lymph nodes adjacent to the oesophageal wall can be visualized, and with certain probes fine-needle aspiration can also be performed.

Radionuclide radiology

The prime role here is in the assessment of motility disorders of the oesophagus and in the investigation of gastro-oesophageal reflux disease. For the former, the patient is placed in a horizontal position under a gamma camera and is given a standard radioactive meal. Similarly, patients with suspected reflux are examined in the horizontal position, having drunk water labelled with ^{99m}Tc-radiofarmaceutical. This investigation may in addition demonstrate complications such as aspiration into the lungs.

Positron emission tomography is a physiological imaging technique that relies on the metabolism of ^{18}F-glucose to yield images. Because of this feature it has found a particular role in the staging and follow-up of tumours, including the oesophagus. The advent of hybrid PET/CT examinines that combine the anatomical accuracy of CT with the physiological feature of PET have enhanced this function.

Magnetic resonance imaging

Magnetic resonance (MR) imaging is the newest modality developed for cross-sectional imaging of the body and nearly all organ systems can be evaluated with this technique. MR imaging of the hollow organs of the gastrointestinal tract is increasingly used to evaluate a wide assortment of gastrointestinal tract disorders. As with CT imaging, mild mucosal diseases and small focal lesions are not well detected with this technique; however, malignancies can be similarly evaluated and staged. With the newer technologies, both CT and MR imaging offer multiple options for viewing the gastrointestinal tract, including multiplanar viewing and 2-D and 3-D reconstructions.

Radiology of esophagus

Normal anatomy of the esophagus

The esophagus is a muscular tube that is normally 25–30 cm long and 2–3 cm wide. The esophagus is divided into three segments: the cervical, thoracic, and ab-

dominal segments. The cervical portion is separated from the cervical vertebrae by only a few mm of prevertebral soft tissue. It is also in contact with the trachea and the left mainstem bronchus, separated only by the connective tissue. There are several structures that are in close proximity to the esophagus and which make normal impressions on it. These structures are the aortic arch, the left mainstem bronchus, the left inferior pulmonary veins (Figures 1.1 A to B).

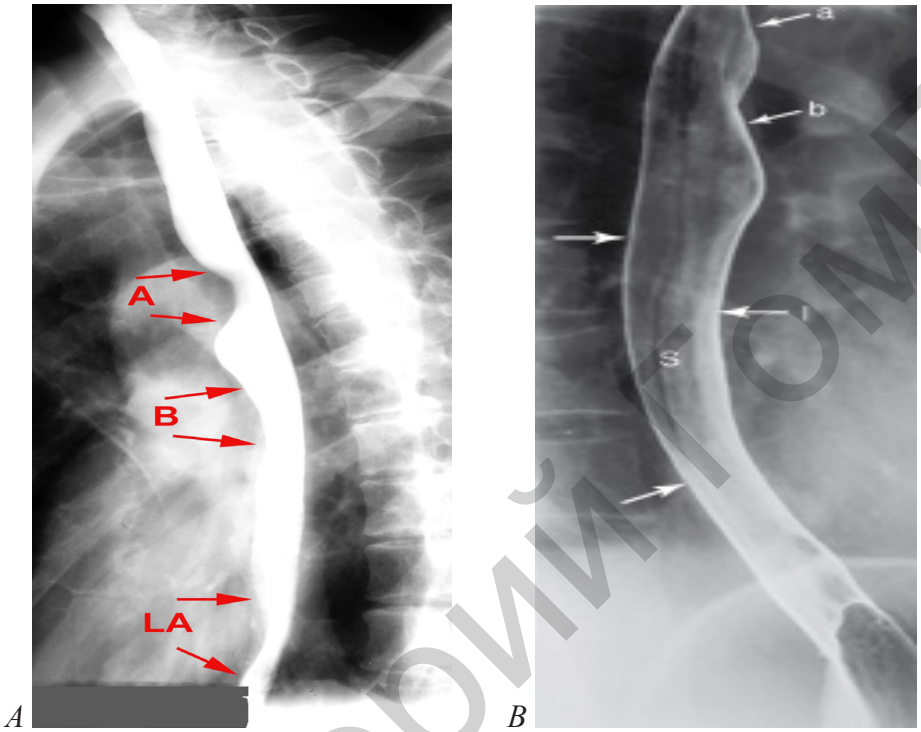

Figure 1.1 — A) A single-contrast radiograph obtained with the patient swallowing barium while in a vertical position. This oblique view of a normal barium swallow shows the normal impressions made by the (A with arrows) aortic arch, (B with arrows) left mainstem bronchus, and (LA with arrows) left atrium on the esophagus.(B) Radiograph shows a normal lower thoracic esophagus. These indentations are identified as the bottom of the aortic arch (a), the left main stem bronchus (b), and the left atrium (l). In this patient, swallowed high-density barium coats the mucosa. The swallowed carbon dioxide (effervescent agent) and swallowed air distend the lumen of the esophagus. The mucosa of the esophageal tube seen in profile appears as a white line (arrows). The mucosal surface of the normal esophagus seen en face is smooth and varies from white to gray (mucosa identified by S). Normal structures in the mediastinum push on the distended esophagus, manifested as alterations of the normal straight tubular contour of the esophagus

Pharyngoesophagography is a valuable technique for demonstrating a wide range of functional and structural lesions of the pharynx and esophagus. The pharyngeal portion of the study enables evaluation of swallowing dysfunction as well as a variety of morphologic abnormalities in the pharynx. The esophageal portion is equally valuable for detecting esophageal dysmotility, gastroesopha-geal reflux disease, infectious esophagitis, esophageal carcinoma, and other morphologic abnormalities of the esophagus.

Conventional radiology imaging diseases of esophagus

Achalasia

Achalasia is a primary esophageal motility disorder characterized by aperistalsis and lower esophageal dysfunction. The gastroesophageal sphincter fails to relax because of wallerian degeneration of Auerbach's plexus. The sphincter relaxes only when the hydrostatic pressure of the column of liquid or food exceeds that of the sphincter; emptying occurs more in the upright than in the horizontal position.

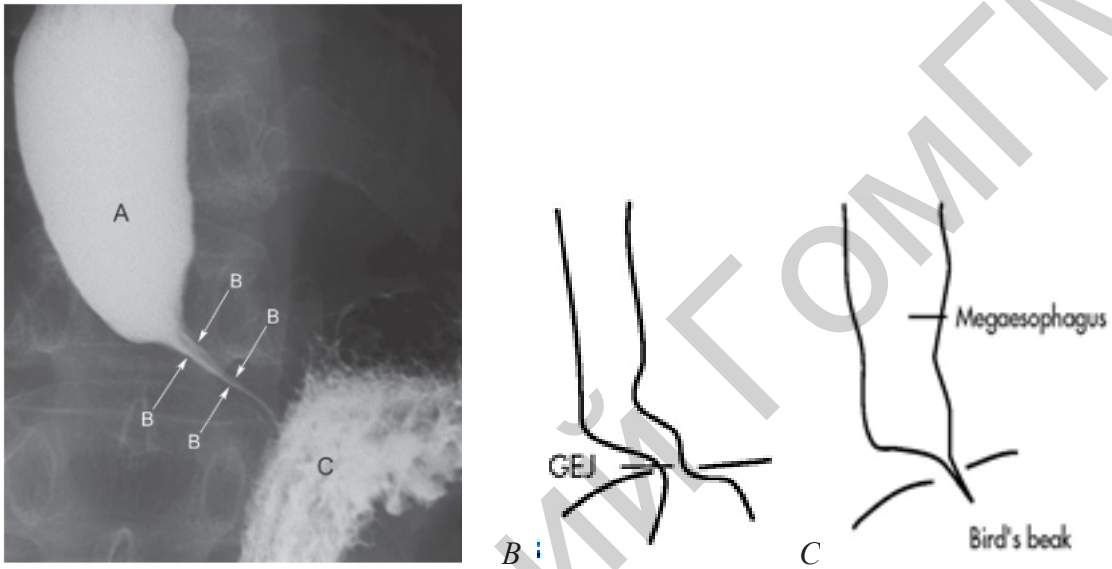

Figure 1.2 — (A) Spot film from a barium swallow showing dilation of the lower oesophagus with pooling of contrast (A) above a tight smooth narrowing ("bird's beak" sign) of the lower oesophageal sphincter. (B). Some contrast has passed through into the fundus of the stomach, with visible rugae (C) (B) Schemes of distal esophagus (GEJ — gastro-oesophageal junction). (C) schematic representation achalasia of esophagus

Radiological findings: on plain films, achalasia can be recognized by massive esophageal dilatation with possible large amounts of retained food and fluid in the esophagus. Typically, the distal esophagus has a smooth, tapered appearance often likened to a "bird's beak" which reflects the dysfunction. Image depicts of the esophagus showing a massively dilated esophagus with retention of contrast in the distal portions of the esophagus, shows the "bird's beak" appearance of the dysfunctional lower esophageal sphincter (Figure 1.2).

Diverticula

Esophageal diverticula can be classified based on their location (i.e. cervical, midesophageal, epiphrenic, intramural, or intraluminal). The diverticula may fill with food or fluids and compress the true lumen of the esophagus causing dysphagia.

Radiological findings: Image depicts the frontal view of a large barium-filled sac. On double-contrast esophagograms, most of the outpouchings are still filled with barium. Diverticula are outpouchings of one or more layers of the intestinal wall that may occur at any level of the esophagus (Figure 1.3).

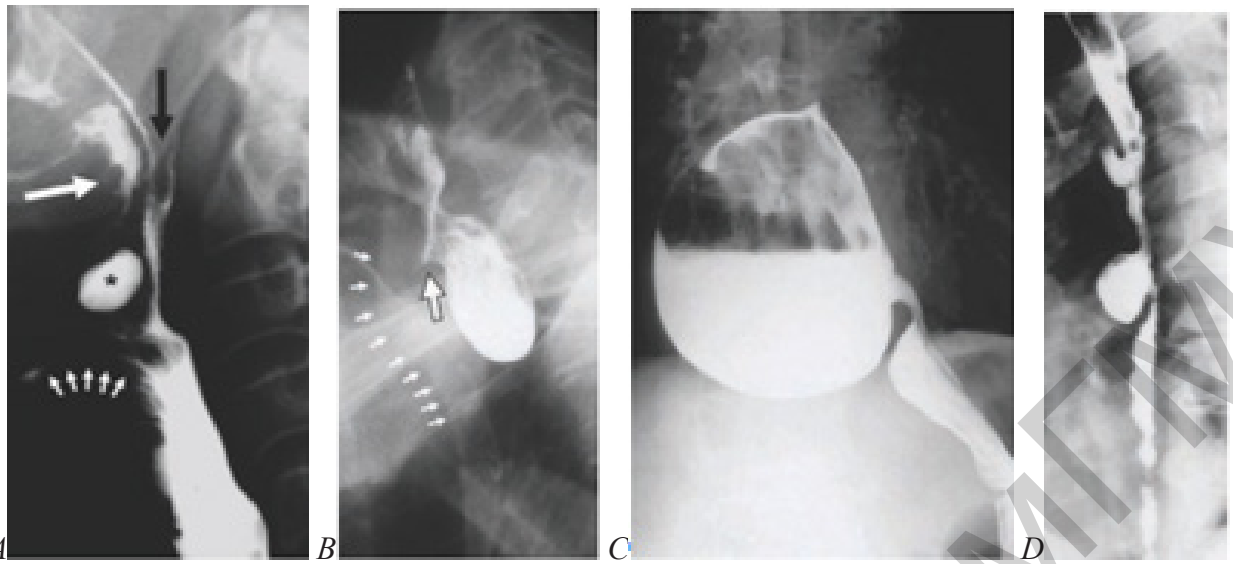

Figure 1.3 — A) This lateral view of the swallowing act shows the appearance after passage of the barium bolus into the esophagus. The soft palate is pressed against the dorsal pharyngeal wall (black arrow), thus preventing the regurgitation of food into the nasal cavity. The tongue base (large white arrow) has moved upward and backward; the epiglottis (small white arrows) seals off the laryngeal entrance. The bolus has entered the proximal esophagus. There is a diverticulum in the area of the epiglottic fold (star). It extends laterally from the tongue base. (B) In a Zenker diverticulum the depiction of the width of the diverticular neck (large arrow) is of particular importance to the surgeon. The esophagus and the trachea (small arrows) are displaced ventrally. (C) Another typical location of a pulsion diverticulum is the distal esophagus. (D) Traction diverticula tend to occur at the level of the pulmonary hila and are usually the consequence of inflammatory lymphadenitis in the mediastinum

Esophageal diverticula can be classified as traction diverticula, which are composed of all esophageal layers, and pulsion diverticula, which are composed only of mucosa and submucosa herniating through the muscularis. Traction diverticula often have a triangular or tented appearance resulting from traction on the diverticulum by the fibrotic process in the adjacent mediastinum. Pulsion diverticula appear on barium studies as rounded wide-necked outpouchings that fail to empty when the esophagus collapses.

Perforation

Untreated thoracic esophageal perforations have a near 100% mortality rate.

Radiological findings: on plain films, subcutaneous emphysema may be visible on AP or lateral films of the neck. Air may also dissect into the chest and produce a pneumomediastinum. Lateral films of the neck may reveal widening of the prevertebral space, anterior deviation of the trachea, or a retropharyngeal abscess with an air-fluid level.

If a cervical perforation is suspected on a plain film, the study should be followed up with a water-soluble contrast study. On the esophogram, one would look for localized extravasation of contrast medium into the neck or mediastinum.

Foreign bodies/food impaction

80% of pharyngeal or esophageal foreign body impactions occur in children, who accidently ingest coins, toys, etc. In adults however, animal/fish bones or large boluses of meat cause most foreign body impactions. The risk of esophageal perforation in foreign body impaction is less than 1%, however, the risk increases significantly if the foreign body remains lodged for greater than 24 hours.

Radiological findings: occasionally, the foreign object may be radiopaque and visualized. Contrast studies can also be performed. Animal/fish bones may be obscured by barium, but they can sometimes be visualized as linear filling defects.

If the food bolus is completely obstructing the esophagus, then contrast studies may reveal a polypoid filling defect outlining the superior aspect of the bolus. If the obstruction is incomplete, contrast may trickle around the bolus and continue downstream towards the stomach. After the food impaction is treated, an esophagram should be completed to look for abnormal esophageal strictures.

Esophagitis

Esophagitis may present with erosions, ulcers, and strictures (Figure 1.4) and rarely with perforations and fistulas.

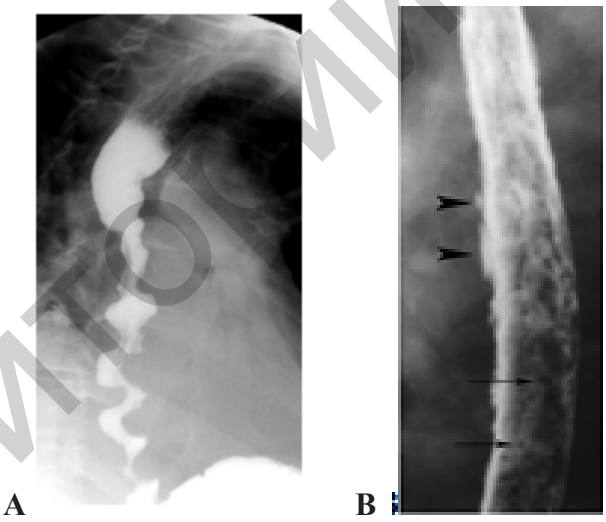

Figure 1.4 — (A) Diffuse esophageal spasm. Single-contrast barium swallow image demonstrating the classical corkscrew appearance of diffuse oesophageal spasm. (B) Reflux esophagitis. A barium esophagram demonstrates stiffness and narrowing of the distal esophagus just above the level of the diaphragm (open arrows). Several prominent sacculations (arrows) are present, indicating long-standing and severe esophagitis

Types esophagitis: infectious (herpes, candidiasis), chemical (reflux esophagitis, corrosives), iatrogenic (radiotherapy, extended use of nasogastric tubes, drugs (tetracycline, antiinflammatory drugs, potassium, iron).

Radiographic features: thickening, nodularity of esophageal folds; irregularity of mucosa (granularity, ulcerations); retraction, luminal narrowing, stricture.

Corrosive/caustic esophagitis

Ingestion of caustic or corrosive agents (i.e. lye, dishwasher detergents, alkali or acidic agents) causes acute and chronic inflammatory changes mostly in the distal two-thirds of the esophagus. There are three characteristic phases of injury in caustic esophagitis: 1) acute necrosis, 2) ulceration-granulation, 3) stricture formation. Chest and abdominal radiographs should be ordered routinely for patients who have ingested these agents. Chest films may reveal a dilated esophagus or evidence of esophageal perforation. Abdominal films may show pneumoperitoneum secondary to gastric perforation. If perforation is suspected, the study should be followed up by a water-soluble contrast study.

Radiological findings: in the acute phase, esophagrams may show abnormal esophageal motility with diffuse spasms and poor peristalsis (Figure 1.1 D).

On double contrast studies, shallow ulcers may appear as punctuate, linear, or serpiginous collections of barium. In severe cases, the esophagus may show diffuse narrowing with an irregular contour. The strictures typically appear as areas of smooth, tapered narrowing in the cervical or upper thoracic esophagus. Image depict irregular narrowing of the esophagus with ulcerations.

Leiomyoma

Leiomyomas make up approximately 50% of all benign esophageal tumors. About 60% of the lesions are located in the distal third of the esophagus, 30% in the middle third, and 10% in the proximal third. They appear as discrete submucosal masses ranging from 2–8 cm in size.

Radiological findings: on chest films, leiomyomas may be recognized as a soft tissue mass in the posterior mediastinum or by punctuate areas of calcification in the tumor. A calcified esophageal mass is pathognomonic of a leiomyoma.

In contrast studies, the leiomyomas appear as discrete submucosal masses with round or ovoid filling defects sharply outlined by barium. Larger leiomyomas may occasionally cause some compression of the lumen significantly enough to narrow the lumen. In image, the ovoid filling defects. The smooth surface and obstuse angles formed are of submucosal masses.

Adenocarcinoma, radiological findings

Early: early esophageal adenocarcinoma may appear as plaques or flat, sessile polyps in the distal esophagus (Figures 1.5–1.6).

Late: advanced esophageal adenocarcinomas appear as infiltrating lesions with irregular luminal narrowing or, nodularity or ulceration of the mucosa. Less frequently, adenocarcinomas can appear as a polypoid mass, ulcerative lesion.

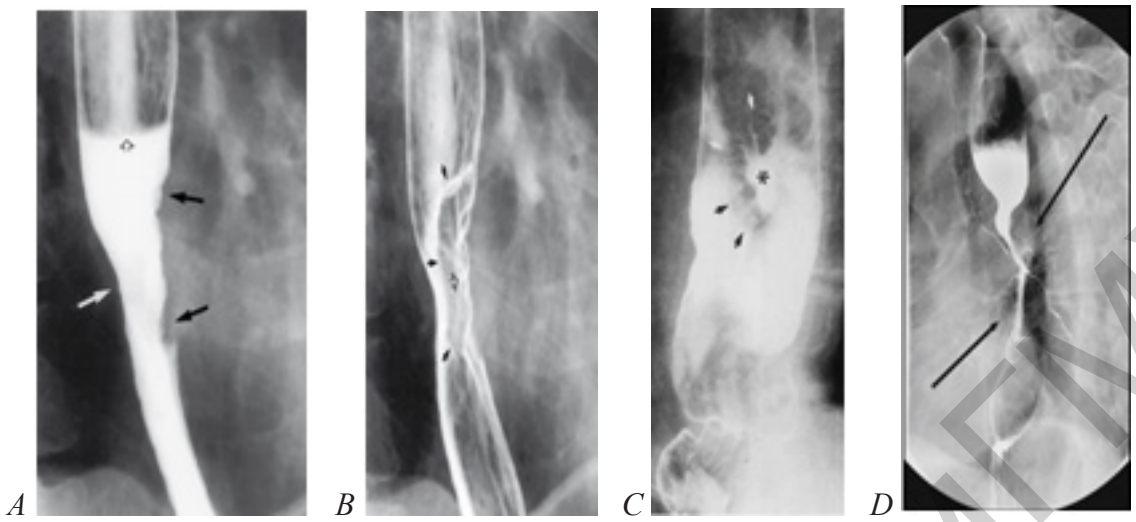

Figure 1.5 — Inflammatory polyp (A, B arrows) and oesophageal carcinoma (C, D). (A) Spot radiograph of the chest performed while the patient stands and drinks high-density barium shows a column of barium (with an air-barium level, open arrow) in the mid-esophagus. The narrowing appears smooth on one wall (white arrow) and has an irregular contour on the opposite wall (black arrows). (B) Spot radiograph performed seconds later after the barium column has passed through the esophagus shows the same circumferential narrowing with a smooth contour on one side and an irregular contour on the other. The mucosal surface is now seen en face as well, however, revealing focal mucosal nodularity (open arrow) and barium-coated lines (arrows) that disrupt the normal smooth surface of the esophagus and outline the outer margin of a mass. (C) Early oesophageal carcinoma. En face there is a central ulcer (asterisk) with a nodular margin (arrows). (D) Esophageal carcinoma, malignant stricture. A squamous cell carcinoma of the mid-esophagus causes an abrupt narrowing with irregular mucosa. Note the irregularity and overhanging edges (arrows)

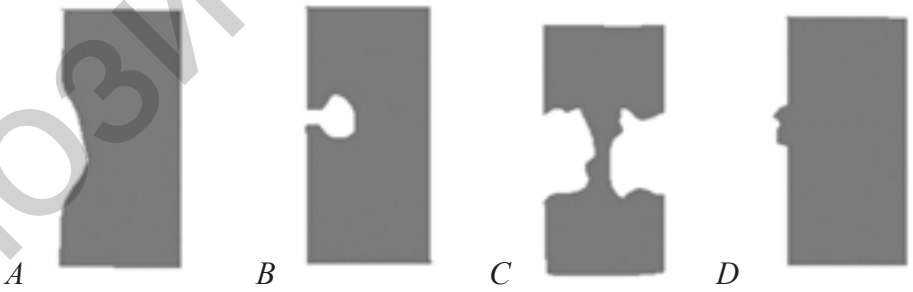

Figure 1.6 — Schemes of esophagogram variants of esophageal tumours. (A) Infiltrative, (B) polypoid, (C) annular stenotic, (D) ulcerative

On contrast studies, esophageal cancer may appear as an infiltrating, polypoid, ulcerative. Infiltrating cancers show irregular narrowing of the lumen with an associated nodular or ulcerated mucosa with well-defined borders. Polypoid lesions are usually greater than 3,5 cm in diameter and appear as lobulated or fungating intra-

luminal masses with possible areas of ulceration. Ulcerative carcinomas appear as well-defined meniscoid ulcers with a radiolucent rim of tumor surrounding the ulcer.

The wide spectrum of motility disorders ranges from the well-defined primary esophageal motility disorders to very nonspecific disorders that may play a more indirect role in reflux disease. Primary motility disorders include nonspecific esophageal motility disorder, achalasia, diffuse esophageal spasm and hypertensive lower esophageal sphincter. The classic finding in diffuse esophageal spasm, most commonly seen during a barium swallow study, is the "corkscrew" or "rosary-bead" appearance of the esophageal body during a simultaneous contraction.

Radiology of stomach

The stomach is not well seen on plain x-ray films. In order to examine well, it is necessary to swallow a barium fluid that can be seen on a fluoroscope screen and on the x-ray films. To X-ray anatomy of stomach: fornix, cardial part, small curvature, large curvature, body of th1.18e stomach, angle of the sto-mach, antral part, pyloric canal.

Single-contrast radiographic study (Figure 1.7): the stomach is filled and distended with dilute barium or a water-soluble contrast agent. Water-soluble contrast should be used when perforation or post-operative anastomotic failure is suspected. The stomach is compressed either manually or by positioning to allow for adequate x-ray penetration in the evaluation of each anatomical segment. Single-contrast technique assesses thickness of the gastric folds and evaluation of gastric emptying. Large luminal defects can be detected.

Double-contrast radiographic study: the stomach is temporarily paralyzed by administration of glucagon, filled with dense barium, and distended with gas using effervescent granules. Hence, both barium and air are used for contrast. Images are obtained as the patient rolls in various positions to coat the gastric mucosa with contrast. Double-contrast technique provides improved visualization of the gastric mucosa. Several films may be made during this time (Figures 1.8–1.9).

Limitation: requires fluoroscopy and requires follow up endoscopy to biopsy lesions.

Patient preparation: the patient should have nothing orally after midnight or the next morning preceding the radiographic study (no smoking or chewing gum). Fluid and food in the stomach degrade the examination by interfering with good mucosal visualization and causing artifacts that may mimic disease.

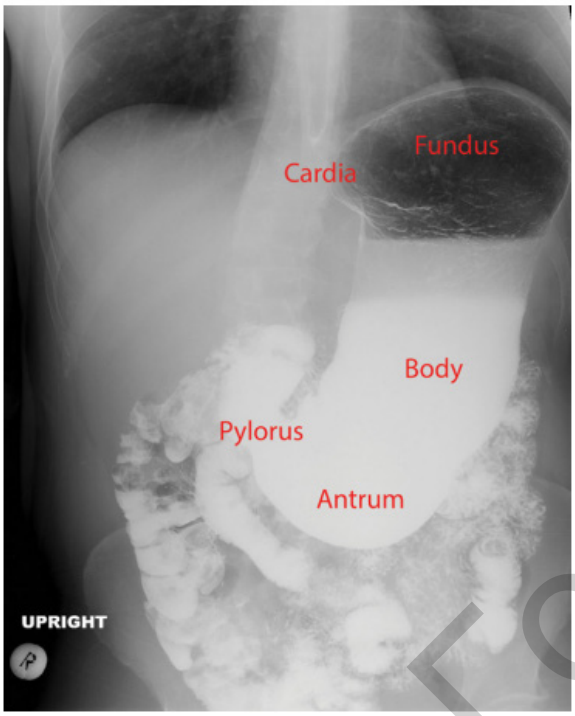

Figure 1.7 — Single fluoroscopic image demonstrates the anatomy of the stomach (cardia, fundus, body, antrum, and pylorus). Small bowel and colon are partially opacified

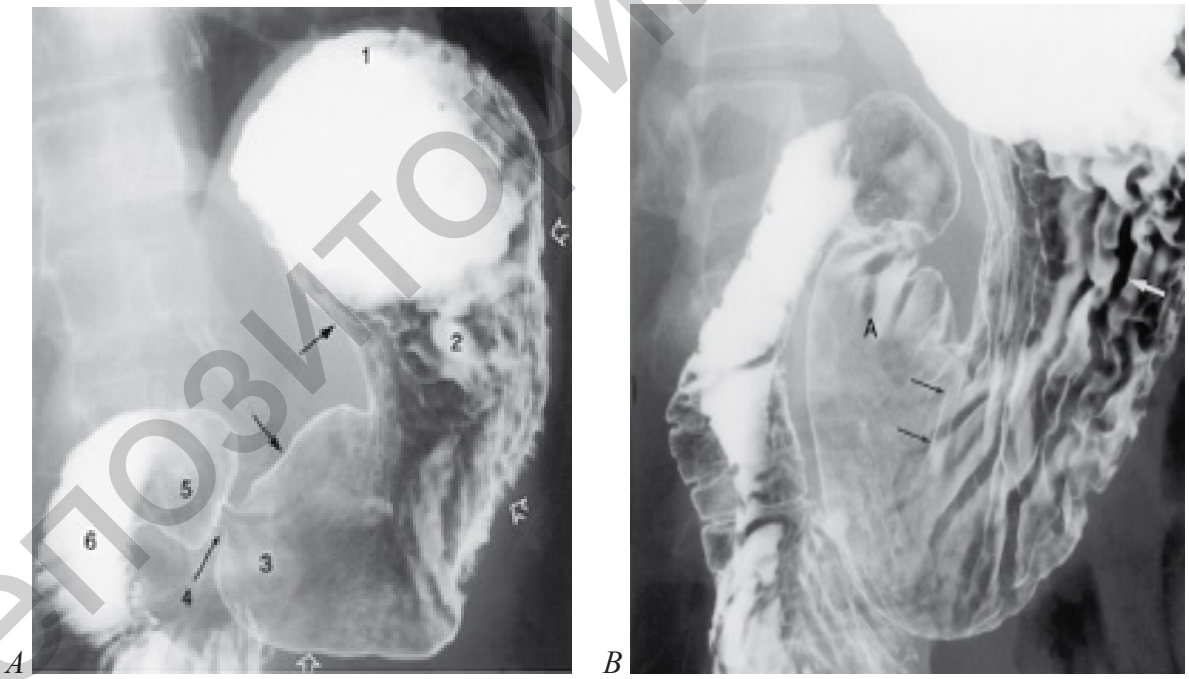

A *B*

Figure 1.8 — (A) Normal stomach. 1 — gastric fundus, 2 — gastric body, 3 — gastric antrum, 4 — pylorus (pyloric channel), 5 — duodenal bulb, and 6 — second portion of duodenum. (B) is a double-contrast image of the distal stomach. Rugal folds are seen as radiolucent filling defects in the barium pool (white arrow) and as parallel barium etched lines (black arrows). Rugal folds are composed of mucosa and submucosa and are most prominent along the greater curvature of the stomach. The normal gastric antrum (A) has few, if any, rugal folds in most patients

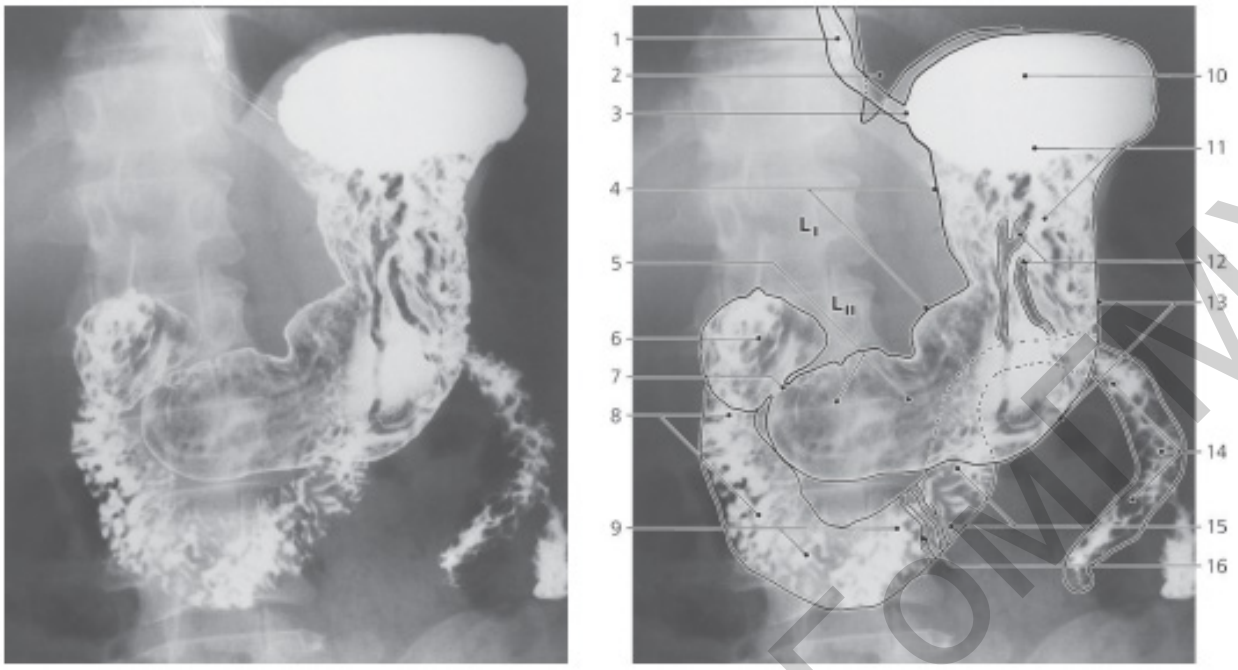

Figure 1.9 — Stomach and duodenum, oblique X-ray, barium meal, double contrast.
1 — Esophagus. 2 : Left lung. 3 — Cardia. 4 — Lesser curvature of stomach.
5 — Pyloric antrum. 6 — Duodenal "cap" (bulbus). 7 — Pyloric orifice.
8 — Descending part of duodenum. 9 — Horizontal part of duodenum.
10 — Fundus of stomach. 11 — Body of stomach. 12 — Rugae gastricae.
13 — Greater curvature of stomach. 14 — Jejunum. 15 — Ascending part of duodenum.
16 — Circular folds (Kerckring)

Magnetic resonance and CT imaging

Magnetic resonance (MR) imaging is the newest modality developed for cross-sectional imaging of the body and nearly all organ systems can be evaluated with this technique. MR imaging of the hollow organs of the gastrointestinal tract is increasingly being used to evaluate a wide assortment of gastrointestinal tract disorders. As with CT imaging, mild diseases and small focal lesions are not well detected with this technique; however, malignancies can be similarly evaluated and staged.

Conventional radiology imaging diseases of stomach

Inflammatory disorders

Gastritis

The appearance of a gastritis can vary. There may be oedema around small ulcers, thickened hyperaemic mucosa, or areas of atrophic mucosa. Islands of more "normal" mucosa may stand proud from a sea of atrophic thinned mucosa, giving the polyps reported in the fundal type "A" gastritis.

Perhaps as diverse as the underlying causes are the varied manifestations including erosions, rugal hypertrophy, rugal atrophy, and mucosal nodularity. Given

that no single finding or combination thereof is specific for a particular etiology, gastritis is most commonly categorized as either acute or chronic.

Acute gastritis

Radiographic findings: thickened gastric rugae (> 5mm) secondary to edema mucosal nodularity, antral narrowing (indicative of h. pylori) (Figure 1.10).

Erosions: manifest by small mucosal defects that collect contrast.

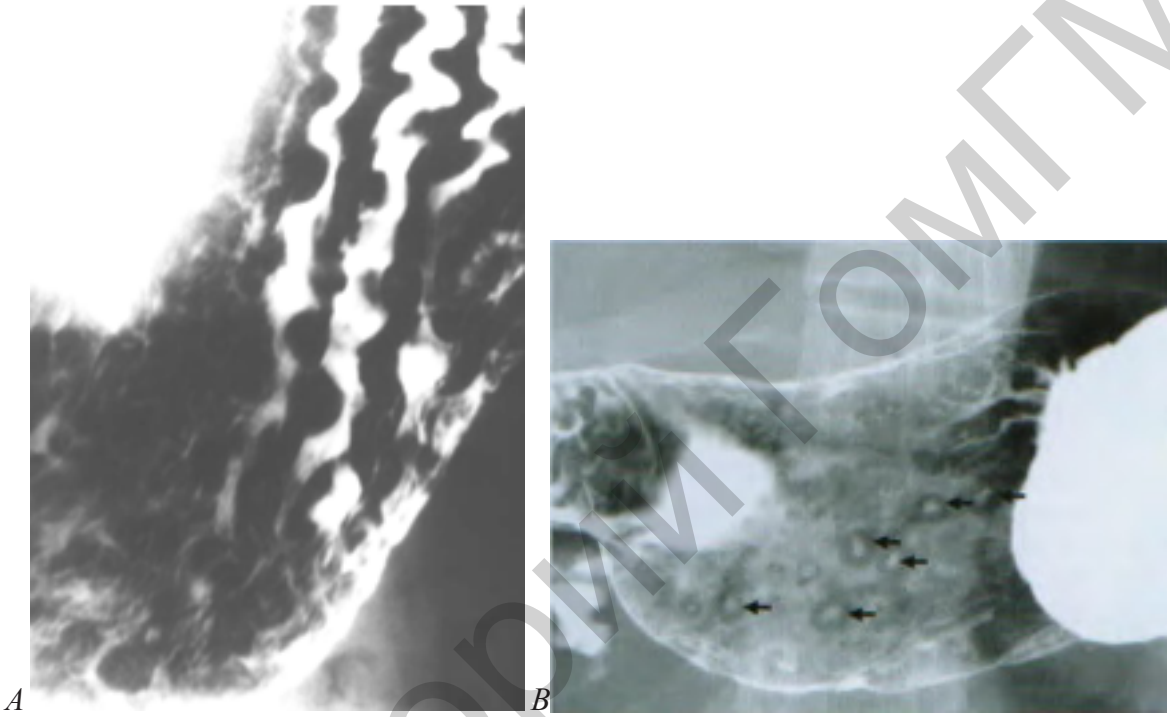

Figure 1.10 — (A) Acute gastritis. Diffuse erosive gastritis with thick nodular folds. Erosions are scattered along the folds.
(B) Acute erosive gastritis. There are numerous erosions in the stomach (arrows). Each erosion consists of a small central collection of barium surrounded by a translucent ring (a small "target" lesion)

Chronic gastritis

Radiographic findings: thinning or loss of rugal folds (however, thickening may be seen in early chronic disease); widening or loss of the area gastricae; as in acute gastritis, erosive lesions may be appreciated; mucosal nodularity; antral narrowing.

Gastric polyps

Gastric polyps are the most common benign gastric tumor with an incidence of 1,5–5%. They are typically solitary, but may be multiple or diffuse. Gastric classification is similar to other GI polyps:

1. Hyperplastic: most common; usually small in size and have no malignant potential. Radiographic findings:

— Shape: sessile or pedunculated. “Mexican hat sign” represents the stalk seen overlying the head of polyp.

— Size: usually < 2cm in diameter.

— Surface: sharply marginated polyp with smooth circular border.

— Location: variable.

— Often multiple.

2. Adenomatous: tend to be larger and papillary in appearance. Are a malignant precursor. Radiographic findings:

— Shape: broad-based elliptical polyp +/- a pedicle.

— Size: usually > 2cm in diameter.

— Surface: contour is generally lobulated, but may be smooth.

— Location: antrum is most common.

Gastric ulcers

The radiologic imaging study of choice in the clinical evaluation of suspected gastric ulcers is a double-contrast upper GI series. Features to evaluate include location, shape, penetration, mucosal folds, and the ulcer mound.

Radiographic findings: the distortion and uninterrupted mucosal folds that radiate from (pulled into) the ulcer crater.

Ulcer crater seen en face: distinct collection of barium that persists on different views; the collection is most often round but can be linear. Ulcer crater seen in profile: barium collection extends outside the projected margin of the gastric or duodenal wall. Double-contrast studies: the crater has a white center with surrounding black “collar.”

Benign ulcers

Benign ulcers constitute approximately 95% of all gastric ulcers. Most benign ulcers heal in 3–4 weeks following treatment with complete resolution by 6 weeks. Radiographic findings:

—Location: most commonly occur on the lesser curvature or posterior wall of the stomach.

—Shape: ulcer crater is smooth and round or oval (Figures 1.11).

— Penetration: the ulcer projects beyond the normal margin of the gastric lumen.

— Mucosal folds: extension of smooth gastric folds to the ulcer crater margin.

—Ulcer collar: an edematous mucosal band across the ulcer neck and around.

Complications includes of penetration, stenosis and deformation of body of stomach. Ulcers are generally classified as either benign or malignant depending upon their radiographic features and underlying etiology.

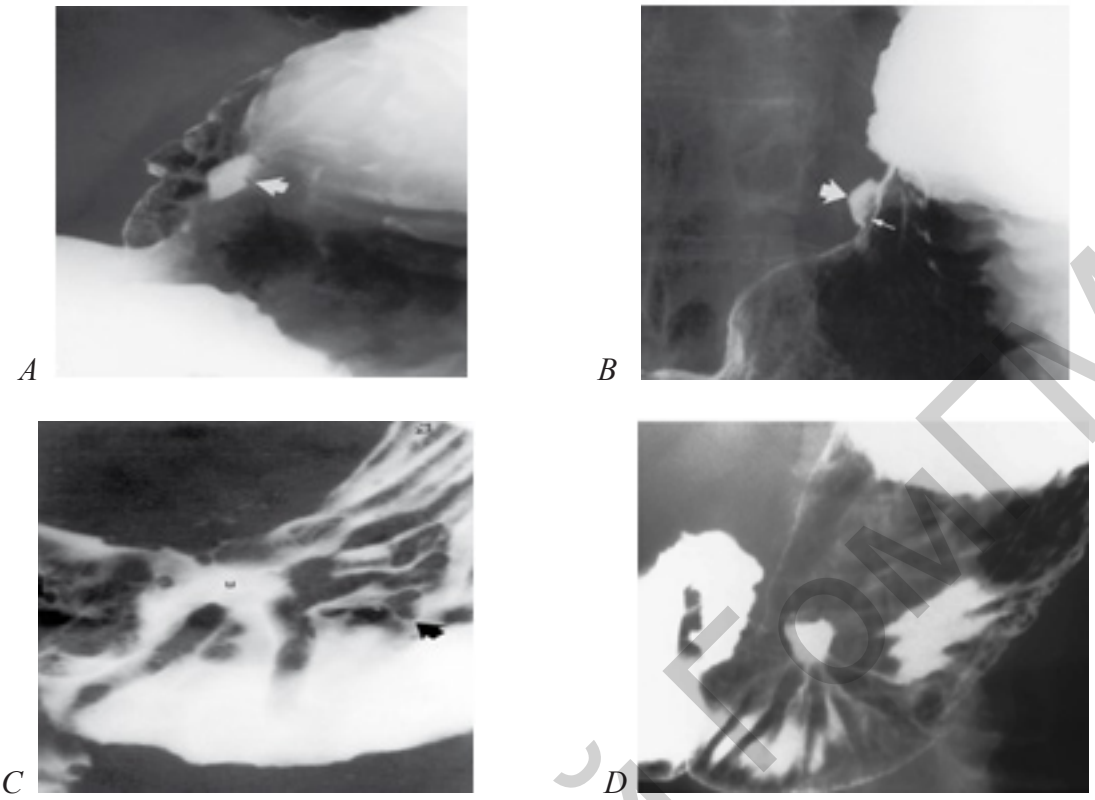

Figure 1.11 — Variants of gastric ulcer crater at double-contrast radiographic examination. (A) A 6-mm focal barium collection (arrow) is seen en face. No mass effect is seen. (B) When the barium collection is viewed in profile, the collection protrudes from the expected luminal contour (large arrow). A thin lucency (small arrow) crosses the collection at its interface with the luminal contour. These are findings of a benign gastric ulcer. The ulcer niche (crater) is filled with barium (large arrow) and protrudes outside the expected contour of the stomach. No mass or mucosal nodularity is seen to indicate that a tumor is present. As the ulcer extends into the soft submucosal fat, it spreads laterally, burrowing under the mucosa. The undermined mucosa is manifested as the lucency (small arrow) crossing the edge of the ulcer, termed a Hampton line. (C) Coarsely lobulated, nodular folds radiate toward a central barium collection (u). Compare a normal-sized fold (open arrow) with an enlarged, lobulated fold (black arrow). (D) Benign gastric ulceration. Small posterior wall ulcer demonstrated en face. Radiating mucosal folds extend to the edge of the crater

Malignant ulcers

Approximately 5% of gastric ulcers are found to be associated with malignancy. Of those, 90% are due to adenocarcinoma, with the remaining 10% divided among lymphoma, sarcoma, and metastases. Radiographic imaging suggestive of malignancy warrants tissue biopsy.

Radiographic features:

— The interrupted mucosal folds and irregular raised edge of the tumour indicate carcinoma of stomach.

— Shape: the ulcer crater is irregular and nodular.

— Non-penetrating: The ulcer does not project beyond the expected normal stomach margin.

— Mucosal folds: do not radiate to the ulcer margin and are often nodular.

— Ulcer mound: irregular and mass-like with eccentric crater.

Benign tumors

Benign tumors of the stomach are usually submucosal (lipoma, fibroma, schwannoma, hemangioma, lymphangioma, carcinoid (malignant transformation in 20%)). Leiomyoma: most common benign tumor; may ulcerate, 10% malignant.

Gastric carcinoma

Gastric carcinoma is the third most common GI malignancy after colorectal and pancreatic cancer, and represents the 6th leading cause of cancer deaths. Although they may present anywhere within the stomach, gastric carcinomas are most commonly located in the antrum or pylorus (50%); 60% are on the lesser curvature and 30% occur at the GE junction.

The diagnosis is usually suggested by endoscopic biopsy. CT is useful in defining the extent of disease as hepatic or peritoneal metastases may be present.

Radiographic findings:

— Gastric mass producing an irregular filling defect (Figure 1.12).

— Possible tumor ulceration. If an ulcer is present, radiating folds may be blunted or fused.

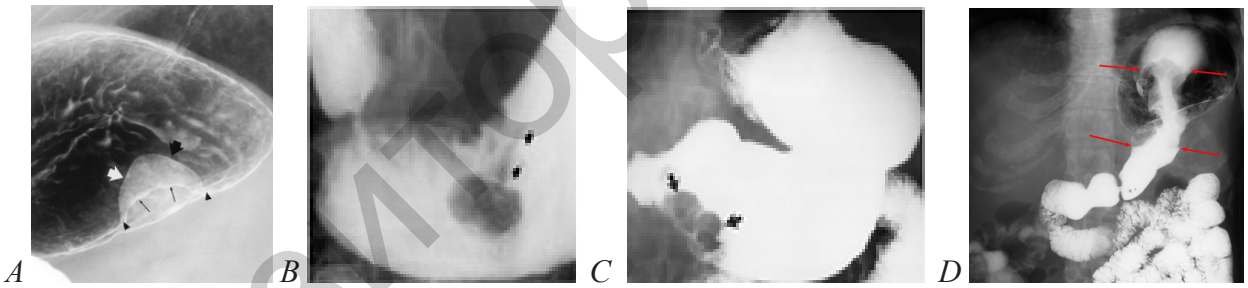

Figure 1.12 — (A) 4-cm, smooth-surfaced mass (large arrows) is protruding into the stomach. The mass has sharp angles to the luminal contour (arrowheads). There is a sharp line between the obliquely oriented tumor and mucosal surface (thin arrows). These are the classic findings of a mass arising in the submucosa or muscularis propria, variably termed a submucosal or extramucosal mass. (B) Adenomatous polyp. A long, thin pedicle (arrows) extends from the head of the polyp to the stomach wall. (C) Polypoid gastric carcinoma. Single-contrast technique upper GI series reveals a lobulated filling defect (arrows) in the antrum of the stomach. (D) Single contrast study from the same patient showing the apple core appearance (arrows) of the stomach due to the invasive gastric adenocarcinoma

CT may provide more insight into the true nature and size of the mass. CT is well-suited to assess for additional findings to support a diagnosis of a malignant tumor, including adjacent organ invasion, hematogenous spread (most often to the liver), and peritoneal spread.

Radiology of intestine

Decreased natural contrast between adjacent structures of roughly similar radiographic density mandates the use of contrast material. Barium suspensions, high-density compounds mixed with water, are commonly used in the examination of the gastrointestinal tract. Barium enema is useful to diagnose problems in the intestine and to identify abnormal growths, ulcers, polyps, diverticula, and intestinal cancer. A satisfactory barium examination depends on the colon carefully cleansed and being empty.

Limitation: discomfort to a patient, requires fluoroscopy, time consuming.

Patient preparation: for small-bowel examination, the patient should have nothing orally after midnight or the next morning preceding the radiographic study. Fluid and food in the stomach and small intestine degrade the examination by interfering with good mucosal visualization and causing artifacts that may mimic disease.

Preparation for the barium enema examination must be performed properly to obtain an accurate evaluation of the colon by this method. Various colonic preparations have been recommended and usually combine the use of dietary changes, oral fluids, and several cathartics the day preceding the barium enema examination. The presence of even small amounts of residual stool in the bowel may mimic colonic disease, or a filling defect in the colon may be passed off as stool but be a neoplasm.

CT imaging

CT imaging of the abdomen can portray the various organs of the gastrointestinal tract. Mucosal disease, such as ulcers, and small neoplasms will not be shown with this imaging modality. Larger intestinal neoplasms, thickening of the walls of the hollow organs, and extrinsic processes can be detected with CT imaging. A major role of CT scanning, especially in the esophagus and colon, is staging malignancy of these organs. In the colon, for example, CT examination is used for initial staging, especially of distant metastases, and for evaluation of recurrence following surgery.

Magnetic resonance imaging

MR imaging of the hollow organs of the gastrointestinal tract is used to evaluate and stage malignancies, especially of the esophagus and rectum, and also to assess inflammatory and obstructive bowel disease.

Conventional radiology imaging diseases of small intestine

The normal dimensions of the small bowel can be remembered by the “Rule of 3’s”: 1) bowel wall < 3 mm thick, 2) bowel folds < 3 mm thick, 3) bowel diameter < 3 cm wide. Patterns that should be assessed when evaluating the small bowel include the location of the abnormality, the caliber of the lumen, the mucosal contour, the fold pattern (Figure 1.13–1.14).

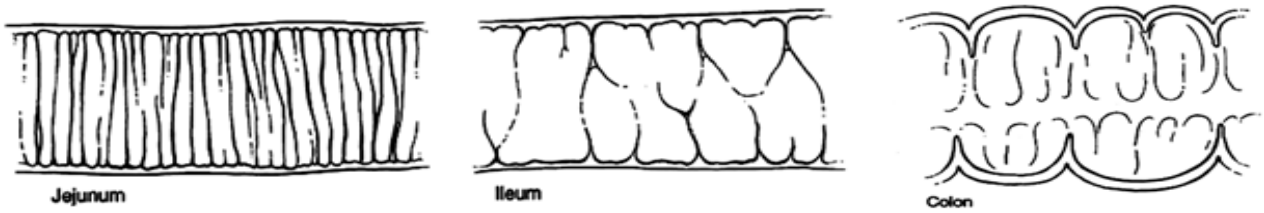

Figure 1.13 — Schematic illustration of portions of bowel. The jejunum shows numerous mucosal folds, whereas the ileum has fewer folds. Both serosa of the jejunum and the ileum are smooth. The colon has serosa indented by haustra, and mucosal folds do not cross the lumen

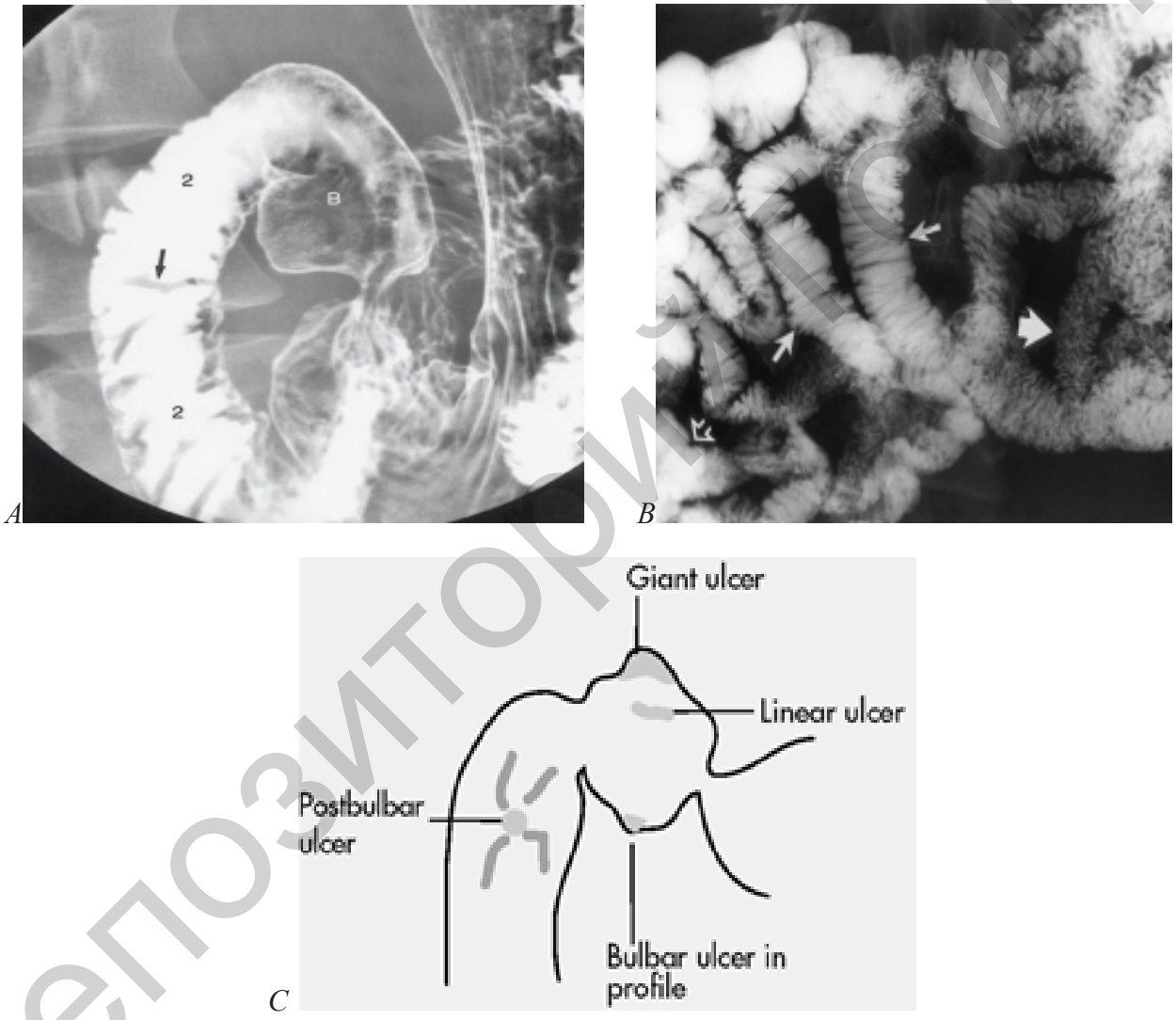

A *B* *C*

Figure 1.14 — (A) Spot radiograph of the duodenal bulb (B) and second portion of the duodenum (2) obtained during a double-contrast upper GI series. The folds of the duodenum (folds of Kerckring) (arrow) cross the duodenum except at the level of the papilla of Vater. (B) Close-up from an overhead view obtained during a normal small bowel follow-through examination demonstrates the normal anatomy. Many loops of small intestine are visible. Two loops are well distended (thin arrows) and show that the valvulae conniventes lie perpendicular to the longitudinal axis of the small bowel. (C) Scheme variants of duodenal ulcers

The small bowel generally lies centrally within the abdomen, “framed” by the large bowel. On imaging (Figure 1.15), the small bowel can be differentiated from the large bowel based on the presence of plicae circulares (circular folds), which traverse the entire diameter of the lumen. The large bowel does not possess these circular folds, but rather has saccular dividers called haustra.

Figure 1.15 — Normal bowel gas pattern. Gas is normally swallowed and can be seen in the stomach (st). Small amounts of air normally can be seen in the small bowel (sb), and this is usually in the left midabdomen or central portion of the abdomen. In this patient, gas can be seen throughout the entire colon, including the cecum (cec). Where the air is mixed with feces, a mottled pattern appears. Cloverleaf-shaped collections of air are seen in the hepatic flexure (hf), transverse colon (tc), splenic flexure (sf), and sigmoid (sig)

Inflammatory diseases

Duodenal ulcer

Duodenal ulcers are two to three times more common than gastric ulcers. All bulbar duodenal ulcers are considered benign. Postbulbar or multiple ulcers raise the suspicion for Zollinger-Ellison syndrome.

Radiographic features of duodenal ulcers: persistent round or elliptical collection of the barium, radiating folds, spasm (Figure 1.16).

Ulcer largely replaces the duodenal bulb. A large ulcer crater may be mistaken for a deformed bulb but does not change shape during fluoroscopy. Duodenal ulcers often heal with a scar; this can lead to deformity and contraction of the duodenal bulb: cloverleaf deformity, or hourglass deformity. Postbulbar ulcers: any ulcer distal to the first portion of the duodenum should be considered to have underlying malignancy until proven otherwise (only 5 % are benign ulcers, mostly secondary to Zollinger-Ellison syndrome).

Crohn's disease (regional enteritis)

Early findings represent active inflammation, while late findings represent chronic inflammation and/or fibrosis. Fluoroscopic findings include:

— Mucosal ulcers (punctate collections of barium surrounded by radiolucent mounds of edema).

— Luminal narrowing from edema, spasm (Figure 1.16).

— Fold thickening.

— Strictures, manifest by the "string sign".

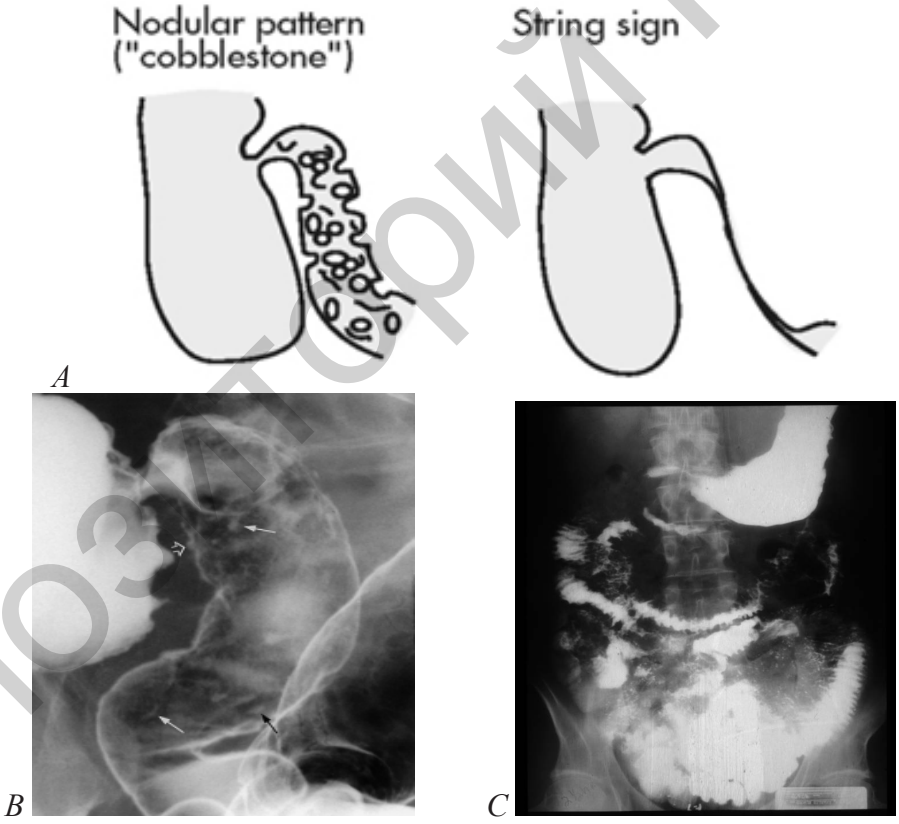

Figure 1.16 — (A) Schemes variants Crohn's disease of the small distal bowel. (B) Spot radiograph of the terminal ileum shows numerous aphthoid ulcers en face as 2- to 5 mm punctate or slightly elongated collections of barium surrounded by radiolucent halos (thin arrows). In profile, the aphthoid ulcers appear as 2- to 4 mm punctate barium collections (open arrow) protruding outside the expected luminal contour. (C) Crohn disease of intestine (luminal narrowing from edema, spasm, fold thickening) with stomach involvement

Ulcers

Fluoroscopy, using either single or double contrast, is the imaging study of choice for evaluating small bowel ulcerations. Barium pools in the ulcer base, seen as a radiopaque collection outside the confines of the small bowel. Ulcers can have a variety of appearances, ranging from aphthoid to linear to "punched-out" to "bull's-eye," depending on the etiology. In addition, pancreatic pseudocysts and diverticula may mimic the appearance of ulcers (Figure 1.17).

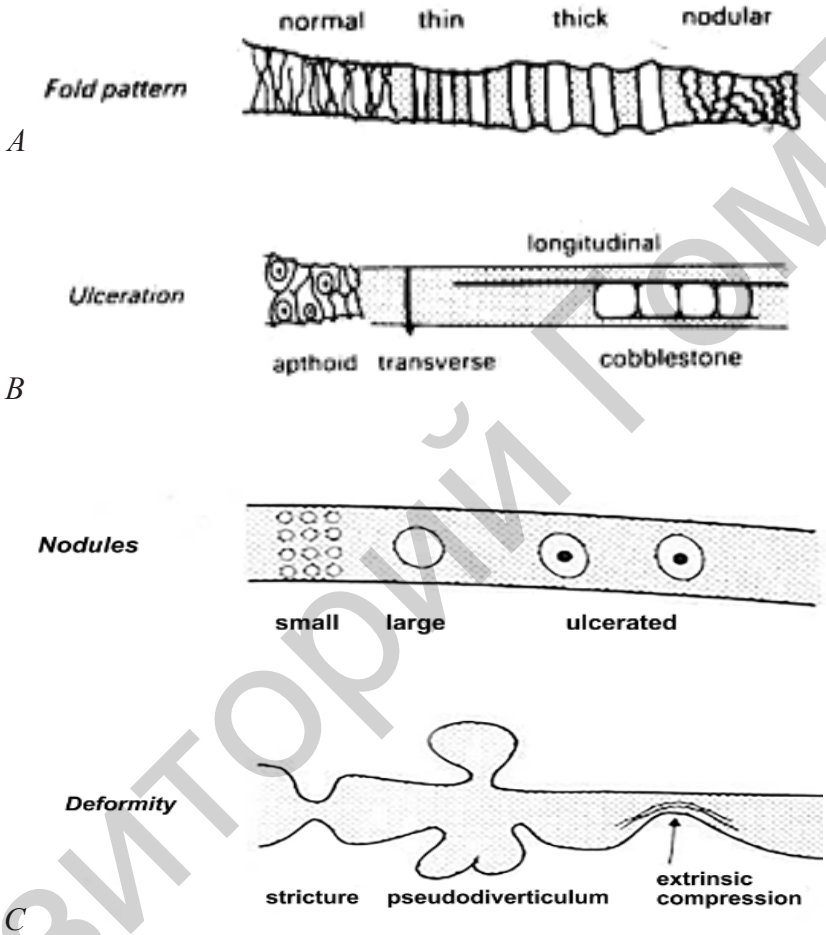

Figure 1.17 — (A-C) Schemes of variants lumen, mucosal and fold patterns of small bowel

Solitary mass

Masses projecting into or occurring with the small intestine appear as filling defects on radiographic studies. These filling defects may represent intraluminal, mucosal, intramural, or extrinsic masses (Figure 1.10).

Diagnostic imaging and in particular cross-sectional modalities (US, CT, and MR) have a critical and complementary role in diagnosis and management of small bowel diseases. Radiologists should be aware of advantages and disadvantages of each imaging test in order to choose the best option, considering the specific small bowel disease and the patient's characteristics (age, gender, clinical status).

Conventional radiology imaging diseases of colon

Large intestine

The radiographic examination of the large bowel evaluates the entire organ from the rectum to the cecum. Reflux of barium suspension into the ileum and the appendix, if present, occurs commonly. As with the upper gastrointestinal examinations, the colon can be evaluated by the following techniques: (1) single-contrast barium enema or (2) double-contrast barium enema. Both examinations require insertion of a rectal tip for installation of the examining materials. The single-contrast barium enema is performed using a low-density barium suspension that flows into the colon through the rectal tip.

Small films with abdominal pressure applied to the area of interest are exposed as each segment of the colon is opacified. A series of larger films is also obtained with the patient in various frontal and oblique positions.

The large intestine consists of the rectum, sigmoid colon, descending colon, splenic flexure, transverse colon, hepatic flexure, ascending colon, and cecum (Figure 1.18). The length of the colon varies considerably, depending mainly on the length and redundancy of the sigmoid colon and the colic flexures. The colon varies in caliber depending on the location and degree of luminal distention. The mucosal surface has a smooth appearance and the colonic contour is indented by the haustra, which are less numerous in the descending portion of the colon.

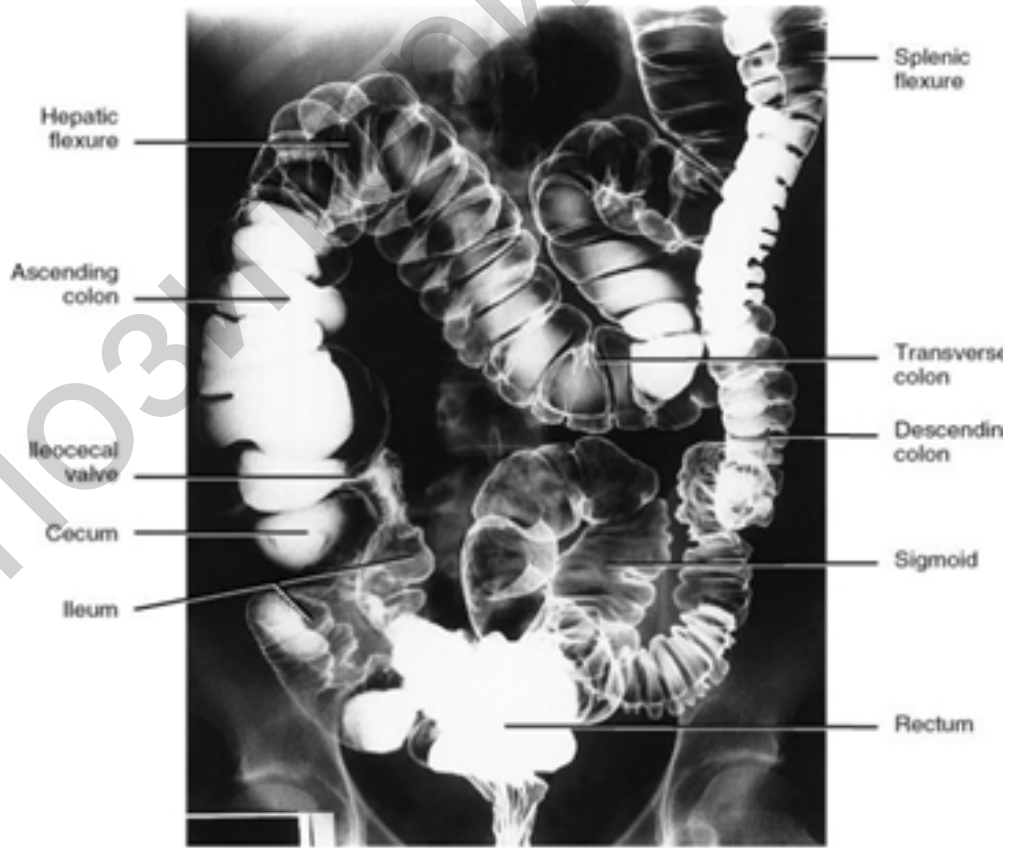

Figure 1.18 — Normal supine film on double-contrast barium enema

Inflammatory diseases

Crohn's disease

Crohn's disease is an idiopathic inflammatory disease of the GI tract that is characterized by ulcerations, erosions, noncaseating granulomas, and full-thickness bowel wall inflammation. The disease may affect any portion of the gastrointestinal system from the esophagus to the anus. The course is progressive in nature, with frequent remissions and relapses. The radiographic hallmarks of Crohn's disease are aphthous erosions, thickened and distorted folds due to bowel wall edema, "cobblestone" pattern of deep ulcerations (Figures 1.16–1.17), fibrosis with thickened walls, contractures, and stenosis resulting in the "string sign", fistula and sinus tract formations, stranding in mesenteric fat due to inflammation, and "skip" lesions with intermittent areas of normal bowel between diseased segments (Figure 1.19).

Colitis

Radiographic features of bowel inflammation (any etiology) depend mainly on the process. Ulceration shallow: granularity of mucosa, aphthoid. Ulceration deeper: flasklike collections of barium: collar button. Edema: displacement of barium (translucent halo around central ulcer). Spasm: localized persistent contraction/ narrowing of bowel lumen.

Ulcerative colitis

Ulcerative colitis is an idiopathic chronic inflammatory disease that is characterized by superficial ulcerations, edema, and hyperemia of the colonic mucosa and submucosa. The disease usually begins in the rectum and extends proximally in a continuous pattern.

The radiographic hallmarks of ulcerative colitis are confluent, circumferencial, shallow ulcerations of the colon, granular mucosa, collar button ulcers, and "thumbprinting" (Figure 1.19).

Diverticulosis

Diverticulosis is a condition in which the mucosa and muscularis mucosae herniate through the muscularis propria of the colon wall and produce a saccular outpouching. Approximately 70% of diverticula occur in the sigmoid colon and 25% in the ascending colon. Plain films and barium studies reveal diverticula as gas/ barium-filled sacs parallel to the lumen of the colon. Most are 5–10mm in diameter, but may range from tiny spikes to 2 cm.

Hallmarks on barium enema include distorted diverticlar sacs, evidence of abscess, and leakage of barium outside the bowel lumen (Figure 1.20).

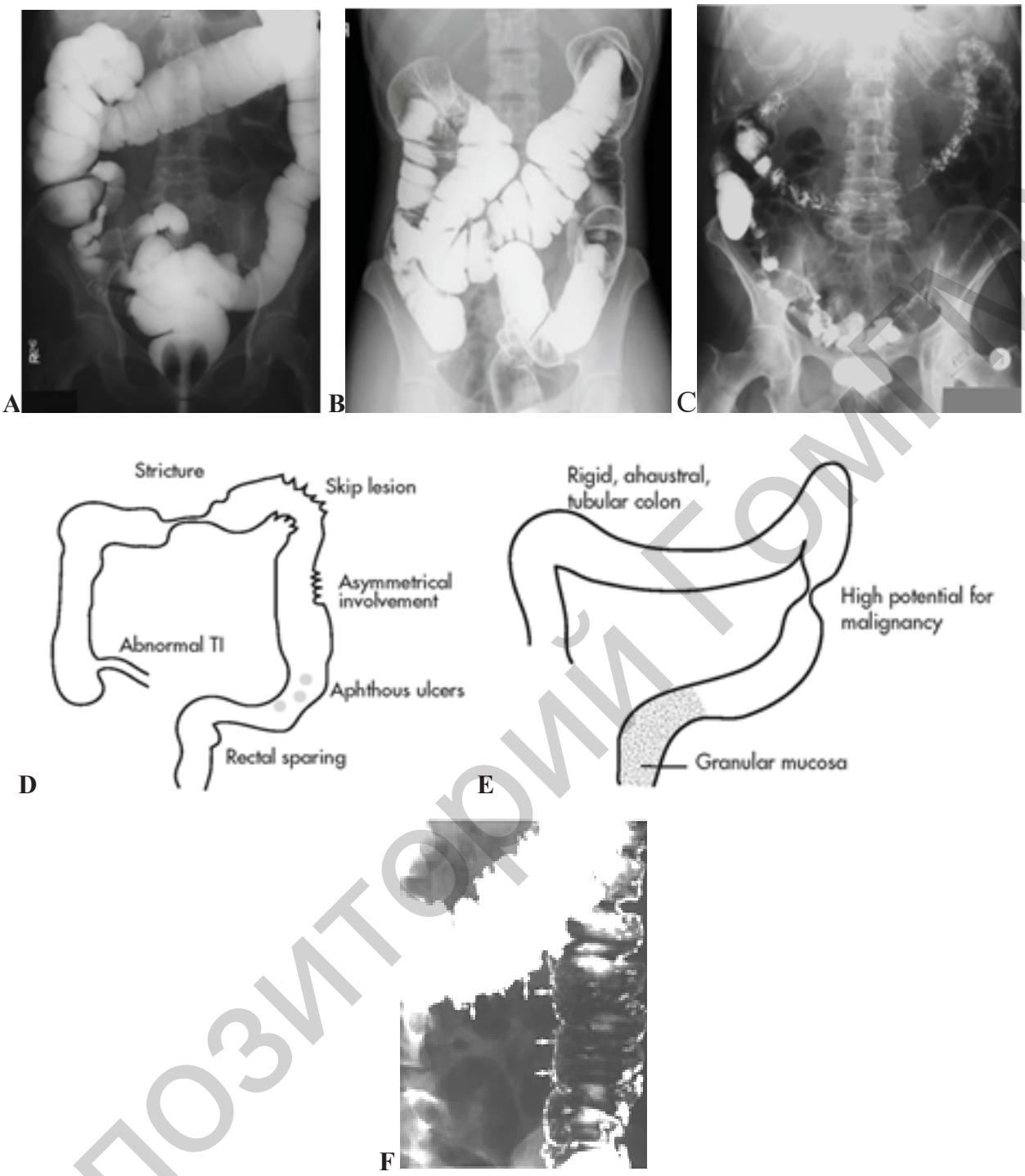

Figure 1.19 — (A) Single-contrast barium enema and (B) double-contrast barium enema of the normal colon. Although a single contrast study may be easier to perform, mucosal detail is better seen on the double contrast study.
(C) Post-evacuation radiograph of abdomen and pelvic.
(D, E) Schemes variants Crohn's disease of the large bowel.
There is a stenosis of the descending and transverse colon. The haustral pattern is lost. Numerous deep fissured ulcers can be seen and there is irregular mucosal thickening at the hepatic flexure with a cobblestone appearance. This portions of bowel is affected asymmetrically. The bowel involvement is thus asymmetrical with skip lesions.
(F) Ulcerative colitis (spot radiograph of the colon with marked multiplies of ulcers craters)

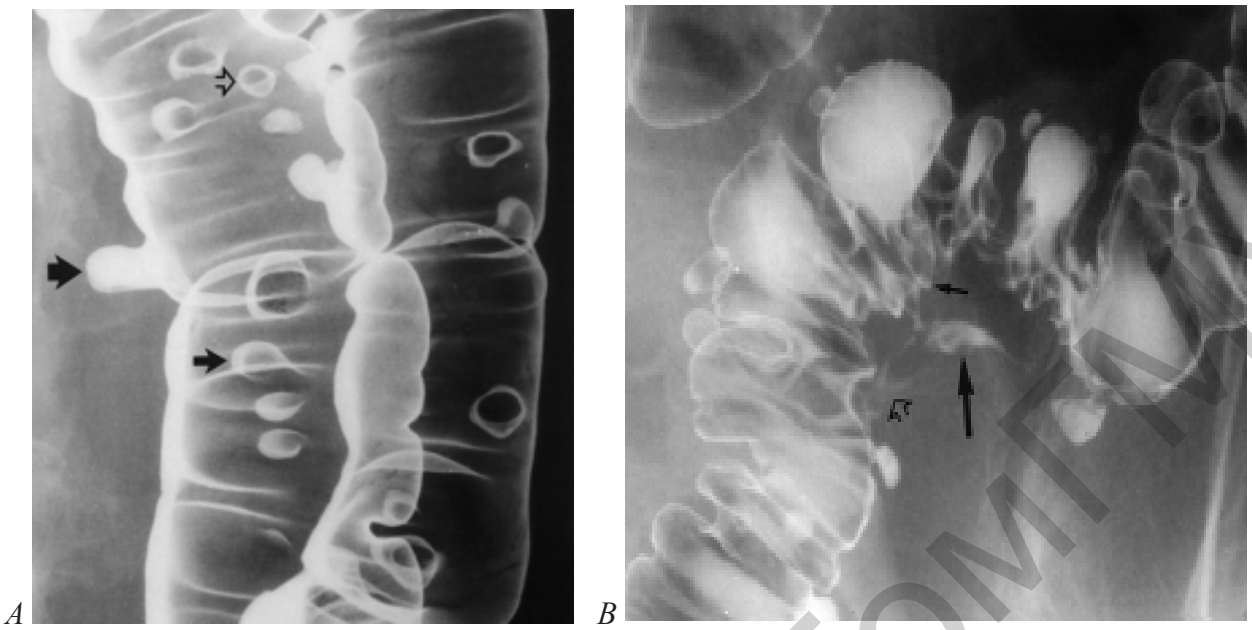

Figure 1.20 — (A) Diverticulosis of the colon. Coned-down image of the splenic flexure from a left-side-down decubitus overhead from a double-contrast barium enema reveals numerous diverticula. Some barium-filled diverticula are seen in profile (thick black arrow). Most diverticula seen en face have a small pool of barium on their dependent surface resembling a meniscus (thin black arrow). Other diverticula are devoid of a barium meniscus and are depicted only as barium-coated ring shadows (open arrow). The normal haustral sacculations and interhaustral folds are preserved. (B) Diverticulitis. Spot radiograph of the sigmoid colon from a double-contrast barium enema shows several small barium-filled tracks (open arrow) forming a flame-shaped collection (large arrow) in the pericolic space. The wall of the adjacent sigmoid colon has a spiculated contour (spicule represented by small arrow). There is an extrinsic mass impression on the inferior wall of the sigmoid colon. Compare the asymmetric inflammatory changes with the normal contour of the opposite colonic wall

Neoplasm

Polyps are focal masses that protrude from the mucosa into the bowel lumen. In general, polyps less than 1cm in diameter have a 1% risk of cancer, 1–2 cm have a 10% risk, and those greater than 2cm have up to a 50% risk. Thus, barium studies are often indicated to detect colon polyps (Figure 1.21).

Radiographic finding: benign polyps are small in diameter, stable in growth, spherically shaped, have normal mucosa, long stalks, and a smooth surface. Malignant polyps on the other hand are large in diameter, sessile, irregularly shaped, may exhibit sudden growth, and have a broader base and puckered mucosa.

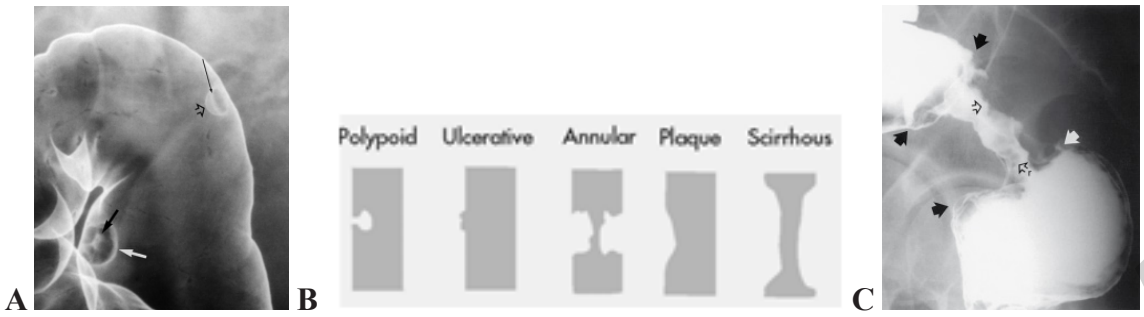

Figure 1.21 — (A) Spot radiograph of the splenic flexure shows two polyps. The small polyp resembles a hat. The top of the hat (open arrow) is the top of the polyp. The brim of the hat (thin black arrow) is barium trapped between the mucosa and the polyp as it is retracted by its stalk. This was a tubular adenoma. The second polyp has a more worrisome morphology – that of an umbilicated, sessile polyp. A small barium collection (thick black arrow) fills a central umbilication or ulceration. The edge of the polyp is coated by barium (white arrow). This polyp was a tubulovillous adenoma. (B) Schemes variants of the colorectal cancer. (C) Annular adenocarcinoma of the rectum. Spot radiograph from the single-contrast phase of a double-contrast barium enema shows a 5-cm-long, circumferential narrowing of the proximal rectum. The lesion has abrupt shelf-like margins (large black and white arrows) and an irregular surface (open arrows). This has been called an "apple core" lesion, but this is a misnomer because the tumor represents the part of the apple that has been eaten away, and the lumen would be the "apple core"

Colorectal adenocarcinoma is the most common GI malignancy and is the second most deadly cancer in the United States. Signs and symptoms depend on the location of the tumor. Approximately 50% of these malignancies develop in the rectosigmoid area and 25% in the cecum and ascending colon. Many likely arise from a malignant transformation of an adenomatous polyp. These tumors tend to form annular constricting lesions or bulky exophytic masses, with raised everted edges and ulcerated mucosa, ranging from 2–6 cm in diameter. They spread by direct invasion into the pericolonic fat and adjacent organs, through lymphatic vessels to regional nodes, and hematogenously via systemic and portal circulation.

Apple-core constricting lesions, tumor masses, nodal involvement, and metastases may be visualized (Figure 1.21C).

Emergency radiology of the abdomen

Intestinal obstruction

Radiographic the main sign of intestinal obstruction is — Kloiber's cup and arches (air-fluid levels). The small bowel obstruction — the width of horizontal fluid level is more than height of a gas bubble above it; on a background of gas the mucosal folds reminding a spring can be visible; the localization of Kloiber's cups is more

often in medial parts of the abdomen. Arches — the intestinal loops, filled with gas and limited by horizontal fluid levels.

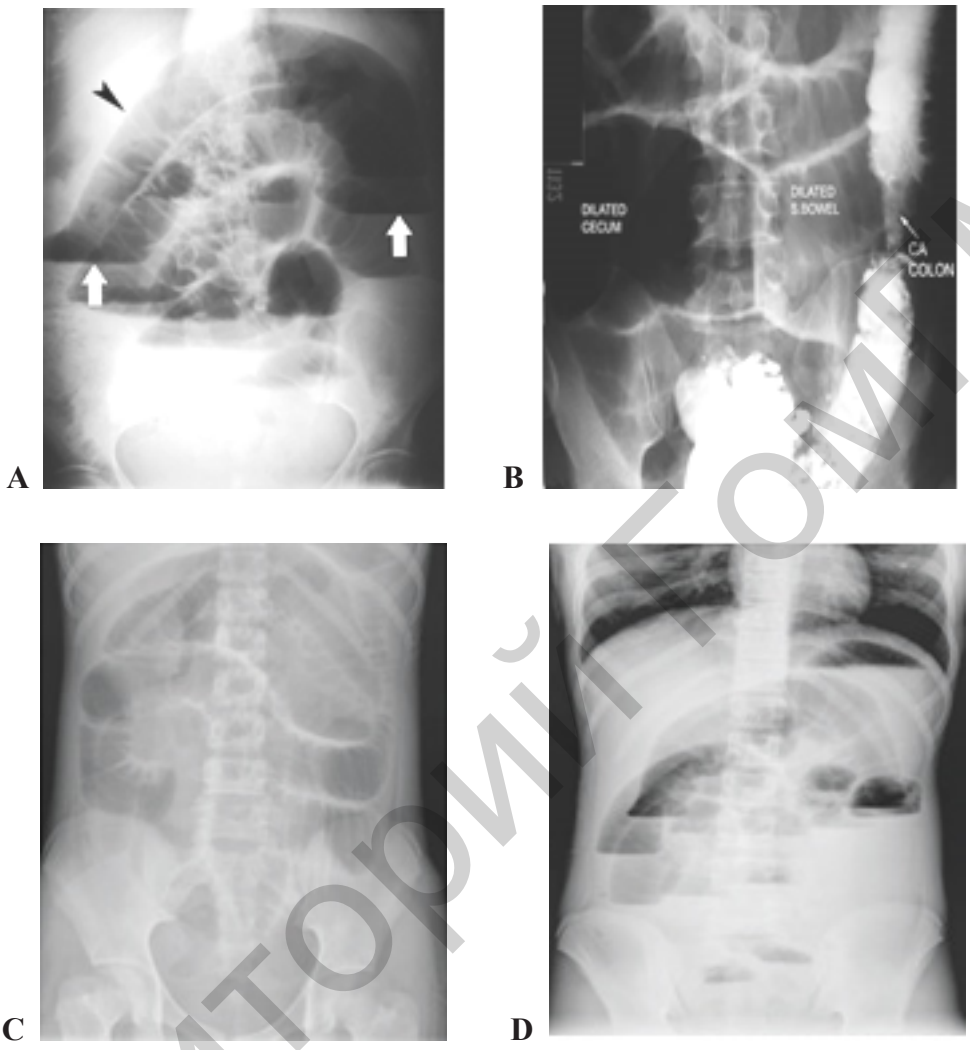

Figure 1.22 — (A) Small bowel obstruction (black arrow – dilated small bowel, white arrows – air-fluid levels). (B) Large bowel obstruction. (C) Supine and (D) upright abdominal radiographs same patient demonstrate a "stacked" appearance of multiple segments of markedly dilated small bowel with numerous air-fluid levels at high-grade distal small bowel obstruction

The large bowel obstruction — the width of a horizontal level is less than the height of a gas bubble above it; the localization of Kloiber's cups is more often in lateral parts of the abdomen; on a background of gas colic haustra are sometimes visible (Figures 1.22–1.23).

The mechanical obstruction — at a roentgenoscopy there has been detected "migration" of a fluid from one loop of an intestine to another, fast motions of fluid levels. The dynamic obstruction — at a roentgenoscopy no motions of fluid levels, barium meal passes very slowly.

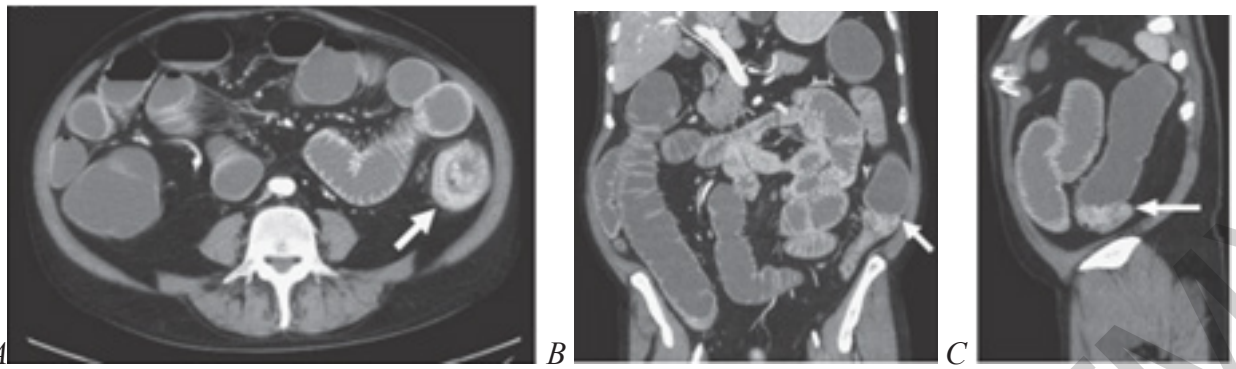

Figure 1.23 — Obstruction of the large bowel secondary to carcinoma of the descending colon (CT features). (A) Axial, (B) coronal reformatted, and (C) sagittal reformatted images show an enhancing, obstructing colonic mass (arrows) with a dilated, fluid-filled proximal colon and small bowel

Colon obstruction is four to five times less common than small bowel obstruction and differs significantly in terms of etiology, pathophysiology, therapy, and prognosis. Since most colonic obstructions are due to cancer, patients are usually elderly and have symptoms related to tumor location. Signs and symptoms are often insidious with right colon lesions because the lumen is large and the contents are semiliquid. Patients with volvulus may develop pain and distention rapidly if a closed-loop obstruction and bowel ischemia are present.

Clinical evidence of colonic obstruction arises through a combination of mechanical obstruction, inadequate propulsion of luminal contents, and often an ischemic component. The causes of large bowel obstruction include carcinoma of the colon (55%), volvulus (11%), diverticulitis (9%), extrinsic cancer (8%), adhesions (4%), fecal impaction (3%), hernia (2%), and intrinsic causes (4%).

In the case of intestinal dilatation, ultrasound contributes to distinguishing obstructive from paralytic ileus. Findings suggestive of intestinal obstruction include dilated fluid-filled loops, increased peristalsis of distended segments (ineffective contractions may cause to-and-fro fluid movements), and collapsed loops distal to the obstruction. A small amount of intraperitoneal fluid is frequently present. Analysis of the dilated loops may help in determining the level of obstruction, and sometimes the cause is also identified (e.g., neoplasm, hernia, Crohn disease, intussusception, bezoar, or gallstone.

Free gas in an abdominal cavity

The free gas in an abdominal cavity — can be the result of perforation of hollow organs (stomach, intestine), penetrating wounds of an abdominal wall; after operations on the organs of an abdominal cavity, or owing to injection of gas in an abdominal cavity with the diagnostic purpose (diagnostic pneumoperitoneum). In a vertical position of a patient there has been detected a falciform accumulation of gas under the right dome of a diaphragm (at presence of a much amount of gas — under the right and the left also) (Figure 1.24), in a latero-position — under a lateral wall of an abdominal cavity.

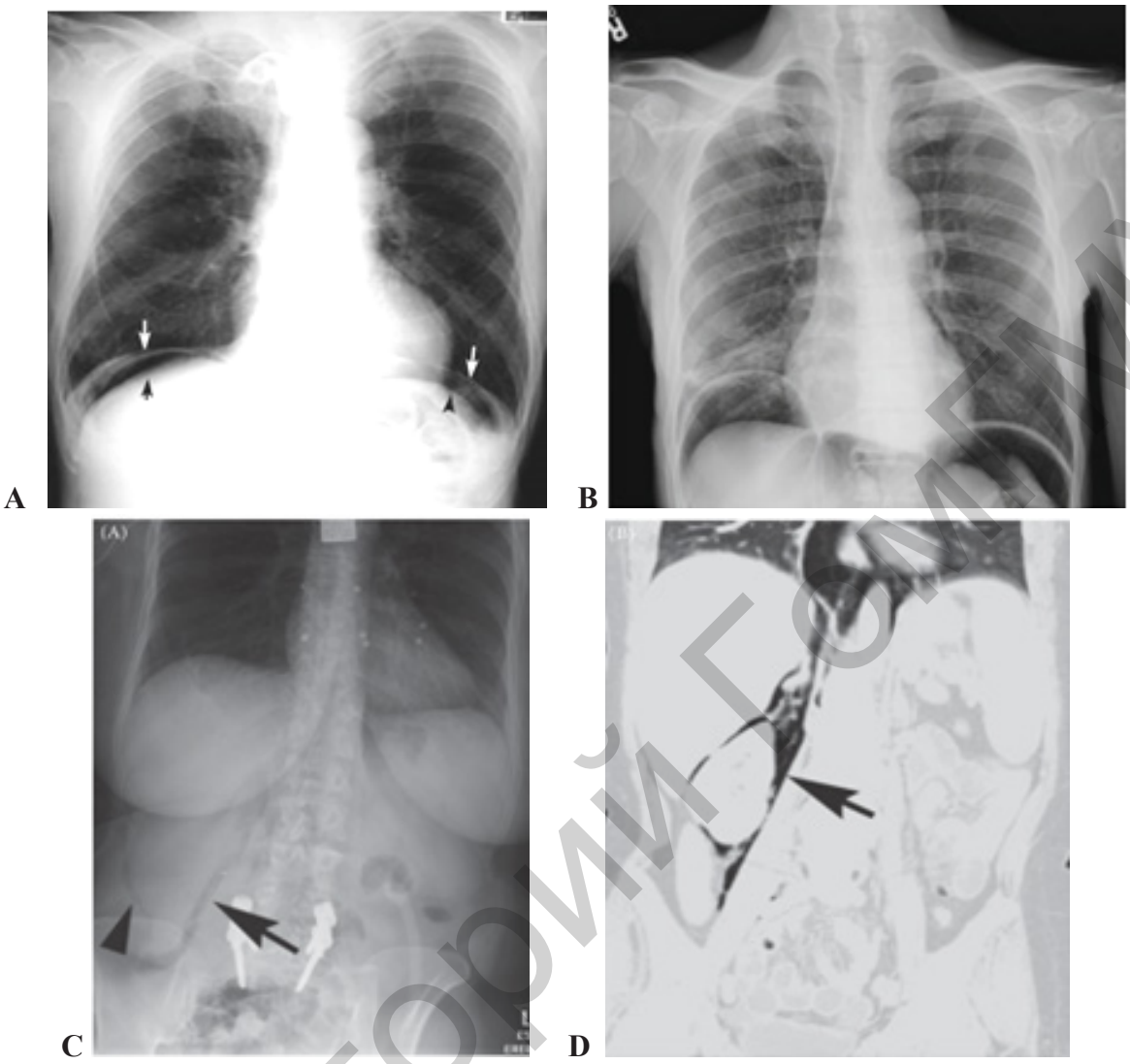

Figure 1.24 — (A) Free gas of abdominal cavity (arrows). (B) This upright chest radiograph demonstrates crescent shaped lucencies under both hemidiaphragms. This is free intraperitoneal gas, or "free gas", which rises up to the top of the peritoneal cavity when the patient is upright (different patient). Pneumoretroperitoneum from endoscopic perforation of the duodenum. (C) Upright abdominal radiograph shows lucency outlining the right psoas muscle (arrow) and kidney (arrowhead). (D) Coronal image from CT scan in the same patient shows air in the retroperitoneum adjacent to the psoas muscle (arrow) and kidney, dissecting into the mediastinum

Pneumoperitoneum is commonly due to recent surgery, but it may also indicate a ruptured abdominal viscus, such as a perforated duodenal ulcer.

Pneumoperitoneum may occur at any age for a variety of reasons. Common etiologies of pneumoperitoneum include gastric or intestinal perforation from trauma, peptic ulcer disease, ischemia, obstruction, tumors, diverticular perforation and other inflammatory diseases, steroids, dehiscence of surgical anastomoses, chemotherapy and radiation therapy, and ingestion of foreign bodies. Pneumoperitoneum may also be seen following abdominal or pelvic surgical procedures, peritoneal dialysis, or from iatrogenic injury to the bowel during endoscopy or other interventional procedures.

II. RADIOLOGY OF ABDOMINAL VISCERA

(liver, biliary tract, and pancreas)

The diagnosis of diseases of the liver, biliary tract, and pancreas optimally depends on using both clinical and radiographic data. Understanding the proper use of these data and ordering radiographic studies in the optimal sequence are helpful for making the diagnosis most efficiently. If clinical information is insufficient or if radiographic confirmation is necessary, plain films and contrast studies may be performed. Upright and supine plain radiographs are helpful for the detection of free air, calcifications, and other abnormalities. Contrast studies such as endoscopic retrograde cholangiopancreatography and percutaneous transhepatic cholangiography are often helpful in analyzing diseases of the liver, bi-liary tree, and pancreas. For instance, pancreatic or biliary ductal systems, fistulae from these ductal systems, and associated abnormalities such as encasing tumors can be diagnosed by cholangiography. Digital cross-sectional imaging, nuclear medicine, positron emission tomography, and angiography have provided considerable information in analyzing diseases of these organs, which cannot be directly visualized with plain radiography, even using traditional contrast material. Cross-sectional techniques consist of ultrasound, computed tomography, and magnetic resonance imaging the use of cross-sectional imaging to evaluate abnormalities of the liver, biliary tract, and pancreas.

Diseases of the liver, biliary system, and pancreas can be conveniently, if arbitrarily, separated into the following categories to help illustrate the optimal sequences of imaging techniques: diffuse hepatocellular disease, focal hepatic diseases, abdominal trauma, inflammatory disease of the biliary tract, and pancreatic inflammation or neoplasm.

Solid organs such as the liver and pancreas are better evaluated by cross-sectional imaging studies than fluoroscopic contrast studies, in which the presence of masses and the like can only be inferred indirectly. Cross-sectional imaging studies of the abdomen reveal a vast quantity of anatomy, and it is important to adopt an ordered approach to avoid missing abnormalities.

Liver

Imaging methods

Plain radiography

Plain radiographs are limited for assessing the liver, but may demonstrate gross hepatomegaly and hepatic calcification. The complex shape of the liver, limited soft tissue contrast and projection acquisition of plain radiographs makes reliable identification of the liver boundaries difficult. As the anterior and inferior border of the liver often extends inferior to the gas-containing lumina of the stomach,

duodenum and hepatic flexure of the colon, these gas-filled structures are unreliable guides to its inferior border.

Computed tomography

CT is the preferred modality for patients with clinical suspicion of appendicitis except in pediatric and pregnant population where US and MR play an important role .The liver is the largest organ in the abdomen and has attenuation of 50 to 70 Hounsfield units (HU) on CT, which on average is about 10 HU greater than that of the spleen.

Unenhanced CT imaging remains valuable for assessing diffuse hepatic changes, such as fat infiltration and iron deposition, and focal changes, such as subtle calcification and haemorrhage. Contrast-enhanced imaging following IV administration of water-soluble contrast medium is widely used for the detection and characterization of focal lesions.

Magnetic resonance imaging

MRI offers major advantages due to its high contrast resolution, multiplanar capability, sensitivity to blood flow and lack of ionizing radiation. On MRI, the liver has high T1-weighted signal intensity relative to spleen secondary to abundant intracellular protein and paramagnetic substances. The normal contour of the liver is smooth, and the liver parenchyma normally homogeneously enhances. MRI is increasingly utilized as the modality of choice in the evaluation of focal and diffuse liver disease (Figure 2.1).

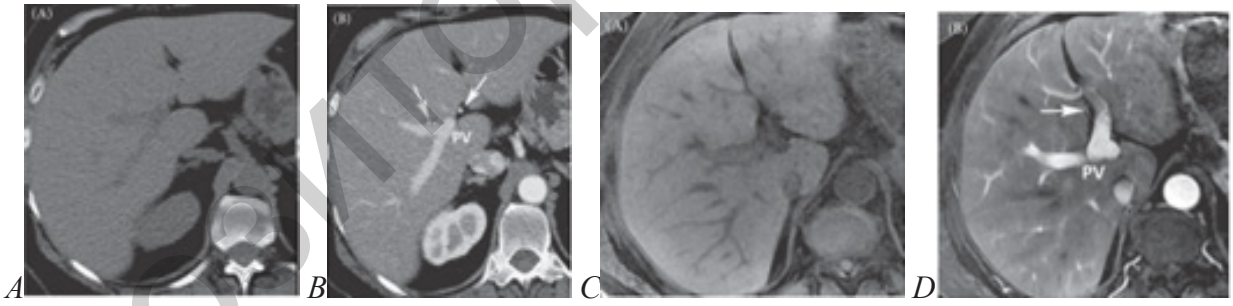

Figure 2.1 — Normal CT of the liver. (A) Unenhanced, (B) late arterial phase. As illustrated in this case, the late arterial phase is characterized by enhancement of the hepatic artery (arrows) and portal veins but not the hepatic veins. The hepatic veins enhance by antegrade flow in the portal venous phase. Normal liver MRI with extracellular intravenous contrast material. (C) Unenhanced, late arterial phase (D). As with CT, the late arterial phase is characterized by enhancement of the hepatic artery (arrow in D) and portal veins but not the hepatic veins. The hepatic veins enhance by antegrade flow in the portal venous phase. PV, portal vein

Abdominal ultrasound imaging

Sonography is a versatile, noninvasive and inexpensive modality for evaluating the liver. It is usually the initial imaging modality used for suspected liver pathology. It

plays a vital role in the evaluation of focal liver lesions, screening for liver metastases in a patient with known malignancy, screening for hepatocellular carcinoma in the setting of hepatitis/cirrhosis, portal hypertension, surgical obstructive jaundice, hepatic veno-occlusive disease and preoperative work up and postoperative follow up of liver transplant patients. Sonography is ideally suited to study the internal architecture of a focal mass and distinguish a solid from a cystic lesion. Ultrasonography is highly portable, and it allows real-time imaging in multiple operator controlled planes. As a result, it is the most widely used cross-sectional imaging modality worldwide.

Increasingly contrast-enhanced US is being used to add an arterial and portal phase study similar to those in CT and MRI.

Doppler ultrasound imaging

Doppler ultrasonography is a noninvasive technique that provides information about the condition of blood vessels and blood flow direction. It also measures flow velocity and can be used to evaluate the vascularity of mass lesions. Color and pulsed-wave Doppler imaging provide complementary information, including spatial orientation and a time velocity spectrum, respectively. Doppler examination of the hepatic vessels can be performed relatively rapidly and is becoming part of the routine US examination of the liver.

Doppler capability, both spectral and colour, is an integral part of the examination of the liver, allowing demonstration of hepatic blood flow and unequivocal identification of the bile ducts. The addition of color Doppler flow imaging further helps in characterizing mass lesions and assessing patency of vessels.

Nuclear scintigraphy of liver

Radionuclide imaging of the liver is commonly performed using ^{99m}Tc-sulphur colloid or albumin colloid, which target the reticulo-endothelial system. Liver scintigraphy lacks anatomical specificity but provides a global view of the liver and is unaffected by bowel gas and the majority of surgical clips and implants. It is infrequently used as a primary diagnostic investigation but can help to further characterize known lesions when CT and MRI are not available.

Cysts appear as cold lesions on nuclear scintigrams because there is no uptake of any radiotracer. Positron emission tomography improves sensitivity and specificity.

Hepatobiliary nuclear imaging

Two commonly used nuclear imaging studies to investigate abnormalities of the GI tract are hepatobiliary imaging and GI bleeding localization. In the setting of acute cholecystitis, a hepatobiliary imaging study has a 95% positive and negative predictive value. The predictive value of this study is improved by concordant US imaging of the right upper quadrant for anatomic correlation. Hepatobiliary imaging is also useful in the setting of biliary surgery or trauma to diagnose intraperitoneal

biliary leaks. Finally, hepatobiliary imaging with additional chemical challenges using cholecystokinin can help in the diagnosis of biliary dyskinesia or acalculous cholecystitis.

On *angiograms* simple hepatic cysts are noted to be avascular.

Diffuse hepatocellular disease

Diffuse diseases are more difficult to detect with imaging than focal lesions as their effect on normal liver architecture may be minimal. Diagnoses are usually made on the basis of clinical features and may require histological confirmation; potential exceptions to this are fatty infiltration and iron deposition. Imaging can help assess the extent and severity of diffuse disease both by demonstrating liver abnormalities and sequelae such as portal hypertension changes.

Liver biopsy is the definitive test, but the presence of cirrhosis can be suggested by several imaging studies. CT, MR, and US all produce high-quality images of the liver parenchyma.

In diffuse hepatocellular disease, *CT* is probably the first study used to survey the liver because it is moderately sensitive to liver lesions and is also helpful for evaluating surrounding organs. Contrast enhanced multidetector CT is the current method of choice for most hepatic imaging.

MR imaging may be the most sensitive modality for detecting and characterizing diffuse diseases of the liver, including cirrhosis and hemochromatosis, especially when combined with contrast agents. MR is preferred whenever iodinated contrast cannot be used (Figure 2.2 B to C).

US is used as a screening method for patients with abdominal symptoms and suspected diffuse liver disease. Color flow and spectral Doppler are used to assess hepatic vessels and tumor vascularity. US is used as a rapid screening modality to detect diseases of the gallbladder, biliary tree, and the liver. Ultrasound may have application unless fatty liver is present, because fat attenuates the US beam (Figure 2.2 A).

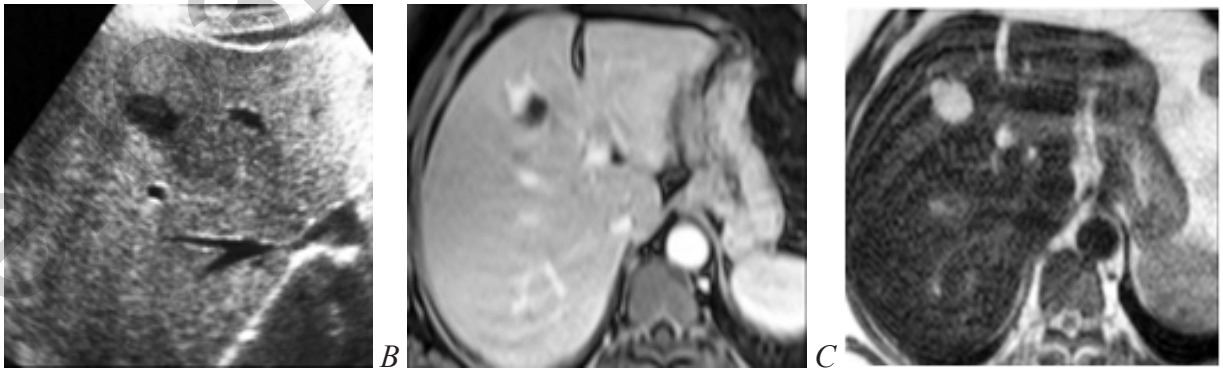

Figure 2.2 — A to C: Fatty liver with hypoechoic hemangioma.
(A) Transverse US of the liver shows a small hypoechoic focal lesion against a background of diffusely increased echogenicity of fatty liver; (B) The lesion is hyperintense on T2W image, with (C) typical peripheral nodular enhancement, suggestive of hemangioma

Radionuclide imaging of the liver is inferior to CT and MR for lesion detection but offers functional information in characterizing lesions, such as focal nodular hyperplasia. Radionuclide blood pool imaging is very useful for definitive diagnosis of cavernous hemangioma. Dynamic bolus radionuclide imaging is used in the characterization of cavernous hemangiomas and focal nodular hyperplasia (Figure 2.3.).

Ultrasound signs include hepatomegaly and irregularity of the hepatic surface, ascites, and evidence of portal hypertension, including varices and splenomegaly. Angiography may be used to study collateral formation in cirrhosis.

CT findings include heterogeneity of the hepatic parenchyma, nodularity of the liver surface, ascites, and signs of portal hypertension. In sclerosing cholangitis, which is characterized by progressive fibrotic inflammation of the biliary tree leading to biliary obstruction and cirrhosis, percutaneous cholangiography demonstrates multiple focal strictures of the bile ducts.

Hepatosplenic scintigraphy

Computed tomography and ultrasound offer better anatomic display of the liver and the spleen architecture than does radionuclide liver-spleen imaging, which is seldom performed. However, there remain some indications for technetium colloid liver-spleen scintigram, such as the confirmation or evaluation of suspected hepatocellular diseases, hepatomegaly or splenomegaly, and the confirmation of specific space-occupying lesions such as hepatic focal nodular hyperplasia. The most commonly used agent is technetium-99m sulfur colloid. The uptake and distribution of ^{99m}Tc-colloid in the liver reflect both the distribution of functioning reticuloendothelial cells. In normal patients, most particles are rapidly accumulated by the phagocytes of the reticuloendothelial system of both the liver (Kupffer cells) and the spleen. Under usual circumstances, 85% of the dose accumulates ^{99m}Tc-colloid in liver, 10% in the spleen and the remainder in bone marrow.

Normal hepatosplenic scintigram

In the normal liver, there is a homogeneous distribution of ^{99m}Tc sulfur colloid throughout the organ (Figure 5.9). The liver usually consists of a dominant right and a smaller left lobe, which may occasionally be absent.

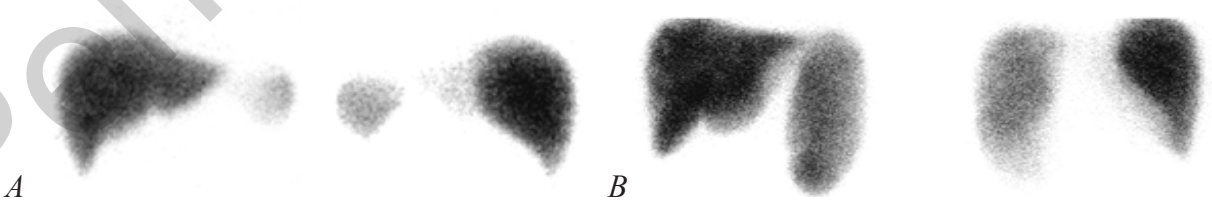

A *B*

Figure 2.3 — (A) Normal planar ^{99m}Tc-sulfur colloid liver-spleen scintigrams (anterior and posterior projections). Activity throughout the liver and spleen are uniform. Splenic activity is less than liver activity. The bone marrow is only faintly seen.
(B) A anterior and posterior projections technetium-99m colloid liver-spleen scintigrams. The basic findings are marked colloid shift, splenomegaly, and an enlarged liver

Evaluation of a liver-spleen scintigram should include (1) the size, shape, and position of the liver and spleen; (2) the homogeneity of activity within the organs; (3) the presence of any focal defects in activity; and (4) the relative distribution of colloid among the liver, spleen, and bone marrow (Figures 2.3).

Focal hepatic diseases

Ultrasonography is highly accurate in the demonstration of cystic lesions in any organ and its diagnostic accuracy in the diagnosis of simple liver cysts approaches 100%. Simple liver cysts appear as defined echo-free lesions with almost imperceptible walls and enhanced through transmission. Thin septations can be present. The presence of internal echoes, debris, thick septations, mural calcification or nodules suggests an alternative diagnosis or a complicated cyst (Figure 2.4). In focal diseases of the liver, US is often used first, because it is inexpensive, widely available, and moderately sensitive to localized lesions in the absence of preexisting diffuse diseases, such as cirrhosis. Ultrasound is often the first investigation perlornied for asuspected liver mass as it is non-invasive and relatively cheap. As with CT it gives good anatomical information.

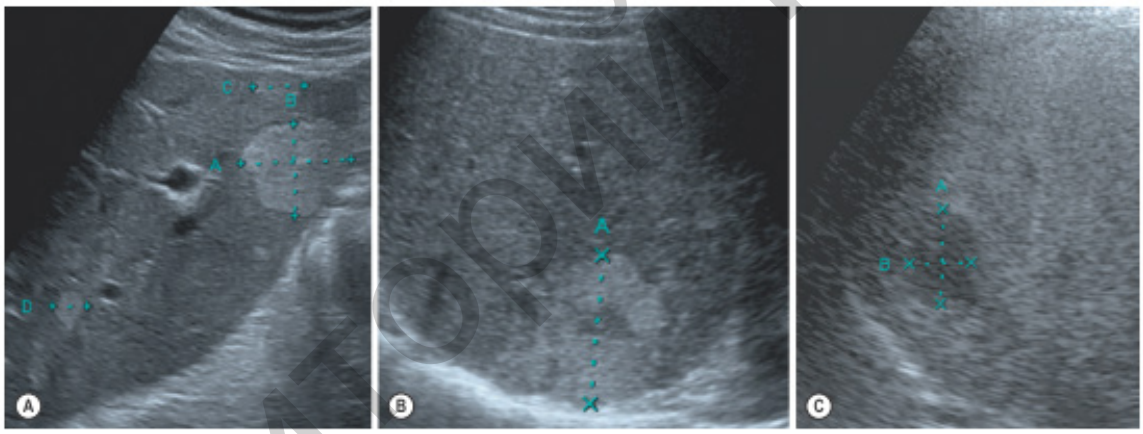

Figure 2.4 —Haemangioma US. (A) Typical appearances of well-defined lobulated peripheral homogeneous increased echo-reflectivity lesions. (B) Atypical haemangiomas with a fibrous central component and a reduced echo-reflectivity lesion (C) resulting from a steatotic liver

Computed tomography has for long been the modality of choice for evaluation of focal liver lesions. CT is a pivotal examination, often employed after US. It is used as a survey of the entire body, is easy to compare in serial studies, and is sensitive to disease. *Contrast-enhanced CT* scanners can be used to perform CT angiography, or CTA, which is a noninvasive means of producing images depicting vessels much like conventional angiography (Figures 2.5 D to F).

MRI imaging is the optimal means for both detection and characterization of focal liver lesions of all types. MRI can often definitively characterize hepatic lesions described as indeterminate on CT scan such as cysts, benign hepatic neoplasms such as hemangioma and focal nodular hyperplasia, hepatocellular carcinoma, and

metastatic disease. It is particularly useful in the evaluation of small 10 mm or less lesions compared with CT. Hepatic cysts appear as homogeneous, sharply marginated masses hypointense on T1 and markedly hyperintense on T2-images. This allows differentiation of these lesions from metastatic disease. No enhancement is seen after administration of gadolinium chelates. In cases of intracystic hemorrhage, a rare complication in simple hepa-tic cysts, the signal intensity is high, with a fluid level, on both T1 and T2-weighted images as mixed blood products are present. Newer MR pulse sequences, contrast agents, and fast scanning techniques arguably make MR imaging the optimal means for both detection and characterization of focal liver lesions of all types (Figures 2.5 B to C).

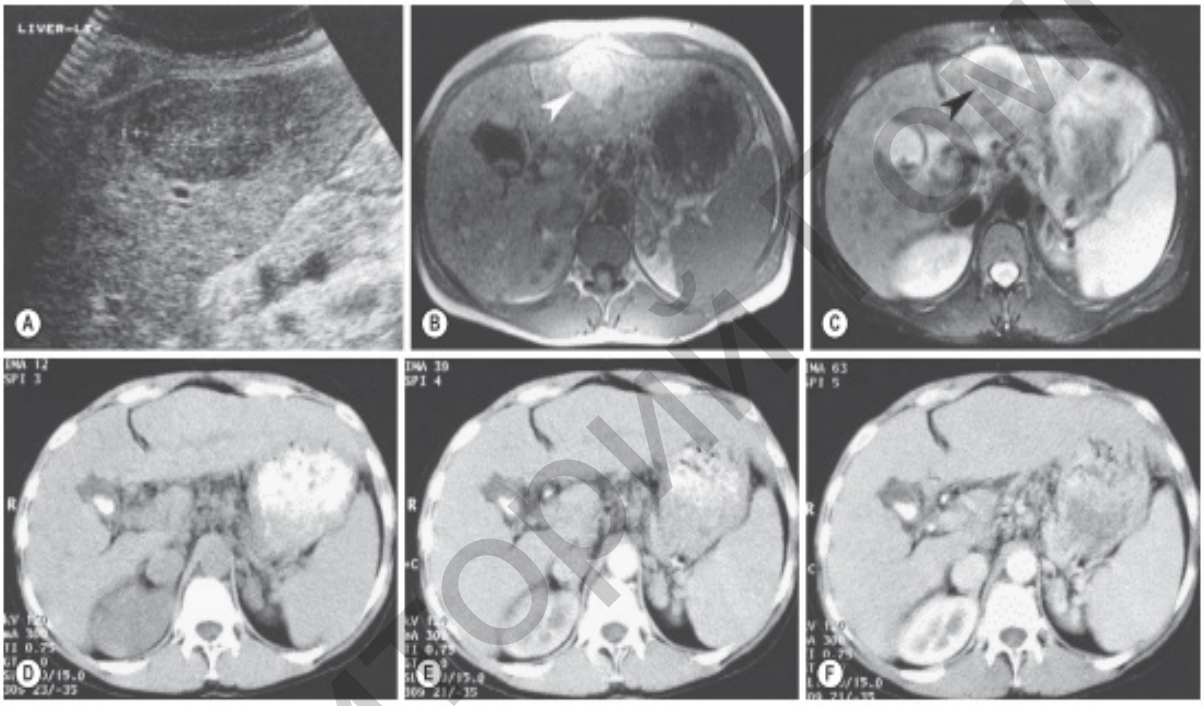

Figure 2.5 — Atypical regenerative nodules. Regeneration in cirrhosis often results in heterogeneity of the parenchyma. Occasionally nodules may become large, "atypical" or "dominant" as in this patient. US (A) demonstrates a reduced echo-reflectivity lesion in the left lobe, initially interpreted as probable tumour. However, on MR the relatively homogeneous lesion (arrowheads) is of increased signal on T1w (B) and decreased signal on T2w (C). These appearances are not typical of malignancy and are recognised as a feature of regenerative nodules (in this case, confirmed on biopsy). Similar smaller nodules are widespread in the liver. Axial CT images (D) unenhanced, (E) arterial phase and (F) portal phase of the same patient demonstrating no differences in enhancement characteristics of the nodule when compared to the rest of the liver parenchyma

On the basis of these features in most cases either CT or MR imaging alone is sufficient to establish an accurate diagnosis of a simple hepatic cyst. However, guided-percutaneous aspiration with cytological analysis may still be required in doubtful cases.

NM techniques can be used to analyze a focal lesion within the liver for possible cavernous hemangioma. NM and MR imaging are considered the optimal means for evaluating the liver for cavernous hemangioma, and both are highly accurate (approximately 95%) in evaluating the liver for cavernous hemangioma.

Angiography is primarily used to provide a vascular road map in planning surgery for focal liver lesions.

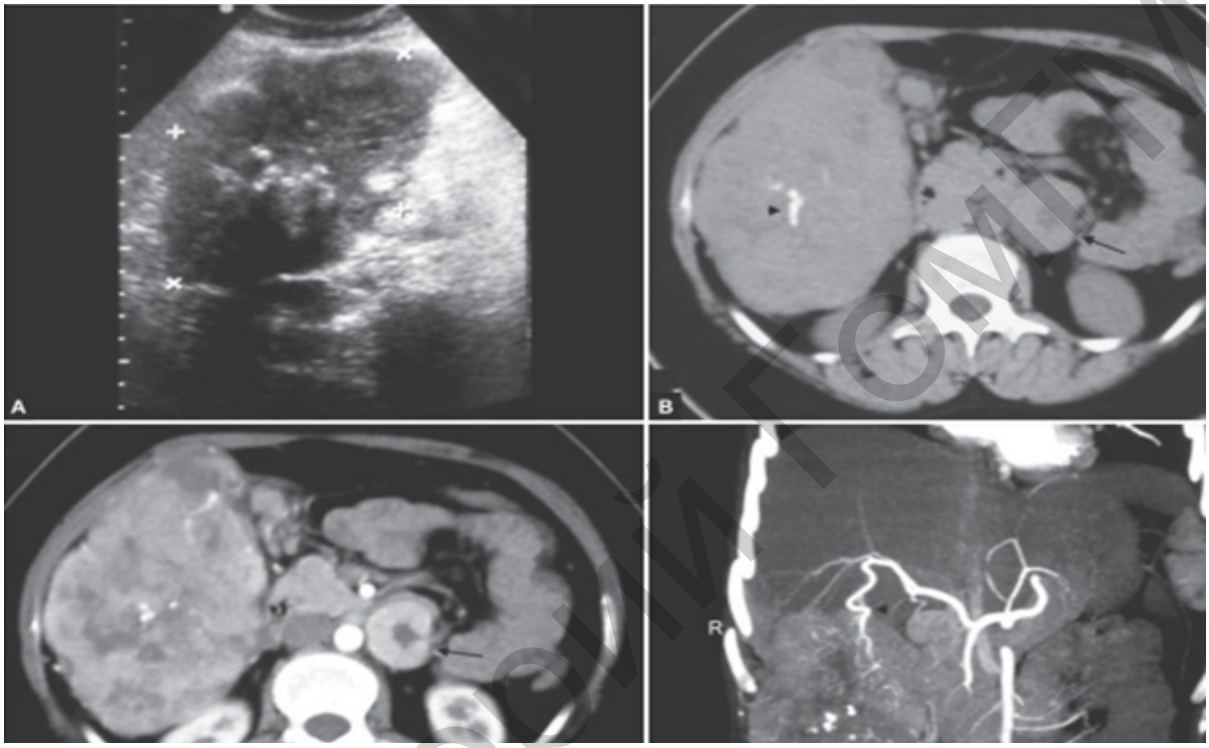

Figure 2.6 — Fibrolamellar carcinoma. (A) Sonogram shows a hypoechoic mass in segment 6 of liver showing central calcification. (B) CT scan shows hypodence mass in the liver with central calcification (arrowhead) and left para-aortic lymphadenopathy (arrow). (C) Contrast-enchanced arterial phase CT tomogram shows heterogeneous enhancement with central scar calcification. The para-aortic node is showing intense enhancement (arrow). (D) The CT scan shows a prominent feeder arising from the right hepatic artery (arrowhead)

CT evaluation of liver masses is usually done with a combination of scans obtained before and after intravenous contrast injection (Figure 2.6 B to D). A simple hepatic cyst appears on CT scan as a well-defined intrahepatic lesion having water attenuation (0–15 HU). It is round or oval in shape, has smooth thin walls and homogeneous appearance. There are no internal structures and no enhancement after contrast administration. These are usually solitary and peripheral but may be multiple which occur more centrally. When more than 10 cysts are present, a polycystic disease should be considered. Cysts that become complicated by hemorrhage or infection may have septations and internal debris as well as wall enhancement. Small cysts often demonstrate attenuation values greater than water density as a result of volume averaging with adjacent liver parenchyma. Multiphase spiral CT, including pre- and post-contrast phases or portal phase and delayed phase is 100% specific for hepatic cyst.

Abnormal liver scintigram

Any localized space-occupying process in the liver may present as a focal area of decreased activity (commonly referred to as a defect) on a technetium colloid scintigram, provided that it is of sufficient size to be detected. Radionuclide imaging simply confirms the presence or anatomic location of focal lesions (Figure 2.7). Metastases, cysts and abscesses all displace normal Kupffer cells and appear as "cold" defects. Some benign focal liver lesions contain Kupffer cells and the benign nature of the mass can be confirmed by showing colloid uptake within it.

Differential of focal hepatic lesions with decreased uptake on technetium-99m colloid scintigrams: metastasis, cyst, hepatoma, adenoma, hematoma, hemangioma, abscess.

Defects in the hepatic parenchyma are nonspecific. Solitary intrahepatic defects may be produced by various lesions, any of which may also be multiple. In any patient with several liver defects, however, metastatic disease must be a prime consideration, particularly when accompanied by hepatomegaly or a known primary lesion. In most instances, particularly in cases of equivocal liver scintigram findings, ultrasonography or CT should be performed.

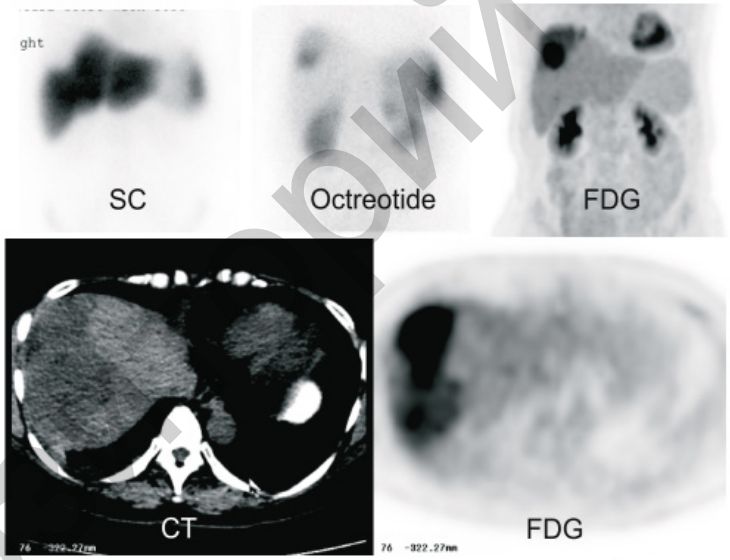

Figure 2.7 — Forty-eight-year-old female with history of pancreatic carcinoid tumor metastatic to liver. Anterior ^{99m}Tc-sulfur colloid scintigram demonstrates a defect in the superior aspect of the liver. Focal uptake is noted on ^{111}In-octreotide anterior planar image and ^{18}F-FDG anterior MIP image, consistent with metastatic carcinoid tumor. On the lower panels, axial PET-CT images illustrate FDG uptake correspond in to a low-density liver metastasis

In addition to primarily intrahepatic lesions, peripheral defects in the liver are frequently produced by adjacent extraparenchymal pathology, including subdiaphragmatic fluid accumulations or renal tumors, or by peripheral lesions of a primary hepatic origin, including subcapsular hematoma.

Increased radiocolloid concentration by the spleen and bone marrow compared with the liver (colloid shift) may be found in patients with diseases that cause derangement of hepatic function and/or portal hypertension. Hepatic cirrhosis is the most common abnormality presenting in this fashion.

Other entities that may cause apparent focal areas of increased hepatic activity are Budd-Chiari syndrome (hepatic vein obstruction), focal nodular hyperplasia, and cirrhosis (regenerating nodules).

PET/CT and image fusion

Computed tomography has a high diagnostic ability by visualizing lesion morphology and by providing the exact localization of sites, but it is unable to provide information about functional status (Figure 2.8 A to D). In contrast, positron emission tomography with fluorine-18 fluorodeoxyglucose (FDG) provides information about the metabolism and viability of the lesions but fails to provide precise topographic localization.

The development of SPECT-CT and PET-CT systems allows the superimposition of nuclear medicine and CT images, a technique known as functional–anatomical mapping (Figure 2.8 E). In a range of clinical scenarios, interpretation of images obtained using these hybrid devices has proved to be more diagnostically accurate than evaluation of the two sets of images separately. This combined imaging approach also allows functional data to be incorporated into the selection of radiation fields during radiotherapy planning.

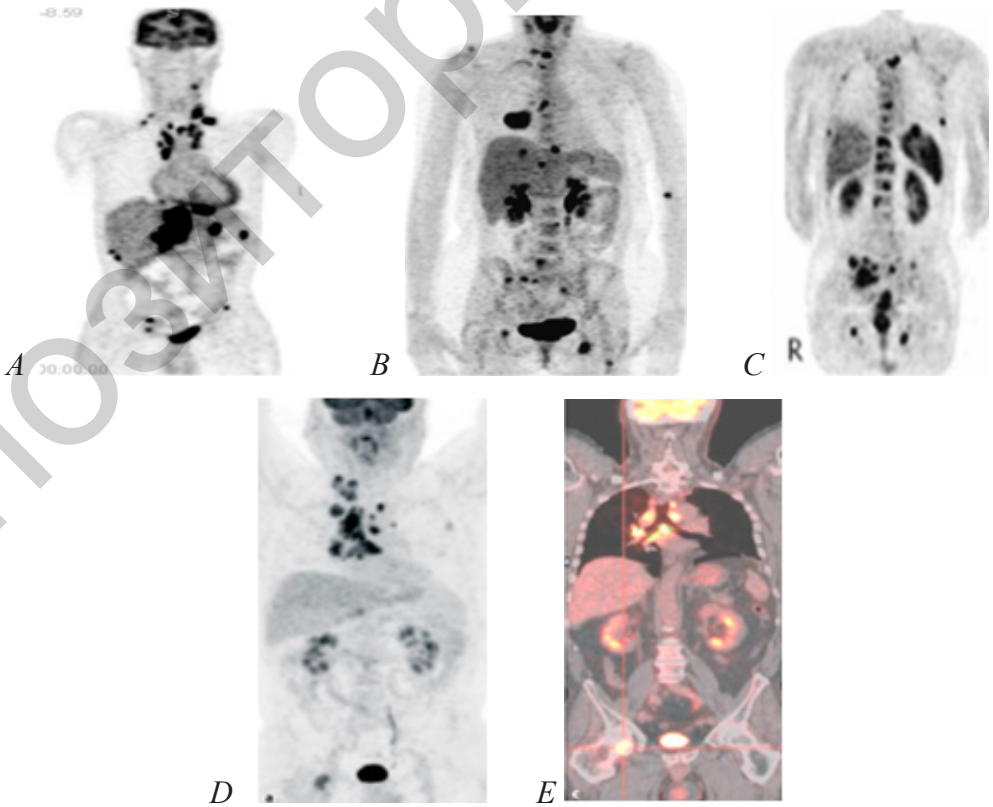

Figure 2.8 — (A, B, C, different patients) PET tomograms and (D) PET, (E) PET/CT (same patient) fusion tomograms demonstrated of multiplies metastasis (hot spots)

Technical and clinical advances in medicine have led to the understanding that one modality cannot be a substitute for the other; they are complementary to each other. A fused image of PET and CT overcomes the inherent limitations of both modalities, resulting in a precise topographic localization of valuable physiologic information. The development of the new technology of PET/CT that allows for combined functional and anatomic data acquisition sequentially has the potential to make fusion an everyday clinical tool.

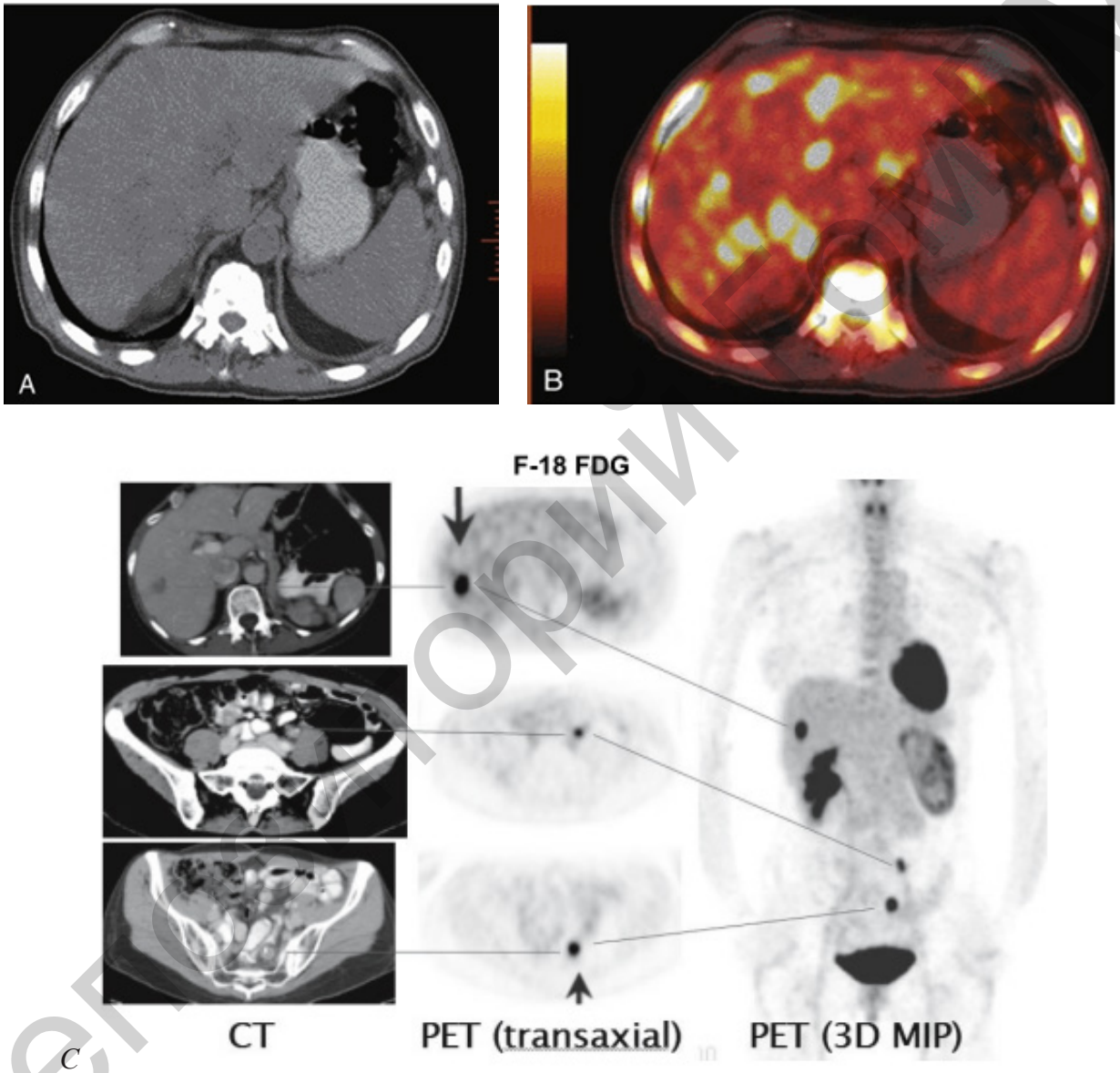

C

Figure 2.9 — (A) Axial noncontrast computed tomogram (CT) image vaguely shows low attenuation bilobar hepatic lesions. (B) These lesions display abnormal increased uptake on transaxial fusion positron emission tomography (PET/CT) image consistent with hepatic metastases. Also noted are hypermetabolic osseous metastases.
(C) CT and FDC tomograms shows metastases to the liver and abdominal lymph nodes (arrows)

Output from PET/CT imaging includes separate CT and PET tomograms, as well as the coregistered fused images that overlay the anatomic CT and metabolic data. The

combined PET/CT is more sensitive and specific for detecting otherwise occult malignancy, tumor staging, and detecting disease recurrence and/or metastasis (Figure 2.9).

Abdominal trauma

CT is reasonably accurate in the detection of trauma-related abnormalities of the liver, biliary system, and pancreas. CT is often used initially in the workup of abdominal pain in the emergency setting especially with history of trauma. CT is the only commonly accepted means for analyzing abdominal trauma, particularly of the liver.

US may be useful if CT is not available or to quickly identify intraperitoneal hemorrhage in patients who are in the emergency department and are going directly to the operating room.

Angiography may be useful to embolize persistently bleeding arteries in the liver or spleen when surgery is not possible.

Two commonly used nuclear imaging studies to investigate abnormalities of the GI tract are hepatobiliary imaging and GI bleeding localization. Currently, NM and MR imaging have no application in studying the liver, biliary tract, or pancreas in trauma.

Gallbladder and biliary tree

Ultrasound should be the first imaging choice for patients with suspected biliary disease. It is often used initially for patients with abnormal liver function tests to exclude biliary dilation and diffuse hepatocellular disease. It also is a good initial study to evaluate the visceral organs and has the added benefits of nonionizing radiation (Figure 2.10–2.11). CT and/or MR imaging are often used as supplements to help delineate or access abnormalities detected by US.

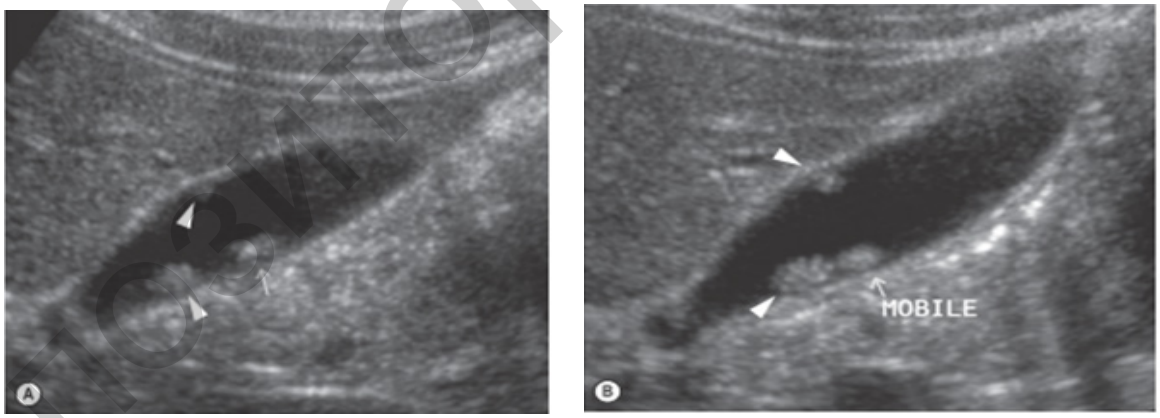

Figure 2.10 — Mobility of gallstones. (A) Ultrasound demonstrates two dependent intraluminal non-shadowing structures. (B) The patient was rolled and reimaged and the lesion marked with an arrow proved to be mobile in keeping with a stone while the fixed dependent and antidependent lesions are polyps (arrowheads)

CT cholangiography has been used to describe two techniques using negative and positive contrast methods, respectively. The former makes use of bile as a negative contrast agent to display the biliary tree using various reformatting techniques. The reformats improve the CT evaluation of bile duct obstruction, though they do not improve the detection of duct stones.

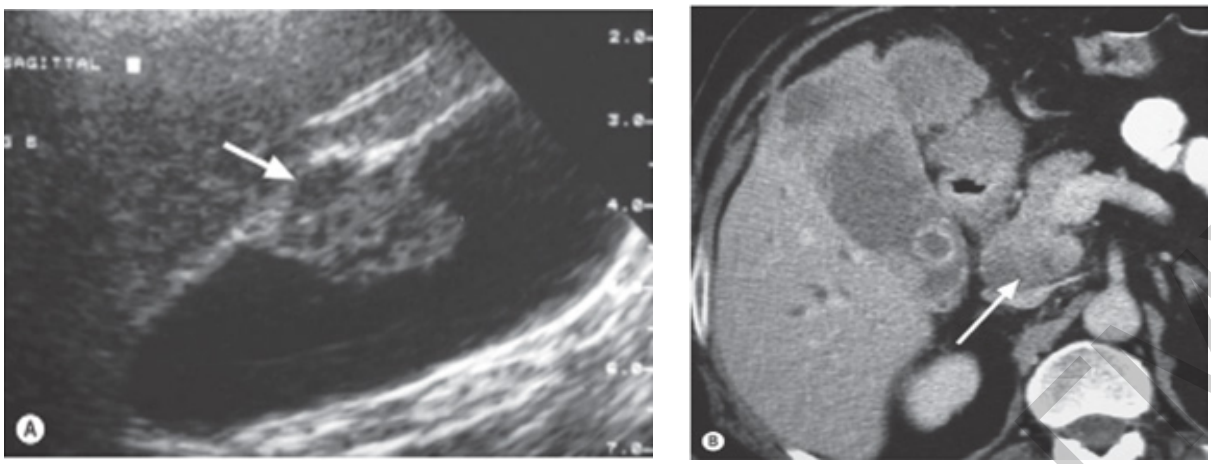

Figure 2.11 — Gallbladder carcinoma. (A) Ultrasound shows a polypoid lesion in the wall of the gallbladder with breach of continuity of the underlying wall (arrow). (B) Advanced carcinoma extending outside the fundus, with a nodal metastasis posterior to the pancreatic head (arrow). An associated stone can be seen in the gallbladder neck

Although MRI is primarily used for lesion detection and characterization, the biliary system information can also be assessed during the same examination. As mentioned earlier, MR excels with respect to evaluation of the biliary tree and in pregnant or pediatric patients where radiation is a concern.

Intraoperative cholangiography

Intraoperative cholangiography is performed either routinely or selectively during cholecystectomy to detect choledocholithiasis, confirm duct stone clearance and provide a roadmap in an attempt to reduce the risk of bile duct injury.

T-tube cholangiography

If the common bile duct has been explored at cholecystectomy a T-tube is usually left in place and cholangiography performed via this tube after about 7 d, prior to its removal. Cholangiography should confirm stone clearance and the free passage of contrast medium into the duodenum. Care must be taken to avoid the injection of air bubbles.

Endoscopic ultrasound

Biliary endoscopic ultrasound provides high-frequency grey-scale imaging (and in some systems colour Doppler imaging) for evaluation of the extrahepatic biliary tree and pancreas. It allows direct visualization of the duodenum and fine-needle aspiration cytology.

Hepatobiliary scintigraphy

The ^{99m}Tc-labeled hepatobiliary agents enable accurate and convenient imaging in acute and chronic biliary disease. After intravenous injection, these organic anions are taken up by hepatocytes in a manner similar to bilirubin.

Common indications are for acute (calculous or acalculous) cholecystitis, biliary patency, identification of biliary leaks, and, in neonates, differentiation of biliary atresia from neonatal hepatitis. Less common uses are for evaluation of biliary dyskinesia and sphincter of Oddi dysfunction. Limitation: none.

The radiopharmaceutical is taken up by the liver and excreted into the biliary tract. ^{99m}Tc IDA (iminodiacetic acid) is injected into a peripheral vein, followed by immediate imaging of the right upper quadrant.

Normal scintigram

In the normal patient, sufficient ^{99m}Tc-IDA (dimethyl-acetanilide-iminodi-acetic acid) is present in the liver in 5 minutes to allow good visualization of that organ. If for any reason additional views of the liver are sought, they should be obtained in the first 10 or 15 minutes of the examination. After this time, there is progressive clearance of the radiopharmaceutical from the liver, and it becomes less apparent. As the radiopharmaceutical is excreted into the biliary tree, the major hepatic ducts and common duct are visualized first. Next, the gallbladder is filled as labeled bile flows through the cystic duct. About two thirds of biliary flow bypasses the gallbladder and enters the duodenum, and about one third enters the gallbladder. In the presence of a patent common duct, activity flows promptly into the duodenal sweep and proximal small bowel (Figures 2.12).

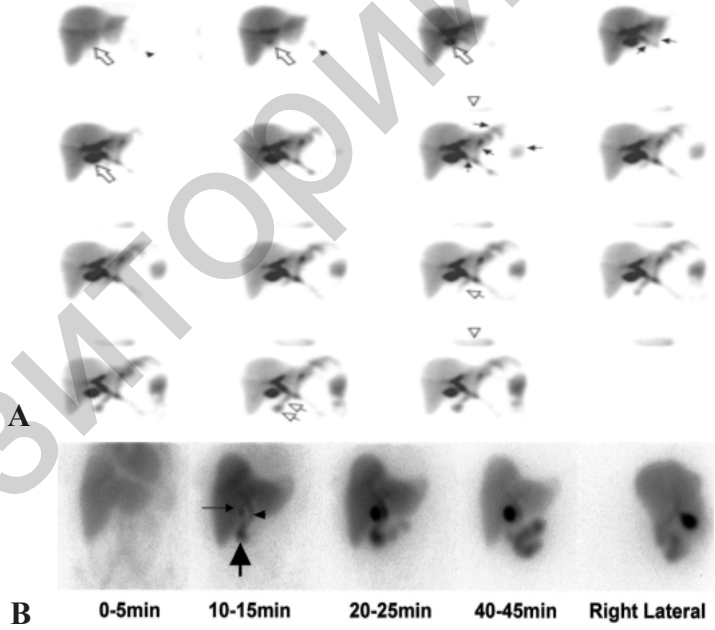

Figure 2.12 — (A) Normal hepatobiliary scans. Hepatic uptake is prompt. The common bile duct (short arrow), gall bladder (long arrow), and duodenum (thick arrow) are visualized within 15 min following intravenous administration of ^{99m}Tc-IDA. (B) Normal hepatobiliary scintigrams. The common bile duct (thick and short arrows), gall bladder (long arrow)

Because the tracer behaves similar to bilirubin, it should be taken up by hepatocytes and excreted into the bile ducts. The liver should be visualized first, followed by visualization of the bowel and gallbladder. The appearance of tracer in the bowel

and gallbladder by 60 minutes after administration is defined as normal. Nonvisualization of the gallbladder by 60 minutes is diagnostic of acute cholecystitis because this implies a functional obstruction of the cystic duct. Falsepositive results can be caused by chronic cholecystitis, hepatic insufficiency, and fasting for less than 4 hours or more than 24 hours as previously described.

Acute cholecystitis

Hepatobiliary imaging has proved to be of the greatest value in the diagnosis of acute cholecystitis. More than 95% of patients with acute cholecystitis have cystic duct obstruction. In this group of patients, radiopharmaceuticals excreted into the bile by the liver cannot enter an inflamed gallbladder through the obstructed cystic duct (Figure 2.13–2.14 for comparison).

In the proper clinical setting, the diagnosis of acute (calculous or acalculous) cholecystitis in a fasting patient may be reliably made in the presence of normal hepatic uptake and excretion of the radiopharmaceutical through the common duct, but without visualization of the gallbladder over a period of 4 hours after injection. A normal hepatobiliary scintigram with gallbladder visualization almost always excludes a diagnosis of acute cholecystitis.

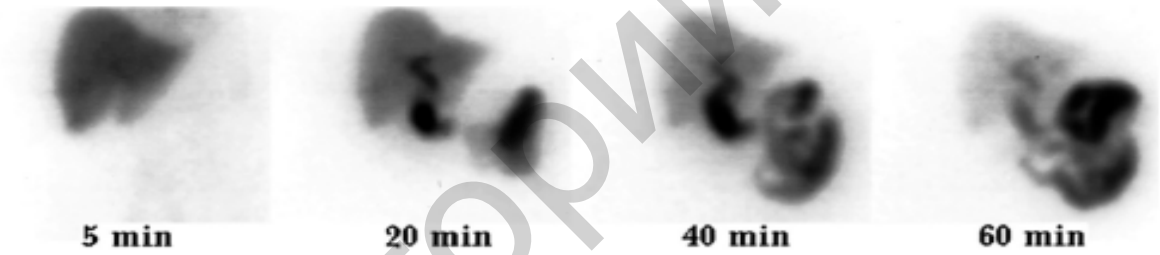

Figure 2.13 — The common bile duct and small bowel are promptly visualized in this study with ^{99m}Tc-IDA, but the gall bladder is not visualized up to 60 min (cystic duct obstruction)

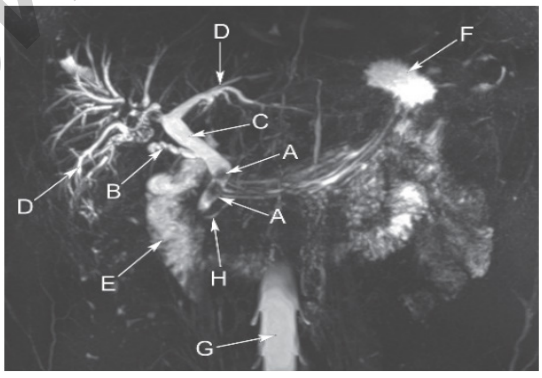

Figure 2.14 — MRT coronal plane from an magnetic resonance cholangiopancreatography. These images are highly fluid sensitive so that fluid appears bright/high signal. Obstructing calculi within the dilated common bile duct (CBD) are seen as low signal filling defects (A). The cystic duct (B) and CBD (C) are also dilated. Note cholecystectomy. The intrahepatic ducts are dilated (D), normal duodenum (E), stomach (F), cerebrospinal fluid in the spinal canal (G) and normal pancreatic duct (H)

Pancreas

Imaging modalities

CT, US, and MR provide high-quality images of the pancreatic parenchyma and are used as the primary imaging modalities for the pancreas (Figure 2.15). Multidetector CT optimizes contrast enhancement for detection of small tumors and provides the capability of CT angiography to detect vascular involvement by pancreatic tumor. Improved techniques and the use of gadolinium enhancement have increased the capability of MR to detect and characterize pancreatic lesions.

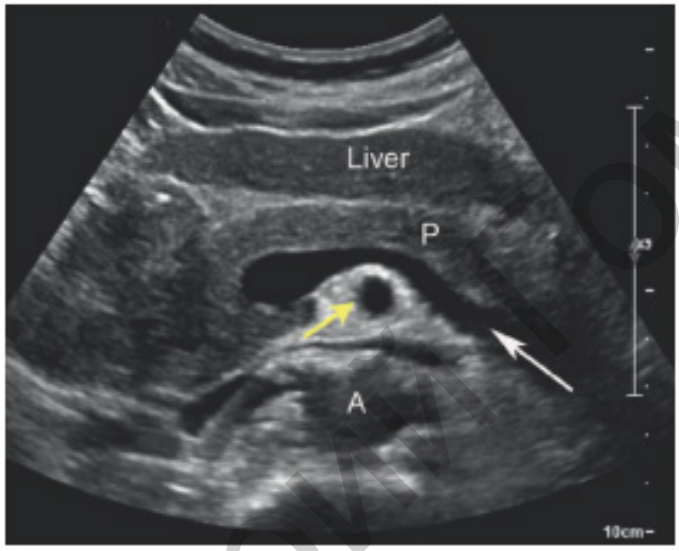

Figure 2.15 — Normal pancreatic body and landmarks. Transverse image of the pancreatic body and its dorsal landmark, the splenic vein (white arrow) and portosplenic confluence. Note the normal parenchymal echogenicity, similar to that of the liver echogenicity. The superior mesenteric artery (yellow arrow) is surrounded by a collar of fat. A, Aorta; P, pancreas

Endoscopic retrograde cholangiopancreatography provides excellent visualization of the lumen of the pancreatic duct, which is usually affected by any mass lesion of the pancreas.

MR cholangiopancreatography offers a noninvasive method of imaging the pancreatic duct as well as the biliary system.

Arteriography is now routinely performed using CT and MR angiographic techniques (CTA, MRA). US- and CT-guided biopsy and drainage procedures play a major role in the diagnosis and treatment of pancreatic diseases.

Pancreatic diseases

Abdominal CT is the technique of choice in the evaluation of patients who present with clinical features suggestive of pancreatitis. However, ultrasonography is widely used. Biliary stones, peripancreatic collections, and pseudocysts can be detected. Normal ultrasound findings can be seen in patients with mild acute pancreatitis. Although the pancreas can appear normal in acute pancreatitis, the most frequent

findings are enlargement of the gland and a diffuse decrease in normal echogenicity. Acute pancreatitis can be focal or diffuse, depending on the distribution. Focal pancreatitis generally occurs in the pancreatic head and manifests as a hypoechoic mass that is sometimes difficult to differentiate from a tumor, especially when focal acute pancreatitis occurs over chronic pancreatitis and the clinical findings are not clear or evident (Figure 2.16).

Figure 2.16 — Acute necrotizing pancreatitis. Axial intravenous contrast–enhanced CT image shows several areas of no enhancement in the pancreatic neck and tail consistent with areas of pancreatic necrosis. In the setting of necrosis, the correct term for early peripancreatic fluid collections is acute necrotic collections

On contrast-enhanced ultrasonography the inflamed pancreatic segment shows increased contrast enhancement. In severe acute pancreatitis, contrast-enhanced ultrasonography may improve the identification and delimitation of areas of parenchymal necrosis, which appear as nonvascular areas. Contrast-enhanced ultrasonography improves the ultrasonographic diagnosis of pseudocyst: the differential diagnosis between pseudocysts and cystic tumors of the pancreas is more reliable thanks to the evaluation of intralesional inclusion vascularization.

Abscesses consist of encapsulated collections of purulent material within or near the pancreas. On ultrasonography they are seen as an anechoic or heterogeneous mass containing bright echoes from pus, debris, or gas bubbles. A pancreatic abscess should be suspected on the clinical evidence and when changes in the echogenicity of the content of pseudocysts are documented at ultrasound examination. Vascular complications including pseudoaneurysms and venous thrombosis may be seen in both acute and chronic pancreatitis. Hemorrhage may occur as a consequence of vascular injury.

Chronic pancreatitis is an inflammatory disease characterized by the replacement of the glandular elements of the pancreas by fibrous tissue. The most significant ultrasound findings of chronic pancreatitis are pancreatic duct dilatation, intraductal calcifications, and pseudocysts.

The pancreas was one of the most elusive organs to image in the past. Although pancreatitis and pancreatic pseudocysts make themselves clinically apparent at a

relatively early stage of the disease, pancreatic carcinoma often does not. Once the patient with pancreatic carcinoma becomes symptomatic, he/she is usually beyond cure from either surgery or radiation therapy. Direct pancreatic imaging, therefore, has become one of the major advances in medical diagnosis in the last three decades. CT is the preferred modality for studying pancreatic pathology as well as for staging and surgical resectability of carcinoma (Figure 2.17).

Imaging

The imaging techniques for evaluation of solid masses in the pancreas include ultrasonography, contrast-enhanced multidetector computed tomography, magnetic resonance imaging, combined positron emission tomography with CT (PET/CT), endoscopic cholangiopancreatography, and endoscopic ultrasonography. Diagnostic imaging of pancreatic solid lesions is aimed at (1) confirming or excluding the presence of a pancreatic mass; (2) differentiating a benign from a malignant lesion and narrowing the differential diagnosis; (3) staging the neo-plastic process, in case it is malignant, and providing a road map for surgery, in case the tumor is considered resectable; and (4) assisting in follow-up of patients after medical and/or surgical treatment.

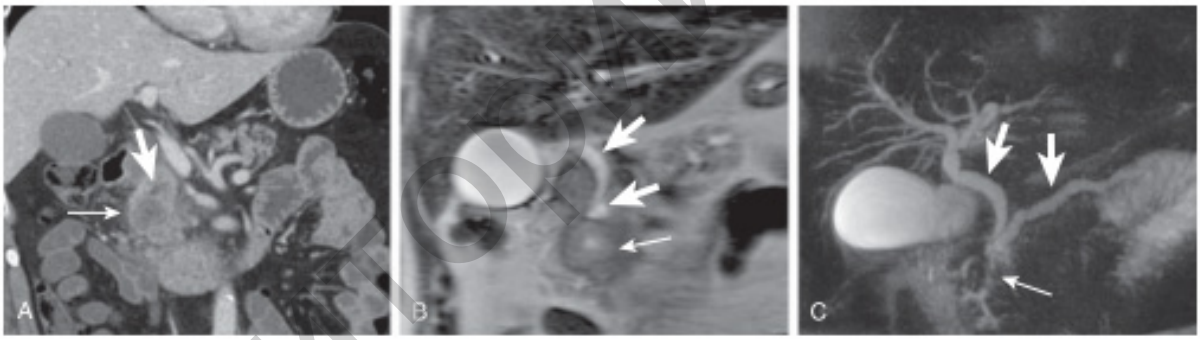

Figure 2.17 — Infiltrating pancreatic adenocarcinoma (thin arrow) causing obstruction and upstream dilatation of both the main pancreatic duct and the common bile duct (thick arrows) and (A) showing the "double duct" sign on coronal multidetector computed tomogram, (B) coronal steady-state fast spin echo T2-wighted magnetic resonance image, and (C) three-dimensional magnetic resonance cholangiopancreatogram

Differential diagnosis

Clinical data are useful to suspect pancreatic adenocarcinoma and contribute to rule out other conditions. Abdominal pain radiating to the back and partially reduced leaning forward, weightloss, jaundice, apalpable gallbladder, thrombophlebitis migrans, recent onset of diabetes, depression, history of smoking and of exposure to carcinogenic agents, and a family or a personal history of breast, colon, and pancreatic neoplasms and of hereditary oncologic syndromes may suggest the occurrence of adenocarcinoma of the pancreas.

Many anatomic variants may be confused with pancreatic adenocarcinoma. Their differential diagnosis is described in the corresponding sections. Collapsed duodenum or small bowel and duodenal diverticula can be misinterpreted as pancreatic adenocarcinoma, but filling with positive oral contrast agent, air/fluid levels, and enhancement characteristic like that of the intestinal wall suggest the correct diagnosis.

Chronic pancreatitis, usually of alcoholic or autoimmune cause, may manifest as a focal mass clinically and radiologically similar to adenocarcinoma. The differential diagnosis with mass-forming chronic pancreatitis is difficult, and different clinical and imaging findings must be carefully satisfied.

The most reliable differentiating finding is the "duct penetrating" sign, characterized by visualization of the main pancreatic duct traversing the pancreatic mass, without stenosis and ductal wall irregularities. If this criterion is satisfied, it is highly specific (96%) for mass-forming chronic pancreatitis. On the other hand, main pancreatic duct with an irregular wall, while traversing a mass, is not considered predictive of a benign cause.

FDG-PET/CT may be useful to differentiate pancreatic adenocarcinoma, which shows an avid FGD uptake, from mass-forming chronic pancreatitis, which demonstrates relatively low levels of FDG uptake. New radionuclides, such as s-receptor ligands and ^{18}F-FLT, are more tumor specific and potentially of better use in the differential diagnosis.

Other neoplasms, such as lymphoma, endocrine tumors, and acinar tumors, enter in the differential diagnosis with pancreatic adenocarcinomas. They all tend to spare the main pancreatic duct, which is not dilated or stenosed; moreover, their size tends to be larger than that of an adenocarcinoma. A lymphoma is usually sharply circumscribed, if focal, and associated with prominent extrapancreatic nodal disease. Endocrine tumors show intense contrast enhancement, and acinar cell tumors are large at presentation and enhance more than adenocarcinomas.

III. RADIOLOGY OF URINARY TRACT

Imaging modalities

Uroradiology remains a discipline that utilizes all imaging techniques to provide answers to specific clinical questions. The required information can be obtained most efficiently by using the correct test or tests performed in the correct order.

Currently ultrasound (US) and computed tomography (CT) are the most important imaging techniques in uroradiology. Renal US is a very important and frequently performed investigation, hence you should be familiar with the fundamentals of this modality. Renal tumors are mainly diagnosed by US, CT, and magnetic resonance imaging (MRI). Renal calculi can be demonstrated on US, renal and ureteric calculi on CT. The intravenous urogram (IVU) or pyelogram (IVP), once the mainstay of imaging of the genitourinary (GU) tract has lost much of its importance.

Computed tomography

Computed tomography has high sensitivity for detection of small renal cell carcinoma, urinary tract stones and transitional cell carcinoma. CT is rapidly replacing IVP in the assessment of renal colic and haematuria.

Magnetic resonance urography

The unique advantage of MR urography (MRU) is the absence of ionizing radiation. The exact clinical role of MRU has not yet been defined and remains under evaluation. There are two basic methods for modern MRU. The first technique uses unenhanced, heavily T2-weighted turbo spin-echo sequences to obtain static-water images of the urinary tract. It is used in poorly functioning hydronephrotic kidneys. The second technique is similar to conventional intravenous urography and is known as excretory MR urography. A gadolinium-containing contrast agent is given intravenously. Following renal excretion, the gadolinium-enhanced urine is visualized using fast T1-weighted gradient echo sequences. MR imaging now plays an important role in the staging of pelvic malignancy, and the appearance of bladder and ureters is critical.

Ultrasound

US is an exceedingly useful technique for examination of the urinary tract. The advantages of using a non-invasive test, which is painless and does not involve irradiation to either patient or operator, are obvious. When a renal mass is found at IVU, then an ultrasound examination will easily and rapidly differentiate a tumour from a cyst. Combining a limited IVU, with its ability to demonstrate the pelvicalyceal system in detail, and ultrasound, which will show abnormalities of the renal outline, is a very efficient method of imaging the urinary tract accurately.

One of the most frequently performed urological ultrasound examinations is the estimation of residual urine in the bladder of patients with outflow obstructive

symptoms. This can be combined with measurements of urinary flow rates, giving vital information to the urologist. A normal flow rate with no residue is reassuring to patient and clinician alike. Slow flow with a large bladder residue, on the other hand, may indicate a decompensated bladder due to outflow obstruction.

US provides information about renal length which is used to estimate renal mass and the presence or absence of hydronephrosis. The normal length in the adult ranges between 11 and 14 cm. Women tend to have smaller kidneys than men. The normal adult renal length approximates to the height of three lumbar vertebral bodies (nearly four in children). A difference in renal size of over 2 cm is usually significant.

Plain abdominal radiography

A plain radiograph of the abdomen should be obtained before any contrast examination because calcification may later be masked by the contrast medium. As small renal calculi may be hidden by bowel shadows, at least two views of the renal area may be required. If there is doubt about the presence of a calculus, an oblique view or tomography of the kidneys may be required.

The perirenal fat gives a lucent outline to the kidneys and allows an assessment to be made of their position. Any mass related to them may be suspected by careful scrutiny of the plain radiographs. The loss of outline of a psoas muscle may point to retroperitoneal pathology but it is a notoriously inaccurate sign. The full-length radiograph should include the bladder base and, in male patients, the prostatic urethra, particularly when there are lower tract symptoms, in order not to miss a urethral calculus. The outline of the bladder can be appreciated and for this reason the patient should empty the bladder before investigation: a large bladder residue may then be recognized.

Intravenous urography

Preliminary films are taken mainly to identify the kidneys and diagnose any area of renal tract calcification. This is particularly important in renal colic where a ureteric stone is being sought. The intravenous contrast is then injected. Films are taken to show the kidneys, the collecting systems, ureters and bladder. When overlying bowel gas obscures the kidneys, tomography and/or oblique projections are used to outline the collecting system. This is especially important in patients with haematuria where a small transitional cell carcinoma (TCC) of the collecting system may be the cause. A postmicturition film confirms drainage of both ureters and the emptying of the bladder. For conditions, such as urinary tract infection and renal cell carcinoma, other imaging techniques, especially ultrasound (US), CT and scintigraphy, have replaced IVP. The number of intravenous urography (IVUs) performed over the last 15 years has decreased as the use of other imaging techniques, particularly US and CT, has increased. The IVU is still a valuable procedure for examination of the urinary tract. It gives excellent anatomical images of the pelvicalyceal systems and, to some extent, an indication of renal function.

Retrograde pyelography

This procedure is usually performed in conjunction with formal cystoscopy. The ureteric orifice is identified and a catheter passed into the ureter. Contrast is then injected via this catheter to outline the collecting system. In my experience better images are attained by performing the contrast injection in the X-ray department after the patient has left the recovery ward, rather than obtaining mobile films in the-atre. Retrograde ureteropyelography is indicated mainly in those patients suspected of having a urothelial tumour of the upper urinary tract and in whom excretion urography is normal or equivocal.

Ascending urethrography

A small catheter is passed into the distal urethra and contrast-injected. Films are obtained in the oblique projection. The posterior urethra is usually not opacified via the ascending method. Should this area need to be examined, a micturating cysto-urethrogram will be required.

Micturating cysto-urethrography (MCU)

The bladder is filled with contrast via a urethral catheter. The catheter is withdrawn and films are taken during micturition. The particular indication will dictate the type and number of films performed. The micturating cystourethrography is the most accurate method of demonstrating vesicoureteric reflux, and is important in children with urinary tract infection and reflux nephropathy.

Nuclear medicine

Nuclear medicine imaging (alsocalled radionuclide, radioisotope scanning) is an excellent diagnostic tool because it shows not only the anatomy (structure) of an organ or body part, but the function of the organ as well. This additional "functional information" allows nuclear medicine to diagnose certain diseases and various medical conditions much sooner than other medical imaging examinations which provide mainly anatomic (structural) information about an organ or body part. Nuclear medicine can be valuable in the early diagnosis, treatment and prevention of numerous medical conditions and continues to grow as a powerful medical tool.

Plain films, US, CT, and MRI produce anatomic images with very high spatial resolution. A viewer can see anatomy very well, but function generally is not assessed. Nuclear medicine studies sacrifice spatial resolution, but in return offer information about organ function. Nuclear medicine studies, in general, are very sensitive, but relatively nonspecific in the detection of pathology.

Sequence of radiographic imaging

Contrast films are usually taken at 1, 5 and 15 minutes after injection. In order to obtain a good demonstration of the renal outlines, a radiograph coned to the renal area should be taken immediately after the injection of contrast medium (the 1-min film). This will coincide with the highest concentration of contrast medium in the nephrons and from this nephrogram the size and outline of the kidneys will be seen.

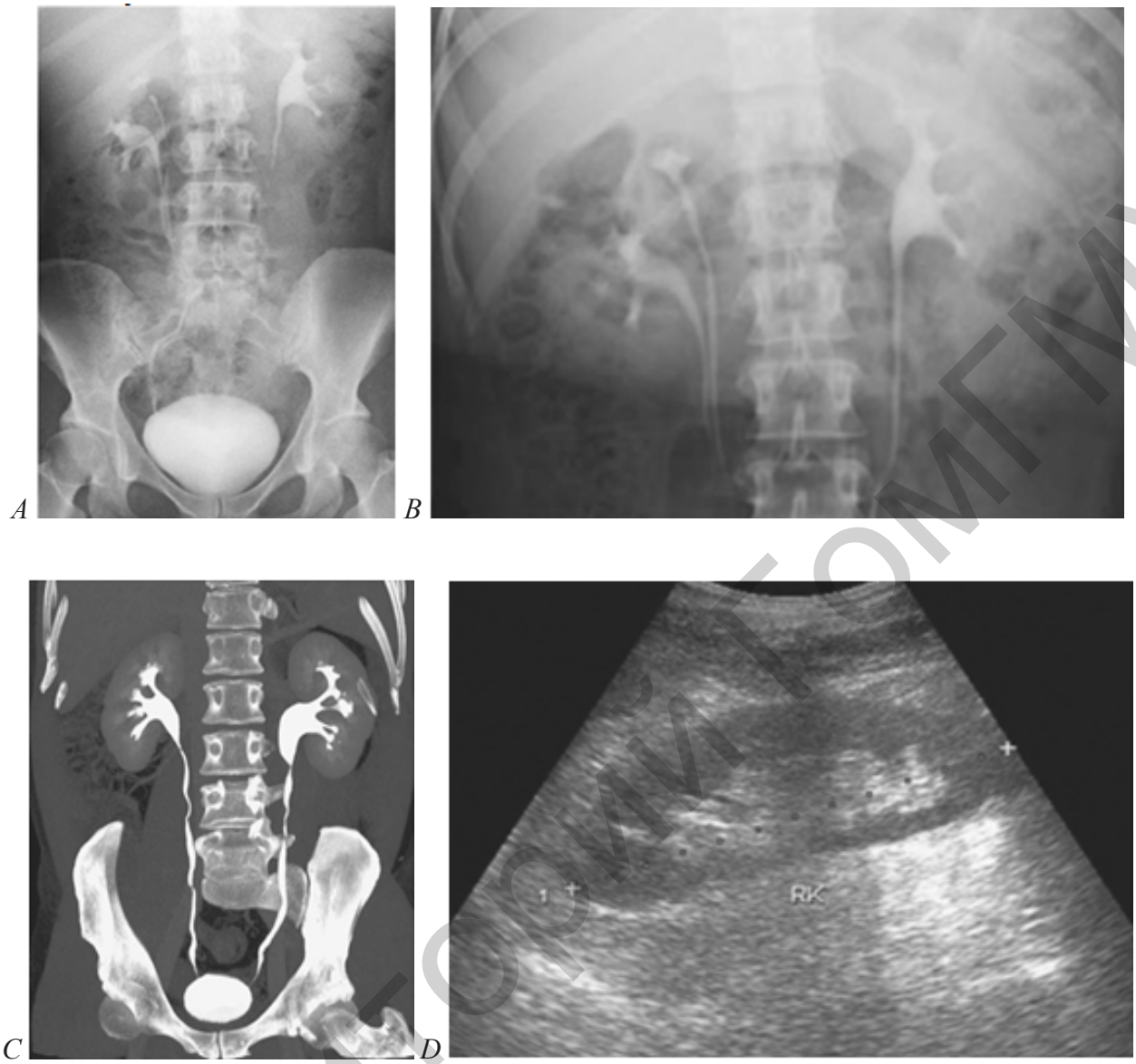

Figure 3.1 — Intravenous normal urogram (A to C). (A) Duplex right ureters on a 15-minute full length radiograph. (B) Designated renal area radiograph for improved visualization of duplex (right) and normal (left) collecting system. (C) CT urography. Coronal maximum intensity projection (MIP) acquired 10–12 minutes following intravenous contrast medium masking the location of a stone in the upper left ureter but demonstrating there is no obstruction and normal in all other respects. (D) Ultrasound of the kidneys. Normal right renal sonogram

An image at 5 min coned to the renal area will show early filling of the pelvicalyceal system and the relationship of the calyces to the renal outline. Again, tomography or oblique images may be useful. Some advocate abandoning the immediate 1-min nephrogram image, as the 5-min tomogram will give an equally good demonstration of the renal outlines, allowing the number of films in the IVU series to be reduced. This decreases the total radiation dose to the patient, the importance of which is now well understood. If there is any doubt about the renal outlines, ultrasound is far better than urography (Figures 3.1–3.3, 3.5).

Radiology diseases of urinary tract

Hydronephrosis and hydroureter

This situation is analogous to an obstructing ureteric stone (pebble) or a tumor encasing the ureter (pinching). On the IVP present signs of obstruction. Radiographic features:

1. Delayed nephrogram and delayed contrast excretion.
2. Hyperdense nephrogram: the affected kidney becomes too white.
3. Dilation of the collecting system and dilatation of the ureter before the obstruction.

Initial films may not show the site of obstruction since it takes longer to outline a blocked system with contrast. Therefore, to locate the site of obstruction, one must ask for delayed films. When there is no delayed nephrogram and no delayed contrast excretion, there is no obstruction.

Renal ectopia

Abnormally positioned kidney that can be found in various locations. The ectopic kidney usually functions, though the nephrogram and pelvocalyceal system may be obscured by overlying bone and fecal contents. Includes pelvic kidney, intrathoracic kidney, and crossed ectopia (the ectopic kidney lies on the same side as the normal kidney and is usually fused with it). Whenever only one kidney is seen on excretory urography, a full view of the abdomen is essential to search for an ectopic kidney (Figure 3.2).

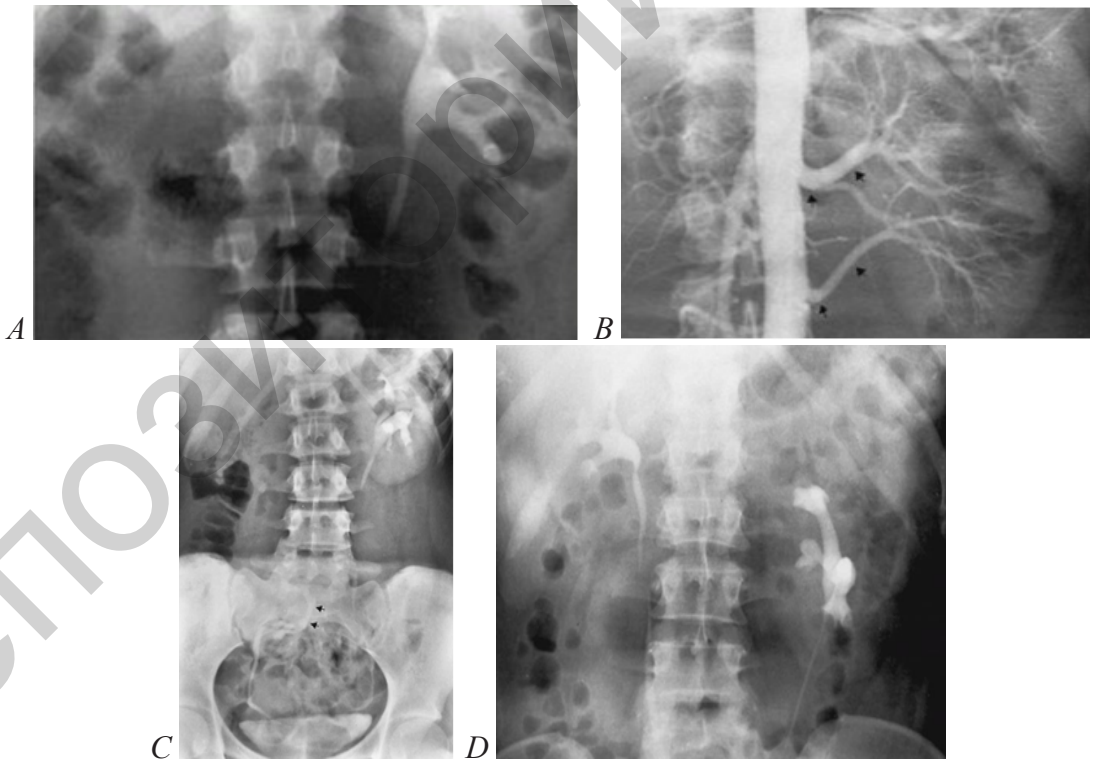

Figure 3.2 — Solitary kidney. (A) Excretory urogram demonstrates a normal left kidney with no evidence of right renal tissue. (B) Aortogram shows two renal arteries to the left kidney (arrows) and no evidence of a right renal artery, thus confirming the diagnosis of unilateral renal agenesis. (C) Pelvic kidney. The arrows point to the collecting system. (D) Malrotation of the left kidney. Note the apparent lateral displacement of the upper ureter and the elongation of the pelvis

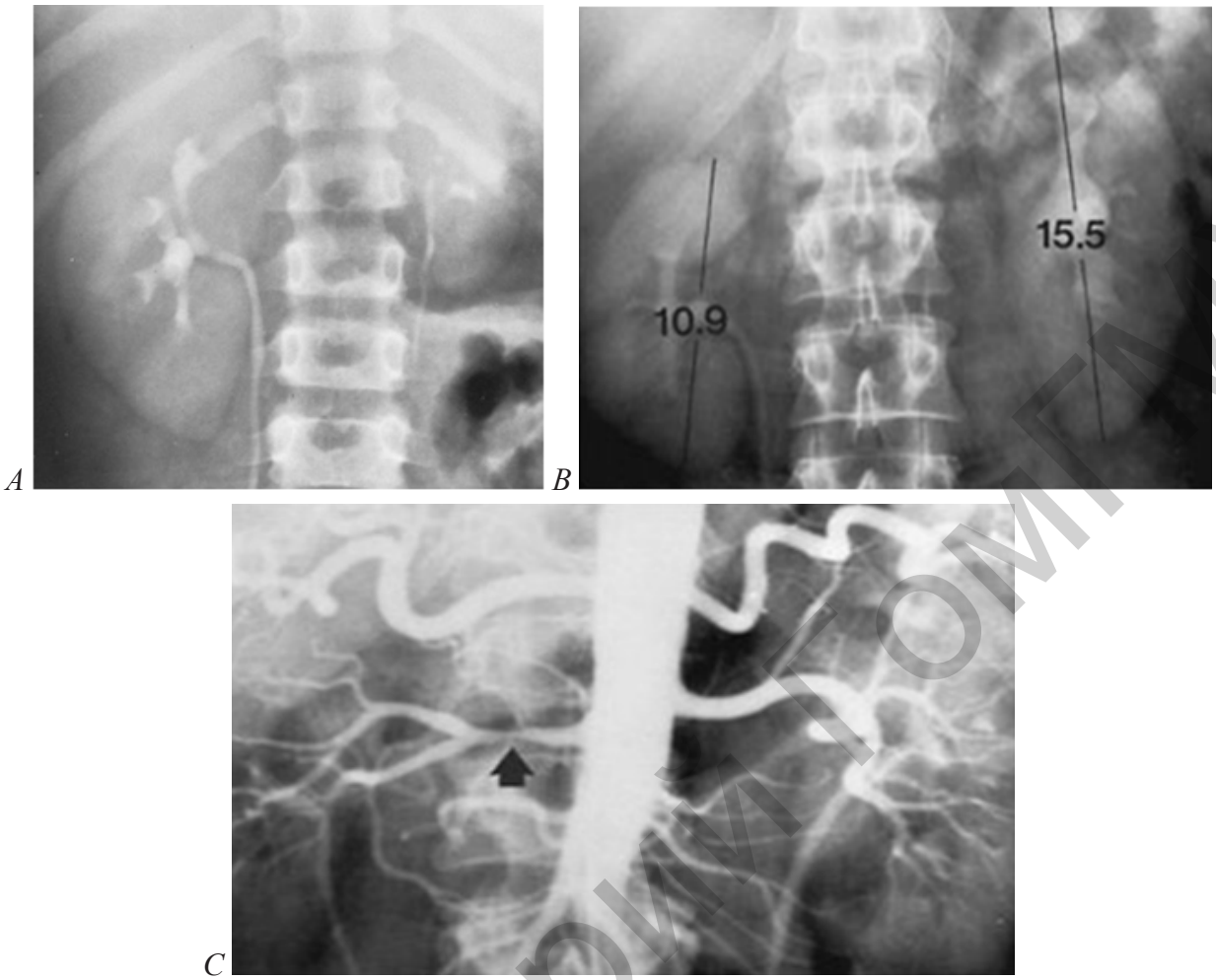

Figure 3.3 — (A) Congenital hypoplasia.
The small left kidney, a miniature replica of a normal kidney, has good function and a normal relation between the amount of parenchyma and the size of the collecting system.
Note the compensatory hypertrophy of the right kidney.
Renal ischemia associated with hypertension.
(B) Diminished size (cm) of the right kidney due (C) to renal artery stenosis (arrow)

Nephroptosis

Excessive caudal movement of a mobile kidney (especially the right) when the patient goes from the supine to the erect position. There may be associated changes in the ureter (angulation at the ureteropelvic junction, loops, kinks, and tortuosity). If a ptotic kidney becomes fixed in its dropped state, permanent ureteral kinking causes impaired drainage, increased hydronephrosis, and a greater chance of infection.

Calculus (kidney stones)

Round or oval, frequently mobile filling defect. Often multiple and bilateral. A large calculus may form a cast of the pelvocalyceal system (staghorn calculus). If the obstruction is acute, the increased intrapelvic pressure may permit little or no glomerular filtration and produce the radiographic appearance of a delayed but prolonged nephrogram and the lack of calyceal filling on the affected side. More than 80% of renal calculi are radiopaque and detectable on plain abdominal radiographs.

Completely lucent calculi are composed of uric acid or urates, xanthine, or matrix concentrations. Cystine calculi are mildly opaque (Figure 3.4).

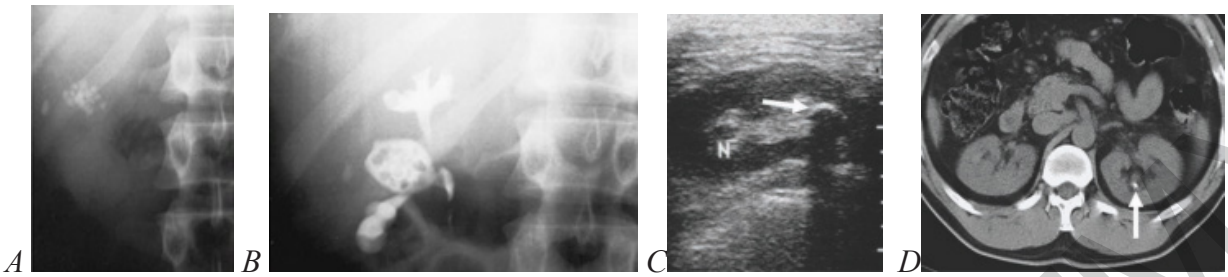

Figure 3.4 — Cystine stones. (A) Plain film shows multiple radiopaque calculi. (B) Excretory urogram demonstrates the stones as lucent filling defects in the opacified renal pelvis. (C) On US renal calculi are strongly echogenic structures (arrow) with posterior shadowing. (D) On CT they are very dense and are demonstrated in the renal pelvis (arrow)

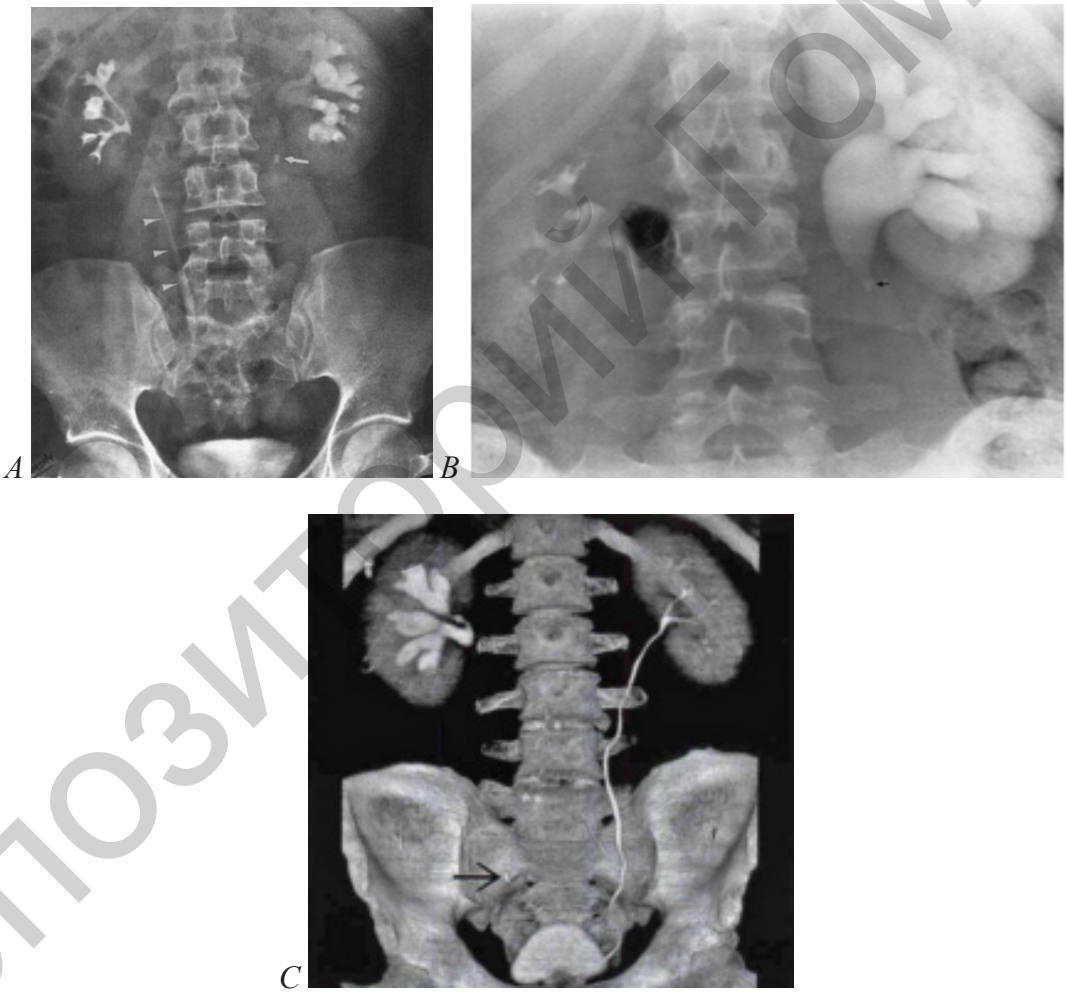

Figure 3.5 — (A) An anteroposterior film from an intravenous urogram was taken at 10 minutes in a patient with a proximal left ureteral calculus (arrow) and associated left collecting system dilatation. The right collecting system is normal, and the right ureter (arrowheads) and bladder are visualized. (B) Obstructing ureteral calculus. Excretory urogram demonstrates a prolonged nephrogram and marked dilatation of the collecting system and pelvis proximal to the obstructing stone (arrow). (C) Coronal CECT shows prompt concentration & excretion of urine from the left kidney. While the right kidney has a delayed nephrogram and dilated calices, due to an obstructing ureteral stone (black arrow)

Acute pyelonephritis

Unilateral global enlargement of the kidney with decreased and delayed contrast material excretion and mild dilatation of the collecting system. There is often focal polar swelling and calyceal compression (Figures 3.6–3.7).

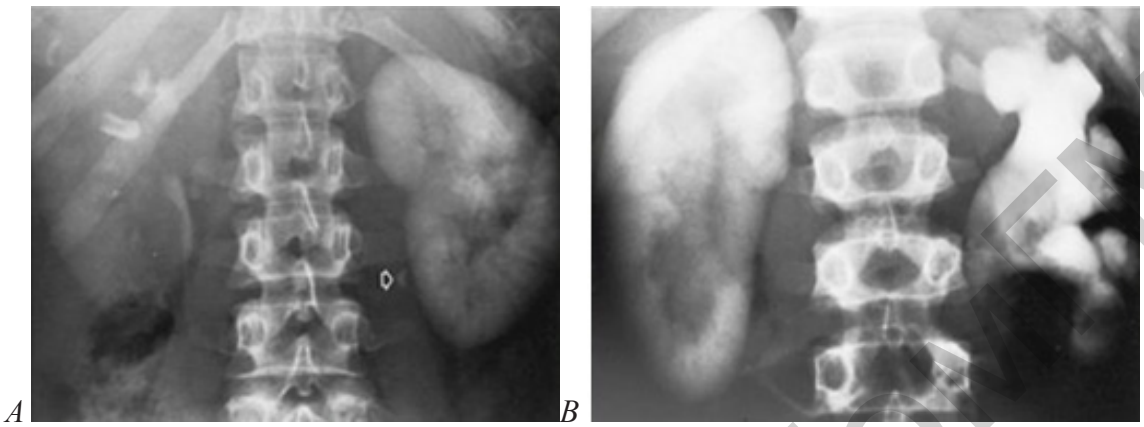

Figure 3.6 — Acute urinary tract obstruction. (A) Excretory urogram demonstrates a prolonged nephrogram on the left with fine cortical striations (alternating radiolucent and radiopaque lines) and no calyceal filling. An arrow points to the obstructing stone in the proximal left ureter. (B) In another patient, there is a prolonged and intensified obstructive nephrogram of the right kidney. On the left, there is marked dilatation of the pelvocalyceal system but no persistent nephrogram, reflecting an intermittent chronic obstruction on this side

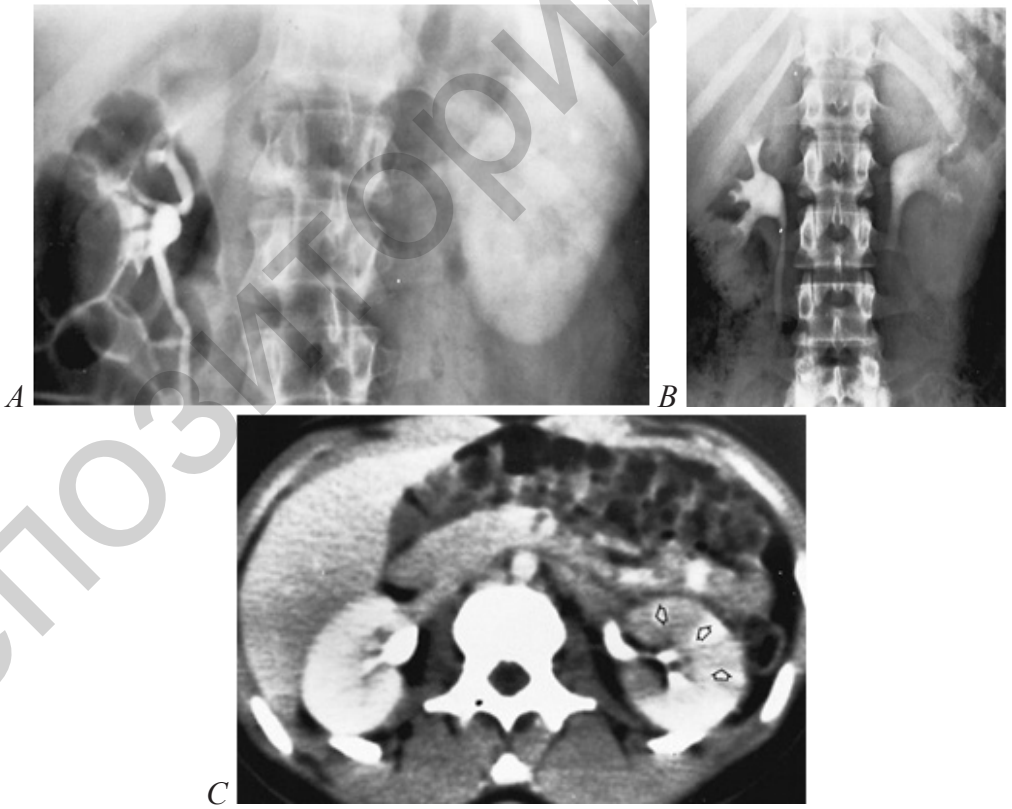

Figure 3.7 — (A) Acute bacterial nephritis. Persistent dense nephrogram on the left with minimal opacification of the collecting system. (B) Acute pyelonephritis. Generalized enlargement of the left kidney with decreased density of contrast material in the collecting system. (C) Acute pyelonephritis. Postcontrast scan shows characteristic low-density striations (arrows) in the left kidney

Compensatory hypertrophy

Unilateral smooth, large kidney that is normal in all respects except for its size and the thickness of the renal parenchyma. The pelvocalyceal system and ureter may appear distended (high urinary flow rate). Response to congenital absence, surgical removal, or disease of the contralateral kidney.

Chronic pyelonephritis

Clubbed, dilated calyces are caused by retraction of papillae and most frequently involve the poles. Depressed cortical scars typically develop over involved calyces (Figure 3.8 A).

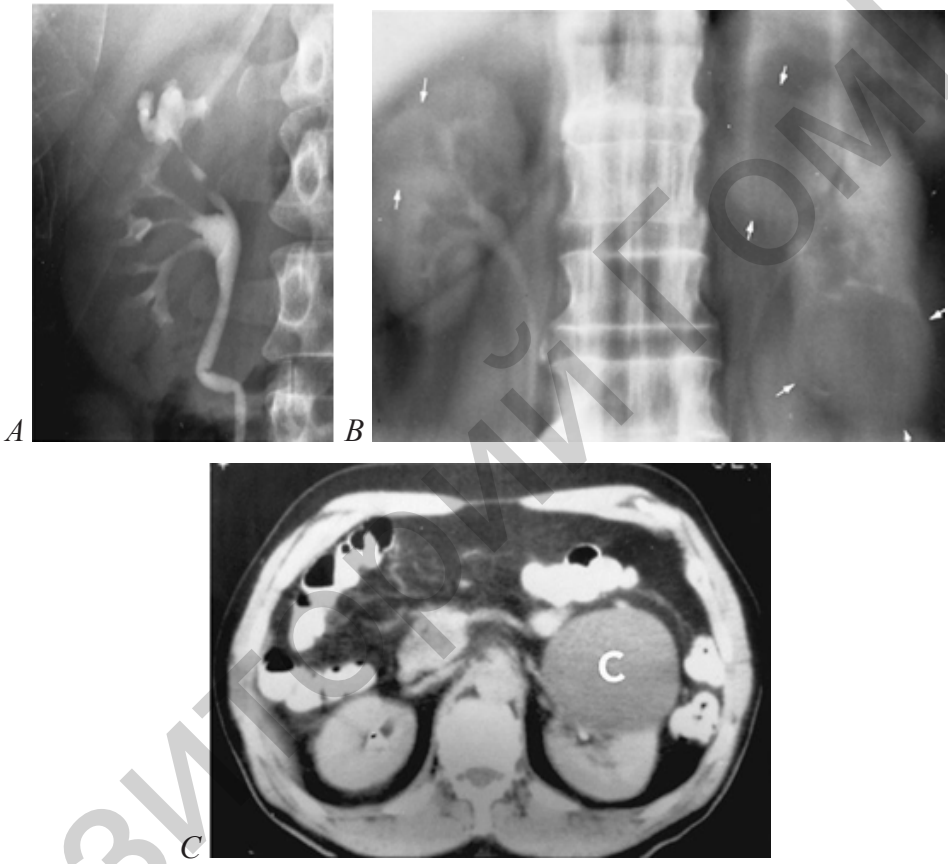

Figure 3.8 — (A) Chronic atrophic pyelonephritis. Focal reduction in parenchymal thickness involving the upper pole of the right kidney.
(B) Renal cysts. Nephrotomogram demonstrates bilateral renal cysts (arrows).
(C) Benign renal cyst. Nonenhancing left renal mass (c) with a sharply marginated border and a thin wall

Renal cyst

This common benign entity is found in approximately 30% of all elderly patients. It often occurs bilaterally and can be associated with hepatic cysts. Simple renal cysts have a thin, smooth margin, have no internal echo on US, and are of water density on CT (less than 20 Hounsfield Units). They are predominantly found in the renal cortex, but can also protrude into the renal hilum, in which case they have to be distinguished from a dilated renal pelvis (Figure 3.8 B to C, 3.9–3.10).

Parapelvic renal cysts located in the renal sinus fat can also create the impression of hydronephrosis but are easily discernible from the actual renal pelvis on the excretory phase of a contrast-enhanced CT scan.

Simple renal cyst

Focal contour expansion of the kidney outline on the nephrogram. The cortical margin appears as a very thin, smooth radiopaque rim about the bulging lucent cyst (beak sign). A thickened wall suggests bleeding into a cyst, cyst infection, or a malignant lesion. When a simple cyst is completely embedded in the kidney parenchyma, the thin rim and beak are absent, and the renal size and contour are normal. A renal cyst causes focal displacement of adjacent portions of the pelvocalyceal system, with the collecting structures remaining smooth and attenuated rather than shaggy and obliterated as with a malignant neoplasm.

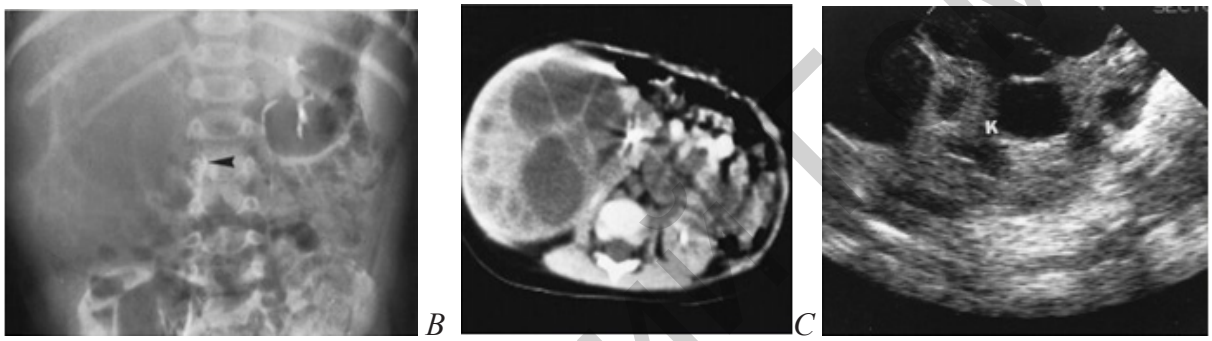

Figure 3.9 —Segmental multicystic dysplastic kidney involving only the medial portion of the right kidney.
(A) Excretory urogram shows a large multiloculated renal mass displacing the opacified collecting system (arrowhead) over the spine.
(B) Enhanced CT scan confirms the intrarenal multiloculated mass.
(C) Multicystic dysplastic kidney. Sagittal sonogram demonstrates the cystic kidney. Note the absence of communication between the cystic structures

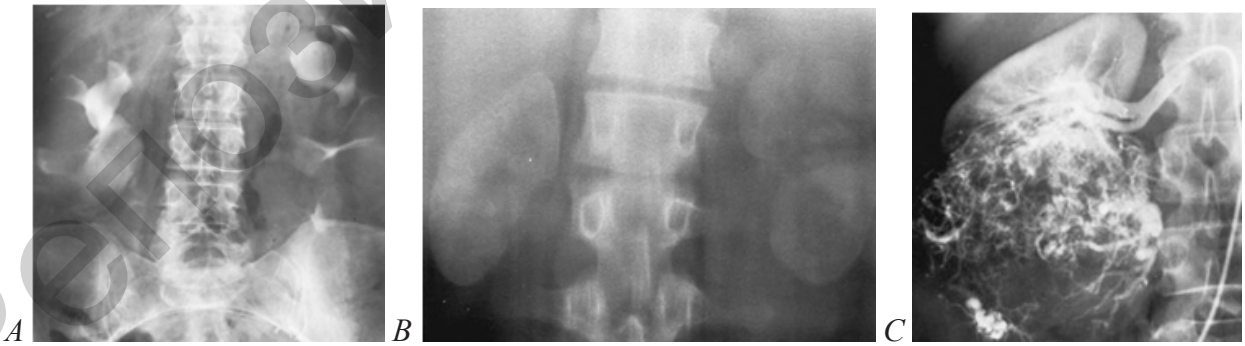

Figure 3.10 — (A) Adult polycystic kidney disease. Excretory urogram shows marked multifocal enlargement of both kidneys, focal displacement of the collecting structures, and normal opacification.
(B) Chronic glomerulonephritis. Plain film tomogram shows bilateral small, smooth kidneys with diffuse fine calcification in the renal parenchyma.
(C) Renal hamartoma. Arteriography shows the mass to be hypervascular

Acute glomerulonephrities

Bilateral large kidneys (may be of a normal size) with global parenchymal thickening and smooth contours. The nephrogram is homogeneously faint or normal. The pelvocalyceal system is normal, though opacification is often faint (ultrasound is the most efficacious test to show that the calyces are not dilated and thus not obstructed). If the disease progresses to a chronic stage (especially in the poststreptococcal type), the kidneys become bilaterally small with smooth contours.

Renal hamartoma

A combined excretory urogram and inferior vena cavagram shows a large mass in the lower pole of the right kidney with displacement but no invasion of the pelvocalyceal system and inferior vena cava. Arteriography shows the mass to be hypervascular (the radiographic appearance is indistinguishable from that of renal cell carcinoma) (Figure 3.11).

Renal cell carcinoma

Eighty percent of all solid renal tumors are renal cell carcinomas.

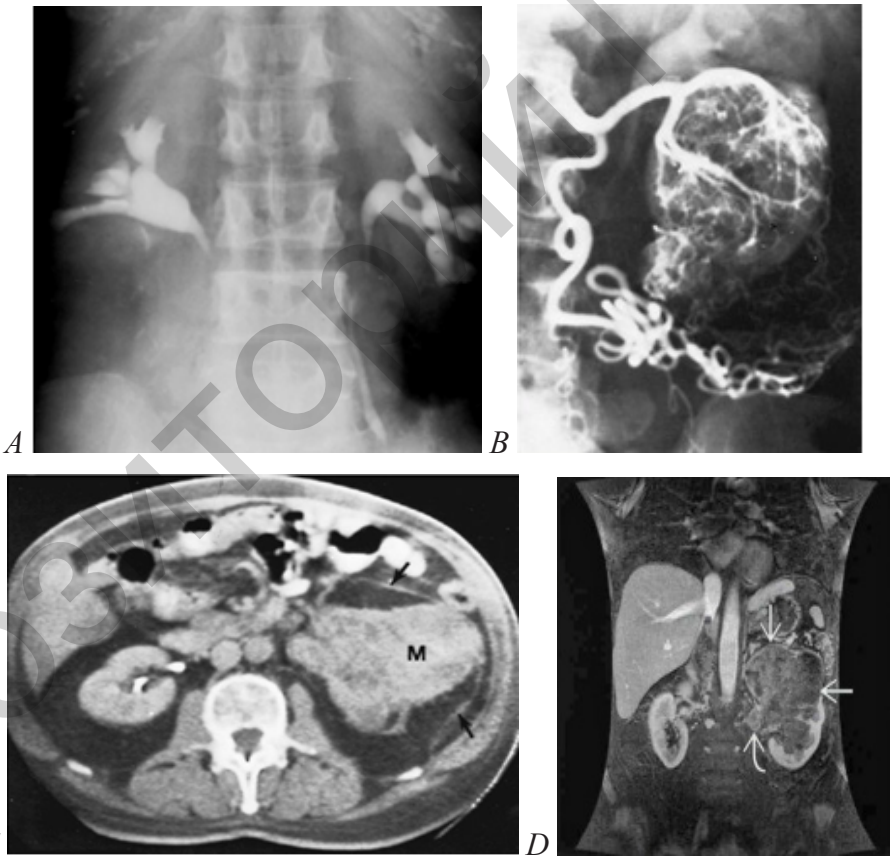

Figure 3.11 — (A) Renal cell carcinoma (urogram). Upward displacement of the right kidney and distortion of the collecting system by the large lower pole mass.
(B) In another patient, left renal arteriogram demonstrates a large hypervascular mass with striking enlargement of capsular vessels (arteriogram).
(C) Renal cell carcinoma. Large mass (M) of the left kidney with thickening of Gerota's fascia (arrows on CT-tomogram).
(D) Coronal T1 MR scan shows a large infiltrative and exophytic mass that invades the renal sinus (arrows), filling both the renal pelvis and the renal vein

They are predominantly found in the elderly. Any solid lesion in the kidney represents a malignant neoplasm until proven otherwise, unless there are definite benign features such as internal fat. Suspicion of renal cell carcinoma always warrants surgery, as tissue biopsy is contraindicated. Renal cell carcinoma is often very vascular and can contain areas of calcification and necrosis; occasionally it can be predominantly cystic. There is a tendency for vascular invasion by the tumor, growing into renal veins, and sometimes also extending into the inferior vena cava, even up to the right atrium (Figures 3.11–3.12).

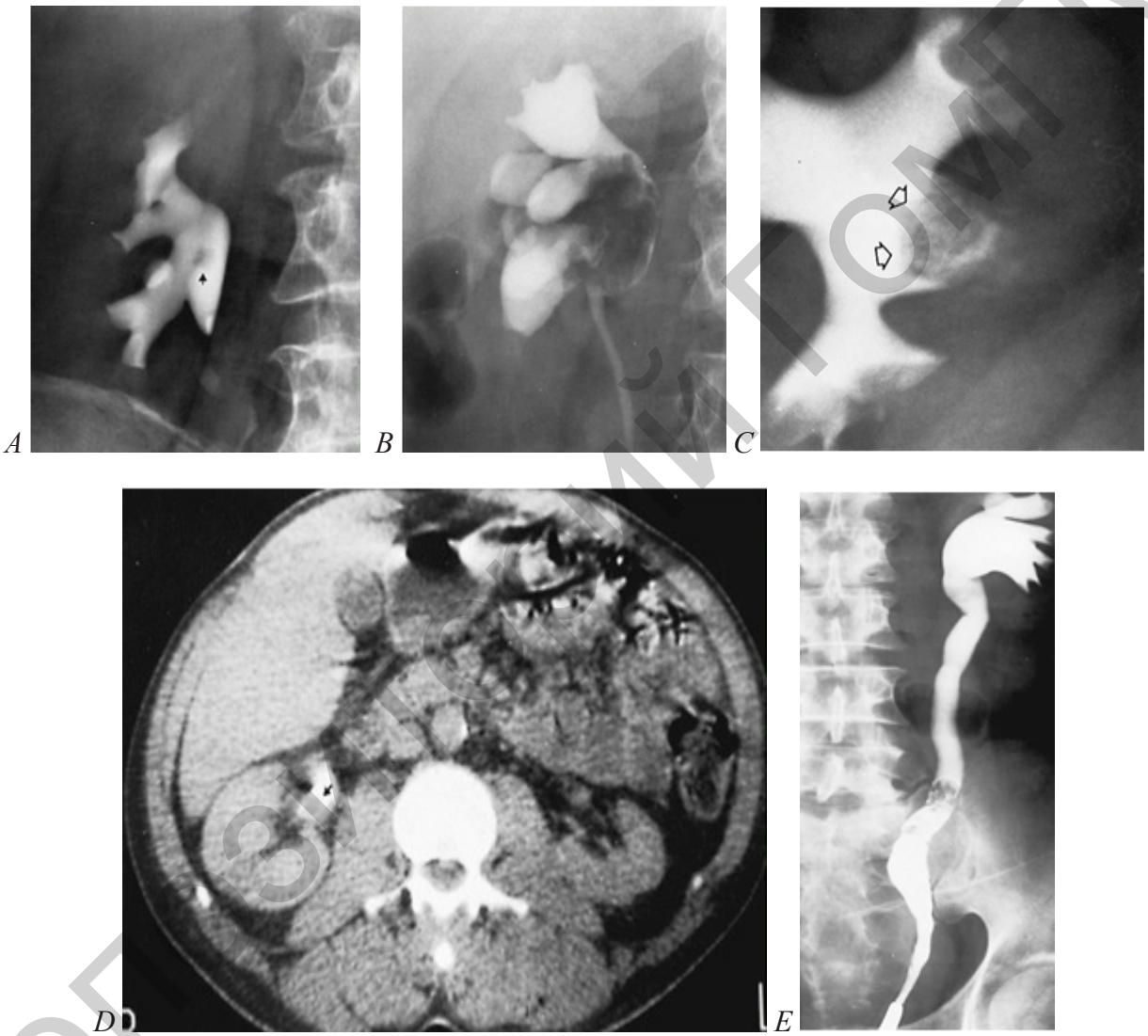

Figure 3.12 — Transitional cell carcinoma of the renal pelvis in different patients. (A) A small filling defect (arrow) in the renal pelvis simulates a blood clot, stone, fungus ball, or sloughed papilla. (B) A huge mass fills virtually all the renal pelvis. (C) A small filling defect occupies an interpolar calyx (arrows). Although the defect might at first be mistaken for a large but otherwise normal papilla, the many small contrast stipples and the suggestively irregular border make its neoplastic nature evident. (D) Transitional cell carcinoma. Filling defect (arrow) in the opacified renal pelvis. (E) Transitional cell carcinoma of the midureter. Irregular stricture with proximal ureteral and pelvocalyceal dilatation (A-C and E – spot-films, D – axial CT-scan)

Cystitis and mass

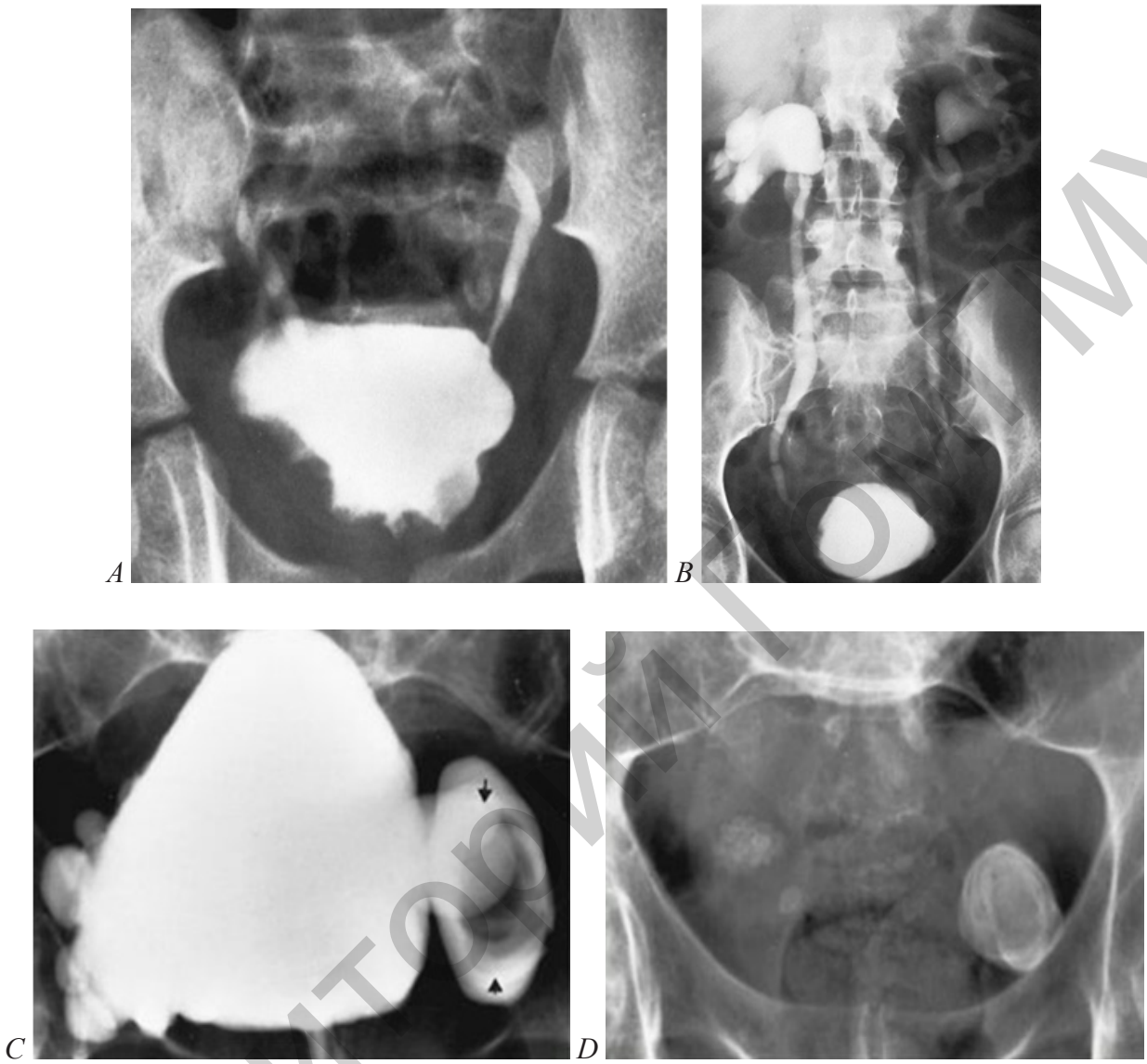

Figure 3.13 — (A) Cystitis. Irregular, lobulated filling defects (representing intense mucosal edema) at the base of the bladder.
(B) Radiation cystitis causing ureteral obstruction. After radiotherapy for cervical cancer, an excretory urogram shows the bladder wall to be thickened and bladder opacity to be reduced. Narrowing of the distal ureters causes bilateral hydronephrosis. Bladder calculi. (C) Excretory urogram demonstrates a large stone (arrows) in a left-sided bladder diverticulum. (D) Plain radiograph of the pelvis shows the laminated stone and multiple smaller calculi that were obscured by contrast material in the right-sided bladder diverticula on the contrast-filled view (A-C – contrasted radiographs)

In acute cystitis, there is a compression of the intramural portion of the ureters by edema and inflammation (unilateral or bilateral obstruction of the distal ureters). In chronic cystitis, the ureterovesical junction is obstructed by fibrosis or an inflammatory mass (Figure 3.13).

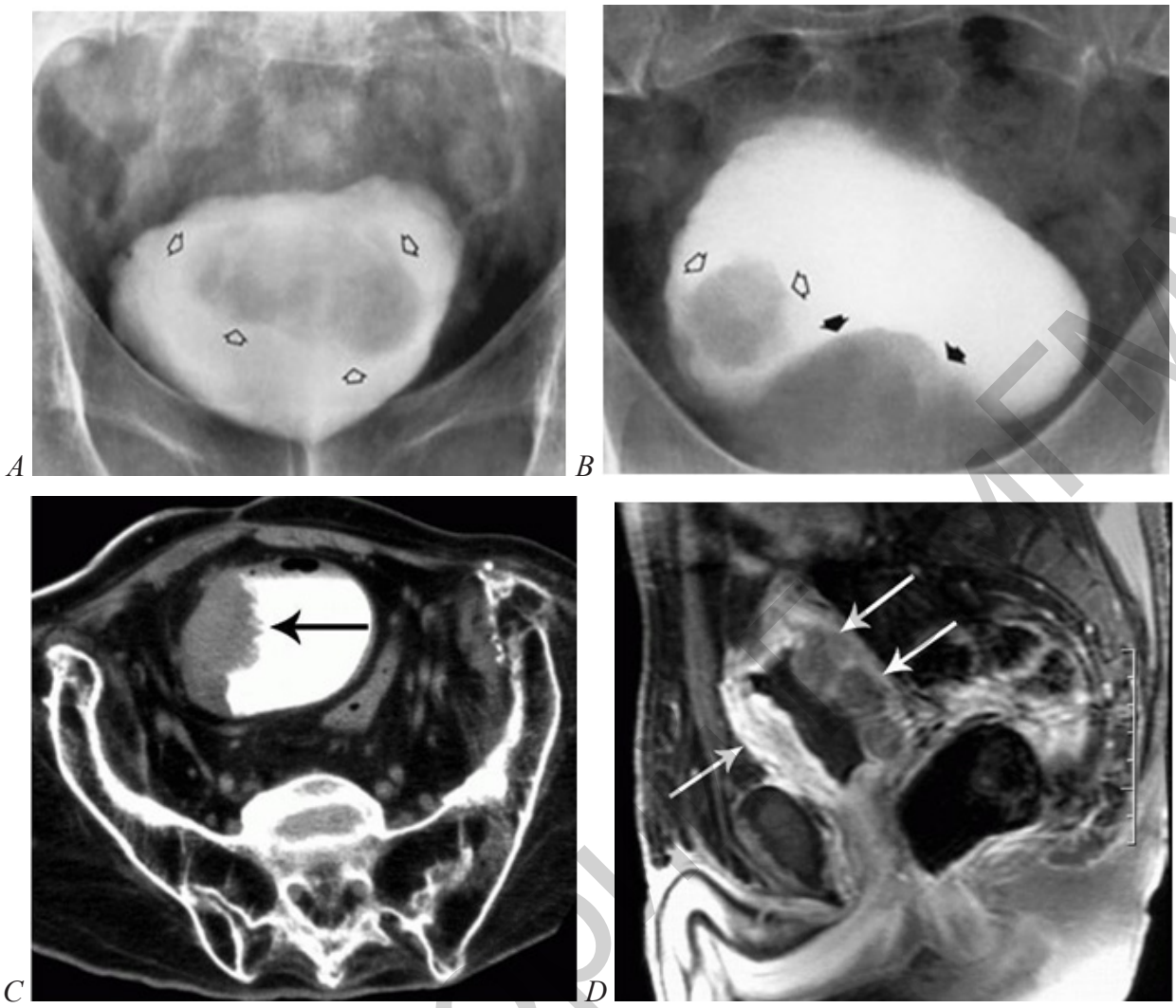

Figure 3.14 —Transitional cell carcinoma.
(A) Large, irregular filling defect (arrows) in the bladder.
(B) In another patient, the irregular tumor (open arrows) is associated with a large filling defect (closed arrows), representing benign prostatic hypertrophy, at the base of the bladder.
(C) Squamous cell carcinoma. CT cystogram shows an irregular mass involving the lateral wall of the bladder. Note the loss of trabecular structure in the bones and fatty infiltration of the muscles in this paraplegic patient. (D) Squamous cell carcinoma. Sagittal enhanced and fat-suppressed T1-weighted MR image shows thickening of the anterior and posterior walls of the bladder (arrows), which represented chronic inflammatory changes with diffuse invasive malignancy (A-B – spot-films, C – axial CT-scan)

Urodynamic studies provide accurate and objective information on the pathophysiology of the lower urinary tract in patients with symptoms suggesting dysfunction of the bladder and/or urethra. The basis of urodynamics is the recording of pressure within the bladder (the cystometrogram) or urethra (the urethral profile) and the flow of urine (during voiding (a flow rate). The relationship between pressure and flow has been studied for many years but refinements in techniques and advances in technology, such as the addition of ultrasound and real-time imaging, have made urodynamics an accurate science. Urodynamic techniques included: cystodynamogram, intravenous urodynamogram, videocystometrography.

Urethra

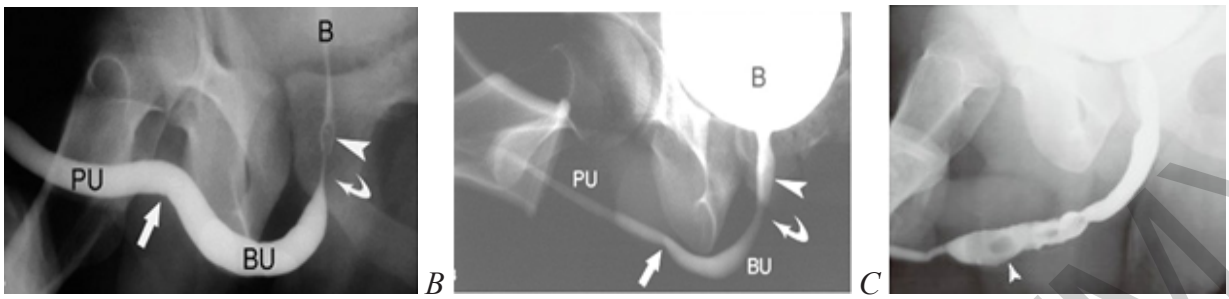

A *B* *C*

Figure 3.15 — Normal male urethra. (A) Retrograde urethrogram (RUG). (B) Voiding cystourethrogram (VCUG). The penile urethra (PU) extends from the urethral meatus to the suspensory ligament of the penis (straight arrows) at the penoscrotal junction. The bulbous urethra (BU) extends from the penoscrotal junction to the urogenital diaphragm (curved arrows), marked by the tip of the cone on the RUG and the slight narrowing of urethral caliber on the VCUG. The membranous urethra (curved arrows) is only 1 cm in length and is entirely within the muscle of the urogenital diaphragm. On a RUG, the membranous urethra extends between the tip of the cone and the verumontanum. The verumontanum (arrowheads) is a nodular structure that produces a filling defect on the urethrograms by bulging into the prostatic urethra. The prostatic urethra extends from the inferior aspect of the verumontanum to the base of the bladder (B). (C) The stones (arrowhead) lie in a segment of an anterior urethral stricture

The urethra is studied by retrograde and voiding urethrography. The retrograde urethrogram is a simple study of the anterior male urethra. Contrast medium is injected into the anterior urethra by means of a syringe or catheter that occludes the meatal orifice. Films are exposed in the right posterior oblique projection.

Voiding cystourethrography is performed by filling the bladder with contrast via a catheter. The catheter is removed, and films are obtained while the patient urinates into a basin on the fluoroscopy table (Figure 3.15).

Imaging methods urinary system of characteristic

The choices for imaging of the pelvicaliceal system and ureters have expanded. An excretory urogram, also called an intravenous pyelogram (IVP), has been the traditional choice. This study is performed by obtaining a series of radiographs at various times and in various projections following IV administration of contrast agent. The images of the collecting system are routinely of high quality and remain the gold standard. However, detection of lesions in the renal parenchyma is limited. With the development of multidetector CT and continued improvement in MR, we now have available the CT-IVP and the MR-IVP, which combine optimal imaging of the renal parenchyma with satisfactory images of the collecting system and ureters. MR urography can be performed without the use of IV contrast utilizing T2 weighting to provide visualization of urine-filled structures. Poor renal function or high-grade obstruction limits the use of IV contrast agents because of poor concentration of contrast within the collecting system. When a percutaneous nephrostomy catheter has been placed in the collecting system, antegrade pyelography is an additional choice. US is the imaging method of choice for screening for hydronephrosis but is limited in its ability to demonstrate small uroepithelial tumors. CT, routinely performed without IV or oral contrast agents, has supplanted plain radiographs and IVP in the diagnosis of renal stones in the kidneys and ureters.

Renal scintigraphy

Scintigraphy has provided a unique tool for the noninvasive evaluation of renal pathophysiology. A renal scintigram is a nuclear medicine examination that measures the function of the kidneys. Renal scans are helpful in evaluating blood flow to the kidney, glomerular filtration, tubular function (resorption and secretion), and drainage of the collecting systems. Functional information is provided as well as anatomical and drainage of the collecting systems.

Example indications: renal function; renal artery stenosis; obstructive uropathy, hypertension acute renal failure.

The preferred agents renal parenchymal static imaging are technetium-99m DMSA. Optimal parenchymal imaging can be obtained 1–3 hours after injection. By this time, collecting system activity will usually not be present. At a minimum, both posterior and posterior oblique views should be obtained.

^{99m}Tc-diethylenetriaminepentaacetic acid (^{99m}Tc-DTPA)

This tracer is a nearly ideal agent for assessment of glomerular filtration. It is a small chelate with a molecular weight of 500, and its only mode of excretion is glomerular filtration. It is neither secreted nor reabsorbed by the kidneys. Its renal extraction reflects the filtration fraction of plasma.

^{131}I-hippurate

Hippurate is mainly excreted by tubular secretion (80%) and, to a lesser extent, by filtration (20%).

^{99m}Tc-dimercaptosuccinic acid (^{99m}Tc-DMSA)

^{99m}Tc-DMSA is used for cortical imaging because about 50% of the injected dose is retained in the renal cortex, bound to sulfhydryl groups in the proximal convoluted tubules. Peak renal activity is seen at 4-6 hours after injection. It is the favored tracer for assessment of renal morphology and is used in the assessment of pyelonephritis and renal scarring.

Renal perfusion can be assessed with the various ^{99m}Tc-labeled tracers with the camera set to take rapid sequence dynamic images at a rate of 1–3 seconds per frame during the first minute of the acquisition. The remaining 20–30 minutes of the study is usually performed at a framing rate of 20–60 seconds to evaluate the uptake and excretion phases (Figures 3.16–3.17).

Acute renal obstruction

Decreased blood flow with decreased function and minimal excretion is noted in the kidney, suggesting an acute obstruction. An acute high-grade outflow obstruction can decrease excretion, overall function and blood flow to the affected kidney. A chronic obstruction will eventually lead to the absence of the function of the kidney.

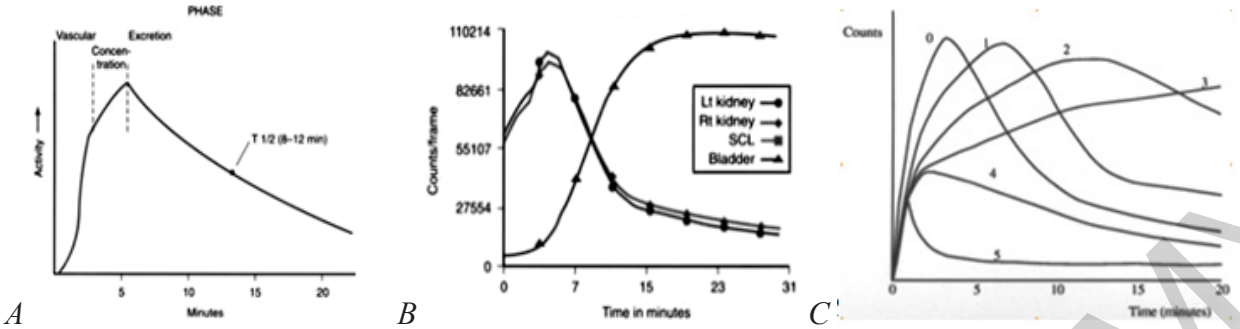

A *B* *C*

Figure 3.16 —Typical renogram curves. (A) Schematic drawing demonstrates the conceptual portions of the time-activity curve within the kidney. (B) An actual renogram shows symmetric activity between right and left kidney, rapid drop off after the peak, and a long tail extending to the right. The curve also shows increasing activity within the bladder after about 4 minutes. (C) Common renogram patterns used for the visual interpretation of renography.
Type 0: normal. Type 1: time to peak (T max) is >5 min.
Type 2: There are more exaggerated delays in time to peak and in parenchymal washout.
Type 3: Progressive renal accumulation (obstruction type, no washout detected).
Type 4: Renal failure pattern, but with measurable renal uptake.
Type 5: Renal failure pattern, representing blood background activity only (non functional type)

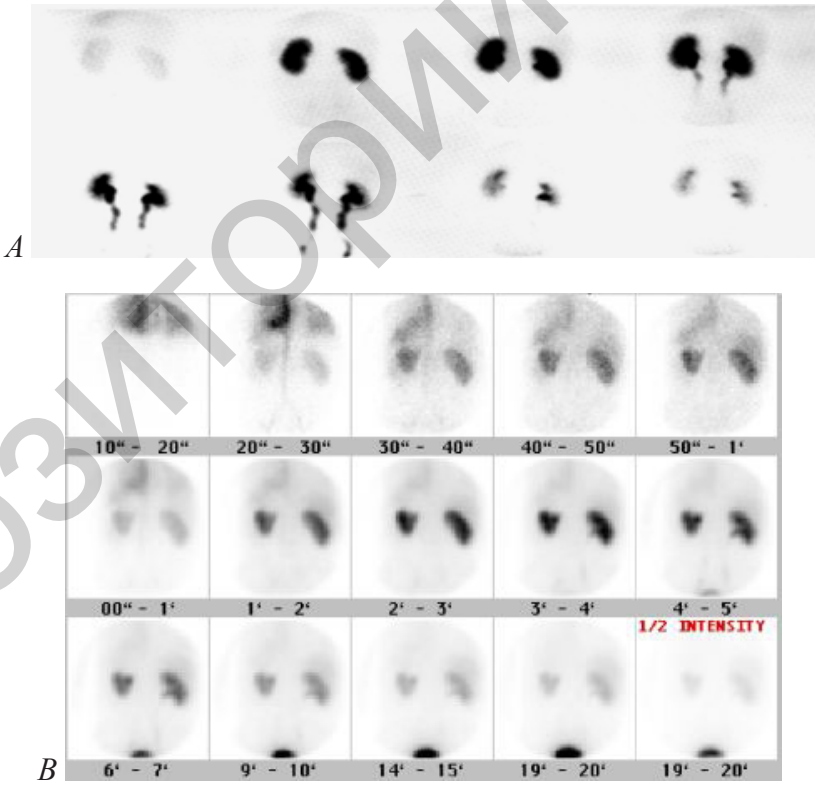

A

B

Figure 3.17 — Variants of normal dynamic renoscintigraphy. After administration of radiopharmaceutical, maximal kidney activity is seen at about 3 to 5 minutes, and by 4 to 5 minutes, the bladder can be identified at the bottom of the images. By about 8 to 12 minutes, most of the activity has cleared the parenchyma and is seen in the collecting systems, making the kidneys appear slightly smaller than on the early images. The temporal sequence here is similar to that identified on intravenous pyelogram

Obstructive uropathy

Interpretation of a diuretic scintigram relies both on visual examination of the dynamic scintigram and on inspection of time-activity curves derived for each kidney using the regions of interest method. Curves represent obstruction with a continuous rise or plateau following diuresis. On images there is progressive accumulation in the collecting system which is unaffected by furosemide injection, is present dilatation of the pelvis and (or) calices. Can is present progressive accumulation of the tracer in both ureters and delayed renal washout (Figure 3.18).

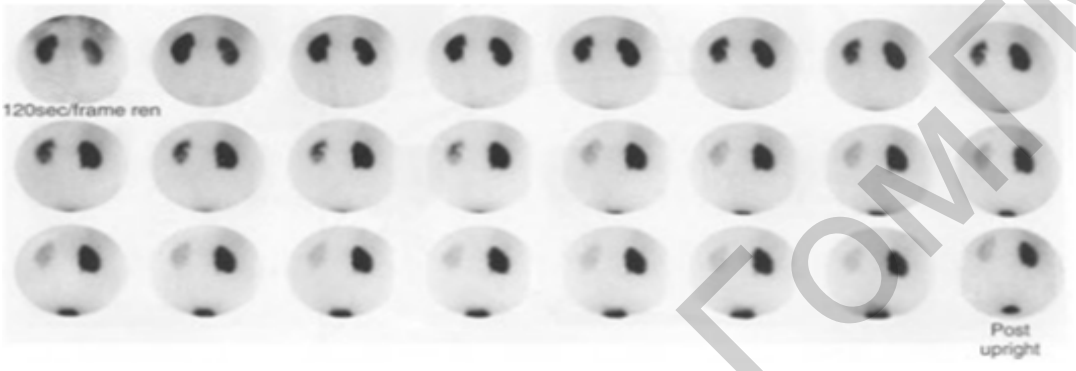

A

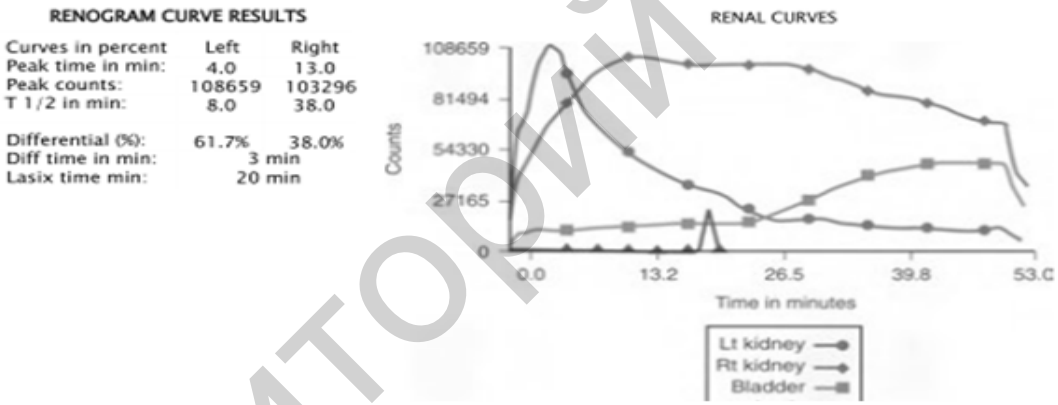

B

Figure 3.18 — (A) After intravenous administration of technetium-99m DTPA, the posterior 2-minute sequential images show a dilated collecting system of the right kidney. (B) Abnormal diuretic renogram with obstruction

Acute pyelonephritis

On the imaging of the renal parenchyma with ^{99m}Tc-DMSA a cortical defect due to pyelonephritis is characterized by preservation of a renal contour, whereas scarring (from a previous infection) typically results in a volume contraction, although the two may be indistinguishable.

Renovascular hypertension

With a filtered agent such as ^{99m}Tc-DTPA, the drop in glomerular filtration results in moderate to severe reduction of tracer uptake by the affected kidney which in extreme cases can be complete with only background activity and no appearance of tracer in the collecting system.

IV. BASIC RADIOLOGY OF REPRODUCTIVE SYSTEM

Imaging of the female reproductive system

Imaging studies have contributed greatly to the diagnosis and management of infertility in women. Hysterosalpingography (Figure 4.1 A) remains the first-line radiologic examination for most women undergoing an infertility investigation. Sonography has a crucial role in monitoring ovarian follicular development in spontaneous and induced cycles and is invaluable as a guidance procedure in reproductive techniques such as oocyte collection and gamete transfer in vitro fertilezation programs.

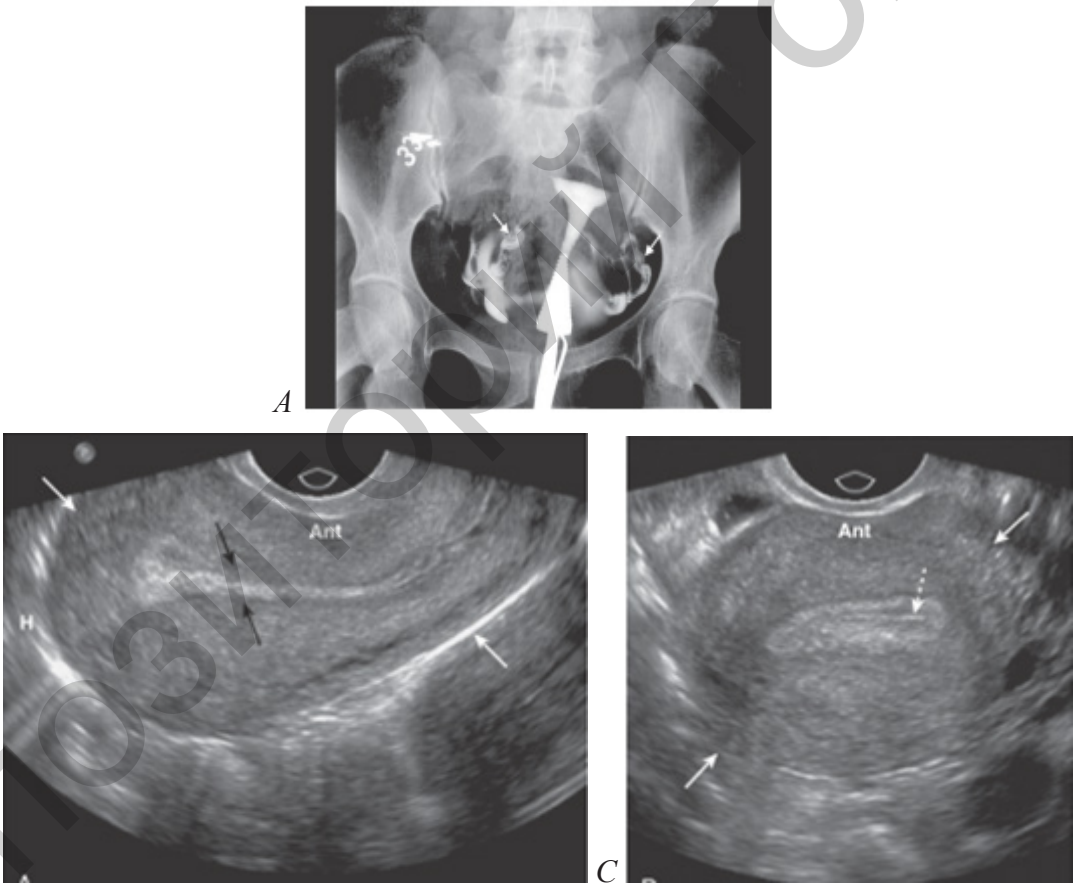

Figure 4.1 — (A) Normal hysterosalpingogram showing an inverted triangle shaped smooth uterine outline. Both fallopian tubes are well outlined by contrast. Note the presence of longitudinal rugal folds in the ampullary portion (arrows). Free intraperitoneal spill is seen on both sides outlining the bowel loops. Normal uterus, longitudinal and transverse. The uterus (solid white arrows) has a pear shape with maximum dimensions of approximately 8 cm in length, 5 cm in width, and 4 cm in the anteroposterior dimension. (B) The endometrium lines the uterine cavity and is measured in the sagittal view (black arrows). (C) The collapsed uterine cavity is within the center of the endometrium and is visualized as a thin line (dotted white arrow). Ant, Anterior; H, head

Ultrasound use is even higher in countries where it is considered a part of routine obstetric care. Indications for ultrasound during the first trimester include pregnancy dating (Figure 4.2 A), assessment of women with bleeding or pain, and assessment of translucency in screening for aneuploidy. In the second trimester, ultrasound is used for pregnancy dating, assessment of interval growth, assessment of patients with abnormal pain or bleeding, assessment of size-to-dates discrepancy, routine survey of fetal anatomy, and assessment of maternal indications related to age, drug use, or history of prior abnormalities. Studies should be conducted with real-time scanners using a transabdominal and/or transvaginal approach, depending on the gestational age and the region of interest. Higher-frequency transducers are most useful in achieving high-resolution scans, and lower-frequency transducers are useful when increased penetration of the sound beam is necessary. Use of Doppler ultrasound and three-dimensional (3-D) and four-dimensional (4-D) imaging depends on the specific indication.

Transvaginal ultrasound (TVUS) is the imaging modality of choice in the evaluation of the first-trimester pregnancy (Figures 4.1 B to C). In rare instances, a transabdominal ultrasound (TAUS) may be sufficient. For example, in cases where there is a known intrauterine pregnancy (IUP), but fetal cardiac activity is not heard, TAUS may be used to verify that the embryo is still alive.

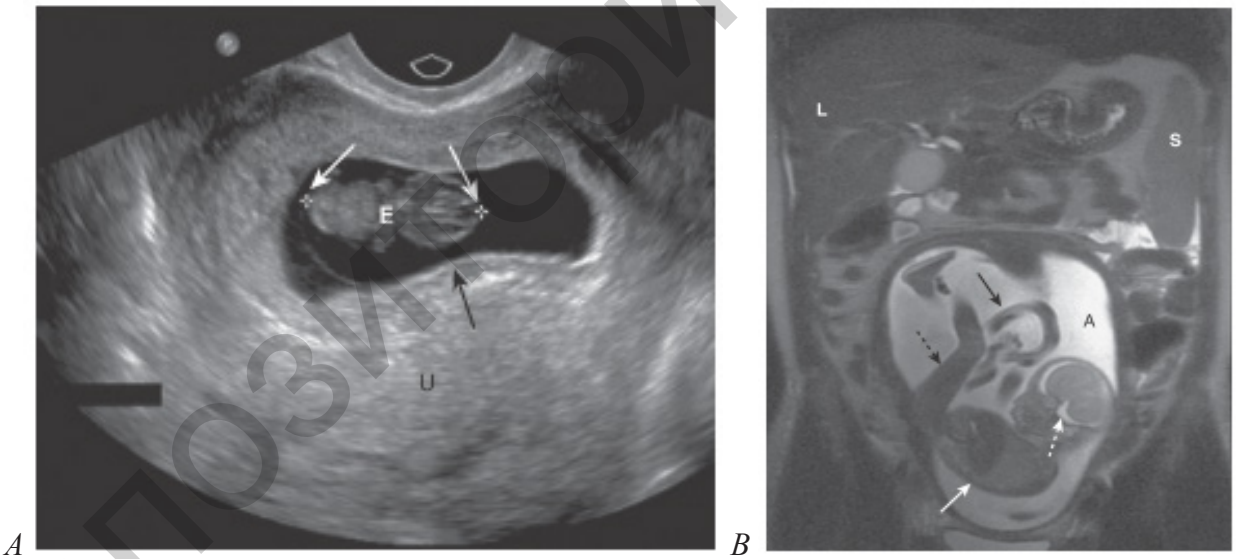

A *B*

Figure 4.2 — (A) Early US intrauterine pregnancy. A single live intrauterine pregnancy (white arrows) is contained within the gestational sac (black arrow) inside the uterus (U). Using a measurement called the crown-rump length (between the white arrows), the embryo (E) was estimated at 9 weeks of age.
(B) Magnetic resonance imaging scan in pregnancy. Coronal T2-weighted image demonstrates an intrauterine pregnancy. The maternal liver (L) and spleen (S) are partially imaged. The right amniotic fluid (A) and fetal cerebrospinal fluid (dotted white arrow) help us to recognize this as a T2-weighted image. The fetal body (solid white arrow) and leg (dotted black arrow) can be seen clearly. The umbilical cord (solid black arrow) is partially visible

Magnetic resonance imaging

Ultrasound is the screening modality of choice for fetal imaging. However, when additional information regarding fetal anatomy or pathology is needed, fast MR imaging is increasingly used as a correlative imaging modality in select cases (Figure 4.2 B). MRI is useful in these cases because it has no ionizing radiation, provides excellent soft tissue contrast, has multiple planes for reconstruction, and has a large field of view, allowing for improved depiction of many complex fetal abnormalities. It is important to tailor the examination to answer specific questions raised either by patient history or by prior sonographic examination.

There are no known biologic risks from MRI. The MR procedure is not believed to be hazardous to the fetus. No delayed sequelae from MR examination have been encountered, and it is expected that the potential risk for any delayed sequelae is extremely small or nonexistent.

Benign diseases of the female pelvis

Ultrasonography is the primary modality for evaluating gynecological abnormalities as it adequately depicts normal and pathological anatomy (Figures 4.3 C to D). Ultrasound provides useful information in confirming the presence or absence of a pelvic mass, determining its site of the origin and precise relationship to other pelvic organs, and evaluating the morphologic characteristics of the mass along with delineating ascites or adenopathy or other features suggesting malignancy. The diagnostic sensitivity and specificity of sonography has increased with the advent and increased use of high resolution transvaginal probes.

Color Doppler sonography (Figure 4.12 B) and sonohysterography are useful adjuncts to conventional gray-scale ultrasonography in the evaluation of gynecologic disorders and can be helpful in clarifying the etiology of some of the masses with nonspecific morphological features.

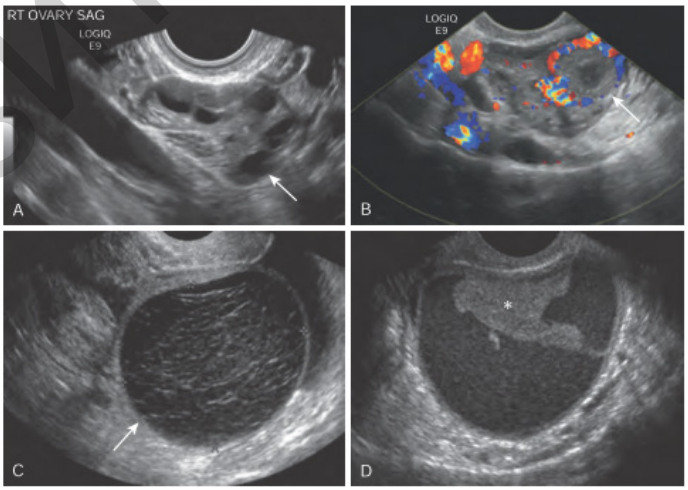

Figure 4.3 — Normal ovary and benign ovarian cysts on transvaginal US. (A) Sagittal image of normal right ovary in premenopausal patient with multiple anechoic follicles (arrow). (B) Color Doppler image of right ovary demonstrates thick-walled corpus luteum with "ring of fire" appearance (arrow). (C and D) Note ovarian hemorrhagic cysts with internal "lace-like" reticular echoes (arrow) and eccentric echogenic blood clot (*)

CT often provides diagnostic information in patients who have suspected pelvic masses in whom the initial ultrasound has proved equivocal as it is capable of detecting adenopathy, assessing fat planes and extent which are important in the staging of malignancy.

Magnetic resonance imaging can reliably diagnose several benign lesions, such as congenital anomalies of the uterus, leiomyomas, adenomyosis, dermoid cysts and in some cases of endometriomas.

Gynaecological mass and cancer

Ultrasound

Ultrasound (transabdominal or transvaginal) is accepted as the primary imaging technique for examining the female pelvis. Currently, the main role of US in gynaecological oncology includes evaluation of a suspected pelvic mass, evaluation of causes of uterine enlargement, identification of endometrial abnormalities in a patient with postmenopausal bleeding and characterisation of ovarian masses. In addition, US has become invaluable in guiding a wide selection of invasive procedures such as transabdominal and transvaginal guidance of fluid or tissue sampling, transvaginal-guided drain placement and guidance for placement of brachytherapy devices for cervical and endometrial malignancies. A full bladder is mandatory for transabdominal US, as it provides a sonic window to image the pelvic organs. It is usual to employ 3,5–5,0 MHz (Mega Hertz) transducers. Transvaginal US, which is optimally performed with an empty bladder, provides greater detail of the anatomy and pathology due to the closer apposition to the pelvic organs, as well as the higher frequencies of insonation (5,0–7,5 MHz) (Figures 4.4–4.11).

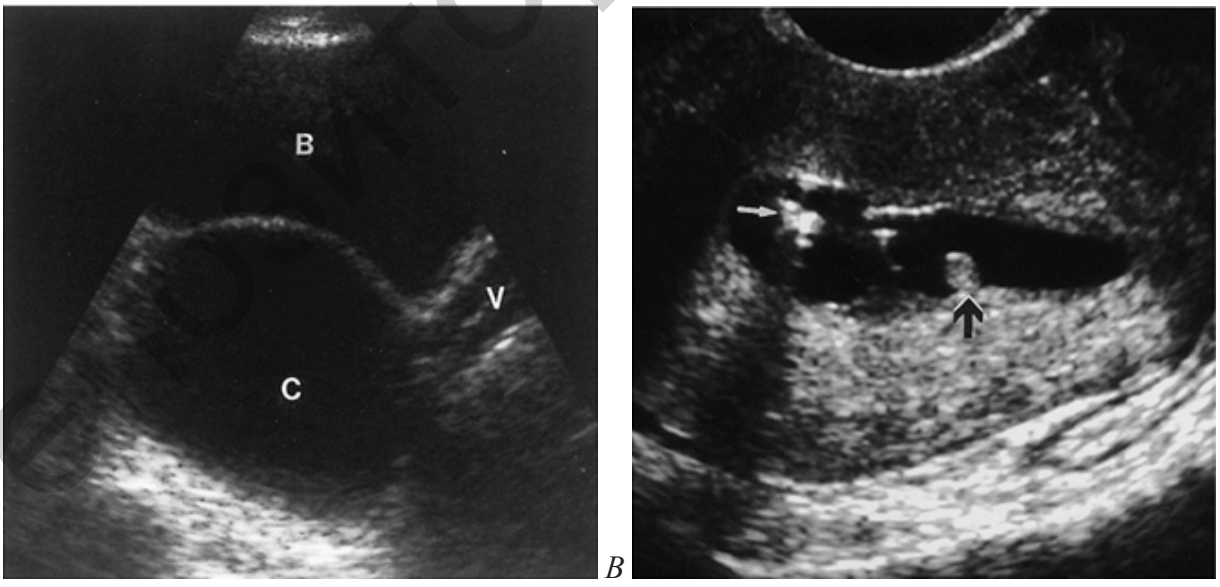

Figure 4.4 — Paraovarian cyst. Sagittal sonogram demonstrates the cyst (C) superior to the vagina (V). The uterus had been removed. (B, bladder)

Endometrial polyp. Sonohysterogram reveals a small polyp attached by a stalk to the endometrium (black arrow). An echogenic focus in the endometrial cavity (white arrow) represents injected air

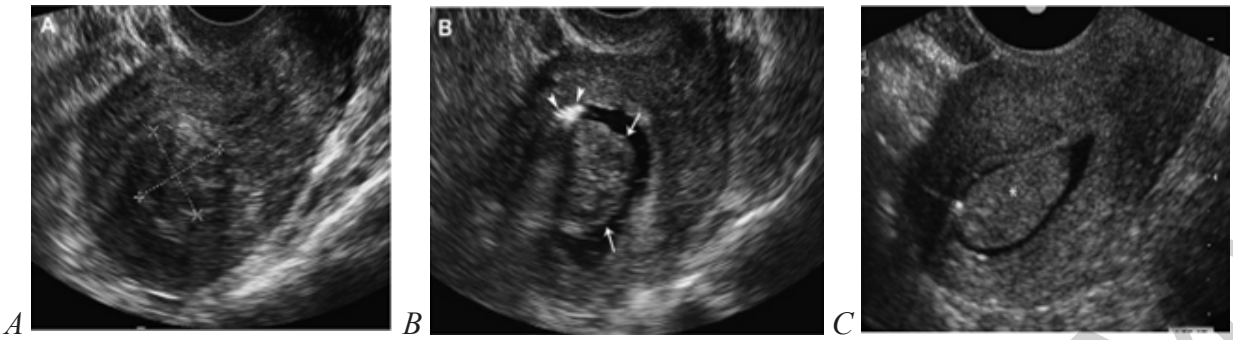

Figure 4.5 — (A) Longitudinal transvaginal US showing a central fibroid (witin cursors) with distortion of the endometrium. (B) Longitudinal sonohystegram reveals fibroid (arrows) with less than 50% extension into the myometrium. Air bubbles (arrowheads). (C) — Longitudinal sonohysterogram showing a large benign endometrial polyp (asterisk)

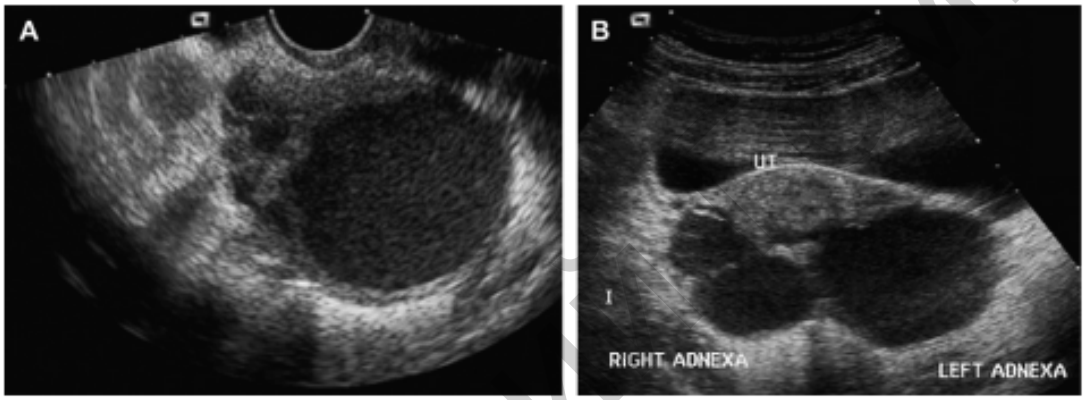

Figure 4.6 — Endometrioma. (A) Transvaginal grayscale image demonstrates a left ovarian cyst with low-level echoes. (B) Transabdominal grayscale image of the pelvis with bilateral endometriomas demonstrates the "kissing ovaries" sign. (UT, uterus)

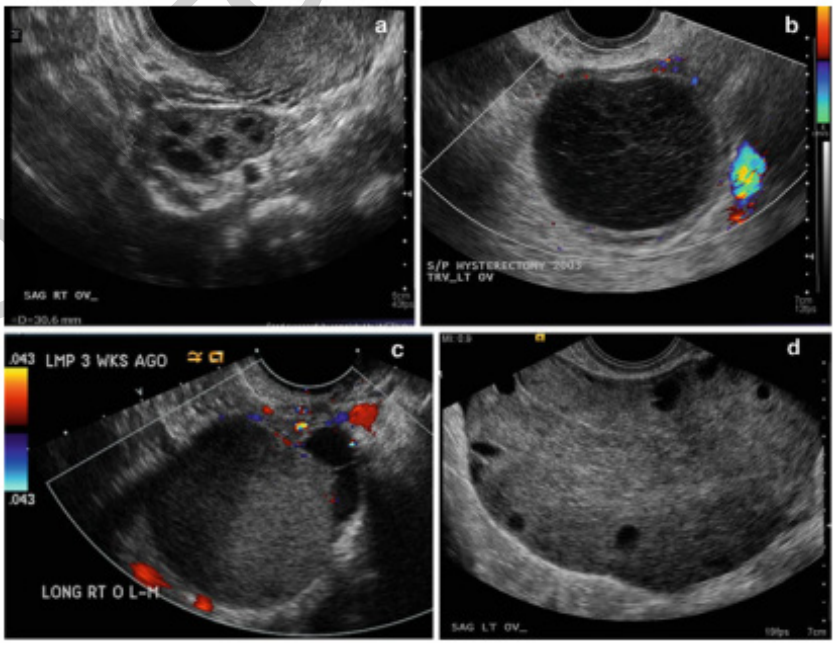

Figure 4.7 — Examples of ovarian ultrasounds. (a) normal ovary, (b) hemorrhagic cyst with reticulated mesh-like echoes, (c) endometrioma with homogeneous echoes, and (d) enlarged torsed ovary with peripheral follicles

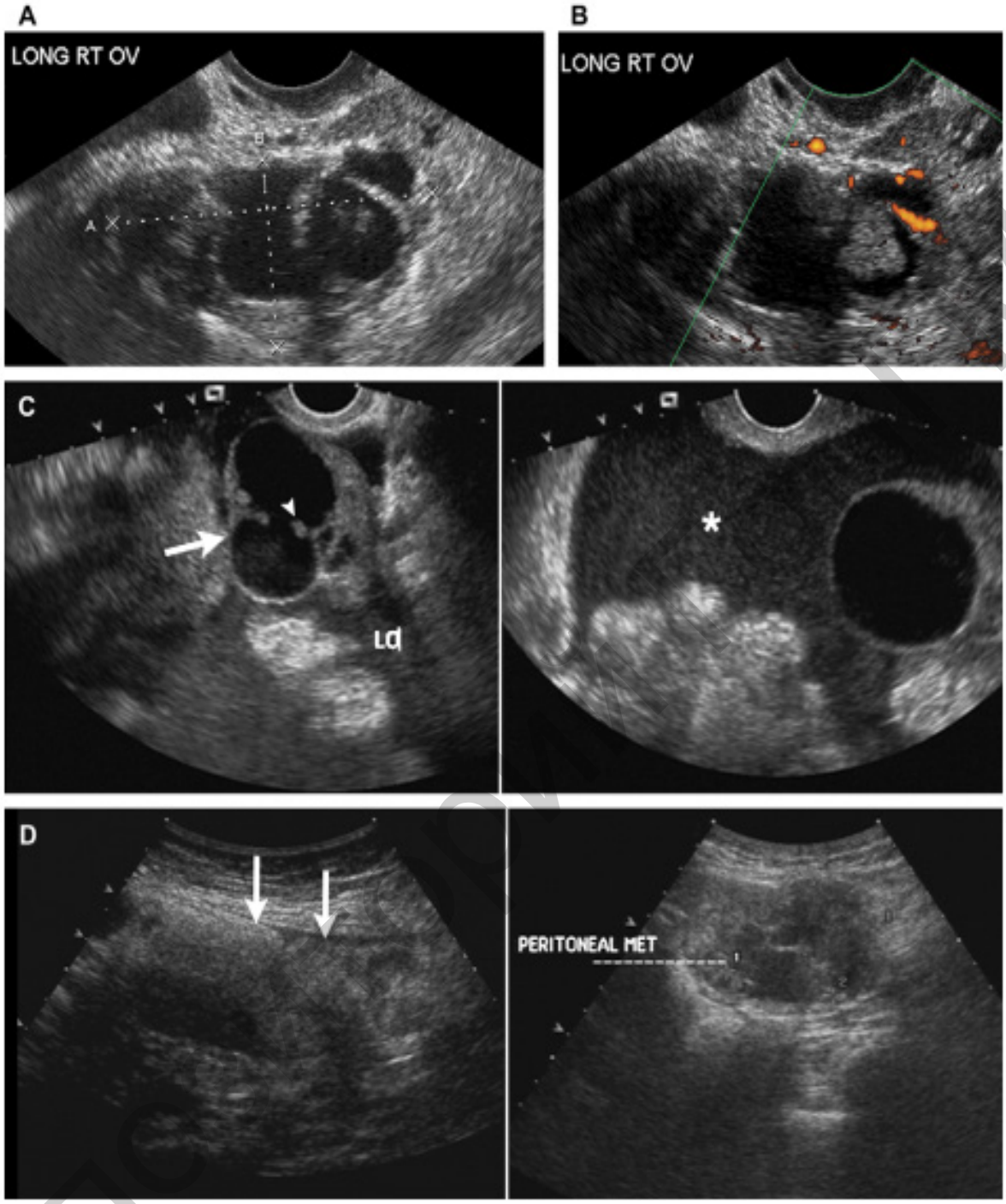

Figure 4.8 — Malignant adnexal masses. (A) Transvaginal grayscale image demonstrates a large right adnexal complex mass with solid and cystic components. (B) Corresponding power Doppler image shows increased vascularity within the septae. Spectral Doppler (not shown) confirmed resistive index of less than 0.4, suggesting an ovarian carcinoma. (C) Mucinous cystadenocarcinoma. Transvaginal grayscale images of left adnexa demonstrate a cystic left ovarian mass (arrow) with mural nodulations (arrowhead) and low-level echoes with complex free fluid (asterisk), consistent with malignant ascites. (D) Omental and peritoneal metastases. Grayscale US of the abdomen demonstrates omental caking (arrows) and peritoneal metastasis in a known case of ovarian carcinoma

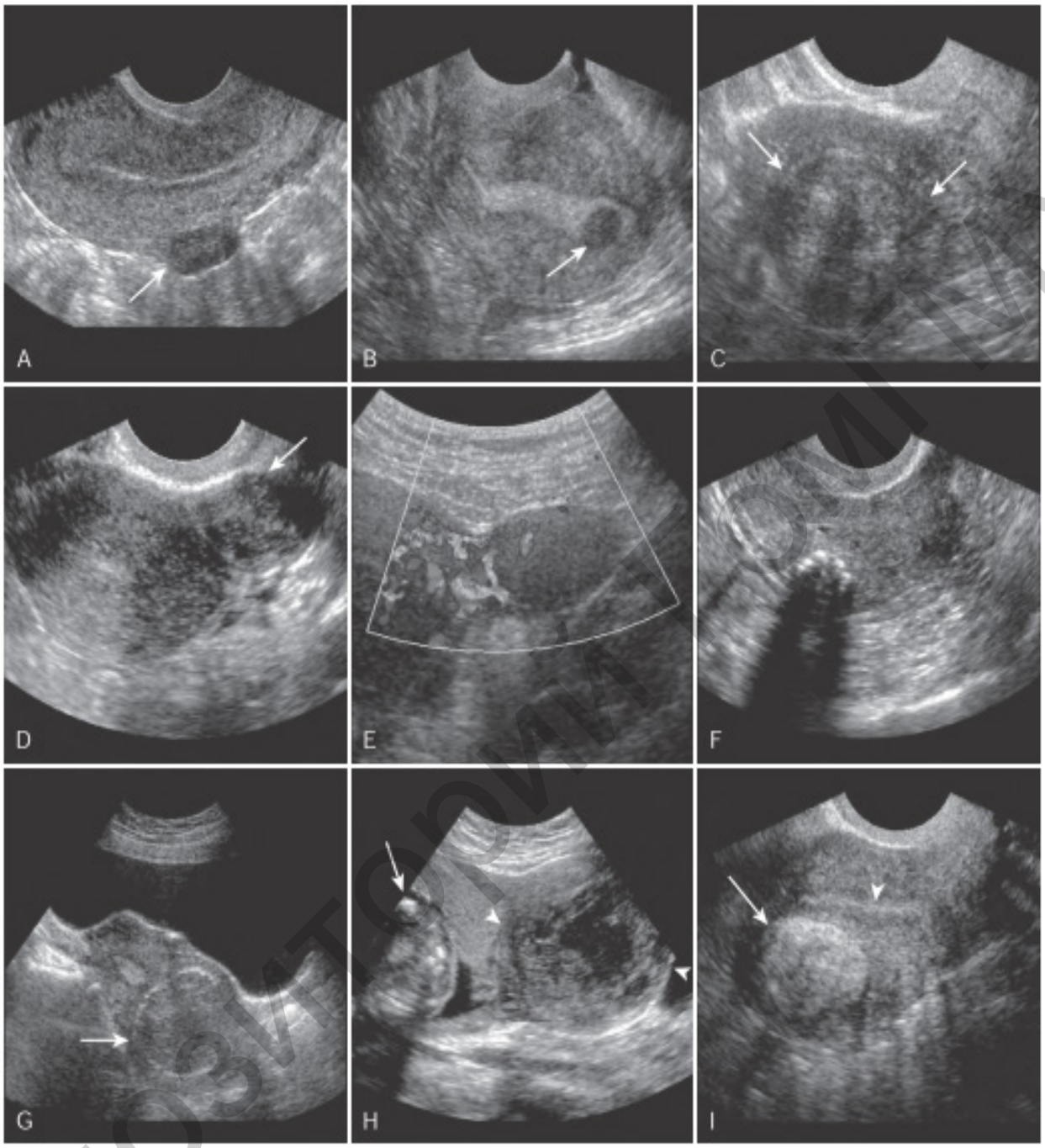

Figure 4.9 — Uterine fibroids: spectrum of appearances. A to D, F, and I, transvaginal scans. E, G, and H, Transabdominal scans. (A), Localized hypoechoic subserosal fibroid (arrow). (B), Hypoechoic submucosal fibroid (arrow). (C), Marked attenuation of sound beam by fibroid (arrows). (D), Pedunculated subserosal fibroid (arrow) presenting as solid left adnexal mass. (E), Color Doppler sonogram of pedunculated subserosal fibroid shows blood supply arising from uterus. (F), Fibroid with calcification causing posterior shadowing. (G), Calcified fibroid with curvilinear peripheral calcification (arrow) mimicking a fetal head. (H), Fibroid with cystic degeneration (arrowheads) in pregnancy. Patient presented with pain and tenderness over degenerating fibroid (arrow, fetus). (I), Lipoleiomyoma. Highly echogenic mass within myometrium (arrow) with posterior attenuation (arrowhead, endometrium)

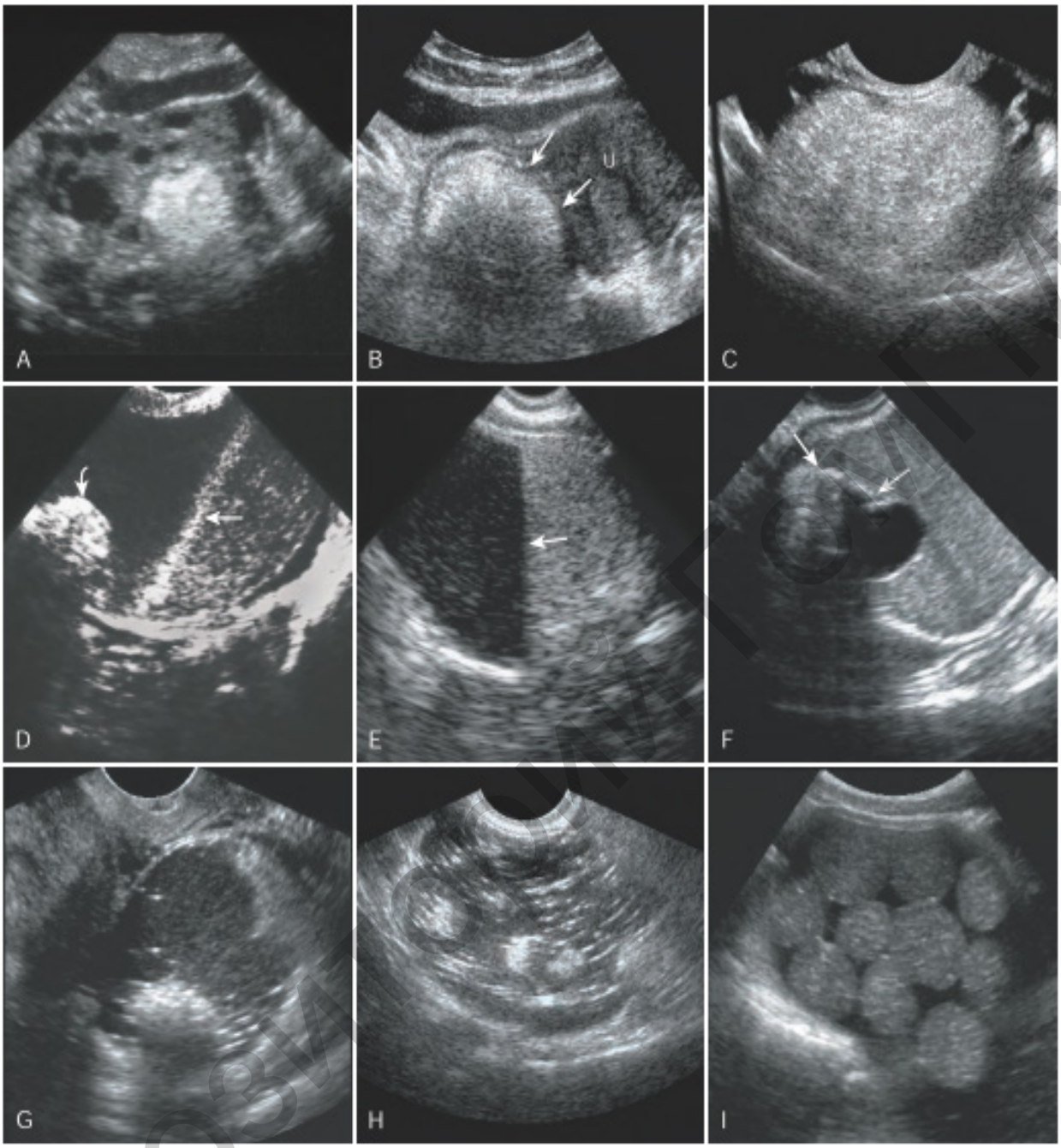

Figure 4.10 — Dermoid cysts: spectrum of appearances. (A), Small, highly echogenic mass in an otherwise normal ovary. (B), Transverse transabdominal scan shows the uterus (U). In the right adnexal region, there is a highly echogenic and attenuating mass (arrows), the "tip of the iceberg" sign. (C), Highly echogenic intraovarian mass with no normal ovarian tissue. (D), Mass of varying echogenicity with hair-fluid level (straight arrow) and highly echogenic, fat-containing dermoid plug (curved arrow) with shadowing. (E), Mass with fat-fluid level (arrow), with dependent layer more echogenic. (F), Mass containing uniform echoes, small cystic area, and calcification (arrows) with shadowing. (G), Combination of dermoid mesh and dermoid plug appearances. (H), Dermoid mesh, multiple linear hyperechogenic interfaces floating within cystic mass. (I), Multiple mobile spherical echogenic structures floating in a large, cystic pelvic mass

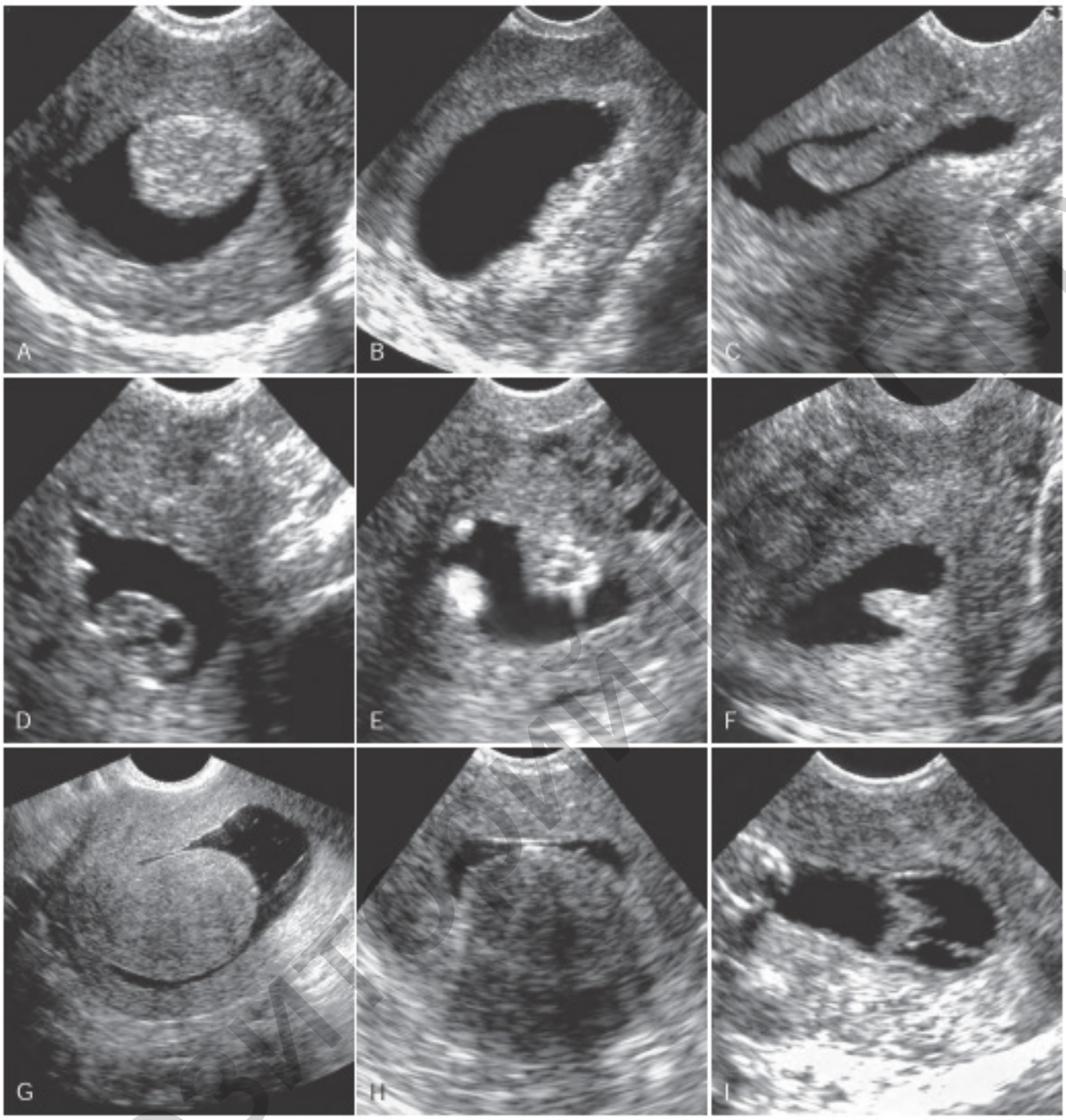

Figure 4.11 — Sonohysterograms of polyps, fibroids, and adhesions. (A), Well-defined, round echogenic polyp. (B), Carpet of small polyps. (C), Polyp on a stalk. (D), Polyp with cystic areas. (E), Small polyp. (F), Small polyp. (G), Hypoechoic submucosal fibroid. (H), Hypoechoic attenuating submucosal fibroid. (I), Endometrial adhesions. Note bridging bands of tissue within fluid-filled endometrial canal

Ultrasound has many advantages: it is relatively inexpensive, provides multiplanar views, is widely available and lacks ionising radiation. Its portability allows use in virtually any setting, including the ultrasound suite, operating room, patient bedside or radiotherapy suite. Colour, power and spectral Doppler provide additional information regarding associated vascularity.

US also has a number of limitations: it is operator dependent and image quality varies with patient body habitus. Although transvaginal, sonohysterography and endorectal US provide improved spatial resolution, they are not as useful as either CT or MRI in the staging of pelvic malignancies, including the evaluation of regional extent or metastatic spread.

Computed tomography

CT is the most commonly used primary imaging study for evaluating the extent of gynaecological malignancies and for detecting persistent and recurrent disease although there is increasing use of MRI. CT-guided biopsy of omental cake or pelvic mass can be used to obtain histological confirmation of ovarian cancer and to confirm pelvic recurrence. Advantages of CT include wide availability, fast data acquisition and high spatial resolution. Disadvantages of CT include the use of ionising radiation, degradation of image quality by body habitus or metallic hip prosthesis and the risk of morbidity and mortality associated with iodinated contrast agents. Although CT is useful in the advanced stages of pelvic malignancy, it often has limited utility in characterising early-stage disease.

CT images of the abdomen and pelvis are acquired in the portal venous phase, 70-s following an injection of intravenous low osmolar contrast medium; this enhances blood vessels and viscera, allowing easier identification of enlarged lymph nodes and parenchymal lesions. Oral contrast medium is utilised to opacify the small and large bowel, which allows detection of bowel serosal deposits and the differentiation of bowel loops from pelvic and nodal disease.

Magnetic resonance imaging

The role of MRI in the evaluation of gynaecological malignancies has evolved during the past two decades. MRI has been shown to be superior to CT in the work-up of endometrial and cervical cancer (Figure 4.12) and may be a useful problem-solving tool in the evaluation of ovarian cancer. In addition, there is evidence that MRI may aid the differentiation of radiation fibrosis from recurrent tumour. The accuracy of MRI assessment of lymph node invasion is similar to that of CT; both rely primarily on size criteria to detect lymph node metastases. Although MRI is still relatively expensive, it has been shown to minimise costs in some clinical settings by limiting or eliminating the need for further expensive and/or more invasive diagnostic or surgical procedures.

Advantages of MRI include superb spatial and tissue contrast resolution, no use of ionising radiation, multiplanar capability and fast (i.e. breath-hold and breathing-independent) techniques. MRI is the technique of choice for patients with previous reactions to iodinated IV contrast media or impaired renal function. However, MRI is contraindicated in patients with implants such as pacemakers, neural stimulators or cochlear implants, certain vascular clips and metallic objects. Some patients may experience claustrophobia, causing difficulty in completing the examination or requiring sedative premedication in subsequent MR examinations.

Dynamic multiphase contrast-enhanced MRI using a three-dimensional (3-D) gradient echo T1-weighted after intravenous gadolinium is often utilised in sta-ging patients with endometrial cancer; it is also useful in the characterisation of complex adnexal lesions and can aid in the detection of small peritoneal and serosal implants, when ovarian cancer is suspected.

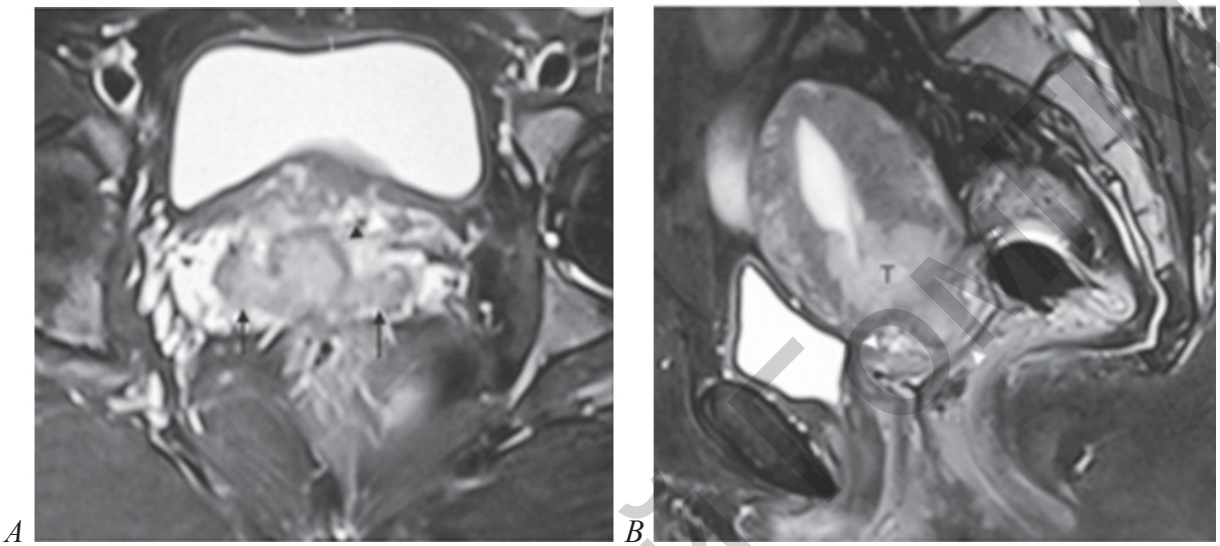

Figure 4.12 — Carcinoma of cervix. (A) T2-weighted axial MR image shows hyperintense mass in the cervix. It is surrounded by hypointense stromal ring anteriorly (black arrowhead); however, this ring is disrupted posterolaterally with tumor sensitivity soft tissue extension in bilateral parametrium (arrows).
(B) Contrast-enhanced sagittal T1-weighted images shows enhancing tumor (T) in the cervix. Preserved hypointense walls of urinary bladder and rectum (white arrowheads) exclude their invasion by the tumor

Increasingly, diffusion-weighted MRI (DW-MRI) is routinely incorporated in MRI staging protocols for uterine malignancies. DW-MRI can be useful for accurately determining the depth of myometrial invasion in patients with endometrial cancer, which can be particularly helpful in cases of tumours that are either iso- or hyperintense relative to the myometrium on T2-weighted or when the use of intravenous contrast medium is contraindicated, and may replace dynamic imaging in the future. DW-MRI may also improve detection of drop metastases in the cervix or metastatic foci outside the uterus, such as adnexa or peritoneum.

Positron emission tomography/computed tomography

The main applications of ^{18}F-fluoro-2-deoxy-d-glucose (FDG) PET/CT in gynaecological oncology are the staging of cervical cancer and detection of recurrent ovarian, cervical and endometrial cancer (Figure 4.13). FDG-PET/CT does not have the same spatial resolution or soft-tissue contrast as US or MRI, but image fusion techniques that overlay FDG-PET images onto MR images are available.

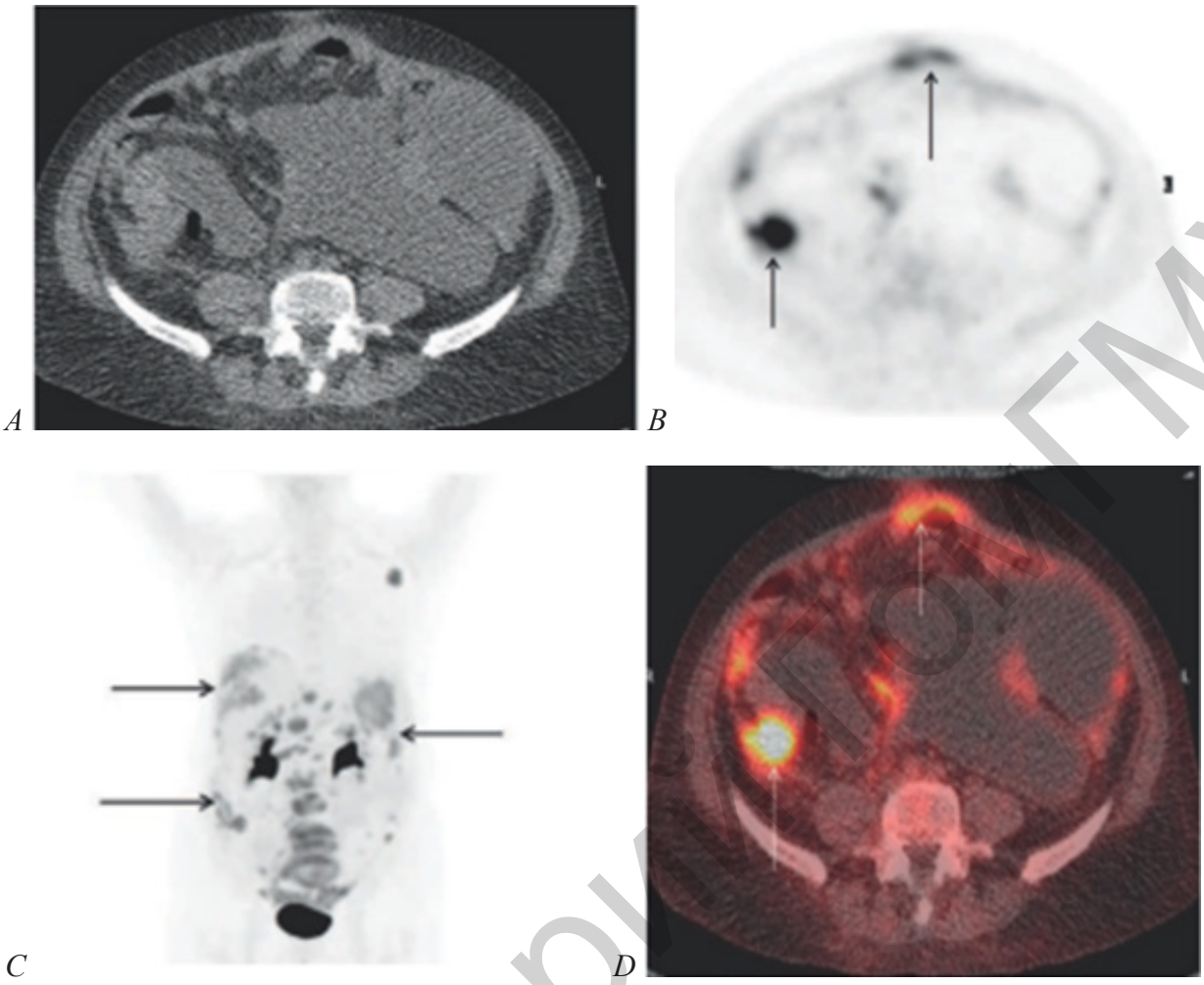

Figure 4.13 — Recurrent ovarian carcinoma, PET/CT. (A) Axial CT, (B–C) PET and (D) fused PET/CT in axial and coronal planes show multiple areas of increased FDG uptake in the anterior peritoneum and paracolic gutters

Imaging strategies in endometrial cancer

Conventional radiography

Chest radiographs are routinely obtained in all patients diagnosed to have endometrial carcinoma. Skeletal radiography or scintigraphy can be performed if bone metastases are suspected. Similar to the carcinoma of cervix, IVU and barium studies are obsolete in evaluation of endometrial carcinoma.

Transvaginal sonography is the most useful modality for detection of endometrial cancer. Patients with abnormal findings on sonography then undergo dilatation and curettage or endometrial biopsy for definitive diagnosis. Trans-vaginal sonography is also useful to determine the extent of myometrial invasion; however, MRI provides more accurate information about the degree of invasion and locoregional extent of the disease. Determining the presence and depth of myometrial invasion on MRI is important. There is six–sevenfold increased prevalence of lymphadenopathy if depth myometrial invasion is more than 50% (stage 1C) when compared with pa-

tients with less than 50% (stage 1B) or absent (stage 1A) myometrial invasion. The preoperative assessment of myometrial invasion helps to plan the extent of lymph node sampling.

MR evaluation of endometrial cancer may be difficult in elderly women with atrophic uterus as junctional zone may be indistinct (Figure 4.14). The junctional zone is also difficult to evaluate when it is irregular and thickened in women with adenomyosis and in presence of myometrial distortion by large tumor or fibroid. MRI has 87% sensitivity and 91% specificity in assessment of myometrial invasion; however, sensitivity for detection of lymph node involvement is only 50%.

Figure 4.14 — MRI, endometrial carcinoma. Sagittal gadolinium-enhanced T1-weighted fat-suppressed MR parasaggital tomogram shows the endometrial tumour (T) relatively hypointense to the avidly enhancing myometrium (black arrows), revealing deep myometrial invasion. The disease extends to the upper third of the vagina (white arrow)

Imaging strategies in carcinoma of ovary

Role of imaging in ovarian cancer is to detect and characterize adnexal masses, recognize unusual findings that may suggest atypical or alternative diagnosis, demonstrate metastases in order to prevent surgical understaging and detect specific sites of the disease that may be unresectable.

Ultrasound is the primary modality, important to detect and characterize the adnexal masses in patients who are clinically suspected to have ovarian cancer. MRI may be used in equivocal cases.

Although staging of the ovarian cancer is always surgical, preoperative CT is recommended and it is now routinely obtained. Preoperative estimation of the gross extent of the disease on imaging may guide the referral to appropriate specialty. Demonstration of GIT and urinary tract involvement helps to modify the surgical plan. Detection of distant metastases on imaging help to prevent surgical under staging, although it does not necessarily makes the patient inoperable. Metastatic ovarian cancer is often similar to primary ovarian cancer in clinical presentation as well as imaging features, hence, careful search to exclude other primary site should be made on CT. The identification of different primary with metastases to ovary on imaging may change the treatment from surgery to chemotherapy.

Similarly, identification of benign or less aggressive tumors like germ cell tumors on CT also change the management as these are treated with more conservative surgery. Although CT is the primary imaging modality for preoperative staging, MRI may be equal to CT. At present, use of MRI in ovarian cancer limited primarily because of long imaging time required for MRI evaluation of entire abdomen and pelvis, high cost and limited availability.

Investigation of a breast lump

The primary role of breast imaging is to detect and characterize abnormalities that could represent malignancy. A large number of benign conditions of the breast are diagnosed and managed clinically. Imaging of benign conditions is required to detect underlying suspicious abnormalities, if any, and to evaluate patients of symptomatic breast diseases with equivocal clinical findings. Mammography is the primary breast imaging modality; ultrasound and MRI have an important complementary role. Imaging findings are generally suggestive but not specific for most breast lesions.

Methods of examination

Mammography

Mammography is primarily a screening and not a diagnostic tool. The mediolateral oblique (MLO) and craniocaudal (CC) views are standard screening views (Figures 4.15). Mammography remains one of the principal imaging modalities for diagnosis, although its use is rarely indicated in women under the age of 35. The main indications for mammography are:

— Evaluation of breast symptoms and signs, including masses, skin thickening, deformity, nipple retraction, nipple discharge and nipple eczema.

— Breast cancer screening.

— Follow-up of patients with previously treated breast cancer.

— Guidance for biopsy, or localisation of lesions not visible on ultrasound.

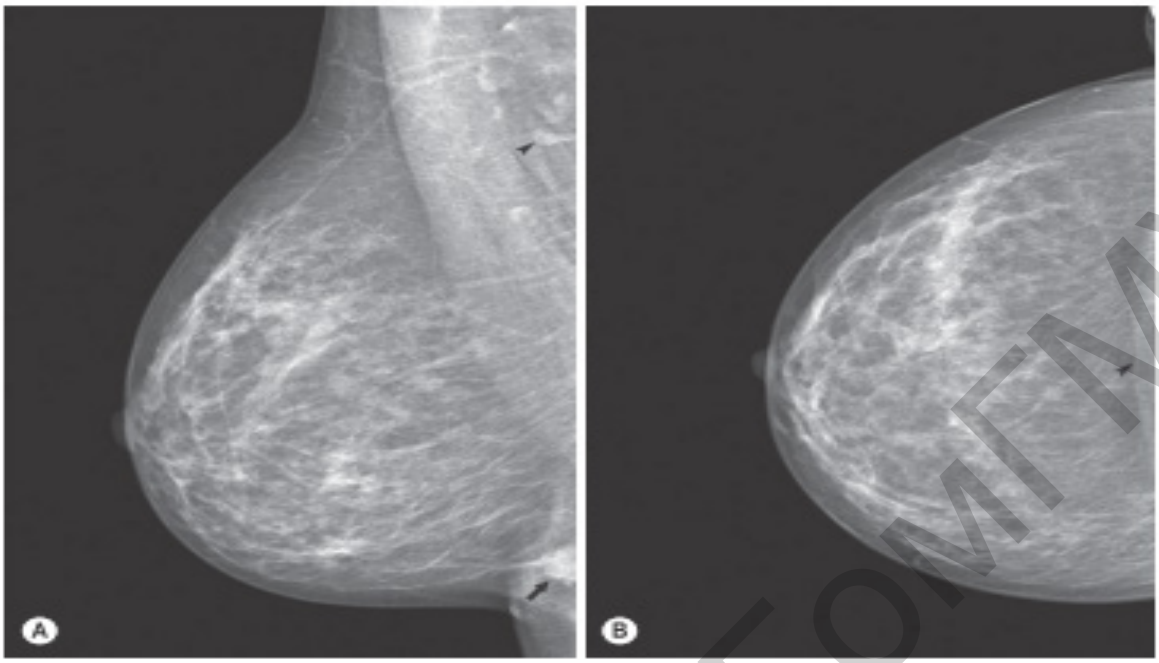

Figure 4.15 — A standard set of mammograms consists of the mediolateral oblique view (A) and the craniocaudal view (B). (A) A cancer is seen in the inframammary area on the MLO view (arrow), illustrating the importance of correct positioning to avoid missing lesions. Normal lymph nodes (arrowhead) are frequently seen on the MLO projection. (B) The cancer is not demonstrated on this correctly positioned CC view, with pectoral muscle visualised at the back of the mammogram (arrowhead)

Mammography places stringent demands on equipment and image quality. The breast is composed predominantly of fatty tissue and has a relatively narrow range of inherent densities. Consequently, special X-ray tubes are required to produce the low-energy radiation necessary to achieve high tissue contrast, enabling the demonstration of small changes in breast density. High spatial resolution is required to identify tiny structures within the breast, such as microcalcifications measuring in the order of 100 μm; and short exposure times are necessary to limit movement unsharpness. Where the breasts are thicker or are composed of denser glandular tissue, higher energy radiation is required, although radiation dose must be kept to a minimum.

Tissue density in a mammogram

According to the ACR BI-RADS Atlas Description of the breast composition and categorization of the glandular density into one of four categories is mandatory before characterization of conspicuous changes in a mammogram. The spectrum extends from the classic involutional breast (almost entirely fat, density type I) to the very glandular breast (extremely dense parenchyma, density type IV). Midrange categories represent breasts with scattered fibroglandular densities (type II) and heterogeneously dense parenchyma (density type III) (Figures 4.16).

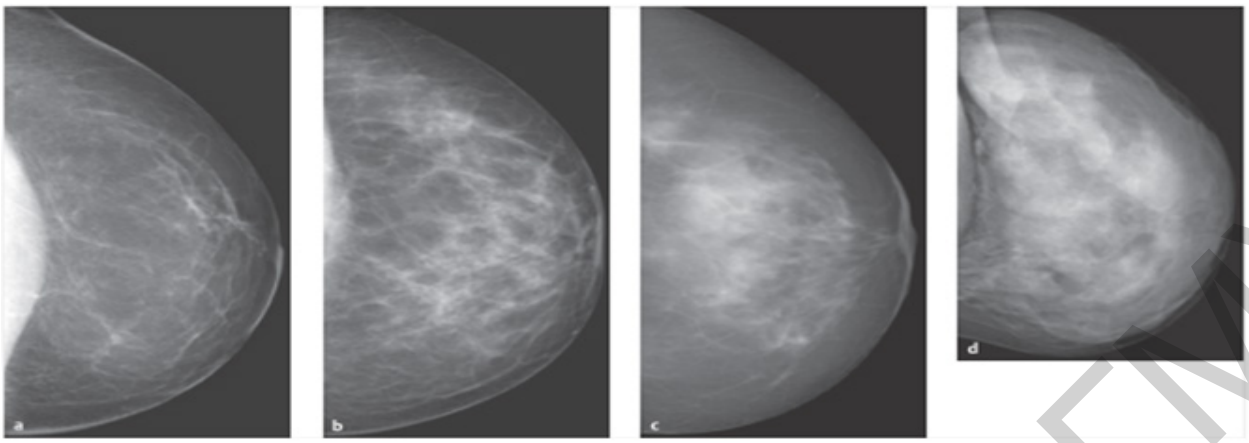

Figure 4.16 — Density types in X-ray mammography. Examples of mammograms of various density types as defined by the American College of Radiology. (a) ACR density type I breast tissue almost entirely fatty. (b) ACR density type II scattered fibroglandular tissue. (c) ACR density type III heterogeneously dense parenchyma. (d) ACR density type IV extremely dense breast

Interpretation criteria and reporting of mammograms

Mammograms should be viewed in optimum lighting conditions, light from around the films and extraneous light in the viewing room should be excluded as far as possible. The films should be checked for correct identification labeling and for radiographic quality. The standard MLO and CC views are studied with the right and left breast films **"**back to back" so that symmetry of the breast tissue can be examined.

American College of Radiology (ACR) has devised the Breast Imaging Reporting and Data System (BI-RADS), a standardized method for descry-bing the morphology of breast lesions and categorizing the findings in an unambiguous report. A lexicon of descriptive terms is an integral part of BI-RADS and is intended to provide a common language for lesion description and assessment.

The BI-RADS lexicon differentiates three primary findings regarding mammographic abnormalities:

— Mass lesions or densities.

— Calcifications.

— Architectural distortions.

The first step in mammographic interpretation should be the assessment of parenchymal density as the diagnostic accuracy of mammogram decreases with increased density of breast. The ACR BI-RADS divides breast parenchyma into four major categories based on the mammographic density. The abnormal mammographic finding is then categorized as a mass, calcification, architectural distortion or asymmetry.

Additional imaging technologies

Ultrasound

The main indications for ultrasound are:

— Evaluation of palpable abnormalities.

— Characterization of palpable mass lesions.

— Assessment of abnormalities detected on a mammogram (e.g., differentiation of cyst vs. solid mass).

— Primary technique for the assessment of breast problems in younger patients.

— Guidance for biopsy and wire localisations.

Breast ultrasound requires high-quality, high-resolution grey-scale imaging,using linear probes with high frequencies typically between 7,5 and 15 MHz (Mega Hertz) (Figures 4.17). Higher frequencies result in greater resolution, but as the frequency increases, the ability of the ultrasound beam to penetrate to deeper breast tissue decreases. Consequently, the frequency selected has to be appropriate for the size of the breast to be examined. Parameters such as harmonics and compounding are available on modern ultrasound machines and can be applied to enhance the displayed image. Their use is subject to operator preference. Techniques such as colour flow imaging (Doppler) and elastography may also have a role in lesion characterisation.

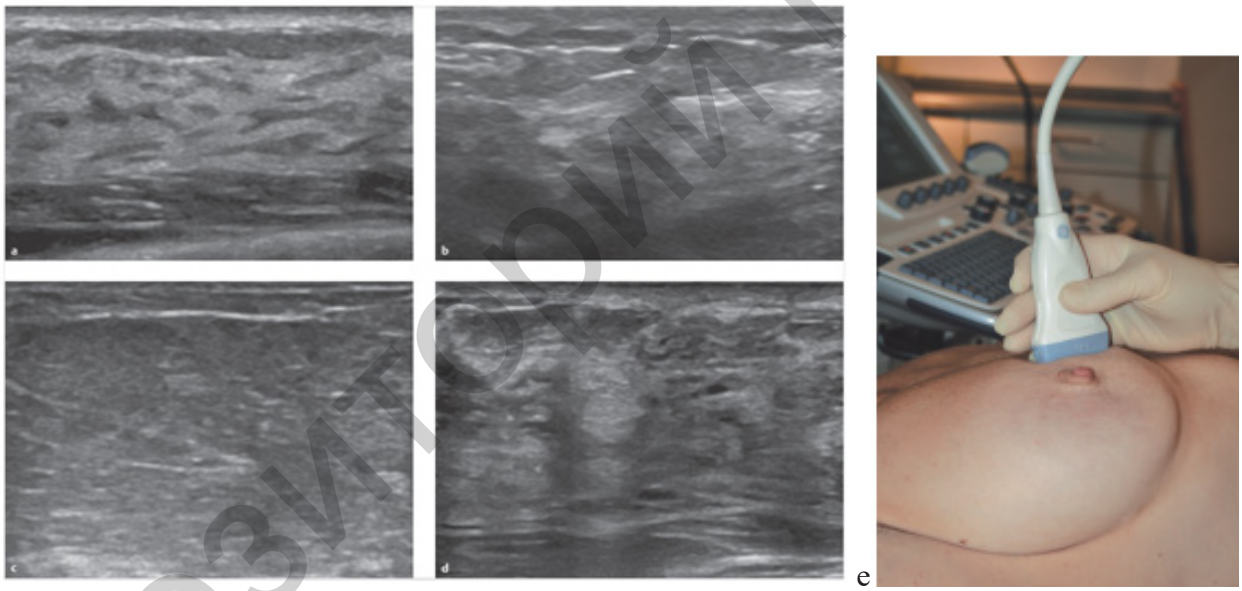

Figure 4.17 — Typical examples of different echo textures in breast sonography. (a) Glandular homogeneous. (b) Mixed lipomatous/parenchyma equivalent. (c) Homogeneous lipomatous. (d) Fibrocystic. (e) Sonographic transducer position for an ultrasound examination of the breast. Typical handling of the transducer with fixation of the base. Movement is carried out from the wrist

Interpretation (BI-RADS lexicon):

— Shape: oval, round, or irregular.

— Margin: circumscribed, or not circumscribed (indistinct, angular, microlobulated, spiculated).

— Orientation of long-axis of lesion to chest wall: parallel or not parallel.

— Echo pattern (relative to fat): anechoic, hypoechoic, hyperechoic, isoechoic, heterogeneous, or complex cystic and solid.

— Posterior features: posterior acoustic enhancement, shadowing, or combined.

— Calcifications: can be seen as echogenic foci with posterior shadowing within a mass, outside a mass, or intraductal (US usually cannot detect small microcalcifications).

— Associated features: architectural distortion, duct changes, skin changes, edema, vascularity, elasticity.

Magnetic resonance imaging

Although mammography and ultrasound remain the most frequently used techniques for imaging the breast, contrast-enhanced MRI is becoming increasingly important, largely because of its high sensitivity for detecting invasive breast cancer, which approaches 100% in many studies. MRI is the technique of choice for assessing the integrity of breast implants. It is more accurate than mammography, ultrasound or clinical examination in identifying implant failure.

Indications

— High-risk screening.

— Preoperative assessment to determine extent of the disease.

— Evaluation for recurrence or residual tumor after surgery.

— Response to therapy.

— Evaluation of postoperative scar versus recurrence.

— Assessment of implant integrity.

Advantages

— Can detect and characterize small lesions.

— Can detect greater extent of disease than depicted by mammography/US.

— Usedeffectively in dense breasts.

— No radiation exposure.

— Evaluation of axillary lymph nodes.

Limitations

— Requires the use of a contrast agent.

— Higher cost.

— Lower specificity.

Normal findings in MRI of the breast

Changes seen in the T1-weighted and T2-weighted (T1W, T2W) MR images are predominantly age-related physiological changes with respect to the composition of the breast, particularly regarding the distribution pattern and proportion of glandular and adipose tissue. The enhancement after the administration of contrast material correlates primarily with the extent of the hormonal stimulation of the glandular tissue, which, in interindividual comparisons, is more pronounced in premenopausal women than in postmenopausal women. Intraindividual fluctuations in premenopausal women depend primarily on the menstrual phase. Before (fourth week of the cycle) and during the menses (first week of the cycle), it is more pronounced than in the second and third weeks of the cycle.

Breast pathology

Cyst

Cysts are the most common cause of a discrete breast mass, although they are often multiple and bilateral. They are common between the ages of 20 and 50 years, with a peak incidence between 40 and 50 years. Simple cysts are not associated with an increased risk of malignancy and have no malignant potential. Breast cysts develop when lumina of ducts or acini become dilated and lined by atrophic epithelium. Cysts arise from terminal acini and enlarge because of obstruction or secretion imbalance. Simple cysts are common lesions and vary in size from microscopic to large palpable masses. These are frequently bilateral and multiple but all may not be identified clinically or by imaging. Cysts are common in perimenopausal age but may be seen in women of all ages. Cysts are benign lesions. Cysts may remain stable for many years or spontaneously resolve.

Cysts are classified according to their size:

— Microcyst (< 3 mm), believed to be a normal finding.

— Macrocyst (> 3 mm), present in up to 50% of adult population.

Radiographic features

Mammography

— Multiple rounded densities may belobulated.

— Cysts may leak and cause inflammation and pericystic fibrosis.

— Cystwall may calcify or the cysts may contain precipitated milk of calcium. In the mediolateral views, the x-ray beam is horizontal, allowing visualization of calcium fluid level within the cyst.

— Some cysts recur and should be reaspirated; if recurrent after second aspiration, many surgeons prefer to take a biopsy of the cyst (although the data supporting this approach are obscure).

— Tumor within a cyst is very rare but if seen usually represents a papilloma (papillary carcinoma would be the most common intracystic malignancy).

— The presence of cysts does not exclude cancer elsewhere in the breast.

On mammography, a cyst is typically seen as well-defined, round or oval mass (Figure 4.18 A). The cyst may be of variable size, solitary or may occur in clumps. A tense cyst is round, but a lax cyst may vary in shape depending upon the degree of compression applied. Calcification is infrequent and it may be seen as a thin peripheral rim or flecks of calcium near the periphery. Rarely, microcysts may contain milk of calcium fluid which on erect lateral mammography layers on the cyst floor forming so-called ‘tea-cup’ calcification. Cysts cannot be accurately diagnosed by mammography, because they cannot be distinguished from other well-circumscribed masses, unless they display characteristic pattern of calcification. However, bilateral multiple benign morphology masses on mammography most commonly represent cysts.

Mammography cannot reliably distinguish between a cyst (fluid-filled) and a proliferative process (solid tissue).

Ultrasound

Ultrasound has an important role in the diagnosis of breast cysts. Typical simple breast cyst is sharply marginated, anechoic with posterior acoustic enhancement (Figure 4.18 B). It may have angular margin, few thin septations or echogenic debris in the dependent part. These features do not necessarily make it suspicious for malignancy and can be ignored.

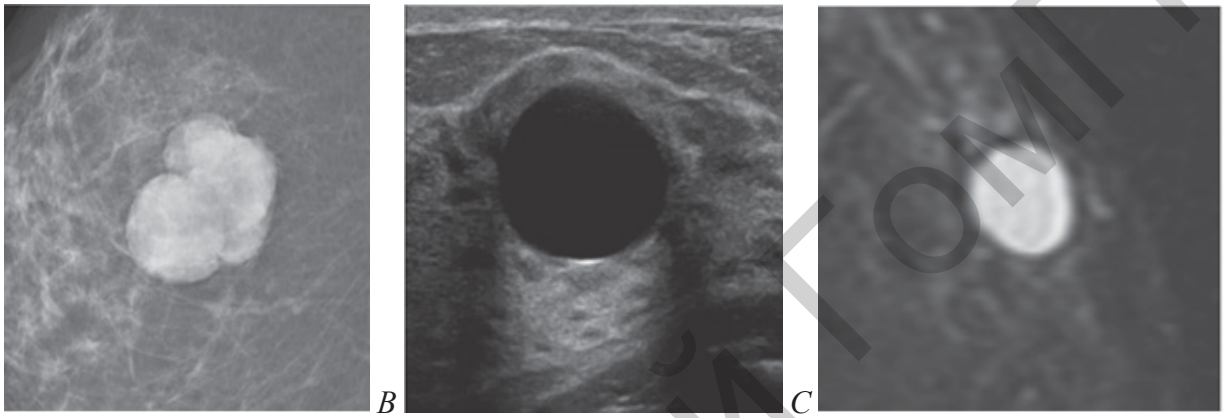

Figure 4.18 — Cyst. (A) Mammogram. A well-defined rounded mass, with an associated lucent halo typical of a cyst. (B) Sonogram. The absence of internal echoes and the posterior enhancement of the ultrasound beam are diagnostic of a cyst.
(C) T2-weighted precontrast breast MR tomogram

Posterior enhancement may not be seen if the cyst is small or close to the chest wall. Sometimes, multiple cysts may be seen forming a cluster. Ultrasound diagnosis of simple breast cyst is important as it obviates the need of any fine needle aspiration biopsy, treatment or follow-up. Cysts with debris, wall thickening and septations are referred to as complicated cysts. Chances of malignancy in a complicated cyst are less than 0,5% and hence, most complicated cysts are appropriately assigned BIRADS 3 category. Intracystic tumors are rare. If present, these are commonly intracystic papillomas; intracystic cancer is extremely rare. Indications for aspiration of complicated cysts include suspicion of cyst being an abscess, significant enlargement on follow-up, solid mass in the cyst or suspicious mammographic findings. Symptomatic cysts may also require ultrasound guided aspiration; however, half of these recur over two years.

US cyst appearance:

— Anechoic with enhanced through-transmission.

— Sharply defined anterior and posterior margins.

— Round or oval.

— Simple cysts are anechoic structures with thin, imperceptible walls and posterior acoustic enhancement.

— Complicated cysts are cysts containing internal echoes (debris).

— Cluster of microcysts are cluster of cysts < 2–3 mm separated by thin septations.

— Oil cysts are hypoechoic and have poor through-transmission. Correlate with mammography for confirmation.

On MRI, most cysts are hypointense on T1-weighted images and brightly hyperintense on T2-weighted images (Figure 4.18 C). The presence of proteinaceous contents or blood products can modify the signal intensity pattern.

Differential diagnosis. Inflamed cyst, complex cyst, cyst with intracystic proliferation, adenoma, papilloma, phyllodes tumor, invasive carcinoma, intramammary metastasis.

Fibroadenomas and related conditions

Fibroadenomas are the most common benign solid breast lesion. They are characterized by the presence of glandular and fibrous components and proli-feration of connective tissue of the lobule. They are commonly found from adolescence to age 40. Fibroadenoma may be single or multiple, unilateral or bilateral, vary in size from few millimeters to a very large size, though most are less than 3 cm in diameter. Fibroadenomas are hormone-dependent lesions. They regress with age and necrosis within the tumor results in coarse calcification.

Radiographic features

On mammography, fibroadenomas are seen as well-defined, rounded or oval masses. Coarse calcifications may develop within fibroadenomas, particularly in older women (Figure 4.19 A).

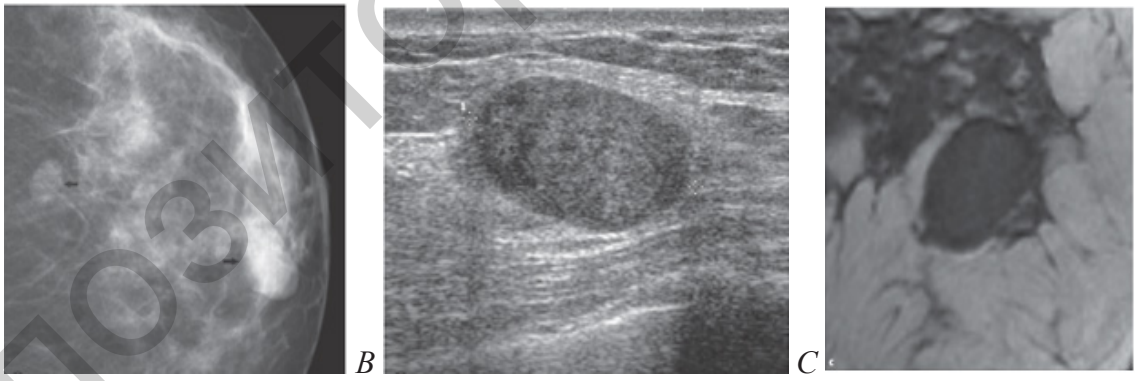

Figure 4.19 — Fibroadenoma. (A) Two well-defined masses on mammogram (arrows). (B) Ultrasound of the lesion nearer the nipple showed a well-defined oval mass. Both lesions were confirmed as fibroadenomas on ultrasound-guided core biopsy. (C) T1-weighted precontrast breast MR tomogram

Ultrasound features have been described that are characteristic of benign masses. These include hyperechogenicity compared with fat, an oval or well-circumscribed lobulated or gently curving shape and the presence of a thin echogenic pseudocapsule. If these features are present with no features suggestive of malignan-

cy, then a mass can be confidently classified as benign. These features are demonstrated by fibroadenomas. Most fibroadenomas are isoechoic or mildly hypoechoic relative to fat, with an oval shape and lobulated contour (Figure 4.19 B). A thin echogenic pseudocapsule may be seen. Percutaneous biopsy may be avoided in women under the age of 25, where the risks of any mass being malignant are very small; however, in most cases, even though the mass appears benign, percutaneous biopsy is undertaken to confirm the diagnosis.

Magnetic resonance imaging is not recommended for a mammographically well-defined mass that is suspected to be a fibroadenoma. If MRI is performed, predominantly fibrous fibroadenomas are hypointense on all sequences and show no enhancement (Figure 4.19 C). Fibroadenomas, which are cellular and contain adenomatous or myxoid tissue, show an intermediate to high-signal intensity on T2-weighted images and most have well-circumscribed margins with low intensity internal septae.

The enhancement is significant and homogenous; usually delayed (type 1). Visualization of nonenhancing septae is diagnostic of fibroadenoma. A fibroadenoma with a diameter of more than 6 cm is defined as a giant fibroadenoma. It may fill a large part of the breast. It is a benign lesion and most commonly seen in adolescent females. Phyllode tumor is a close differential diagnosis however; it is generally seen in later decades of life. Lactating fibroadenoma occurs in young females, and is associated with pregnancy or lactation. The lactating fibroadenoma may attain enormous size. Juvenile fibroadenoma is another variant which may be seen in teenage females. It often grows rapidly and becomes very large.

Fibroadenomas are not premalignant lesions. As there is epithelium within fibroadenoma, cancer can develop just as it can in normal ductal epithelium. Hence, ill-defined margins, microcalcifications and increase in size on follow- up should arouse concern.

Fibroadenomas must be distinguished from well-circumscribed carcinomas; this is done by percutaneous biopsy. Phyllodes tumour can also have a similar appearance to fibroadenoma, leading to diagnostic difficulties. The pathological characteristics can also be similar to those of large fibroadenomas. Most phyllodes tumours are benign, but some (less than 25%) are locally aggressive and may even metastasise. When a diagnosis of phyllodes tumour is made, surgical excision must be complete with clear margins to prevent the possibility of recurrence. Many larger fibroadenomas (over 3 cm) and those that show a rapid increase in size are excised in order to avoid missing a phyllodes tumour.

Abscess

A breast abscess is a localized intramammary collection of pus in a cavity formed by an inflammatory degeneration of tissue. Abscesses may occur after interventional or surgical procedures, or in association with mastitis.

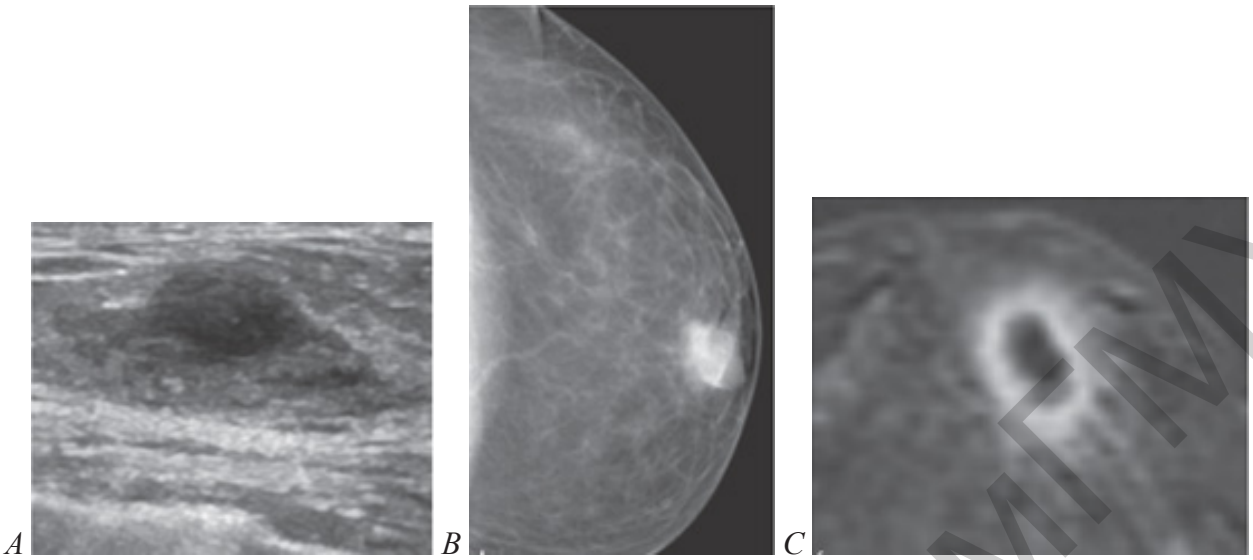

Figure 4.20 — Abscess. (A) Ultrasonogram. (B) Mammogram. (C) Contrast-enhanced breast MRI tomogram

Imaging (Figures 4.20)

— Sonography: hypoechogenic mass with internal echoes; thickened walls.

— Mammography: hyperdensity, nonspecific.

— Breast MRI: mass:

○ T1-weighted precontrast image: hypointense, nonspecific.

○ T2-weighted: hyperintense, nonspecific.

○ After administration of contrast medium: obligatory strong enhancement of the thickened abscess wall; reactive hyperemia of the surrounding structures.

Differential diagnosis. Carcinoma with central necrosis, triple-negative carcinoma.

Breast cancer

Breast cancer is the second leading cause of cancer death (lung is first) in women. The presumed cause of breast cancer is DNA damage, with estrogen playing a key role. Seventy-five percent of breast cancers occur in women with no risk factors.

Diagnosis of the breast cancer

Breast cancer may be detected in preclinical stage on screening mammo-graphy. Others are detected by self breast examination (SBE) or clinical breast examination (CBE). Symptomatic breast cancers present with a palpable mass, focal tenderness, nipple discharge, skin retraction or ulceration, or sometimes as a metastatic disease with occult primary site.

Mammography is the primary modality for detection of breast cancer; ultrasound and MRI complement mammography in detection of breast cancer. However, there are no characteristic features of breast cancer on imaging. It is interesting to note that mammographic interpretation has a category of definitely benign lesions (BIRADS 2), but there is no category of definitely malignant lesions.

Mammography only detects lesions which are either suspicious (BIRADS 4) or highly suspicious (BIRADS 5) for malignancy. Hence, all such lesions need to be subjected to biopsy for the definitive diagnosis of breast cancer. Image guided breast biopsy is an important tool for the diagnosis of breast cancer.

Breast cancers are classified into various pathological subtypes according to the WHO system. These cannot be determined on imaging. There are no imaging features which are specific to any pathological subtype of the breast cancer.

Imaging appearance of invasive breast cancer

Mammography

Carcinomas typically appear as ill-defined or spiculate masses on mammography. Lower-grade cancers tend to be seen as spiculate masses, due to the presence of an associated desmoplastic reaction in the adjacent stroma. Higher-grade tumours are usually seen as an ill-defined mass, but sometimes a rapidly growing tumour may appear relatively well defined, with similar appearances to a benign lesion such as a fibroadenoma (Figure 4.21 A).

Primary signs. With these findings, 20%–30% will have breast cancer:

— Mass with spiculated or ill-defined margin.

— Malignant intratumoral calcifications.

Secondary signs (occur as a result of the tumor; less specific signs):

— Architectural distortion.

— Skin, nipple, trabecular changes (thickening, retraction).

— Abnormal ductal patterns.

— Lymphadenopathy.

— Asymmetry of breast tissue.

Many breast cancers arise from areas of ductal carcinoma in situ (DCIS) and are associated with microcalcifications on mammography. This is particularly true for high-grade invasive ductal carcinomas that are often associated with high-grade DCIS.

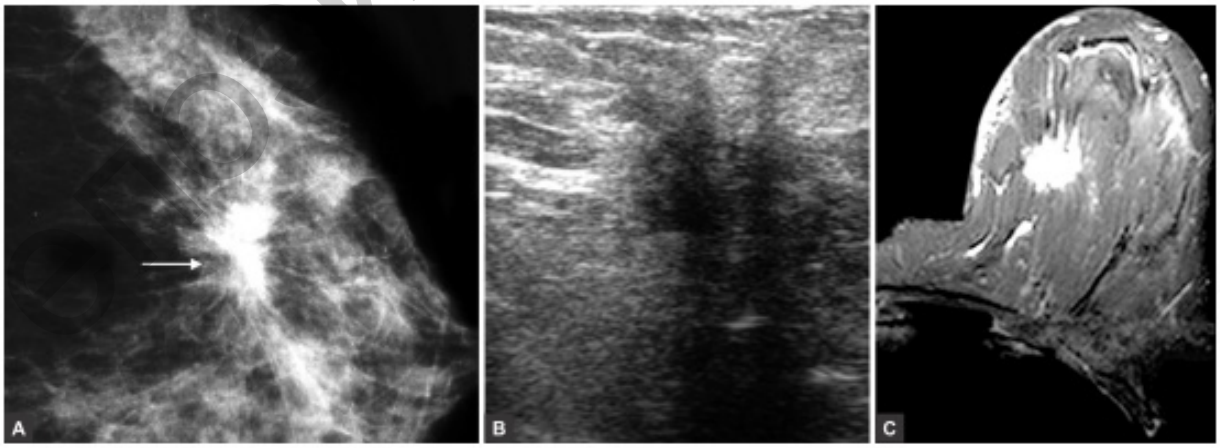

Figure 4.21 — Invasive ductal carcinoma. (A) Mammogram shows a high density, irregular, spiculated mass (arrow); (B) Ultrasound shows a hypoechoic, irregular, spiculated mass with distal acoustic shadowing; (C) Contrast enhanced T1-weighted MRI scan of another woman shows a spiculated, intensely enhancing mass

Sometimes the only clue to the presence of an invasive tumour may be abnormal trabecular markings, known as an architectural distortion, or the presence of microcalcifications, which tend to be visible even when the breast parenchyma is dense. The ability to perceive small or subtle cancers on a mammogram is improved by having the two standard mammographic views available and seeking out previous studies for comparison. An increase in the size of a mass or the presence of a new mass is suspicious of malignancy, whereas a lesion that remains unchanged over many years is invariably benign. Multiple masses in both breasts would favour a benign disease such as cysts or fibroadenomas.

Ultrasound

There are characteristic malignant features on ultrasound (Figure 4.21 B):

— Carcinomas are seen as ill-defined masses and are markedly hypoechoic compared with the surrounding fat.

— Carcinomas tend to be taller than they are wide (the anterior to posterior dimension is greater than the transverse diameter).

— There may be an ill-defined echogenic halo around the lesion, particularly around the lateral margins, and distortion of the adjacent breast tissue may be apparent, analogous to spiculation on the mammogram.

— Posterior acoustic shadowing is frequently observed, due to a reduction in the through transmission of the ultrasound beam in dense tumour tissue.

Poorly differentiated, high-grade tumours are more likely to be well defined, without acoustic shadowing; hence, the importance of carrying out a biopsy of solid masses even when the ultrasound appearances are benign. Microcalcifications are sometimes observed, associated with high-grade tumours arising in areas of DCIS, although this is less frequently encountered than with mammography. Lobular carcinomas can be difficult to demonstrate on ultrasound. They may produce vague abnormalities, such as subtle alterations in echotexture, or the ultrasound findings may even be normal.

Doppler imaging and elastography can help differentiate benign from malignant masses. Doppler may show abnormal vessels that are irregular and centrally penetrating in a malignant mass. Conversely, benign lesions such as fibroadenomas tend to show displacement of normal vessels around the edge of a lesion. Shear wave elastography of malignant lesions tends to demonstrate areas of increased elasticity, with the area of increased tissue stiffness larger than the grey-scale abnormality.

Ultrasound is a useful tool in the local staging of breast cancer preoperatively. It tends to be a better predictor of tumour size than mammography and may detect intraductal tumour extension. Ultrasound may also detect small sa-tellite tumour foci not visible on mammography.

It has long been recognised that involvement of axillary lymph nodes is one of the most important prognostic factors for women with breast cancer. Traditionally, the axilla has been staged at the time of surgery by lymph node sampling procedures,

sentinel node biopsy or clearance of the axillary lymph nodes. Surgical clearance of axillary lymph nodes carries the risk of significant postoperative morbidity, with some women developing disabling lymphoedema in the arm. Ultrasound can identify abnormal nodes preoperatively that can then be biopsied percutaneously under ultrasound guidance, allowing a preoperative diagnosis of lymph node involvement to be made in just over 40 % of patients who are lymph node positive. This enables the more radical axillary clearance to be targeted to those patients with a preoperative diagnosis of axillary disease, with the sampling or sentinel node procedures reserved for those patients with a much lower risk of axillary involvement.

Breast MRI: focus, mass:

— T1W precontrast image: hypointense, nonspecific.

— T2W: 70% hypointense, otherwise isointense, nonspecific.

— After administration of contrast medium: typically displays strong initial enhancement (Figure 4.21 C); in 30 to 50% of cases there is subsequent washout phenomenon; 50% show ring enhancement.

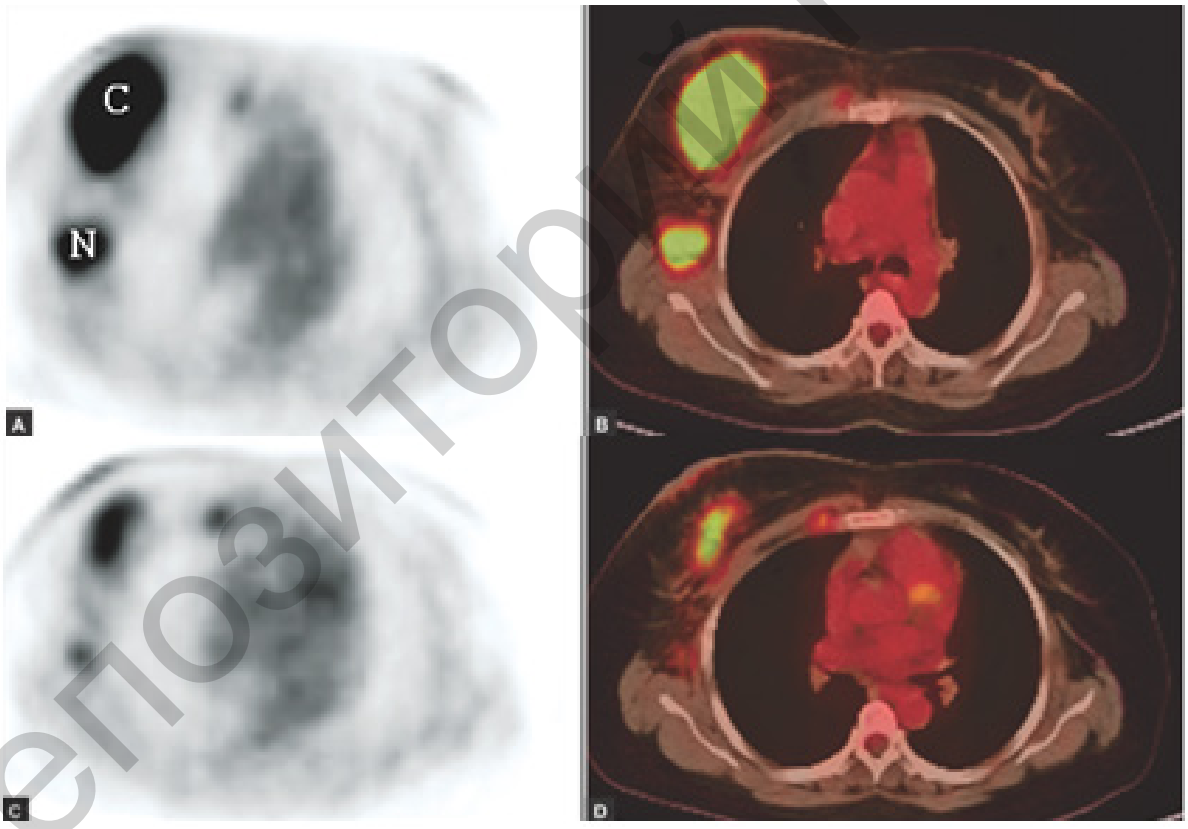

Figure 4.22 — A 43-year-old lady with ductal carcinoma of right breast with ipsilateral axillary lymph node metastasis. Baseline PET (A) and PET-CT (B) tomograms show FDG avid primary breast mass (C) with FDG avid metastatic axillary nodes (N). PET-CT was repeated after 3 cycles of neoadjuvant chemotherapy to response. Postchemotherapy images (C and D) showed significant reduction in size as well as FDG uptake of both the primary tumors as well as lymph nodes. The PET-CT impression was responder which was confirmed on histopathology

Nuclear medicine techniques

Sestamibi imaging using ^{99m}Tc-MIBI and PET imaging techniques using ^{18}F-FDG have been developed following the observation that many breast cancers show uptake of these isotopes. Breast-specific gamma imaging (sometimes referred to as scintimammography) and FDG positron emission mammography (PEM) have significantly improved in recent years with the development of high-resolution mini-camera detectors designed specifically for imaging the breast (Figures 4.22). Indications for use overlap with those for MRI, including local staging, searching for a mammographically occult primary, particularly where there is dense mammographic background pattern, and detecting recurrence in the postsurgical breast. Research is continuing, but so far these techniques have failed to establish a place in routine practice.

PET-CT is a powerful metabolic imaging method for breast cancer. Currently, it has limited role in primary tumor detection and axillary nodal staging. The major utility of PET-CT lies in detection on extra-axillary nodal metastasis and distant metastasis (Figures 4.22). It also appears to be very useful for monitorring treatment response and detection of recurrent disease. The availability of newer tracers, hybrid PET-MRI and positron emission mammography might redefine its role in management of breast cancer.

The differential diagnosis of malignancy

Many apparently suspicious findings seen on mammography or ultrasound can be caused by benign disease or even normal breast tissue. A surgical scar may result in a spiculate mass or an architectural distortion. Radiographers should be encouraged to record the presence and position of any scars when performing a mammogram to aid image interpretation by the film reader.

Infection and inflammatory processes in the breast can be mistaken for malignancy on mammography and ultrasound. Breast abscesses are typically encountered in young lactating women. Treatment is with antibiotics and aspiration of the pus, frequently under ultrasound guidance. Inflammation in a non-lactating breast is a more worrying feature, although infections and more unusual inflammatory conditions such as granulomatous mastitis can occur.

Superimposition of normal breast tissue may produce apparent masses, distortions or worrying asymmetric densities on mammography. These summation shadows are usually evaluated with additional mammographic views. Ultrasound of the area of mammographic concern can help to determine whether a lesion is truly present.

Brief notes on breast screening

Mammographic screening is of benefit in reducing mortality in the over-50–year age group. The aim of a screening programme is to reduce mortality in the 55 – 69 age group. X-ray mammography is the initial screening test of choice.

Male reproductive system imaging

Imaging of the prostate gland

The prostate gland is an extraperitoneal fibromuscular gland surrounding the prostatic urethra at the bladder base. It is separated into a peripheral zone posteriorly, and a central zone and transitional zone more anteriorly. These zones constitute 70%, 25%, and 5% of the prostate gland, respectively. The transitional zone surrounds the proximal prostatic urethra, whereas the central zone surrounds the transitional zone and ejaculatory ducts. The prostate gland is also divided craniocaudally into the prostate base (superiorly), mid gland, and apex (inferiorly). The anterior fibromuscular stroma is a thick layer of nonglandular tissue that forms the anterior surface of the prostate gland, and the paired neurovascular bundles, responsible for erectile function, are located within the periprostatic fat posterolateral to the prostate gland at the 5 o'clock and 7 o'clock positions. The central and transitional zones are not well demarcated on cross-sectional imaging and are collectively referred to as the central gland. On US, the peripheral zone is homogeneous and hyperechoic, whereas the central gland is more heterogeneous and hypoechoic, a differentiation that becomes more marked as the prostate ages and undergoes changes of benign prostatic hyperplasia (BPH).

On CT, the peripheral zone is homogeneous and hypoattenuating relative to the more heterogeneously enhancing central gland. However, CT is not generally used for primary evaluation of the prostate gland and seminal tract, given its suboptimal soft contrast resolution.

On T1-weighted MR images, the peripheral zone and central gland have low-intermediate signal intensity relative to the skeletal muscle and are not well demarcated. On T2-weighted MR images, the peripheral zone has predominantly high signal intensity with thin linear low signal intensity fibrous septa, whereas the central gland has low-intermediate signal intensity relative to skeletal muscle. The anterior fibromuscular stroma has low T1-weighted and T2-weighted signal intensity.

The seminal vesicles are extraperitoneal paired accessory sex glands that are located superior and posterior to the prostate gland. They are essentially long tubes that are convoluted to become approximately 3 cm in length and 1.5 cm in width. The seminal vesicles narrow inferomedially to form the seminal vesicle ducts. On US, the seminal vesicles appear as elongated hypoechoic septated cystic structures. On CT, they are seen as fluid-containing structures with a bow tie configuration. On T1-weighted MR images, the seminal vesicles have intermediate signal intensity. On T2-weighted images, the multiple tubular convolutions are well seen and contain very high signal intensity fluid surrounded by low signal intensity walls (Figure 4.23).

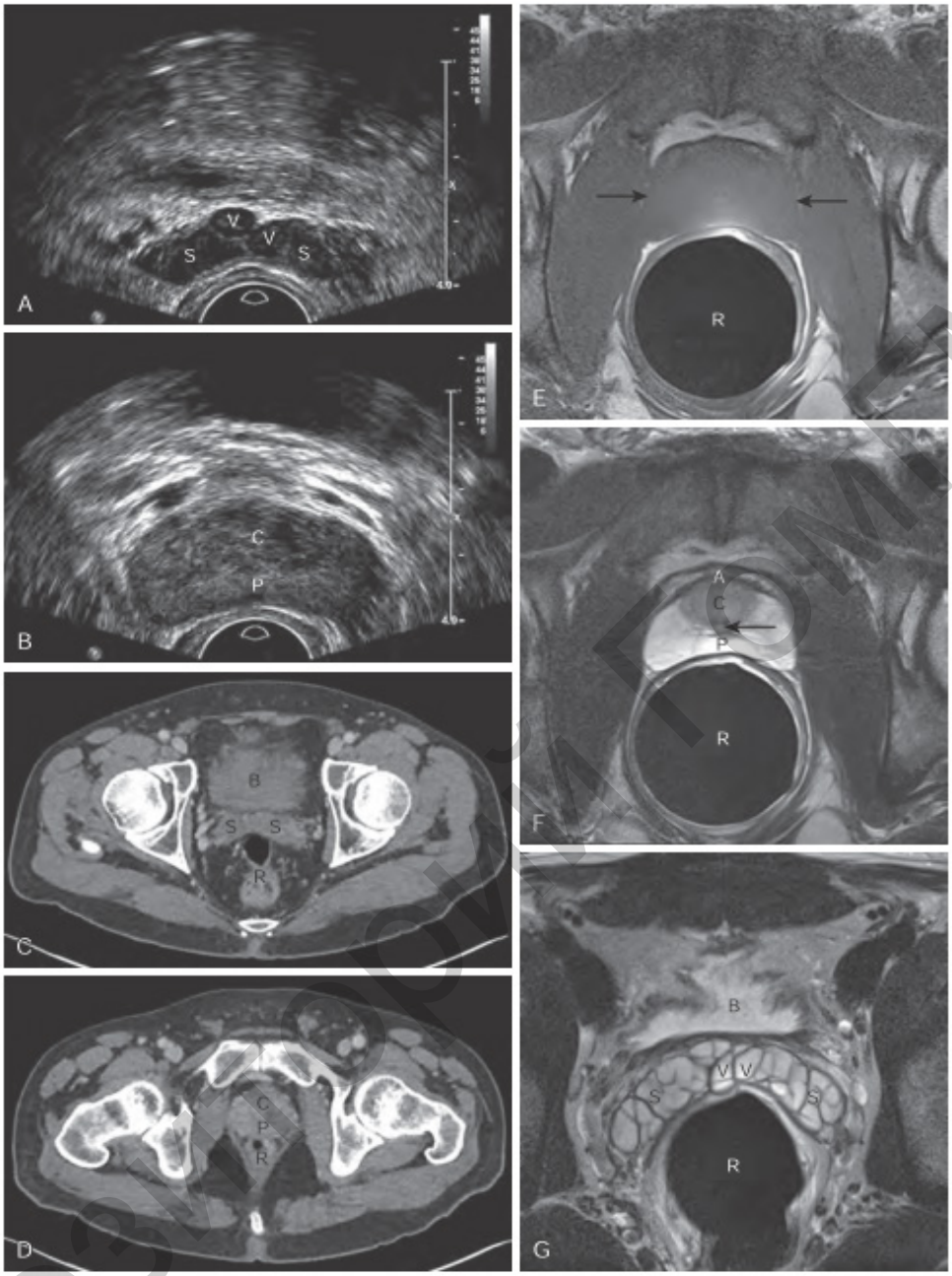

Figure 4.23 — Normal prostate gland and seminal tract on US, CT, and MRI. (A and B) Transverse transrectal ultrasound (TRUS) images through pelvis show seminal vesicles (S), ampullary portions of vasa deferentia (V), and peripheral zone (P) and central gland (C) of prostate gland. (C and D) Axial contrast-enhanced CT images through pelvis demonstrate seminal vesicles (S) along with peripheral zone (P) and central gland (C) of prostate gland and their relationships to urinary bladder (B) and rectum (R). (E) Axial T1-weighted MR image through pelvis reveals prostate gland (between arrows) anterior to rectum (R). Note that peripheral zone and central gland are not well demarcated. (F and G) Axial T2-weighted MR tomograms through pelvis show high signal intensity peripheral zone (P), low-intermediate signal intensity central gland (C), and low signal intensity anterior fibromuscular stroma (A) of prostate gland, prostatic urethra (arrow) within posterior aspect of central gland, seminal vesicles (S), and ampullary portions of vasa deferentia (V) and their relationships to urinary bladder (B) and rectum (R)

The paired vasa deferentia are continuations of the epididymal tails, which ascend from the scrotum within the spermatic cords and into the pelvis via the deep inguinal rings, course posteriorly along the lateral pelvic walls, cross over the ureters, and then curve along the superiomedial aspect of the seminal vesicles, where they become more dilated with thicker walls to form the ampullary portions. These then join with the paired seminal vesicle ducts to form the ejaculatory ducts, which are 1 to 2 mm in width, and extend inferiorly through the central zone of the prostate gland to drain into the prostatic urethra on both sides of the verumontanum.

The paired Cowper (bulbourethral) glands are peasized structures that are located within the urogenital diaphragm on either side of the membranous urethra. They each have a single duct that extends through the corpus spongiosum to drain into the bulbar urethra. Given their small size, they are not well visualized on cross-sectional imaging studies.

Imaging

Imaging of the prostate and the urinary tract is not recommended in the routine evaluation of men with prostatism unless there are symptoms suggesting complications of BPH, findings suggesting another diagnosis (e.g., hematuria, marked prostatic asymmetry), or a history of previous urologic surgery.

TRUS and MRI provide detailed information about the internal structure of the prostate and pathologic prostate enlargement. These modalities are more accurate in estimating prostate volume than transabdominal ultrasound. Transabdominal ultrasound is the preferred method of determining postvoid residual volume. The significance of an increased postvoid residual volume is that it indicates bladder dysfunction and is associated with a less favorable response to treatment or treatment failure.

Differential diagnosis

In the setting of lower urinary tract symptoms, other causes of bladder outlet obstruction, including urethral stricture, prostate cancer, bladder neck contracture, and neurogenic disease, should also be considered.

Prostate enlargement, specifically involving the transitional zone, is most commonly secondary to changes of BPH. However, up to 20% of prostate cancers will occur in the transitional zone. Identifying a transitional zone cancer in the setting of BPH can be a diagnostic challenge, even at high-quality MRI.

BPH nodules, particularly stromal nodules, can mimic tumor because they often show restricted diffusion and abnormal perfusion. Recognition of well-marginated borders on small T2-weighted imaging, sometimes best appreciated on coronal and sagittal sequences, is key in distinguishing stromal nodules from tumor. If tumor is not identified in the peripheral zone on MRI in the setting of an elevated PSA, indeterminate or suspicious nodules in the transitional zone can be targeted with fusion biopsy.

Benign and malignant focal prostate lesions

The most commonly used diagnostic imaging techniques for prostate evaluation are transrectal ultrasound (TRUS) and MRI. Benign findings such as cysts and calcifications are typically incidental, usually found on routine investigation for other conditions; most benign processes such as BPH and prostatitis require little investigation. TRUS can provide high-resolution images of the prostate and real-time guidance for intervention such as biopsy, aspiration, and drainage, without the use of radiation. Magnetic resonance imaging accurately delineates the internal prostatic anatomy but is not routinely used for the investigation of benign prostate lesions owing to its high cost and relatively limited availability. Relative to these modalities, radiography and computed tomography have limited roles in the evaluation of most prostate processes.

Differential diagnosis of malignancy

An elevated PSA level is suggestive of prostate cancer. However, the PSA value may be elevated in benign conditions such as BPH and prostatitis. The probability of prostate cancer is 1% with a PSA level between 0 and 2 ng/ml, 15% with a PSA level between 2 and 4 ng/ml, 25% with a PSA level between 4 and 10 ng/ml, and more than 50% with a PSA level greater than 10 ng/ml. Local prostate cancers can be difficult to differentiate from prostatitis and BPH on imaging alone. TRUS sextant and/or fusion biopsy is often necessary for histologic diagnosis.

In the setting of lower urinary tract symptoms, other causes of bladder outlet obstruction, including urethral stricture, prostate cancer (Figures 4.24–4.25), bladder neck contracture, and neurogenic disease, should also be considered.

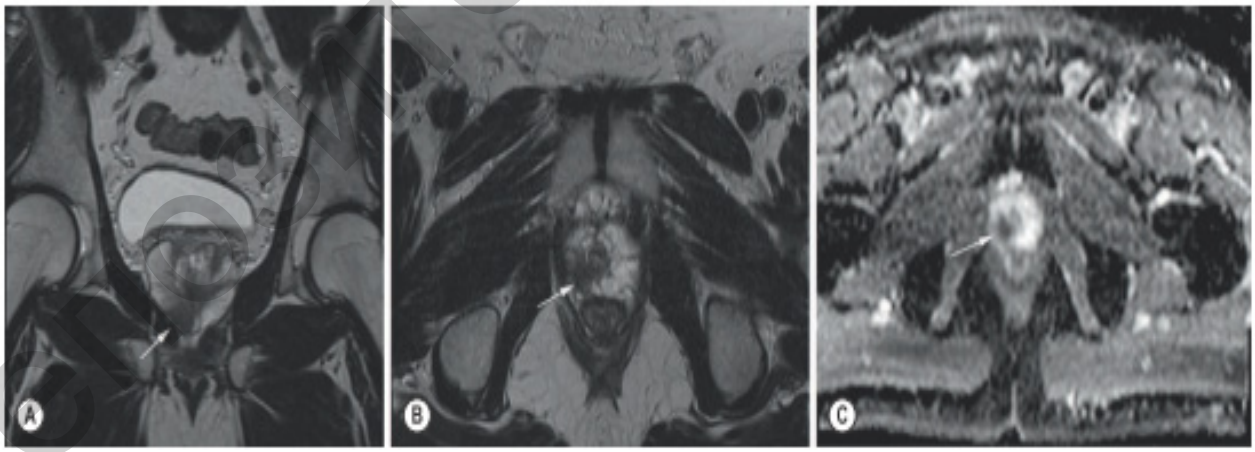

Figure 4.24 — (A) MRI of a primary prostate cancer. T2-weighted coronal and (B) axial images show there is low signal right apical peripheral zone tumour. The tumour extends to the capsular margin (arrow) but there is no confirmatory evidence of extracapsular spread indicating T2 disease. (C) Diffusion-weighted imaging demonstrates restriction within this tumour, depicted as a low signal intensity area on the apparent diffusion coefficient map

Prostate enlargement, specifically involving the transitional zone, is most commonly secondary to changes of benign prostatic hyperplasia. However, up to 20% of prostate cancers will occur in the transitional zone. Identifying a transitional zone cancer in the setting of BPH can be a diagnostic challenge, even at high-quality MRI.

Benign prostatic hyperplasia nodules, particularly stromal nodules, can mimic tumor because they often show restricted diffusion and abnormal perfusion. Recognition of well-marginated borders on small T2-weighted imaging, sometimes best appreciated on coronal and sagittal sequences, is key in distinguishing stromal nodules from tumor. If tumor is not identified in the peripheral zone on MRI in the setting of an elevated PSA, indeterminate or suspicious nodules in the transitional zone can be targeted with fusion biopsy.

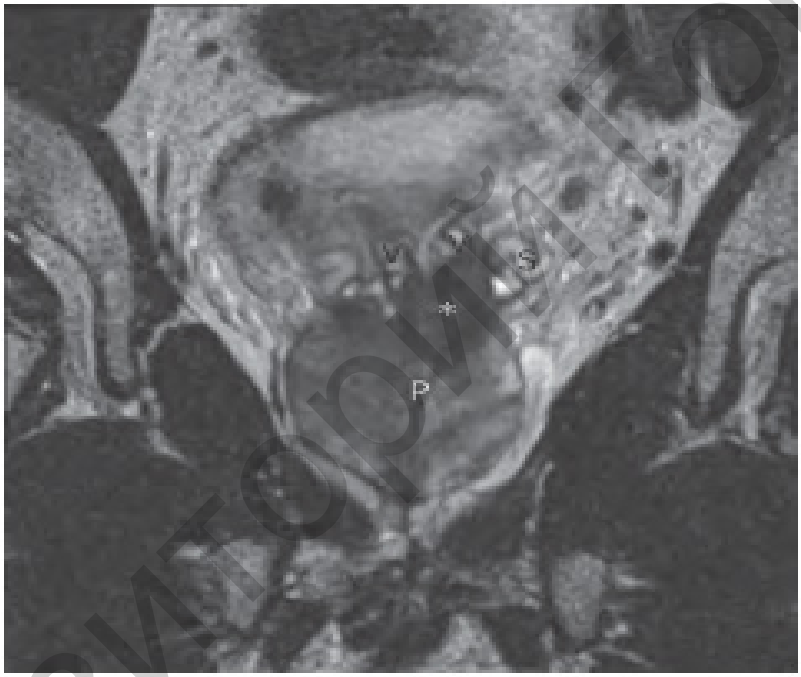

Figure 4.25 — Extracapsular spread of prostate adenocarcinoma on MRI.
Coronal T2-weighted MR image through pelvis shows low signal intensity mass (*) in left base of prostate gland (P) which invades left seminal vesicle (S) and vasa deferentia (V)

Imaging of the scrotum

Scrotal imaging (Figures 4.26–4.27) has been one of the undeniable success stories of modern radiology. The scotum is predominantly imaged for two clinical indications: the painless scrotal mass and the acute scrotum. Both conditions predominantly affect young men in the second through fourth decades of life. Rapid and accurate diagnosis is the goal of all imaging. Among several imaging modalities available, ultrasonography and magnetic resonance imaging are used predominantly, whereas computed tomography, angiography, and nuclear medicine studies are rarely used as primary imaging modalities for disorders of the scrotum.

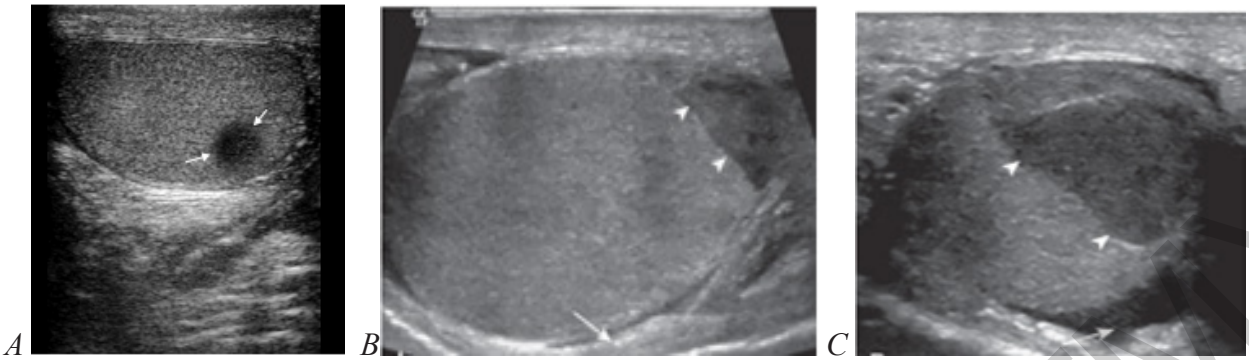

Figure 4.26 — (A) Ultrasonogram showing a nonpalpable seminoma (arrow) of testis. Testicular hematoma. (A) Sagittal gray-scale ultrasound image of the testis in a young man struck in the scrotum with a baseball bat shows a testicular parenchymal hematoma (arrow-heads) with edema and thickening of the scrotal skin (arrow). (B) Transverse ultrasound tomogram of the testis shows the testicular hematoma (arrowheads) and a small hematocele (arrow)

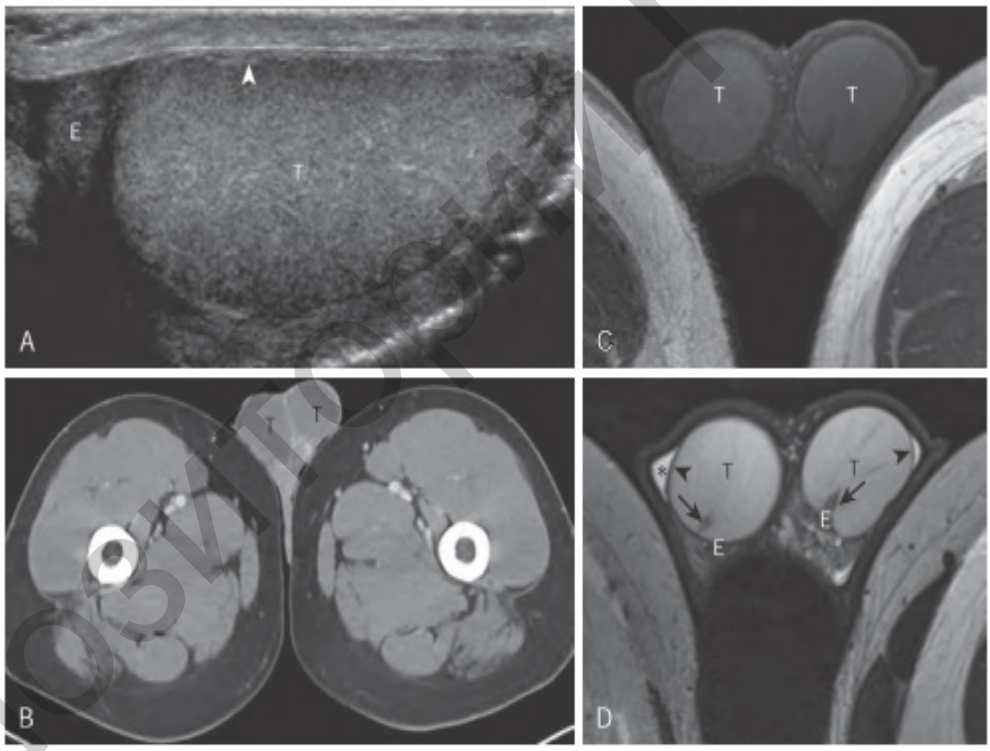

Figure 4.27 — Normal testicles and epididymides on US, CT, and MRI. (A) Longitudinal US image through scrotum demonstrates homogeneous echotexture of testicle (T) and epididymal head (E) along with thin echogenic tunica albuginea (arrowhead). (B) Axial contrast-enhanced CT image through scrotum reveals homogeneous soft tissue attenuation of testicles (T). (C) Axial T1-weighted MR image through scrotum shows homogeneous intermediate signal intensity of testicles. (D) Axial T2-weighted MR image through scrotum demonstrates high signal intensity of testicles along with low signal intensity linear septa that radiate toward mediastinum testis (arrows), low signal intensity epididymides (E), thin low signal intensity tunica albuginea (arrowheads), and physio-logic fluid (*) between visceral and parietal layers of tunica vaginalis

Modern ultrasonography provides high-resolution images of the scrotum and its contents, is relatively inexpensive and quick to perform, has no known bioeffects, and allows dynamic maneuvers such as the Valsalva maneuver to be incorporated into the examination. However, ultrasound imaging requires skill and is therefore operator dependent. Scrotal torsion is a medical emergency. It occurs mostly in adolescents and produces acute scrotal pain. US can confirm the diagnosis by demonstrating absence of flow in the torsed testicle.

MRI provides excellent tissue detail. Contrast-enhanced MRI may allow diagnosis of some benign masses that are indeterminate on ultrasonography. MRI also may aid detection of undescended testes that are not visualized on ultrasonography. In the acute scrotum, MRI can help diagnose testicular torsion; and when dynamic contrast-enhanced MRI is used in combination with T2- and T2*-weighted images, testicular necrosis may be diagnosed. MRI is more expensive, takes slightly longer to perform, and cannot be used in patients with pacemakers, implants, and claustrophobia.

V. INTRODUCTION IN RADIOLOGY ENDOCRINE SYSTEM

Thyroid uptake and imaging

The use of iodine-131 (^{131}I) for measuring thyroid functional parameters and imaging the gland has historically served as the nucleus of the evolution of the field of nuclear imaging (Figure 5.1).

Most thyroid imaging techniques capitalize on some phase of hormone synthesis within the thyroid gland. Iodides or iodide analogs are actively transported into the thyroid gland, a process called trapping. Technetium-99m pertechnetate does not undergo organification to form thyroid hormone; instead, after trapping, it slowly "washes" from the gland.

The major advantages of ^{131}I are its low price and ready availability. The high thyroid dose makes ^{131}I undesirable for routine imaging of the thyroid. Technetium-99m pertechnetate is trapped by the thyroid in the same manner as iodides but is not organified; therefore, it is released over time as unaltered pertechnetate ($^{99m}TcO4^-$) ion. The low absorbed dose to the thyroid permits administration of higher doses and therefore allows for more rapid imaging of the gland.

Iodine uptake test

The diagnosis of hyperthyroidism or hypothyroidism, however, is not made by using radioactive iodine uptake but should be made by serum measurements of thyroid hormone and thyroid-stimulating hormone (TSH). However, the thyroid uptake can be used to differentiate Grave's disease from subacute thyroiditis or factitious hyper-thyroidism.

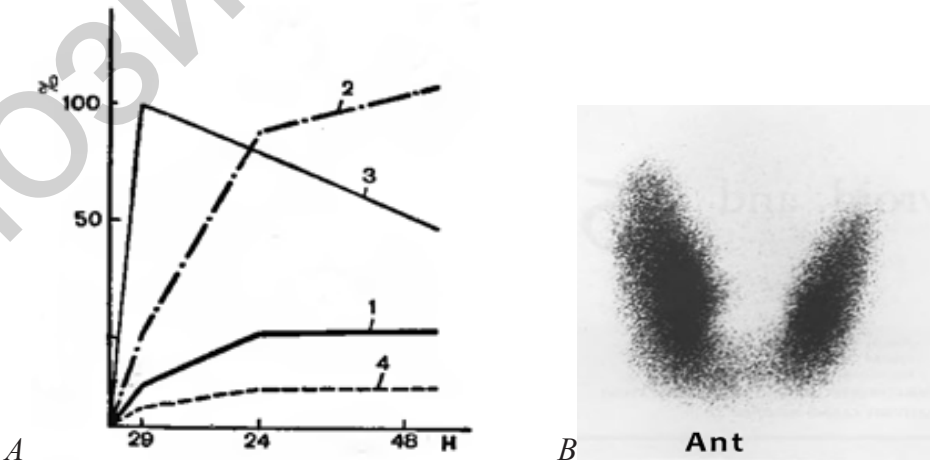

A *B*

Figure 5.1 — (A) Thyroid uptake (radiometry) types:
1 — normal, 2–3 — hyperfunction, 4 — hypofunction.
(B) Iodine-123 anterior scan (scintigram) of the thyroid.
The normal bilobed gland with an inferior isthmus is easily appreciated

Thyroid uptake is based on the principle that the administered radiopharmaceutical is concentrated by the thyroid gland in a manner that reflects the gland's handling of stable dietary iodine and therefore the functional status of the gland. The higher the uptake of the radiopharmaceutical, the more active the thyroid; conversely, the lower the uptake, the less functional the gland. Uptake is conventionally expressed as the percentage of the administered activity in the thyroid gland at a given time after administration (usually 4 to 6 and 24 hours) (Figure 5.1 A). Normal range is about 10 to 30% for 24-hour uptake determinations. The normal range for a 4- to 6-hour uptake is about 6 to 18%. To begin the test, about 5 μCi (0,2 MBq) (Mega becquerel) of ^{131}I-sodium in either liquid or capsule form is administered.

Primary hyperthyroidism

Primary hyperthyroidism (Grave's disease or toxic nodular goiter) and secondary hyperthyroidism commonly produce elevated iodine uptakes. On the other hand, hyperthyroidism produced by toxic nodular goiters may yield uptake values in the high, normal, or mildly elevated range. Therefore, a normal or borderline elevated radioiodine uptake alone cannot be used to exclude the diagnosis of hyperthyroidism when it is clinically suspected.

The radiotracer uptake by this patient's hyperplastic and hyperfunctioning gland is uniform and intensely increased in the right lobe, left lobe, and isthmus. Therefore, the clinical manifestations and abnormal thyroid function tests correlate with the scintigraphic imaging findings.

Hyperthyroidism

On examination, there were no specific signs of a thyroid disease and the thyroid was normal in size. Images obtained from technetium-99m-pertechnetate ($^{99m}TcO_4$), thyroid scintigraphy show abnormally increased homogeneous radiotracer uptake throughout the thyroid, which is normal in size. The intensity of thyroid gland uptake exceeds the uptake in both salivary glands, background activity is markedly decreased, and the pyramidal lobe is clearly visible. All of these findings indicate a hyperfunctioning gland. There is no focal photopenic or focal hot area to suggest a nodule.

Thyrotoxicosis

Although the diagnosis of thyrotoxicosis is established by clinical and biochemical means, radioiodine uptake and thyroid scintigrams are very useful in the differential diagnosis of the various causes of thyrotoxic states. Radioiodine uptake and scintigrams in thyrotoxic patients may be obtained at 4 to 24 hours post administration iodine-131 uptake together with ^{99m}Tc-pertechnetate scintigram is effective.

Thyroid scintigraphy

Although ^{131}I may be used for obtaining thyroid uptakes, ^{99m}Tc-pertech-netate remain the agents of choice for obtaining maximum morphologic detail of the thyroid gland with the gamma camera. Either radionuclide, however, provides images of excellent quality (Figure 5.1 B, 5.2).

Technetium-99m-pertechnetate (TcO_4) radiotracer provides a lower radiation dose per unit administered than any of the radioiodines (I-131 and I-123) that are used for thyroid imaging. The thyroid is imaged 20 minutes after the intravenous administration of 5 mCi (185 MBq) of ^{99m}Tc-pertechnetate. On a ^{99m}Tc-pertech-ne-tate scintigram, the salivary glands are usually well seen in addition to the thyroid. Technetium-99m pertechnetate is preferred over radioiodine when the patient has been receiving thyroid-blocking agents.

The normal thyroid gland is a bilobed organ with reasonably homogeneous distribution of activity in both lobes. Slight asymmetry in the sizes of the lobes is common, with the right lobe generally dominating.

The indications for scintigraphic thyroid imaging include:

To relate the general structure of the gland to function, in differentia-ting Grave's disease from toxic nodular goiter.

To determine the function in a specific area, for example, to see if a palpable nodule is functional.

To locate ectopic tissue, such as a lingual thyroid.

To assist in evaluation of congenital hypothyroidism (uptake in the gland is low and visualization is poor).

Grave disease

Uniformly increased activity in the both lobes of the enlarged thyroid gland. There is no evidence of nodular increased activity to suggest a toxic nodular goiter, nor decreased uptake to suggest thyroiditis (Figure 5.2 D).

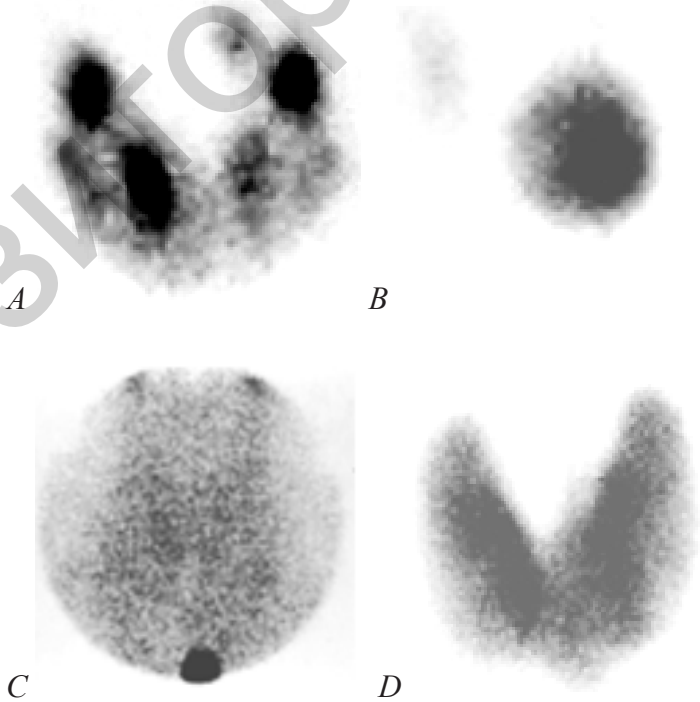

Figure 5.2 — Scintigrams in four types of hyperthyroidism. (A) multinodular goiter, (B) solitary hyperfunctioning thyroid nodule, (C) thyroiditis, (D) Grave's disease

Hyperfunctioning thyroid adenoma

Thyroid scintigraphy with ^{99m}Tc-pertechnetate demonstrates intense uptake of the radiopharmaceutical (*hot thyroid nodule)* corresponding to the palpable nodule in the left lobe of the thyroid. There is also suppression of uptake in the remainder of the left lobe as well as the entire right lobe. The scintigraphic findings in conjunction with the patient's history and elevated thyroid function tests are most consistent with an autonomous toxic nodule (Figure 5.2 B).

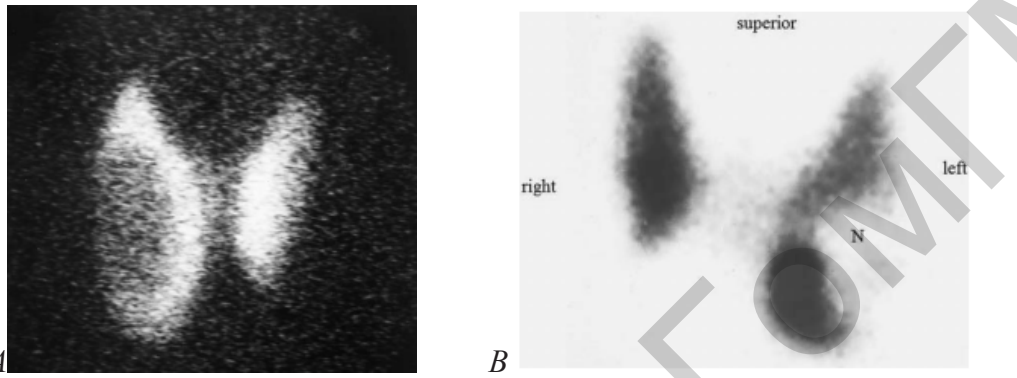

Figure 5.3 — (A) Thyroid scan showing a nodule as a photopenic area in the right lobe of the thyroid. (B) There is a cold nodule (N) in the left lower pole

Cold thyroid nodules are nonspecific and have both benign and malignant causes (Figure 5.3). 75% of cold nodules are secondary to colloid cysts or adenomas. Although the incidence for carcinoma is more common in cold nodules than hot nodules, the incidence is still low and ranges from 15 to 25%. Factors suggesting a benign etiology include older, female patients as well as multiple nodules. A nodule that decreases in size while on thyroid hormone is suggestive of a benign etiology.

Adrenal glands

Adrenal glands are small but their common involvement in many disease processes has made cross-sectional imaging modalities essential to detect abnormal morphological and functional alterations. Radiology also plays a critical role in the characterization of adrenal mass lesions. Therefore, it is important to first understand the normal anatomy and functional characteristics of the adrenal gland (Figure 5.3).

Pathognomonic imaging features have been established for many of these lesions, including myelolipomas, adenomas, haematomas and cysts. Most adrenal lesions are benign. However as the adrenal gland is also a frequent site for metastatic disease, distinguishing between benign and malignant masses on imaging in patients with primary cancers elsewhere is essential. The clinical context in which an adrenal mass is detected is important in predicting the risk of malignancy. Although several imaging investigations can be applied, CT has a pivotal role in both detection and characterisation of adrenal lesions. In functioning adrenal disease, clinical and biochemical findings should direct the radiologist to the correct interpretation and

diagnosis. This chapter looks at adrenal characteristic imaging features of common adrenal lesions, the application of modern imaging techniques in evaluating an incidental adrenal mass and functioning and non-functioning adrenal disease.

Ultrasonography

The adrenal glands are relatively large in infancy and are therefore easy to identify via sonography on both sides. Sonographic images of the adrenal glands in adulthood may be difficult on account of, for example, intestinal gas. Therefore, masses often become detectable only after reaching a size of > 2 cm.

Magnetic resonance tomography

MR imaging is used to characterise adrenal gland lesions and to localise extra-adrenal pheochromocytoma. It is frequently used for planning the surgical treatment of patients with reported allergic reaction to contrast material or other contrast-related reactions. For MRI a body array coil with high-resolution technique is used with a slice thickness of < 5 mm.

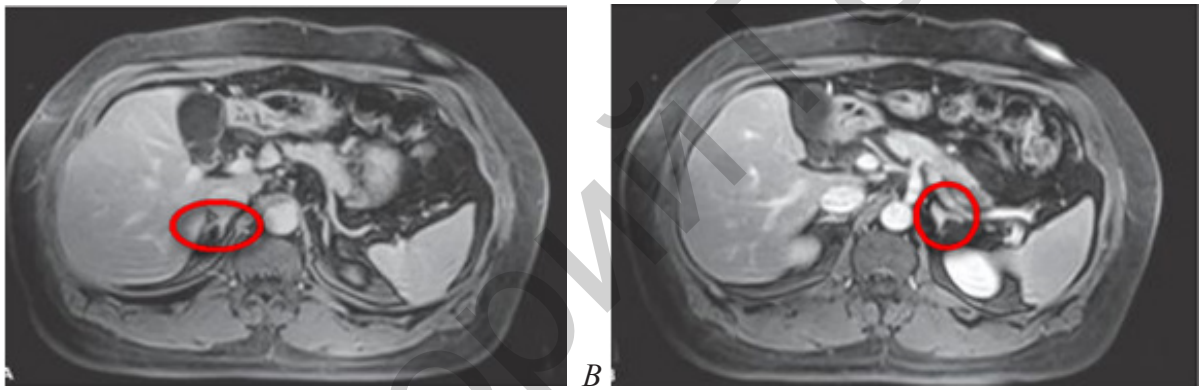

Figure 5.4 — Gradient echo T1W axial tomograms showing the normal inverted 'V' configuration of the adrenal gland (into the oval).
(A) Marked by oval an right adrenal gland, (B) – left adrenal gland

Computed tomography

With the increasing use of cross-sectional imaging, adrenal lesions are frequently identified in routine practice and are seen in up to 5% of abdominal CTs. CT is the imaging technique of choice (Figure 5.4). It not only produces high resolution images of the adrenals but may also facilitate puncture in unclear cases. Thin-section tomography (0,5–1 mm) is used when assessing the adrenals alone; its narrow collimation also serves as a basis for multiplanar reconstructions. An examination can be performed with thicker sections for larger adrenal tumors. In the suspicion of pheochromocytoma, the entire retroperitoneum (at least up to the aortic bifurcation) is commonly examined as well. Percutaneous biopsy of the adrenal lesion under CT guidance has an accuracy of 80–90%.

Nuclear medicine techniques

Among nuclear medicine techniques, MIBG scintigraphy and sometimes PET and PET/CT are useful for the diagnosis of pheochromocytoma and suspicion of

malignant tumours. MIBG scintigraphy uses radiolabelled metaidobenzylguanidine, which is a norepinephrine analogue. PET and PET/CT imaging predominately uses the tracer ^{18}F-FDG (fluorodeoxyglucose); other tracers like, e.g., ^{18}F-DOPA (dihidroxyphenulalanine) are seldom used. Integrated information obtained from anatomic and functional imaging is essential for characterization of adrenal disease. Due to expenditure in time for patients and staff as well as high costs, this diagnostic technique is only used for selected cases.

A number of imaging modalities are available for evaluation of the adrenals. Before the advent of imaging modalities of US, CT and MRI, the radiological techniques available for evaluation of adrenals were plain X-ray abdomen, excretory urography, invasive techniques of perirenal air insufflation, adrenal venography and angiography. Most of these techniques have become obsolete. Angiography may be sometimes indicated to look for extra-adrenal pheochromocytoma in situations when MIBG scintigraphy is not available. Adrenal venous sampling may be recommended in patients with aldosteronism, both for distinguishing unilateral from bilateral disease and for localizing unilateral tumor. However, this technique is invasive, technically difficult to perform and requires long fluoroscopy time with resultant high radiation dose and needs hospitalization.

Recent technical advances in computed tomography and magnetic resonance imaging have resulted in improved detection of subtle changes in adrenal gland morphology. The different morphologic patterns of adrenal gland enlargement on imaging can be classified as follows:

— Diffuse enlargement.

— Focal nodule or mass in a limb.

— Multiple nodules in the gland.

— Nodule with a smaller nodule within the nodule, the so-called nodule within a nodule appearance.

The causes of diffuse enlargement include adrenal hyperplasia, lymphoma, metastatic disease, tuberculosis, and histoplasmosis. Enlarged adrenal glands are common and may be due to both benign and malignant causes.

— Imaging plays an important role in both the detection of adrenal enlargement and its characterization in concert with appropriate endocrine/oncologic/infectious history and testing.

— Image-guided biopsy is less commonly required for diagnosis but can sometimes be helpful for characterization of adrenal enlargement that has remained indeterminate by imaging.

Benign lesions and adrenal diseases

Adrenal hyperplasia

Adrenal cortical hyperplasia may be primary or secondary to a pituitary or hypothalamic lesion or ectopic production of adrenocorticotropic hormone (ACTH). Clinically, adrenal hyperplasia often manifests as Cushing's disease. It may also be associated with Conn's syndrome or adrenogenital syndrome.

Imaging

On CT and MRI, hyperplasia of the adrenals is commonly present as enlarged glands bilaterally but maintains an adreniform shape with a smooth surface (Figure 5.4). Rarely, adrenal hyperplasia may have a normal appearance or nodular enlargement. The maximum diffuse enlargement of the adrenals in hyperplasia is associated with ectopic ACTH production secondary to various tumors, such as bronchial carcinoid. In a patient with hyperaldosteronism, differentiation of adrenal hyperplasia versus hyperfunctioning adenoma is critical because adrenal hyperplasia is treated medically, whereas a hyperfunctioning adenoma requires surgery. Renal venous sampling is usually indicated in patients with hyperaldosteronism, particularly when a focal nodule on cross-sectional imaging is not identified.

Most often, hyperaldosteronism is associated with micronodules that are not usually detected on CT or MRI; hence, even if hyperplasia is identified on CT or MRI, renal vein sampling is still performed to exclude unilateral hypersecretion of aldosterone. If a focal nodule is not identified on imaging in patients with hyperaldosteronism, further evaluation is usually performed with renal vein sampling.

Adrenal cysts

Cysts of the adrenal gland are rare. They are generally of lymphangiomatous origin and their dimensions tend to be small and asymptomatic. Seven percent of adrenal cysts may be parasitic.

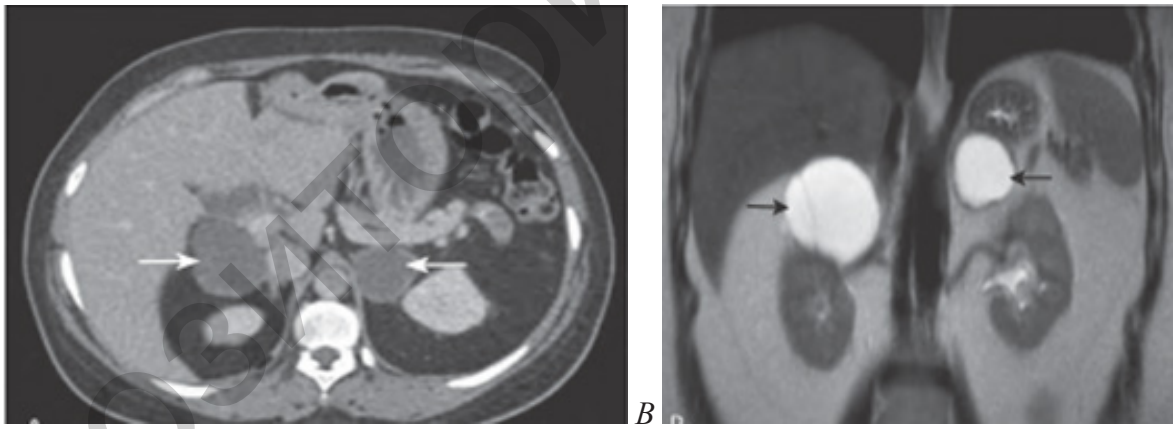

Figure 5.5 — Adrenal pseudocysts on CT and MRI. (A) Axial contrast-enhanced CT image through abdomen demonstrates bilateral oval fluid attenuation cystic lesions of adrenal glands (arrows) with thin walls and without solid enhancing components. (B) Coronal heavily T2-weighted MR tomogram through abdomen reveals very high signal intensity of adrenal lesions (arrows) in keeping with cystic nature. Note thin internal septation in right adrenal gland lesion as well

Imaging

Cysts (Figure 5.5) exhibit usual characteristics with dorsal sound amplification in ultrasonography and a noticeably hypodense appearance in CT. Density values in CT reveal watery fluid and possible wall calcifications. In MR tomography, simple

cysts have a significantly hypointense signal in T1-weighted images and a hyperintense signal in T2-weighted images. Hence, the differentiation and diagnosis of a simple adrenal cyst may be easy as long as typical patterns are present.

Pheochromocytoma

As the term indicates pheochromocytoma is an symptomatic adrenal tumour found by coincidence via imaging techniques. However, syndromic pheo-chromocytoma may be small, multiple and extraadrenal.

Imaging

Computer tomography and sonography most frequently detect abdominal pheochromocytoma by coincidence. The criteria for enlargement of adrenal are taken as length more than 4 cm, anteroposterior diameter of more than 3 cm and limb thickness of more than 6,0 mm or more than adjacent diaphragmatic crus.

Figure 5.6 — Pheochromocytoma (spectrum of appearances).
(A) Unenhanced scan shows a heterogeneously attenuating mass in the right adrenal gland (arrow). (B) Contrast scan shows a mass in the right adrenal gland (arrow) with peripheral enhancement and a central area of low attenuation due to necrosis.
(C) Unenhanced scan shows a mass with cystic and solid components in the left adrenal gland.
(D) Contrast scan shows a cystic adrenal lesion with a calcified rim (arrow)

Besides these absolute measurements, any alteration in the contour, focal bulge, calcification, pattern of enhancement, CT attenuation values on nonenhanced, enhanced and delayed enhanced techniques, and displacement of surrounding structures should be evaluated. MRI may be recommended for further differentiation (Figure 5.6).

Lymphoma

Adrenal involvement occurs in nearly 25% of patients with non-Hodgkin's lymphoma (NHL) at autopsy. Adrenal involvement in NHL is usually associated with diffuse enlargement similar to hyperplasia. However, here the enlargement is either asymmetric or unilateral. On CT, adrenal lymphoma appears as unilateral or bilateral homogeneous solid involvement without calcifications. The shape of the adrenals may be maintained, and mild enhancement may be noted after intravenous administration of a contrast agent. In NHL, the adrenal gland involvement may be due to a primary or metastatic lymphoma.

MRI features of lymphoma are nonspecific and may resemble metastases. Typically, the enlargement is hypointense on a T1-weighted image and has variable or heterogeneous hyperintensity on T2-weighted images. Positron emission tomography with CT (PET/CT) is helpful in identification of adrenal as well as extra-adrenal involvement. The ^{18}F-fluorodeoxyglucose (FDG) uptake will be greater than the liver uptake in adrenals with lymphomatous involvement.

Malignant adrenal tumours

Adrenal carcinoma

Adrenal carcinoma is predominately unilateral; they are bilateral in up to 10% of cases. First detection often shows hormonally active tumours with a diameter of 2–5 cm and hormonally inactive tumours with a diameter of up to 10 cm.

Imaging

CT reveals growing, invasive tumours with central areas of necrosis and contrast-enhanced inhomogeneity. Calcification and haemorrhages are common. Adrenal carcinomas tend to metastasise to regional and pulmonary lymph nodes. Tumours reveal inhomogeneous signal intensity in MRI. Their invasive character, e.g., the invasion of the inferior vena cava or renal parenchyma, becomes easily distinguishable through the use of MR tomography. In contrast to ultrasonography and angiography, FDG-PET(/CT) plays a significant role in diagnosis of the extent of spread.

Conclusion

Adrenal imaging has become increasingly important with the emergence of incidental adrenal masses. Imaging is also an essential adjunct to clinical and biochemical findings in the evaluation and management of adrenal dysfunction. Close collaboration is required between the endocrinologists and radiologist to obtain the correct diagnosis and to select the most appropriate imaging strategy.

VI. RADIATION THERAPY

Millions of cancer patients receive radiation therapy each year, either alone or in conjunction with surgery, chemotherapy or other forms of cancer therapy. Other terms for radiation therapy (RT) include radiotherapy or irradiation. Radiation therapy is useful in cases where surgical removal of the cancer is not possible or when surgery might debilitate the patient (for example, when tumors that are located close to the spinal cord). Together with image guided treatment planning, radiation therapy is a powerful tool in the treatment of cancer, particularly when the cancer is detected at an early stage.

Radiation treatment principles and methods

Radiotherapy or radiation treatment (radiology therapy) is the use of ionizing x-rays, electrons or gamma rays to treat cancer. Radiation can cure or control cancer by inhibiting the cancer cells from dividing or reproducing. About fifty or sixty percent of patients with cancer will require radiation during their lifetime. Radiation is a effective form of treatment for patients.

Radiation therapy uses high-energy of ionizing radiation to stop cancer cells from dividing. During radiation therapy, ionizing radiation deposit energy in the area being treated, damaging the genetic material of cells and making it impossible for these cells to divide. Although radiation damages both cancer cells and normal cells, the normal cells are usually able to repair themselves and function properly.

Radiation therapy is commonly applied to the cancerous tumor because of its ability to control cell growth. Ionizing radiation works of exposed tissue leading to cellular death. Ionizing radiation passes through tissues and dislodges electrons from atoms. Ionization, in turn, can cause cell death or a genetic change. To spare normal tissues (such as skin or organs which radiation must pass through in order to treat the tumor), shaped radiation beams are aimed from several angles of exposure to intersect at the tumor, providing a much larger absorbed dose there than in the surrounding, healthy tissue. **The basic principles of radiotherapy remain unchanged, radiotherapy is a locoregional treatment suitable for radical treatment of tumours in their early stages with high success rates where metastatic spread has not evolved.**

Radiation therapy may be used to treat localized solid tumors, such as cancers of the skin, head and neck, brain, breast, prostate and cervix, it can also be used to treat leukemia and lymphoma. The goal of radiation treatment can be:

— **Radical** (or curative) — radiation can be a very effective treatment for prostate cancer.

— **Palliative**, that is, to alleviate or reduce symptoms (a pain).

— **Symptomatic** — elimination symptoms (compression vein cava).

Curative radiation therapy is used for the purpose of curing the patient where one is willing to engender a small risk of significant side effects in return for the

possibility of cure. An example is the use of radiation therapy for the treatment of early stage breast cancer. In return for a high probability of cure, one is willing to engender a small risk of pneumonitis, for example. Palliative radiation therapy is designed to ameliorate a specific symptom such as pain, obstruction, or bleeding. In palliative radiation therapy used in the context of an incurable malignancy, one is not willing to engender a significant risk of side effects to achieve a palliative goal. Thus, if one wishes to relieve pain from lung cancer metastatic to a bone, one would pick a dose and technique of radiation therapy sufficient to achieve the relief of pain but not enough to run a risk of radiation osteonecrosis.

There are basically two types of radiation treatment:

1. **External** (distant) radiation therapy.

2. **Brachytherapy**, or radiation at a short distance (contact radiation therapy).

A patient may receive one or the other, or assotiated of both. The combined of an irradiation with operation or chemotherapy is possible. The complex the-rapy included operation-, chemo- and radiotreatment.

Types of radiation used to treat cancer:

Ionizing radiation can be divided into 2 major types:

— Photons (x-rays and gamma rays).

— Particle radiation (electrons, protons, neutrons, alpha and beta particles).

Some types of ionizing radiation have more energy than others. The higher the energy, the more deeply the radiation can penetrate into the tissues. The way a certain type of radiation behaves is important in planning radiation treatments. The radiation oncologist selects the type and energy of radiation that is most suitable for each patient's cancer.

The more common types of radiation used for cancer treatment:

— High-energy photons come from radioactive sources such as cobalt, cesium, or a machine called a linear accelerator.

— Electron beams produced by a linear accelerator are used for tumors close to a body surface since they penetrate less into deeper tissues.

— Protons are a newer form of treatment. Protons are parts of atoms that cause little damage to tissues they pass through but are very effective in killing cells at the end of their path. This means that proton beam radiation may be able to deliver more radiation to the cancer while reducing side effects of nearby normal tissues. Proton beam radiation therapy requires highly specialized equipment and is currently only available in a few medical centers.

— Neutrons are used for some cancers of the head, neck, ets. They can be effective when other forms of radiation therapy do not work.

The periods of radiation treatment included:

1. Preradiation (before treatment, treatment planning).

2. Treatment (sessions).

3. After treatment a period.

I. Treatment planning

The objective of treatment planning is to determine the configuration and parameters of beams that will lead to an optimum dose distribution. The parameters include the number and directions of proton beams. Computerized dose planning systems are used to construct an isodose distribution with beams of appropriate energy, size, weighting, gantry angle and wedge to give a homogeneous result over the target volume. In a complex procedure called dosimetry, computer programs are used to determine how much radiation the surrounding normal structures would be exposed to in order to deliver the prescribed dose to the cancer.

The doctor and dosimetrist will work together to determine the amount of radiation patient will receive and the best way to aim it at the cancer, based on the size of the tumor, how sensitive the tumor is to radiation, and the ability of the normal tissue in the area to tolerate the radiation.

Steps in radiation treatment planning:

Consultation: At the beginning, the patient will be seen by the radiation oncologist for a consultation. During the consultation, the radiation oncologist will perform a history and a physical examination. He will review all the pertinent data and all of the investigations that have been performed. He may also request other tests or consultations to be made.

Simulation: After the consultation, the radiation oncologist will formulate a treatment plan. Here, the patient comes to the radiation department and lies down on a table under a machine, called a simulator. Iimmobilization devices may be necessary, such as a face mask, in order to make sure the patient is positioned correctly for each treatment. There will be various markings that will be made on the skin and various x-rays will be taken (Figures 6.1).

During simulation, the area of the patient's body to be treated is marked directly on the patient's skin with markers. Very tiny permanent marks, or tattoos are sometimes made to ensure that daily treatments are delivered accurately. These are also useful for future treatment planning sessions and treatment updates. CT scans may have to be taken in order that the computers can calculate and prescribe the dose distribution of the radiation.

The radiotherapy simulator is the mechanical analog of an isocentric therapy unit. It serves several functions, but its primary purpose is to help establish the optimal beam and setup parameters for a patient before the first treatment. These parameters may include the gantry angle, field size, target-to-skin distance and treatment couch position for each beam. The patient setup position, skin marks, and immobilization devices can also be determined during the treatment simulation.

Radiation physicists and dosimetrists use computer models to plan the treatment. This computerized treatment planning allows the treatment to be delivered more accurately, both in terms of the "beam shape" that is achieved with precise collimator settings and in terms of the angles and directions used to deliver the radiation to the cancer. By using the computer to help, the radiation oncologist can deliver the radiation precisely to cancer, delivering a minimal amount of radiation to healthy tissues.

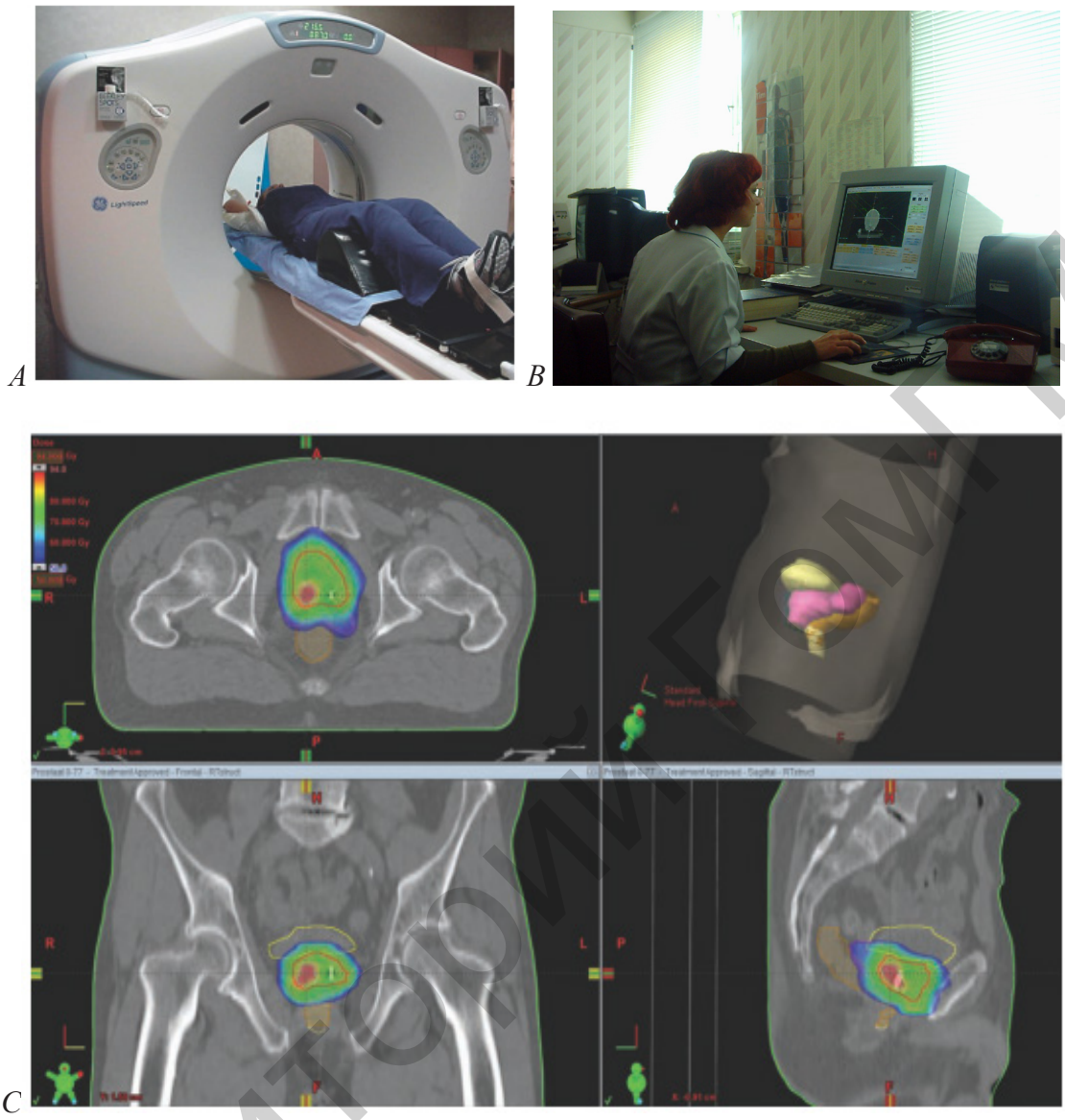

Figure 6.1 — (A) Modern CT simulator. (B) Simulation of individual radiotherapy. (C) Example of the result after CT simulation. Coronal, sagittal and transversal of a CT scan in the treatment position. The prostate as (red line) and the macroscopic tumour as (light blue line) are delineated based on registration with a multiparametric creating (rectum in orange, bladder in yellow). Creation of the "virtual" patient to plan RT

The radiation treatment planning models usually use a three-dimensional (3D) recreation of the patient's anatomy. Images of the patient are acquired from the CT or MR scanner and then sent by network or computer disk to the radiation treatment planning computer.

II. Radiology treatment (of treatment sessions are similar and follow this procedure):

1. Radiation treatments are divided over many sessions encompassing several weeks. Because of this, very tiny marks, or tattoos, are made on the patient's skin to ensure the accuracy of the treatment.

2. For daily treatments, the patient is positioned by the therapist on the treatment table. Patient positioning is very important for treatment delivery accuracy. The patient may communicate at any time with the therapist.

3. The actual treatment delivery session can last anywhere from 5 to 15 minutes.

III. After treatment a period. The patient is observed for estimation of efficiency of radiology treatment, correction of side effects, symptomatic therapy (usually one week).

Dose

The amount of radiation used in photon radiation therapy is measured in *gray* (Gy), and varies depending on the type and stage of cancer being treated. For curative cases, the typical dose for a solid epithelial tumor ranges from 60 to 80 Gy, while lymphomas are treated with 20 to 40 Gy.

Fractionation

The total dose is fractionated (spread out over time) for several important reasons. Fractionation allows normal cells time to recover, while tumor cells are gene-rally less efficient in repair between fractions. Fractionation also allows tumor cells that were in a relatively radio-resistant phase of the cell cycle during one treatment to cycle into a sensitive phase of the cycle before the next fraction is given. Similarly, tumor cells that were chronically or acutely hypoxic (and therefore more radioresistant) may reoxygenate between fractions, improving the tumor cell kill.

The total dose is fractionated (spread out over time) for several important reasons. Fractionation allows normal cells time to recover, while tumor cells are generally less efficient in repair between fractions. Fractionation also allows tumor cells that were in a relatively radio-resistant phase of the cell cycle during one treatment to cycle into a sensitive phase of the cycle before the next fraction is given. Similarly, tumor cells that were chronically or acutely hypoxic (and therefore more radioresistant) may reoxygenate between fractions, improving the tumor cell kill. Fractionation regimens are individualised between different radiation therapy centers and even between individual doctors. In North America, Australia, and Europe, the typical fractionation schedule for adults is 1,8 to 2 Gy per day, five days a week. In some cancer types, prolongation of the fraction schedule over too long can allow for the tumor to begin repopulating, and for these tumor types, including head-and-neck and cervical squamous cell cancers, radiation treatment is preferably completed within a certain amount of time. For children, a typical fraction size may be 1,5 to 1,8 Gy per day, as smaller fraction sizes are associated with reduced incidence and severity of late-onset side effects in normal tissues.

Conventional fractionation*:*

Fraction dose 1,8–2 Gy

Number of fractions per day 1

Number of fractions per week 5
Number of fractions per treatment 25–35
Total dose 45–70 Gy

Hyperfractionation*:*
Fraction dose 1,1–1,2 Gy
Number of fractions per day > 2
Number of fractions per week 10
Number of fractions per treatment 60–70
Total dose 45–70 Gy or > 10%

Aims of hyperfractionation:
— To decrease the fraction dose and increase the total dose.
— To increase local control.
— To decrease late effects in normal tissues.

*In hyperfractionation a*cute side effects are similar or slightly increased compared to conventional fractionation. Late side effects are decreased compared to conventional fractionation.

Accelerated fractionation*:*
Fraction dose 1,1–2 Gy
Fraction number/day > 1
Fraction number/week > 5
Fraction number/treatment 25–35
Total dose 45–70 Gy or less

*The aim of accelerated fractionation: t*o decrease overall treatment time, to decrease accelerated repopulation.

In accelerated fractionation early side effects are more than conventional fractionation. Late side effects are same as conventional fractionation. Treatment may be stopped early or the total dose may be decreased due to the excess amount of early side effects → this may cause a decrease in local control.

Hypofractionation*:*
Fraction dose > 2 Gy
Number of fractions per day < 1
Number of fractions per week < 5
Number of fractions per treatment < 25–35
Total dose < 45–70 Gy

*The aim of hypofractionation: h*ypofractionation is generally used for palliative purposes in the management of metastatic tumors. Late side effects are undervalued and palliation is provided over a very short time period.

In hypofractionation early side effects are similar to those associated with conventional fractionation. Late side effects are increased compared to conventional fractionation.

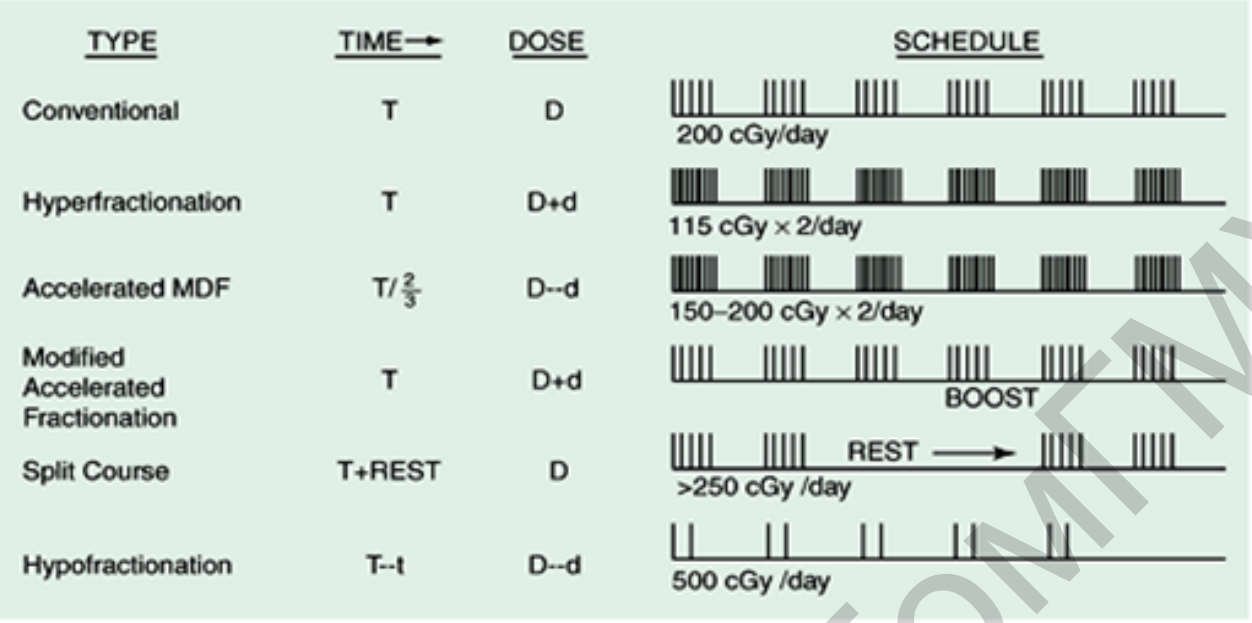

Figure 6.2 — Various types of fractionation used in radiation therapy

In Europe, the typical fractionation schedule for adults is 2 Gy per day, five days a week (Figures 6.2).

Effect on different types of cancer (radiosensitivity**)**

Different cancers respond differently to radiation therapy. The response of a cancer to radiation is described by its radiosensitivity. Highly radiosensitive cancer cells are rapidly killed by modest doses of radiation. These include leukemias, most lymphomas and germ cell tumors. The majority of epithelial cancers are only moderately radiosensitive, and require a significantly higher dose of radiation (60–70 Gy) to achieve a radical cure. Some types of cancer are notably radioresistant, that is, much higher doses are required to produce a radical cure than may be safe in clinical practice. Renal cell cancer and melanoma are generally considered to be radioresistant.

It is important to distinguish the radiosensitivity of a particular tumor, which to some extent is a laboratory measure, from the radiation "curability" of a cancer in actual clinical practice. For example, leukemias are not generally curable with radiation therapy, because they are disseminated through the body. Lymphoma may be radically curable if it is localised to one area of the body. Similarly, many of the common, moderately radioresponsive tumors are routinely treated with curative doses of radiation therapy if they are at an early stage. For example: non-melanoma skin cancer, head and neck cancer, breast cancer, non-small cell lung cancer, cervical cancer, anal cancer, prostate cancer. Metastatic cancers are generally incurable with radiation therapy because it is not possible to treat the whole body.

Effect on different types of cancer (tumor response to radiation)

Different cancers respond differently to radiation therapy. The response of a cancer to radiation is described by its **radiosensitivity**. Highly radiosensitive can-

cer cells are rapidly killed by modest doses of radiation. These inclu-de leukemias, most lymphomas and germcell tumors. The majority of epithelial cancersare only moderately radiosensitive, and require a significantly higher dose of radiation (60–70 Gy) to achieve a radical cure. Some types of cancer are notably radioresistant, that is, much higher doses are required to produce a radical cure than may be safe in clinical practice. Renal cell cancer and melano-ma are generally considered to be radioresistant.

Bergonie and Tribondeau law:

The radiosensitivity of a tissue depends on:

— The excess amount of less-differentiated cells in the tissue.

— The excess amount of active mitotic cells.

— The duration of active proliferation of the cells.

According to the Bergonie and Tribondeau law, the effect of radiation on undifferentiated divided cells with high mitotic activity is much greater than the effect of radiation on undivided differentiated cells.

Single dose (Gy)		Fractionated dose (Gy)	
Lymphoid	2-5	Testes	1-2
Bone marrow	2-10	Ovary	6-10
Ovary	2-6	Eye (lens)	6-12
Testes	2-10	Lung	20-30
Eye (lens)	2-10	Kidney	20-30
Lung	7-10	Liver	35-40
Gastrointestinal	5-10	Skin	30-40
Colorectal	10-20	Thyroid	30-40
Kidney	10-20	Heart	40-50
Bone marrow	15-20	Lymphoid	40-50
Heart	1-20	Bone marrow	40-50
Liver	15-20	Gastrointestinal	50-60
Mucosa	5-20	Spinal cord	50-60
Skin	15-20	Peripheral nerve	65-77
Peripheral nerve	15-20	Mucosa	65-77

Figure 6.3 — Examples of the doses used for radiotreatment

Radiosensitivities of the tumor and its surrounding tissues are important considerations when determining the best treatment. It is important to distinguish the radiosensitivity of a particular tumor, which to some extent is a laboratory measure, from the radiation “curability” of a cancer in actual clinical practice (Figures 6.3). For example, leukemias are not generally curable with radiation therapy, because they are disseminated through the body. Lymphoma may be radically curable if it

is localised to one area of the body. Similarly, many of the common, moderately radioresponsive tumors are routinely treated with curative doses of radiation therapy if they are at an early stage. For example: non-melanoma skin cancer, head and neck cancer, breast cancer, non-small cell lung cancer, cervical cancer, anal cancer, prostate cancer. Metastatic cancers are generally incurable with radiation therapy because it is not possible to treat the whole body.

Therapeutic index

The therapeutic index defines how the tumor control probability (TCP) relates to the normal tissue complication probability (NTCP) for different doses (Figures 6.4–6.7).

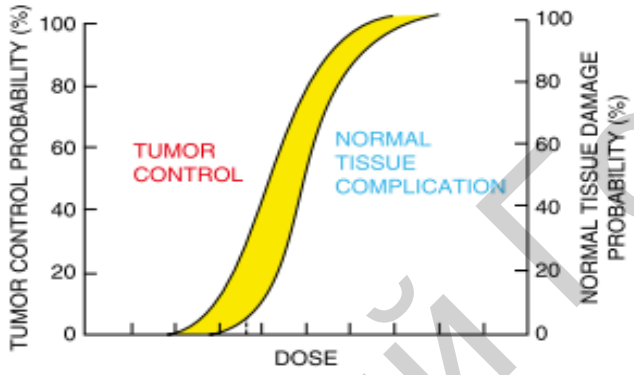

Figure 6.4 —Tumor control probability (TCP) and normal tissue complication probability (NTCP) curves

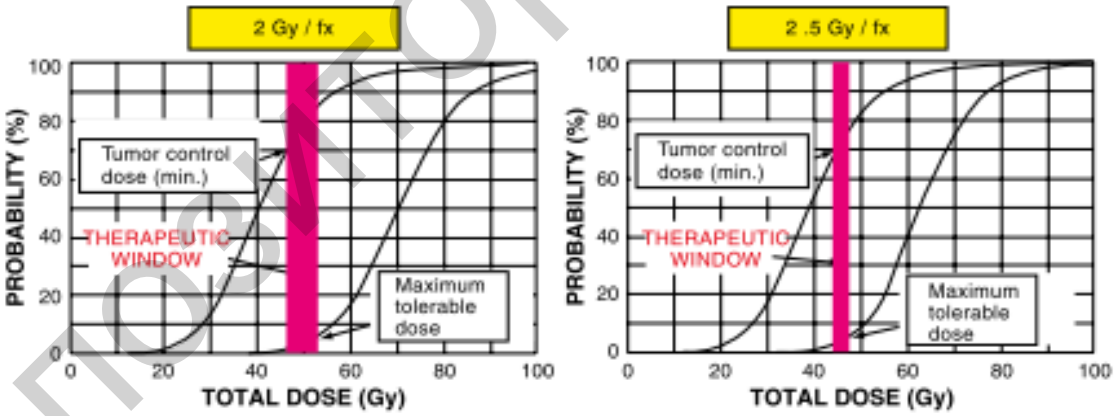

Figure 6.5 — Relationships between fraction dose, total dose, and different therapeutic windows

Normal tissues may get damaged by the dose required to control the tumor; on the other hand, the tumor may not receive an adequate dose if the normal tissues require protection. Achieving the optimal balance between TCP and NTCP is a basic aim of radiotherapy. All new technologies are directed towards this aim. TCP and NTCP curves are sigmoid in shape. The purpose of treatment is to move the TCP curve to the left and the NTCP curve to the right.

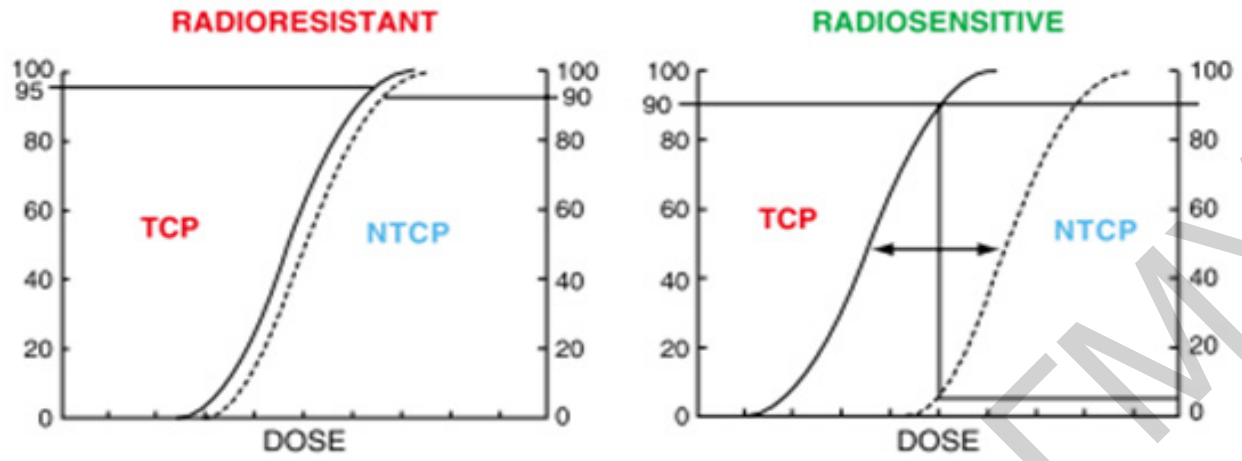

Figure 6.6 — Relationship between tumor control probability (TCP), normal tissue complication probability (NTCP), and radiosensitivity

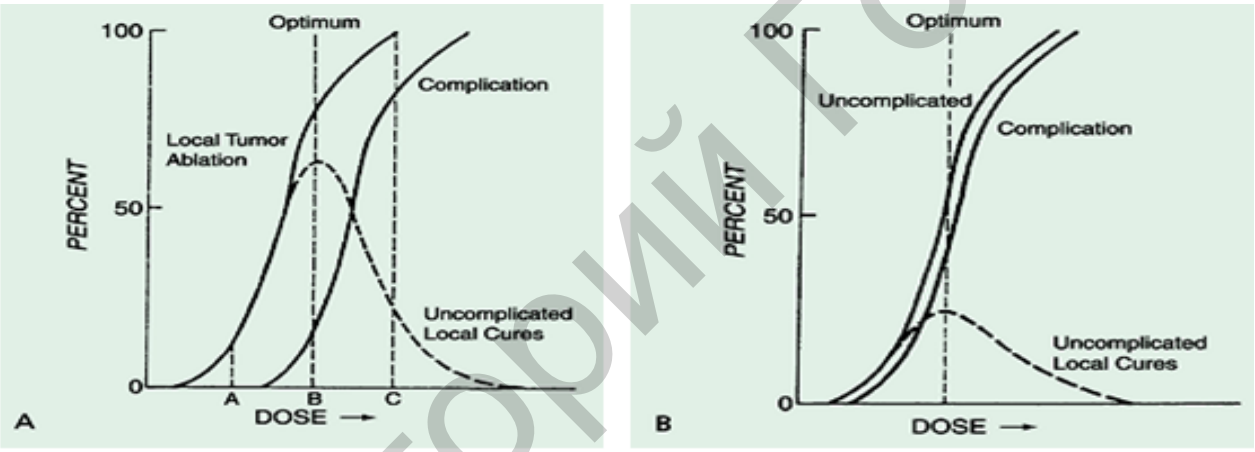

Figure 6.7 — Treatment outcomes. Uncomplicated curves (dashed line) are the desired results of treatment. This is illustrated as a function of the therapeutic index ratio; that is, the greater the separation of the tumor-control curve and the normal tissue-complica-tion curve, the greater the number of uncomplicated cures that will result. The letters A, B, and C represent three different dose levels, which, if chosen, would lead to three different outcomes: A would result in few tumor cures but no complications; C would lead to complete cure in many cases, but virtually all patients would suffer complications. The optimal choice in this group of dose levels is B, which would result in the greatest number of cured patients without complications

The therapeutic index (= therapeutic window) increases if the region the between two curves becomes large, and the expected benefit from treatment increases.

Main methods of radiation therapy

Historically, the three main divisions of radiation therapy are **external beam radiation therapy, brachytherapy** and **sealed source radiation therapy** (by radionuclide of the radiotreatment). The differences relate to the position of the radiation source*; external radiotreatment (distant)* is outside the body, *brachytherapy (contact)* uses sealed radioactive sources placed precisely in the area under treatment,

and systemic radionuclides are given by infusion or oral ingestion. Brachytherapy can use temporary or permanent placement of radioactive sources. The temporary sources are usually placed by a technique called afterloading. In afterloading a hollow tube or applicator is placed surgically in the organ to be treated, and the sources are loaded into the applicator after the applicator is implanted. This minimizes radiation exposure to health care personnel.

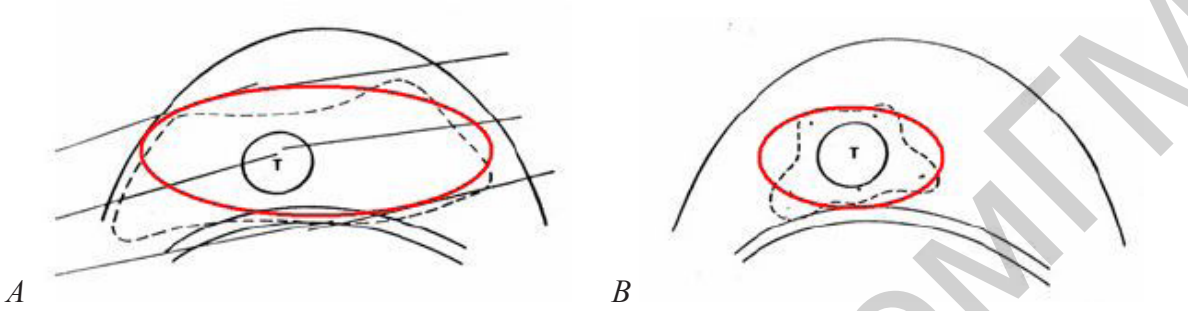

Figure 6.8 — Comparison of the 50% dose distribution between (A) a distant photons cobalt-60 two beams RT and (B) contact interstitial radiotherapy (minimal field of irradiation normal tissues after contact radiotherapy)

Particle therapy is a special case of external beam radiation therapy where the particles are protons or heavier ions (Figure 6.2 B).

Intraoperative radiation therapy is a special type of radiation therapy that is delivered immediately after surgical removal of the cancer. This method has been employed in breast cancer, brain tumors and rectal cancers.

External beam radiation therapy

External beam radiation is the most widely used type of radiation therapy. The radiation is focused from a source outside the body onto the area affected by the cancer. It is much like getting an x-ray, but for a longer time. This type of radiation is most often given by machines called linear accelerators. External beam radiation allows large areas of the body to be treated and allows treatment of more than one area such as the main tumor and nearby lymph nodes. External radiation is usually given in daily treatments over several weeks (Figure 6.8 A).

External beam sources

Linear accelerators are the common source of high energy X-ray beams producing megavoltage photons of between 4 and 20 million volt energy able to penetrate to the most deep-seated tumours in the largest of patients. Clinically, 4–8 MV beams are the most useful providing a balance between penetration and adequate surface dose. The fundamental property of megavoltage beams to have skin sparing is both beneficial in terms of reducing skin reaction but also potentially hazardous in reducing dose to surface or superficial tumour (Figures 6.7).

Modern high-energy linear accelerators offer a choice of ***photon*** and ***electron*** high-energies. The production of high-energy photons can be described briefly as

follows. Electrons are emitted from the heated gun filament, and their energy is gradually increased as they move through the waveguide. The beam of electrons is focused and to hit a high atomic number target. The resultant X-ray beam is collimated. The beam is collimated using of diaphragms and a set of multileaf collimator leaves (Figures 6.9).

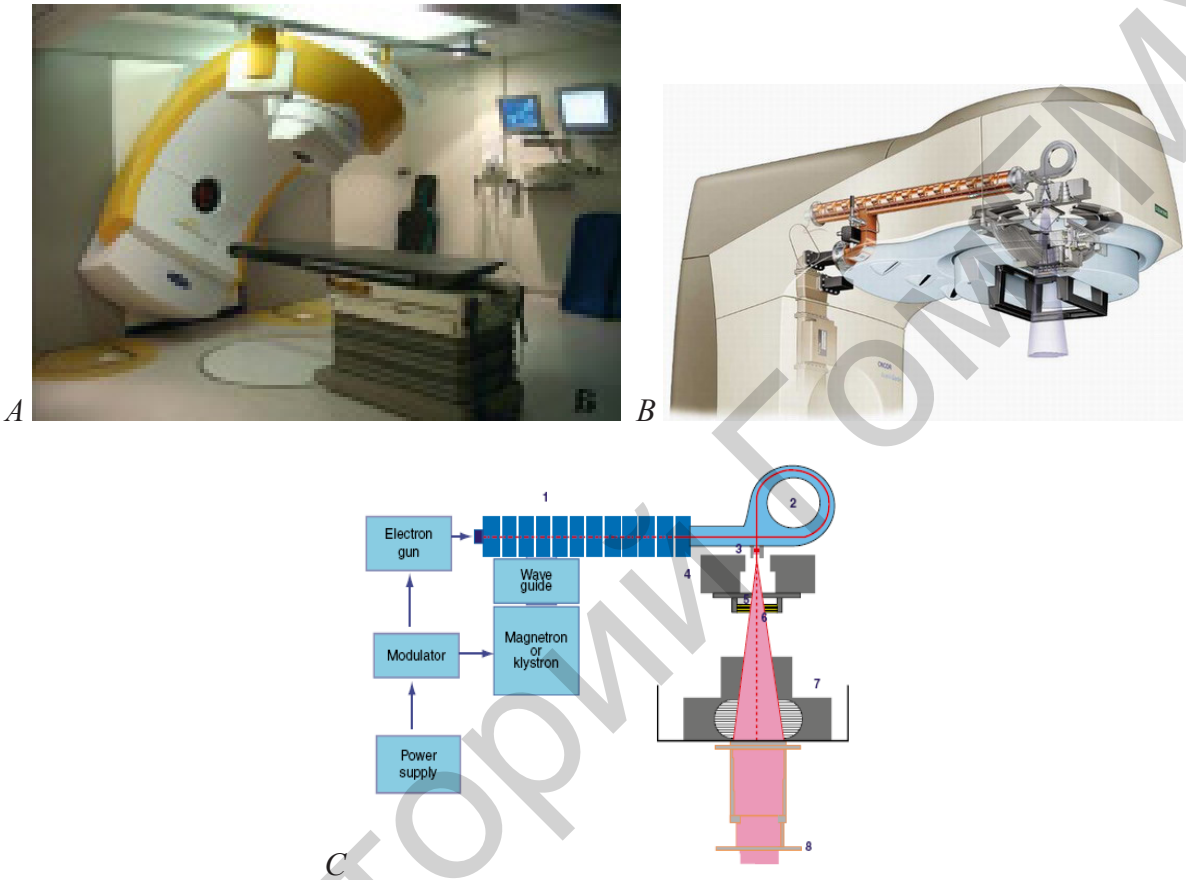

Figure 6.9 — (A) General illustration of a linear accelerator. (B) Treatment head of a linear accelerator. (C) Scheme of linear accelerator. (1) The production and the acceleration of electrons, (2) the 270° bending of electrons, (3) target and primary filter, (4) primary collimators, (5) main filter, (6) ionizing chamber, (7) multileaf collimator, (8) electron applicator

Electron beams used for treatment can be produced either by rapidly scanning the narrow beam of electrons across the desired area or more commonly the beam is broadened by the use of a scattering foil in place of the X-ray target. In normal use, a series of openings in an electron "applicator" are used to collimate the beam at or close to the patient's skin.

Cobalt machines were widely used in the past and in some centers still have their place. They require less maintenance comprising a cobalt source that releases gamma rays with energy equivalent 1 MV and a relatively simple mecha-nism exposing the source to provide the beam. The penetration of the beam, however, is relatively

poor and because it arises from a source of finite size the penumbra of the beam is quite large. Such considerations have led most centers to relegate cobalt units to be replaced by modern linear accelerators or, where retained, for palliative treatments and out of hours work where their simplicity does have advantages (Figure 6.10).

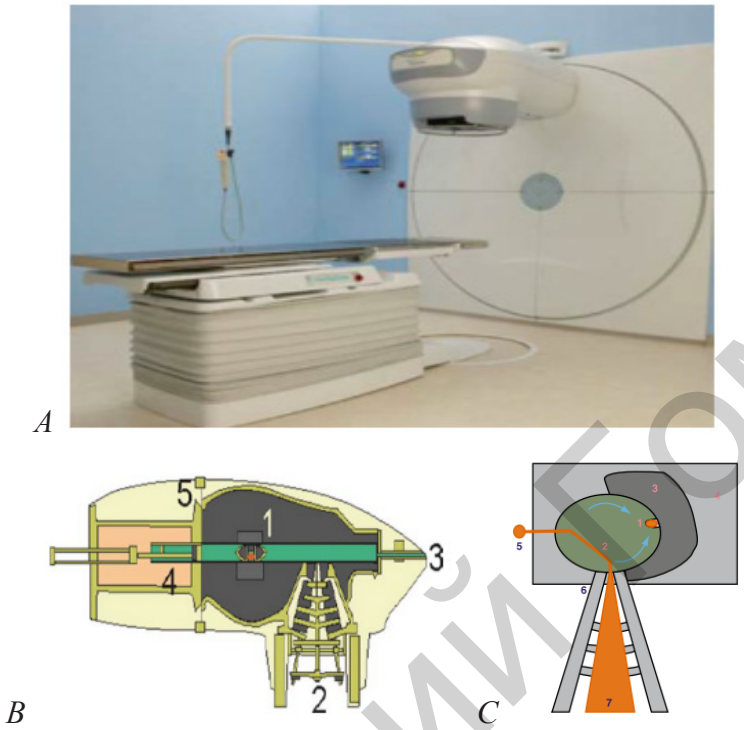

Figure 6.10 — (A) Modern cobalt-60 therapy unit.
(B) Scheme treatment head of a cobalt-60 teletherapy unit.
The cobalt source (1) is situated in a drawer, and surrounded by lead. When the device is in the resting position, the source is protected by layers of enriched uranium.
The source is then pushed by a pneumatic system (4) to the treatment position.
The collimator system (2); manual system that can pull the source to the resting position in case of emergency (3); link between the head and the rotating part of the machine that is used to change the source when its activity is no longer sufficient for treatment (5).
(C) Scheme cobalt-60 head variant: 1, cobalt-60 source; 2, tungsten cylinder; 3, enriched uranium; 4, lead; 5, laser source; 6, collimator; 7, γ-rays cobalt-60

Particle therapy

There are, however, many other particles that can be used in therapy. Neutrons have been evaluated over many years and their clinical utility remains limited and they cannot be regarded as part of routine clinical practice. Protons in contrast have excited increasing interest in recent years. Their main advantage is that their energy deposition follows the Bragg peak with a high-intensity highly localized deposition of energy at a fixed depth. This has advantages in the treatment of certain sites; for example, retinal tumours and tumours of the brain stem where highly localized energy deposition avoiding surrounding structures is required. They have also been used in other sites, for example, prostatic carcinoma, as a means of enabling dose escalation within normal tissue tolerance.

In particle therapy (proton therapy being one example), energetic ionizing particles are directed at the target tumor. The dose increases while the particle penetrates the tissue, up to a maximum (the Bragg peak) that occurs near the end of the particle's range, and it then drops to (almost) zero. The advantage of this energy deposition profile is that less energy is deposited into the healthy tissue surrounding the target tissue.

Internal radiation therapy

Also known as *brachytherapy* (break-e-THER-uh-pee), internal radiation is typically used when doctors needs to deliver a high dose of radiation to a small area. Rather than coming from machines outside body, the radiation source is placed inside body. Most often, the radioactive material — encased in wires, seeds, capsules or tubes (catheters) — is placed inside tumor (Figure 6.11).

Internal radiation implants containing radioactive material are usually placed during surgery or using a needle (interstitial radiotherapy). Brachythe-rapy may include placing implants inside a body cavity, such as the vagina (a technique called intracavitary radiation) or by putting radioactive material directly into body tissue (called interstitial radiotreatment). In both instances placement is usually done once, though it may be done up to several times, and is temporary, lasting from a few minutes to several days.

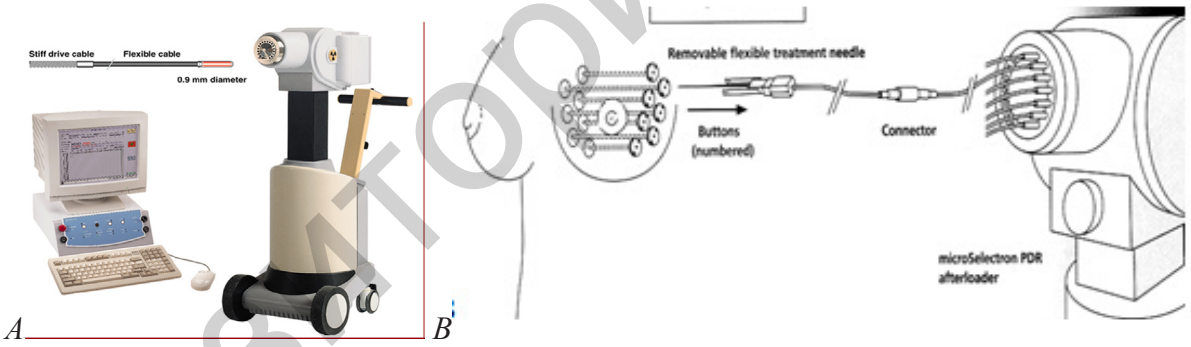

Figure 6.11 — (A) The device of contact radiotherapy "MICROSELECTRON" and (B) scheme using it for breast brachytherapy

As one example of the localized nature of breast brachytherapy, the device delivers the radiation dose through multiple catheters, each of which can be individually controlled (Figure 6.11 B). This approach decreases the exposure of healthy tissue and resulting side effects, compared both to external beam radiation therapy and older methods of breast brachytherapy. Severe pain or illness is not likely to occur during implant therapy.

In brachytherapy, radiation sources are precisely placed directly at the site of the cancerous tumour. This means that the ionizing irradiation only affects a very localized area — exposure to radiation of healthy tissues further away from the

sources is reduced. These characteristics of brachytherapy provide advantages over external beam radiation therapy — the tumour can be treated with very high doses of localized radiation, whilst reducing the probability of unnecessary damage to surrounding healthy tissues. A course of brachytherapy can often be completed in less time than other radiation therapy techniques. This can help reduce the chance of surviving cancer cells dividing and growing in the intervals between each radiation therapy dose.

Radionuclide therapy

Internal radiation can also be given systemically, meaning it travels throughout the body. Also called radiopharmaceutical therapy, systemic radiation uses radioactive material mixed in a solution. This type of radiation can be given intravenously through an IV, by mouth or it can be injected into a body cavity. For instance, if cancer has spread to bones, it might be inefficient to aim external radiation at every small spot where cancer has spread. But by giving radiation through an IV, the radioactive material can travel through the blood to each cancer site.

Systemic radionuclide therapy is a form of targeted therapy. Targeting can be due to the chemical properties of the nuclide such as radioiodine which is specifically absorbed by the thyroid gland a thousand fold better than other bodily organs. Examples are the infusion of oral iodine-131 to treat **thyroid cancer or thyrotoxicosis**.

A radioactive material is inserted directly into or next to a tumour and concentrates the dose there. The dose falls off very rapidly according to the inverse square law, and surrounding normal tissues receive substantially lower doses than the tumour. When 65 Gy are delivered at 0,5 cm from the source, the dose at 2 cm is only 4,0 Gy.

A major use of systemic radionuclide therapy is in the treatment of **bone metastasis** from cancer. The radionuclides travel selectively to areas of damaged bone, and spare normal undamaged bone. Isotopes commonly used in the treatment of bone metastasis are strontium-89 and samarium (^{153}Sm) lexidronam.

Dose distributions

An isodose curve connects points of equal dose in a single plane. The shape of the isodose curves is affected by the beam parameters such as field size and beam filter characteristics (Figures 6.6–6.9).

The penetrability, or energy, of an x-ray or gamma ray totally depends on its wavelength: The shorter the wavelength, the more penetrating the photon; conversely, the longer the wavelength, the less penetrating the photon. A low-energy beam (≤ 120 kVp) of radiation tends to deposit all or most of its energy on or near the surface of the patient and is suitable for treating lesions on or near the skin surface. In addition, with the low-energy beam, a greater amount of absorption or dose deposition occurs in bone than in soft tissue.

A high-energy beam of radiation (≥ 1 MeV) (Mega electron volts) tends to deposit its energy throughout the entire volume of tissue irradiated, with a greater amount of

dose deposition occurring at or near the entry port than at the exit port. In this energy range, the dose is deposited about equally in soft tissue and bone. The high-energy (megavoltage) beam is most suitable for tumors deep beneath the body surface.

Cobalt-60 units

The 60-Co unit was the first skin-sparing machine. The use of 60-Co units has declined significantly since the 1980s, and 60-Co is rarely used for conventional external beam radiation therapy today. This decline has been basically attributed to the introduction of the more sophisticated linac, which has greater skin-sparing capabilities and more sharply defined radiation fields. The radiation beam, or field, from a 60-Co unit also has large penumbra, which results in fuzzy field edges, another undesirable feature.

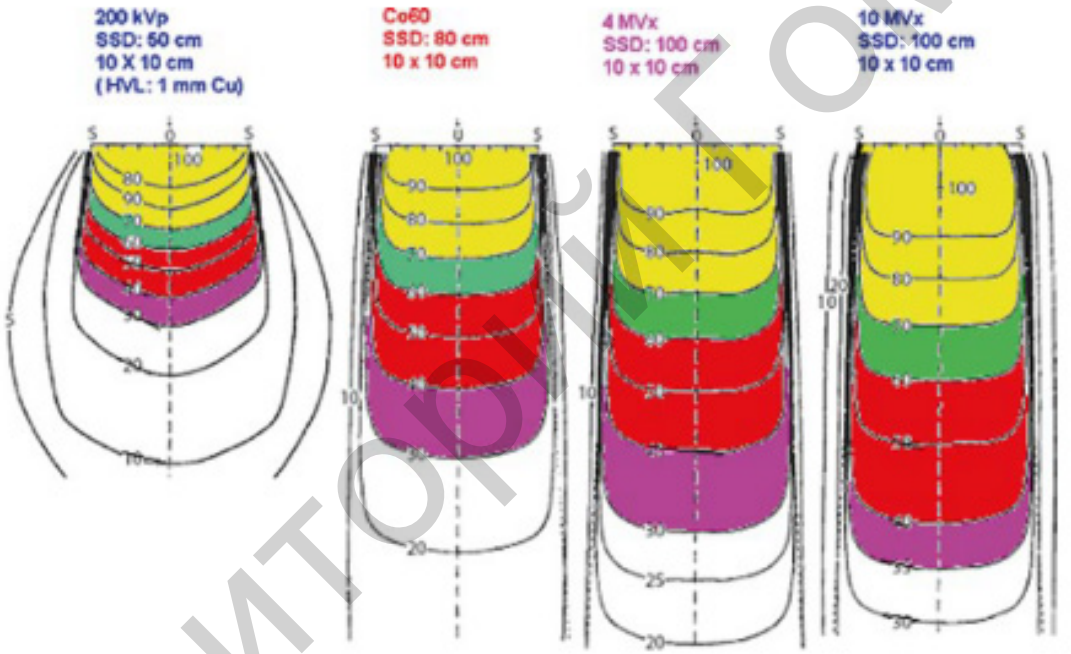

Figure 6.12 — Isodose curves (dose distribution) for various photon energies

Linear accelerators

Linacs are the most commonly used machines for cancer treatment. A linac is capable of producing high-energy beams of photons (x-rays) or electrons in the range of 4 million to 35 million volts. These megavoltage photon beams allow a better distribution of dose to deep-seated tumors with better sparing of normal tissues than their earlier counterparts — the orthovoltage or ^{60}Co units. The photon beam is produced by accelerating a stream of electrons toward a target. When the electrons hit the target, a beam of x-rays is produced. By removing the target, the linac can also produce a beam of electrons of varying energies.

Linacs can now be purchased with a single photon energy or a dual photon machine with two x-ray beams. Typically a dual photon energy machine consists of

one low-energy (6-MeV) and one high energy (18-MeV) photon beam plus a range of electron energies (Figure 6.14). The dual photon energy machine gives the radiation oncologist more options in prescribing radiation treatments. As the energy of the beam increases, so does its penetrating power. A lower energy beam is used to treat tumors in thinner parts of the body, whereas high-energy beams are prescribed for tumors in thicker parts of the body. A brain tumor or a tumor in a limb would most likely be treated with a 6-MeV beam; conversely, a pelvic malignancy would be better treated with an 18-MeV beam.

Electrons are advantageous over photons in that they are a more superficial form of treatment. Electrons are energy dependent, which means that they deposit their energy within a given depth of tissue and go no deeper, depending on the energy selected. An 18-MeV beam has a total penetration depth of 3,5 inches (9 cm). Any structure located deeper than 3,5 inches (9 cm) would not be appreciably affected. This is important when the radiation oncologist is trying to treat a tumor that overlies a critical structure (Figures 6.14).

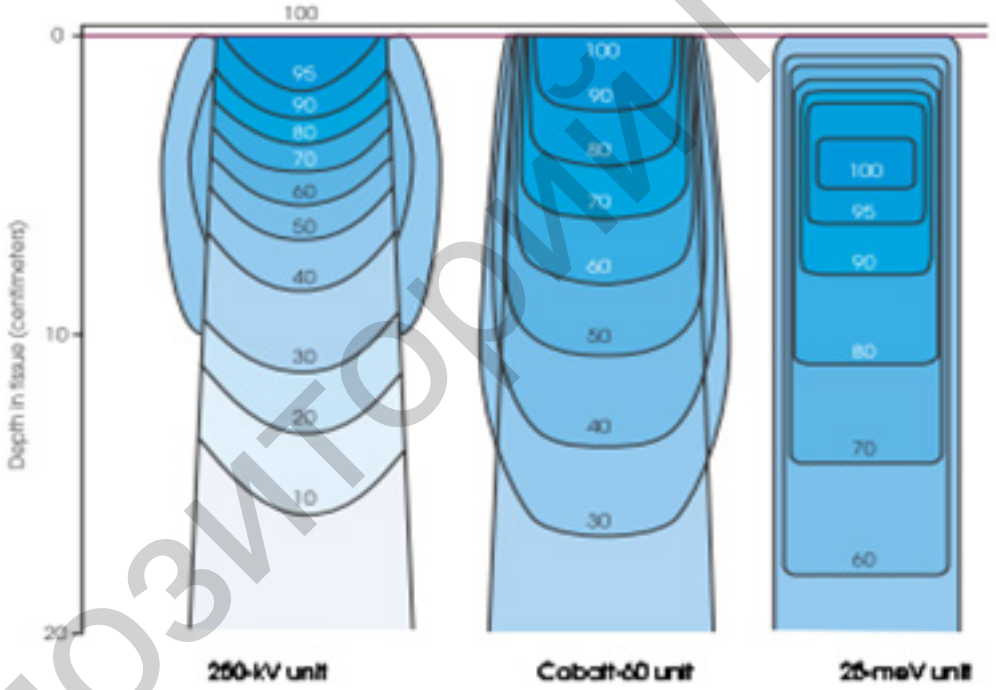

Figure 6.13 — Three isodose curves showing comparison of percent of dose deposition from three x-ray units of different energies. As the energy of the beam increases, the percentage of dose deposited on the surface of the patient decreases

The skin-sparing effect, a phenomenon that occurs as the energy of a beam of radiation is increased, is valuable from a therapeutic standpoint. In the superficial and orthovoltage energy range, the maximum dose occurs on the surface of the patient, and deposition of the dose decreases as the beam traverses the patient (Figures 6.13).

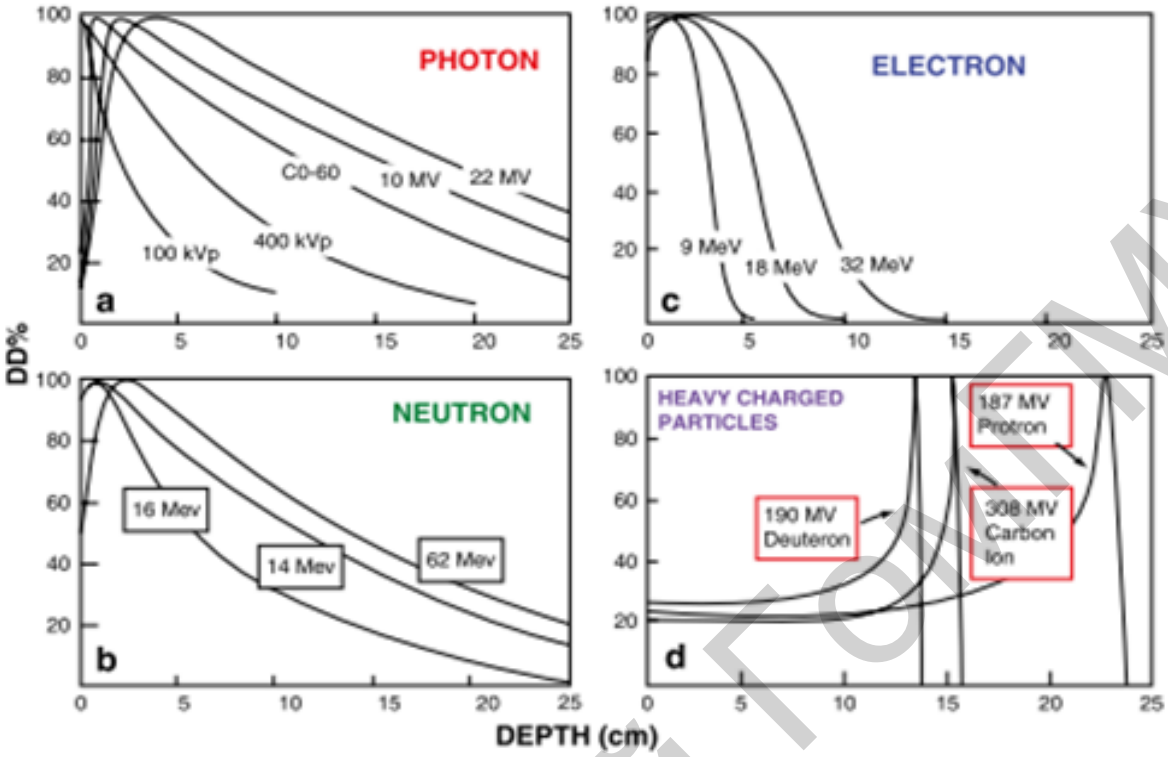

Figure 6.14 — Percentage depth dose curve for photon, electron, neutron and heavy charged particles

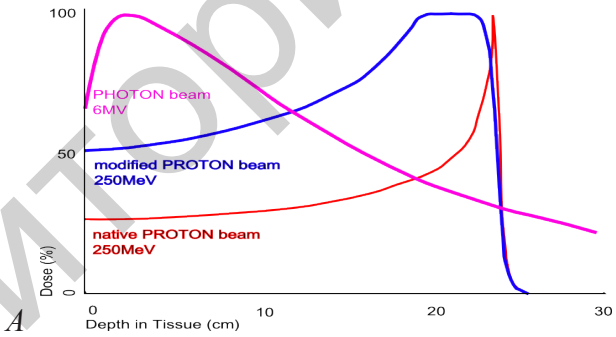

A

B C D

Figure 6.15 — (A) Examples of the percent depth doses as a function of depth. In 20 cm the proton dose is absorbed while a greater depth is needed to absorb the photon dose. (B) Protons (250 MeV) and photons (X-ray 6 MeV) percent depth dose curves. (B to D) Examples of interstitial dose distribution different quantity intratissues sources radiation (internal radiation implants)

As the energy of the beam increases into the megavoltage range, the maximum dose absorbed by the patient occurs at some point below the skin surface. The skin-sparing effect is important clinically because the skin is a radiosensitive organ. The greater the energy of the beam, the more deeply the maximum dose is deposited (Figure 6.14).

For megavoltage photons, the maximum dose does not occur at the surface but at a depth of a few millimeters (D*max*). The depth at which the maximum dose occurs is dependent primarily on the beam energy. After D*max*, a gradual decrease in the dose deposited occurs as the number of photons in the beam is reduced (Figure 6.15). In contrast to photons, electron beams begin to deposit energy immediately on entering the patient.

Radiology therapy of malignant tumours

Radiation therapy may be used to treat localized solid tumors, such as cancers of the skin, head and neck, brain, breast, prostate and cervix, it can also be used to treat leukemia and lymphoma.

RT is commonly applied to the cancerous tumor because of its ability to control cell growth. Ionizing radiation works of exposed tissue leading to cellular death. To spare normal tissues (such as the skin or the organs which radiation must pass through in order to treat the tumor), shaped radiation beams are aimed from several angles of exposure to intersect at the tumor, providing a much larger absorbed dose there than in the surrounding, healthy tissue.

External radiotherapy techniques

These cases include tumors of the parotid, ear, oral cavity, and oropharynx. Electron beams may be the primary mode of therapy or combined with photon beams. There are major clinical applications, such as treating a radically dissected neck or areas in which there is a high risk of residual disease. Electron beam therapy can also be used to boost the dose to specific sites, such as the breast or to lymph nodes.

Shielding electron beams clinically is easily done with high-density materials, such as lead. One centimeter of lead transmits only 5% of an 18 MeV electron dose. Electrons produced at the 7 MeV level require only 2 mm of lead. Added distance alone offered by intervening tissues significantly decreases the dose to deeper structures. For treating lesions of the oral cavity, intraoral stents contain lead, and protection of adjacent tissues is achieved by increasing the distance with tissue-equivalent Lucite. Because of the easy blocking of the beam by dense materials, lead is used extensively for defining treatment fields and for actual field shaping. The fields may be defined by lead cutouts placed on a tray attached to the head of the accelerator. Special electron beam cones are commercially available. The area covered to the 80% line of the 18 MeV electron beams is decreased by 0,5 cm at all margins of the field by shielding, requiring a proportionately larger field to ensure

coverage of the entire lesion and a satisfactory surrounding margin. A differential in depth dose may be achieved by plastic energy moderators placed over a portion of the field.

Clinical applications of electron beam therapy

Electron beams are particularly useful in the treatment of superficial and subcutaneous volumes of tissue, particularly if the treatment should be limited to a unilateral lesion requiring a low dose to the opposite side of the body (Figures 6.16 A to B).

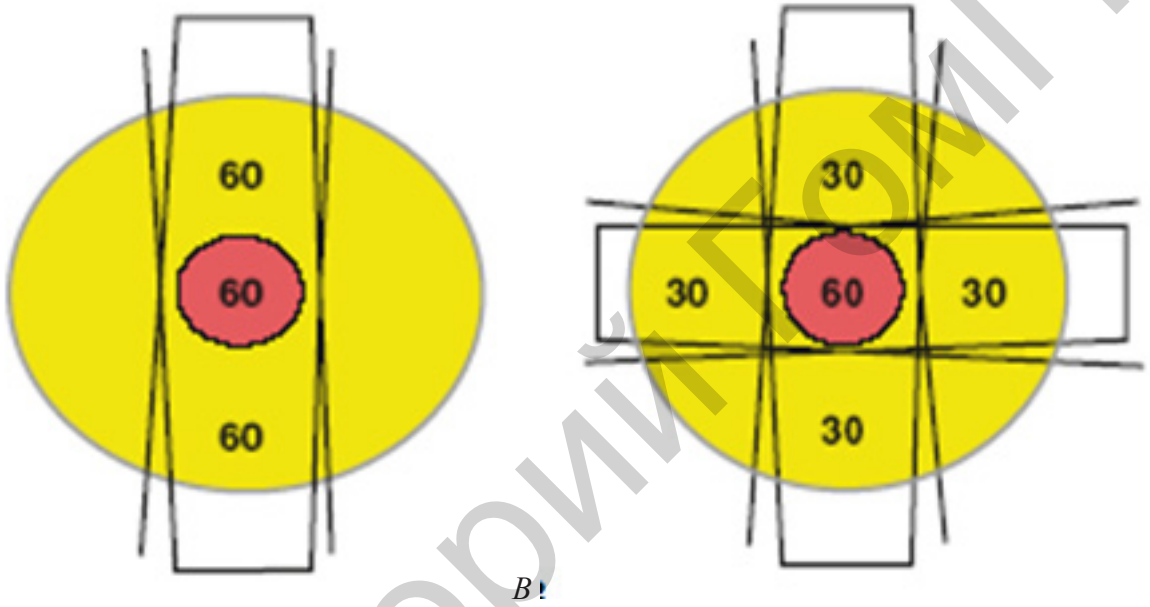

Figure 6.16 — Multiple radiotherapy fields, doses distribution and isodose arias. (A) Two field irradiations. (B) Four fields irradiations

Skin and lip tumors RT

Electron beam therapy is ideal for radiation therapy of all skin and lip cancers and is particularly useful in the treatment of lesions that present problems or are critically located (e. g., lesions involving the eyelid, nose, or ear). For small superficial basal cell carcinomas, a 1-cm margin surrounding the gross lesion is adequate. In large infiltrative lesions with diffuse induration associated with a surgical scar, 2- or 3-cm margins are required, with wide borders of uninvolved tissue. For squamous cell carcinoma, the field usually can be reduced at 50 Gy. Most lesions located on the eyelids, external nose, cheeks, or ears are not deeply invasive and are treated with electron beams at energies of 6 MeV to 9 MeV. If the lesion approaches 2 cm in thickness, 9-MeV to 12 MeV electron beams should be used. Protective devices should be designed to delineate the treatment field and to conform to the irregular shape of a lesion. A wax ledge placed around the opening in a lead mask may provide a seating for the treatment portal and enhance precision in directing the beam.

To achieve almost complete protection, 3 mm of lead, which absorbs almost 98% of 7 MeV electron beams, should be used. Lead is also used for protection of the deeper structures. In treatment of the cheek or the lip, lead in an intraoral stent made for the patient protects the gingiva and tongue. For treatment of the eyelid or near the eye, a lead shield is placed under the lid. Because the eye shields must be thin, they are suitable only for 7 MeV electron beams. Thicker external blocks may be necessary to protect the eye at higher electron energies.

Upper respiratory and digestive tracts RT

Electron beams alone may be used to treat carcinomas of the upper respiratory tract and digestive passages, frequently combined with external beam high-energy photons or with interstitial brachytherapy, as in the treatment of well-lateralized lesions of the oral cavity, oropharynx, hypopharynx, or larynx.

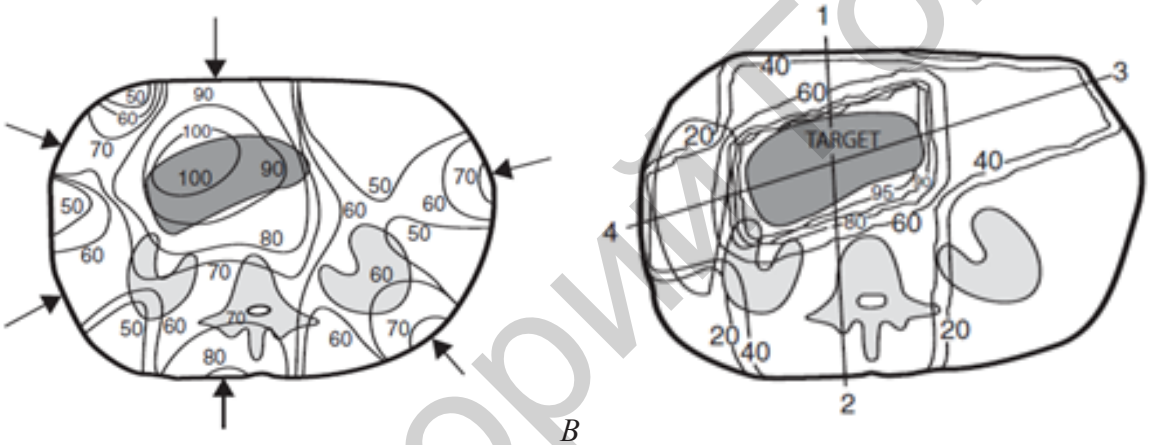

Figure 6.17 — Comparison of treatment plans axial isodoses (dose distribution) for the distant radiotherapy of a case pancreas carcinoma using different photons beams. (A) 250 keV 6 fields and (B) 18 MeV X-rays 4 fields

Electron beam therapy for lesions of the oral cavity may be used with intraoral cones, which must provide coverage of the lesion with an adequate margin of normal mucous membrane on all sides. An intraoral stent may be necessary to maintain the position of the cone and to reproduce the placement of the cone at each treatment session. The electron energy (6, 9, or 12 MeV) is chosen according to the characteristics of the tumor and the depth of extension of the tumor (Figure 6.17).

Breast cancer RT

Electron beam therapy has been of particular value in the treatment of breast cancer, both for administering an additional dose to the site of tumor excision in conservation treatment and for treating subclinical disease in patients who have had surgical removal of the primary breast lesion and axillary lymphatics. During radiation therapy, the supine patient has the arm abducted to 90 degrees and the forearm maintained in an upright position by a hanging bar, which the hand grasps.

The head may be turned sharply to the contralateral side. The beam remains vertical. Various manipulations of the machine, collimator, and other factors may be needed to achieve proper placement of the treatment field.

Radiation therapy may also be designed for the chest wall. Because the average chest wall thickness after radical mastectomy is the 2,0 cm, low-energy electron beams (6 to 9 MeV) may be appropriate. If the chest wall thickness is greater, electron beams of high energy (12 MeV) may be necessary. Computed tomography offers an excellent means of measuring the thickness of the chest wall and aids in the choice of the appropriate energy level to be used.

Salivary gland tumors RT

Treatment for salivary gland tumors generally uses electrons (80% of dose) in combination with photons (20% of dose). The application of electron beam therapy alone or with photon beams is most effective after the bulk of the tumor has been removed. The area to be irradiated includes the entire parotid bed and the full extent of the surgical scar. However, special consideration should be given to potential seventh cranial nerve involvement in all patients with adenocystic carcinomas. The temporal bone must be irradiated. The entire ipsilateral neck may be irradiated in treating the parotid gland area if the primary tumor is a high-grade malignancy, if the tumor is found in connective tissues, if there is extensive invasion of perineural lymphatics, or if there are positive nodes in the operative specimen.

Neoplasm of other sites RT

Certain lymphomas that present as subcutaneous masses or dermal lesions can be treated by electron beam therapy. In many soft tissue sarcomas, electron beam therapy can be used as total treatment or as an adjunct to photon beam treatment, with preservation of function and diminution in the number of late side effects of the treatment. Primary or recurrent carcinomas of the vulva, distal vagina, urethra, suburethral area, or other areas that recur after surgical removal and carcinomas of the cervix that recur in the vagina may be treated with electron beams (6, 9, or 12 MeV), incorporating an appropriate bolus. Intraoperative electron beam used as a boost followed by photon beam treatment represents an innovative regimen, particularly in treating gastric cancer, retro-peritoneal sarcomas, head and neck cancers (Figure 6.18), and genitourinary and gynecologic cancers.

For curative cases, the typical dose for a solid epithelial tumor ranges from 60 to 80 Gy, while lymphomas are treated with 30 Gy. Preventative (adjuvant) doses are typically around 50 Gy in 2 Gy fractions (for breast, head, and neck cancers).

Brachytherapy

Skin cancer

Radiation therapy is an important management option in selected patients, offering an advantage in treating large lesions with deep tissue infiltration. Treatment mar-

gins may be as wide as necessary for facial tumors, obviating the need for extensive surgical reconstruction. Radiation may be preferred for elderly, debilitated, or medically inoperable patients as anesthesia is not necessary, and when cosmesis is not a factor, fractionation can minimize the number of treatments.

Skin cancers with perineural invasion are particularly difficult to control, and salvage after surgical recurrence is unlikely. Treatment fields encompass the nerve at risk to the base of skull with postoperative radiation to 60 Gy to the tumor bed, 50 Gy to the proximal involved nerve with negative surgical margins, and 70 Gy for microscopic or gross positive margins (Figure 6.19).

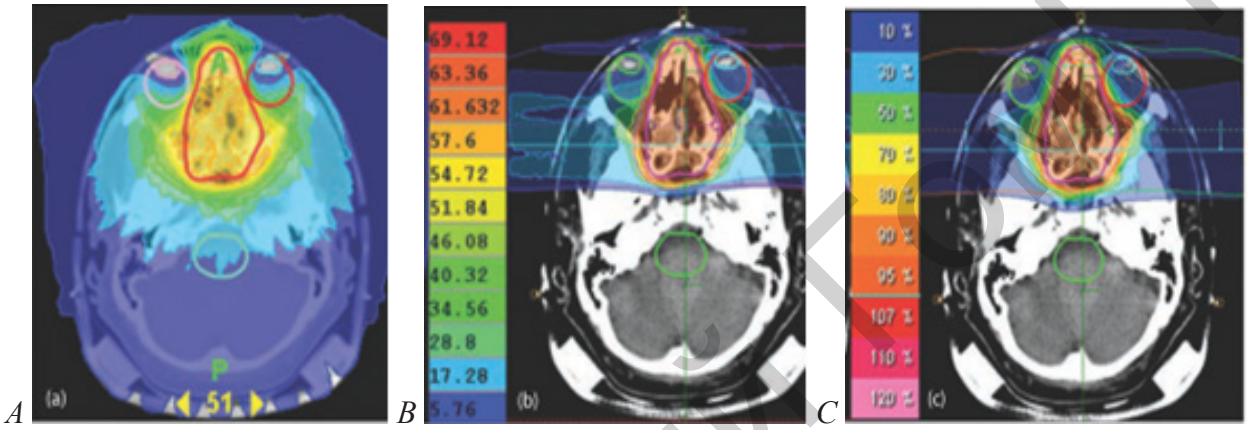

Figure 6.18 — Comparison of dose distributions between different RT for the treatment of an ethmoid sinus meningioma. (A) 6 MeV, tomotherapy, 57.6 Gy in 32 fractions. (B) 160 MeV, 57.6 Gy equivalent in 32 fractions. (C) Carbon ions 60 Gy (in 20 fractions)

Figure 6.19 — (A) Skin cancer of the face before and 181 days after a single brachytherapy treatment. (B) Wide ulcerated skin cancer of the temple before and 83 days after a single BT treatment

Customized surface molds employing afterloading ^{192}Ir or high-dose-rate brachytherapy sources are useful when protracted daily treatment fractionation is inconvenient or for treatment of lesions on the shin or dorsum of the hand, where conventional radiation therapy is poorly tolerated. Low-dose-rate interstitial brachytherapy can treat periorificial tumors of embryonic fusion regions of the face. Excellent disease control and cosmesis are reported with doses of 50 Gy at dose-rates 2 Gy/hr with low risk of late complications.

Esophageal cancer

In addition to external beam radiation therapy, intracavitary therapy can be used with curative or palliative intent. The advantage of brachytherapy centers on exploitation of the inverse square law and quick dose falloff, thus sparing surrounding tissues from radiation while providing focal dose escalation. The radioactive source of choice is usually iridium-192 (^{192}Ir). High-dose-rate (HDR) techniques can deliver 100 to 400 Gy per hour, allowing treatment to be given in 5 to 10 minutes.

With brachytherapy, an afterloading catheter is introduced through the nose into the esophagus to the primary tumor site under fluoroscopic guidance. After localization films are taken and dosimetry generated, the catheter is then attached to a remote afterloader through a guide cable and the ^{192}Ir source inserted through remote control. Dose can be shaped and modified through the use of dwell times.

For patients treated with curative intent (unifocal thoracic tumors < 10 cm, no distant metastases, no airway involvement or cervical esophageal location), the American Brachytherapy Society recommends a brachytherapy dose of 10 Gy in 2 weekly fractions of 5 Gy each or 20 Gy in a single course at 1 Gy per hour. The recommended active length is the visible mucosal tumor with a 1- to 2- cm proximal and distal margins. Ideally, brachytherapy is started 2 to 3 weeks following completion of concurrent external irradiation/chemotherapy to allow mucositis resolution.

Prostate cancer

Brachytherapy for early-stage disease: preplanned transperineal implantation. With the advent of transperineal CT and ultrasound-guided permanent prostatic implantation, the accuracy of isotope source placement has dramatically improved compared with older retropubic methods.

A computerized plan is generated from the transverse ultrasound images, producing isodose distributions and the ideal location of seeds within the gland to deliver the prescription dose to the prostate. Several days to weeks later, the implantation procedure is performed. Needles are then placed under ultrasonographic guidance through a perineal template according to the coordinates determined by the preplan. Radioactive seeds are individually deposited in the needle with the aid of an applicator or with preloaded seeds on a semirigid strand containing the preplanned number of seeds.

At present, the commonly used dose for interstitial implantation is 140 Gy, prescribed to the isodose surface that completely encompasses the prostate as contoured from imaging studies.

Soft tissue sarcomas

Brachytherapy may be used as the sole radiation therapy mode of treatment, using doses of 50 Gy. For unresectable sarcomas, doses above 70 Gy are used, limiting the high-dose volume to the tumor plus a minimal margin.

Interstitial brachytherapy can be used to deliver all or part of the radiation dose. After surgical excision of the tumor, hollow plastic afterloading catheters are inserted using sharp metal troacars in a single plane at approximately 1cm intervals within the tumor bed (Figure 6.20). Surgical clips placed at the margin of the tumor bed permit the target volume to be delineated for planning purposes, and the catheters are secured in place.

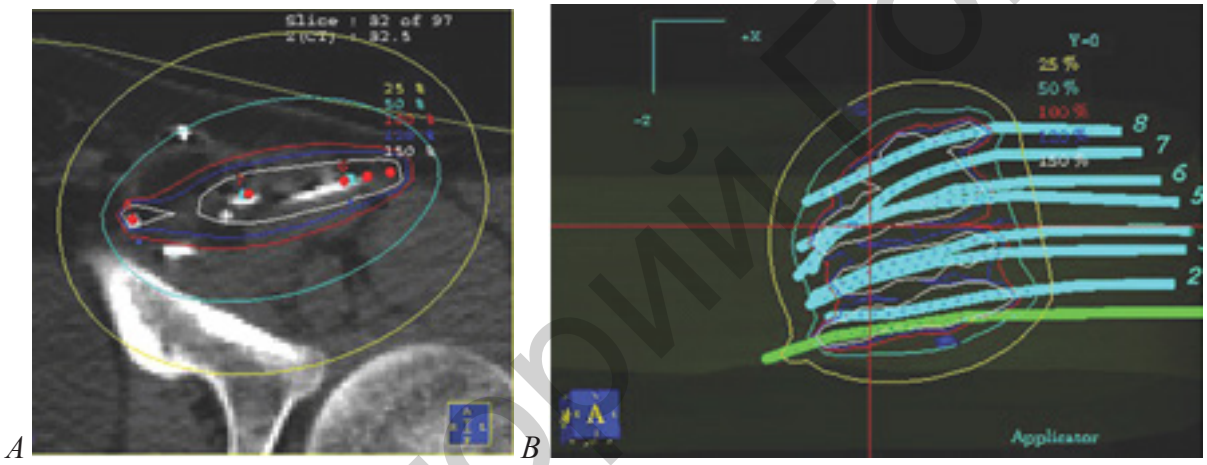

Figure 6.20 — (A) Example dose distribution from radionuclide interstitial a needles. Parasagittal CT reconstruction with isodose distributions in soft tissues. (B) Three-dimensional computer-generated image of radioactive applicators inside of the tumor and isodose lines, demonstrating excellent coverage with the prescription dose

Catheters are loaded with wired ^{192}Ir seeds no sooner than the sixth postoperative day to reduce the risk of wound complications. After completion of the treatment, sources are removed and catheters are cut at one end for removal by pulling through the skin.

For radioimplants, a dose of 45 Gy has been shown to be adequate adjuvant treatment when used alone for high-grade lesions. Brachytherapy treatments are usually given twice daily at 5 Gy per fraction to 50 Gy.

Treatment of thyroid cancer

The thyroid gland absorbs nearly all of the iodine in the blood. Because of this, radioactive iodine (also known as radioiodine or iodine-131) can be used to destroy the thyroid gland and thyroid cancer with limited effects on the rest of the body. This

treatment is often used after thyroid cancer surgery to destroy any thyroid cells that may have been left behind, or to treat some types of thyroid cancer that have spread to lymph nodes and other parts of the body. An international trial has been performed for ablation of cancer cells thyroid tissue using 3.7 GBq (100 mCi) of ^{131}I.

Iodine-131 therapy may be combined with external radiation therapy. The dose to metastases from ^{131}I may be calculated using single-photon emission computed tomography (SPECT) imaging.

In patients with unresectable or inoperable primary tumors, ^{131}I does not seem to affect the rate of tumor regression appreciably or to prolong survival. A combination of ^{131}I and external radiation therapy seems to offer the best results.

Side effects of radiation therapy

Radiation therapy is painless in itself. Many low-dose palliative treatments (for example, radiation therapy to bony metastases) cause minimal or no side effects, although short-term pain flare up can be experienced in the days following treatment due to oedema compressing nerves in the treated area. Higher doses (after radiology treatment of malignancy) can cause varying side effects during treatment (acute side effects), in the months or years following treatment (long-term side effects), or after re-treatment (cumulative side effects). The nature, severity, and longevity of side effects depends on the organs that receive the radiation, the treatment itself (type of radiation, dose, fractionation, concurrent chemotherapy), and the patient.

Most side effects are predictable and expected. Side effects from radiation are usually limited to the area of the patient's body that is under treatment. One of the aims of modern radiation therapy is to reduce side effects to a minimum, and to help the patient to understand and to deal with those side effects which are unavoidable.

The extent and the exact type of side effects are determined by the location of the tumor and the location of the radiation being delivered. The side effects of radiation therapy depend on the treatment dose and the part of the body that is being treated. The most common side effects may be loss of hair in the area being treated, tiredness, skin reactions (such as rash or redness) in the treated area, loss of appetite, and nausea. Radiation therapy may also cause a decrease in the number of white blood cells (cells that help protect the body against infection).

The main side effects reported are fatigue and skin irritation, like a mild to moderate sun burn. The fatigue often sets in during the middle of the course of treatment and can last for weeks after the treatment ends. The irritated skin will heal, but may not be as elastic as it was before.

For instance, patients who are undergoing breast irradiation will typically experience a redness, dryness or itchiness of the breasts that usually begins two to three weeks after the treatment is commenced. It will then continue, but will eventually leave several weeks after the radiation treatment course is completed.

Another example of a side effect is diarrhea, nausea or vomiting. This is sometimes experienced by patients undergoing radiation treatment to their abdomens or bowels. In most cases, these side effects, which are called acute, take place during the radiation treatment course and will continue for a few weeks after the course is completed.

In almost all cases, these side effects will go away and patients will be fine. In rare instances, some patients will experience long-term side effects or complications, because the radiation causes damage to an internal organ adjacent to or near the tumor site.

Normal tissue reactions

Normal tissues vary in their response to radiation. As with tumors, normal tissues that are dividing more rapidly may be affected and cause some of the side effects of radiation treatment. Since radiation is a local treatment, side effects are usually confined to the area being treated (Figure 6.21).

Figure 6.21 — Typical skin patient reaction after external beam therapy

The early reactions are seen during the first days or weeks after irradiation (for example diarrhea or acute mucositis) and may continue for several weeks after treatments are completed. They are temporary because the cell deficit is compensated for by the repopulation of stem cells, and subsequently of differentiated cells. Late reactions due to the damage of the late-reacting tissues, for instance blood vessel damage, fibrosis, telangiectasia, etc, may be seen several months later.

Common side effects of radiation therapy

— Hair loss in the area being treated.
— Fatigue.
— Skin reactions in the treated area.
— Loss of appetite.
— Nausea.

Acute side effects

Fatigue is a general effect of radiation but the exact cause is unknown. The tumor may cause the immune system to make substances that lead to fatigue. Fatigue may also be caused by anemia (low red blood cell count), poor nutrition, pain, medicines such as steroids or chemotherapy, depression, and stress. There is no single treatment for fatigue, but if possible, the cause of the fatigue is addressed. For example, if the fatigue is in part caused by anemia, some patients will benefit from blood transfusions or from medicines to stimulate the body to make more red blood cells.

Epithelial surfaces may sustain damage from radiation therapy. Depending on the area being treated, this may include the skin, oral mucosa, pharyngeal, bowel mucosa and ureter. The rates of onset of damage and recovery from it depend upon the turnover rate of epithelial cells. Typically the skin starts to become pink and sore several weeks into the treatment. The reaction may become more severe during the treatment and for up to about one week following the end of the radiation therapy, and the skin may break down. Although this moist desquamation is uncomfortable, recovery is usually quick. Skin reactions tend to be worse in areas where there are natural folds in the skin, such as underneath the female breast, behind the ear, and in the groin.

Skin

Modern radiation therapy may cause less damage to the skin than in earlier types of therapy because most of the radiation dose is delivered below the surface of the skin. During the first 2 weeks of the treatment, a faint and short lasting redness may occur. Dryness and peeling of the skin, called dry desquamation, may occur in 3 to 4 weeks. The skin over the treatment area may become darker. This is because of the effect radiation has on the cells in the skin that produce pigment.

The skin may also become dry and itchy. Moisturizing the skin with aloe vera, lanolin, or vitamin E may help. After a month of treatment, some people receiving radiation may experience some extreme peeling and weeping (moist) areas. Let your medical care team know if this occurs. Later effects of radiation may include thinning of the skin. The skin may feel hard, especially if surgery has also been done in the same area. Some people may have trouble with wound healing in the area that was treated.

Lung

When radiation treatments include the chest area, the lungs can be affected. One early change is a decrease in the levels of surfactant, the substance that helps keep the air passages open. This keeps the lungs from fully expanding, which may cause shortness of breath or cough. These symptoms are sometimes treated with steroids.

A possible late effect of radiation on the lungs is fibrosis (stiffening or scarring), which reduces the ability of the lungs to inflate and take in air. If a large area of the lungs is irradiated, these changes can cause shortness of breath and less tolerance for physical exercise.

Digestive tract

Radiation to the thorax and abdomen may result in swelling and inflammation of the esophagus, stomach or intestines, causing nausea, vomiting, or diarrhea. The

lower bowel may be treated directly with radiation (treatment of rectal or anal cancer) or be exposed by radiation therapy to other pelvic structures (prostate, bladder, female genital tract). Typical symptoms are soreness, diarrhea, and nausea. Antacids, sometimes combined with a numbing medicine such as lidocaine, may be helpful in relieving pain from inflammation of the esophagus. Nausea and vomiting can also be treated with medicines. If it is severe, some patients may need intravenous fluids to avoid or treat dehydration. Diarrhea can be treated with medicines and by avoiding spicy.

Swelling (edema or oedema) — as part of the general inflammation that occurs, swelling of soft tissues may cause problems during radiation therapy. Surgical intervention may be considered prior to treatment with radiation. If surgery is deemed unnecessary or inappropriate, the patient may receive steroids during radiation therapy to reduce swelling.

Late side effects

Late side effects occur months to years after treatment and are generally limited to the area that has been treated. They are often due to damage of blood vessels and connective tissue cells.

Fibrosis — tissues which have been irradiated tend to become less elastic over time due to a diffuse scarring process.

Epilation (hair loss) may occur on any hair bearing skin with doses above 1 Gy. It only occurs within the radiation field/s. Hair loss may be permanent with a single dose of 10 Gy, but if the dose is fractionated permanent hair loss may not occur until dose exceeds 45 Gy.

Dryness — the salivary glands and tear glands have a radiation tolerance of about 30 Gy in 2 Gy fractions, a dose which is exceeded by most radical head and neck cancer treatments. Dry mouth (xerostomia) and dry eyes (xero-phthalmia) can become irritating long-term problems.

Radiology therapy of benign diseases

Radiation therapy attacks reproducing cancer cells, but it can also affect reproducing cells of normal tissues. The damage to normal cells is what causes side effects. Each time radiation therapy is given it involves a balance between destroying the cancer cells and sparing the normal cells.

Radiation therapy has several applications in non-malignant conditions, such as the treatment of trigeminal neuralgia, severe thyroid eye disease, and prevention of keloid scar growth. The use of radiation therapy in non-malignant conditions is limited partly by worries about the risk of radiation-induced cancers. Radiation can sometimes play a role in the development of cancer, particularly if people are exposed to it at an early age. We are all aware of the increased frequency of cancers, especially leukemias, among Japanese survivors of World War II. Patients should bear in mind that radiation, as delivered in a radiation department, is a very careful, precise and well monitored treatment which very rarely leads to the development of cancer.

The use of radiation in the treatment of benign diseases has a long history. Soon after the discovery of x-rays by Roentgen in 1895, the therapeutic potential of radiation was recognized. In the first half of the 20th century, radiation therapy was used empirically for a host of conditions, both benign and malignant. In many situations in which no effective therapeutic alternatives existed, radiation therapy may have been one of the few treatment options available. Even with recognition of the risks of late skin injury, carcinogenesis, leukemogenesis, and genetic damage from all ionizing radiation, radiation therapy also continues to be accepted treatment for benign diseases that do not respond to other methods of traditional therapy.

In many cases, the use of radiation therapy for benign disorders may be able to spare the patient morbidity associated with the progression of the disease, or additional medical or surgical therapy.

The need for informed consent exists everywhere in radiation oncology, and certainly in the use of radiation therapy for benign diseases. Patients should be informed of the rationale, potential side effects, and treatment alternatives to radiation treatment before it is delivered.

Radiation carcinogenesis, although always a concern when ionizing radiation is used, appears to be a greater risk for pediatric patients and young adults than for older adults, and must be weighed in relation to the consequences of progressive disease and the side effects associated with alternative therapies. Special caution should be used before radiation is delivered to pediatric patients and young adults for benign conditions. These young patients may be at increased risk of second malignancy induction and late atrophy, especially if the area to be treated is in proximity to the breasts or thyroid, tissues that may be sensitive to carcinogenesis. As in all aspects of radiation therapy, care should be taken to use beams of appropriate energy and to shield adjacent normal structures.

Technical considerations

1. Before institution of therapy, the quality of irradiation, total dose, overall time, underlying organs at risk, and shielding factors should be considered.

2. Meticulous radiation protection techniques, including cones and lead shields, should be used in all instances.

3. The depth of penetration of the ionizing radiation beam should be chosen in accordance with the depth of the pathologic process.

As in all radiation therapy, the choice of beam ionizing energy depends on the depth of the target volume, and every effort is made to spare normal underlying tissue in superficial lesions. Absorption data for ionizing radiation therapy are readily obtained from standard depth-dose tables.

Internal lead shields placed in oral or nasal cavities tend to increase the dose to overlying tissue for both x-ray and electron-beam treatments. This increase is caused by backscattered electrons and may be minimized by encasing the shields in plastic.

Exophthalmos

Signs and symptoms of Grave's ophthalmopathy include bilateral exophthalmos, extraocular muscle dysfunction, diplopia, blurred vision, eyelid and periorbital edema, chemosis, lid lag and retraction, and compressive optic neuropathy. The pathogenesis is believed to be an autoimmune disease in which activated T-lymphocytes invade the orbit and stimulate glycosaminoglycan production in fibroblasts, resulting in tissue edema, lymphocytic infiltration, and marked enlargement of the extraocular muscles. Because lymphocytes and fibroblasts are sensitive to radiation, retrobulbar irradiation is a logical method of treatment. Systemic high-dose steroids are customarily used, but they must be given for long periods and have many side effects. Surgical orbital decompression is used when there is rapidly progressive optic neuropathy or severe proptosis.

Megavoltage external-beam irradiation using precise planning with high-resolution computed tomography (CT) scans and complete patient immobilization is recommended for optimization of dose distribution and to avoid unwanted irradiation of sensitive structures (e. g., lens, pituitary gland).

Small opposed bilateral fields are used to encompass both retrobulbar vo-lumes with customized blocks to shield periorbital structures. Either a split-beam technique or a 5-degree posterior angulation should be used to avoid the lens. The total dose is 20 Gy to the midplane, given in 10 fractions over 2 weeks. Photons of 5 MV are used in most cases.

Keloids

Some persons have a tendency to react to skin trauma with excessive production of fibrous tissue that extends beyond the wound, becomes hyalinized, and does not regress spontaneously. These keloids become unsightly masses, and they frequently cause itching and pain. They may occur in susceptible individuals after infection, burns, or (most commonly) surgical wounds.

Although suture tension and stitch infection in the wound may be contribu-ting factors, the recurrence rate after excision is very high even in their absence, and surgical treatment alone is not recommended.

Radiation therapy is usually started within 24 hours after excision, using 120 kV x-rays or low-energy electrons. The radiation field is custom-shaped with lead, with a 0,5 cm margin around the suture lines. The ear lobes, when treated, are taped away from the face, and a direct anterior or posterior field is used with a small cone. If the lobe is more than 1-cm thick and the wound extends around it, a higher-energy beam is needed. The total dose is 10 to 15 Gy in two to five fractions in 1 to 2 weeks.

Treatment of established keloids by irradiation alone is not as successful but may be attempted if surgery is not indicated (e. g., in an elderly patient with a large symptomatic lesion or in presternal and shoulder keloids that commonly recur even after combined treatment.

Cutaneous lesions

Treatment of cavernous hemangiomas of the skin in infants by repeated doses of radium in surface applicators was commonplace many years ago. A trial of oral steroids is now the preferred treatment for skin hemangiomas requiring intervention, such as rapidly growing facial lesions causing disfigurement, and radiation therapy is reserved for lesions that threaten function or life and have failed alternative therapies.

For minor superficial hemangiomas, contact radiation therapy is most suitable. The skin dose is 5 to 10 Gy per treatment. For thicker lesions, orthovoltage irradiation is recommended, with doses of 1 to 4 Gy per treatment.

Bursitis and tendinitis

Bursitis and tendinitis most commonly affect the shoulders. These disorders are caused by degenerative and inflammatory changes in the supraspinatus and infraspinatus tendons that lead to calcium deposition, inflammation of the surface of the subdeltoid bursa, and even rupture and discharge of calcific material into the bursa. Calcification may occur without symptoms, or there may be pain, tenderness, and limitation of motion in acute, subacute, or chronic forms. It is probably true, however, that irradiation is equally effective and is sometimes successful when invasive local treatments are not.

Limited fields encompass the joint only, using either opposed or occasionally a single anterior field. A daily dose of 1,5 to 2 Gy is given on 3 to 5 successive days for a total of 6 to 10 Gy. One or two additional treatments may be added after 1 or 2 weeks in chronic cases, in which results are much less satisfactory.

Rheumatoid arthritis

The patients selected had severe rheumatoid arthritis with active synovitis and significant disability treated unsuccessfully with nonsteroidal antiinflammatory agents, gold, and penicillamine. All patients would have been suitable candidates for cytotoxic therapy with agents such as azathioprine or cyclophosphamide, which, although effective in controlling advanced disease, may be accompanied by significant side effects.

In the Stanford trial, the regimen consisted of mantle field treatment with 20 Gy in 10 fractions of 2 Gy in 2 weeks. Patients were evaluated before and after therapy with respect to joint tenderness and joint swelling, duration of mor-ning stiffness, and a global composite score. Complications of treatment included mild systemic effects, such as nausea and fatigue, and local effects, including dysphagia, xerostomia, and esophagitis.

Conclusion

Radiation therapy continues to be used in the treatment of various benign disorders because the profile of efficacy and morbidity compares well with the available treatment alternatives. There is a well-established role for radiotherapy in the management of benign neoplasms when surgical therapy is medically contraindicated or would carry undue morbidity. In addition, there are situations in which anatomically

limited proliferations of lymphoid, epithelial, or mesenchymal tissue can cause significant morbidity that can be avoided or mitigated with local radiation treatment rather than systemic medical therapy or repeated surgical procedures.

Basic radiobiology of tumor

Biological effects of ionizing radiation

Interaction variants of radiation (Figure 6.22)

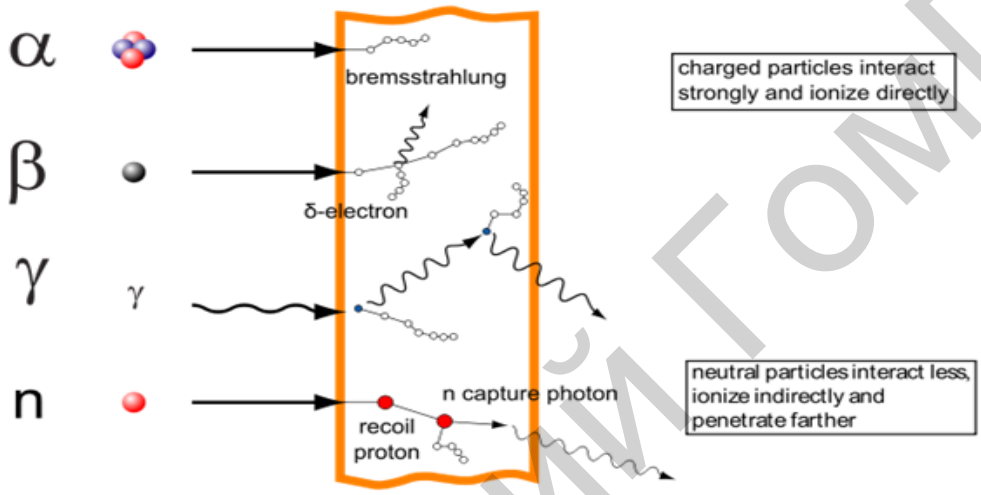

Figure 6.22 — Main types interaction forms of ionizing irradiation with matter

Cell damage

Current thinking suggests that there are two mechanisms for damage:

Direct action: is damage to the DNA material in the cell nucleus. The structure of DNA is a double helix which forms the "backbone" of the structure across which are a series of base pairs composed of adenine-thyamine or cytosine-guanine. Damage to DNA may take the form of strand breaks either in the sugar-phosphate backbone or one or more of the base pairs (Figure 6.23).

Indirect action: is caused by the radiolysis of water, the most common molecular constituent of tissue. Ionisation of the water molecule liberates an electron and produces hydrogen (H) and hydroxyl (OH) free radicals. These are highly reactive and will readily recombine, some to reform the water molecule, H_2O, and others to form more toxic compounds such as hydrogen peroxide, H_2O_2. The effect of toxins produced in this manner may lead to cellular damage.

Damage to cells is not irreparable. However those cells which do not repair will either cease to function or will continue to function in a modified way. Cells which are modified may also be non-viable in the long term but some may be modified in such a manner that they undergo a neoplastic transformation characterized by unlimited proliferation (i.e. malignant tissue).

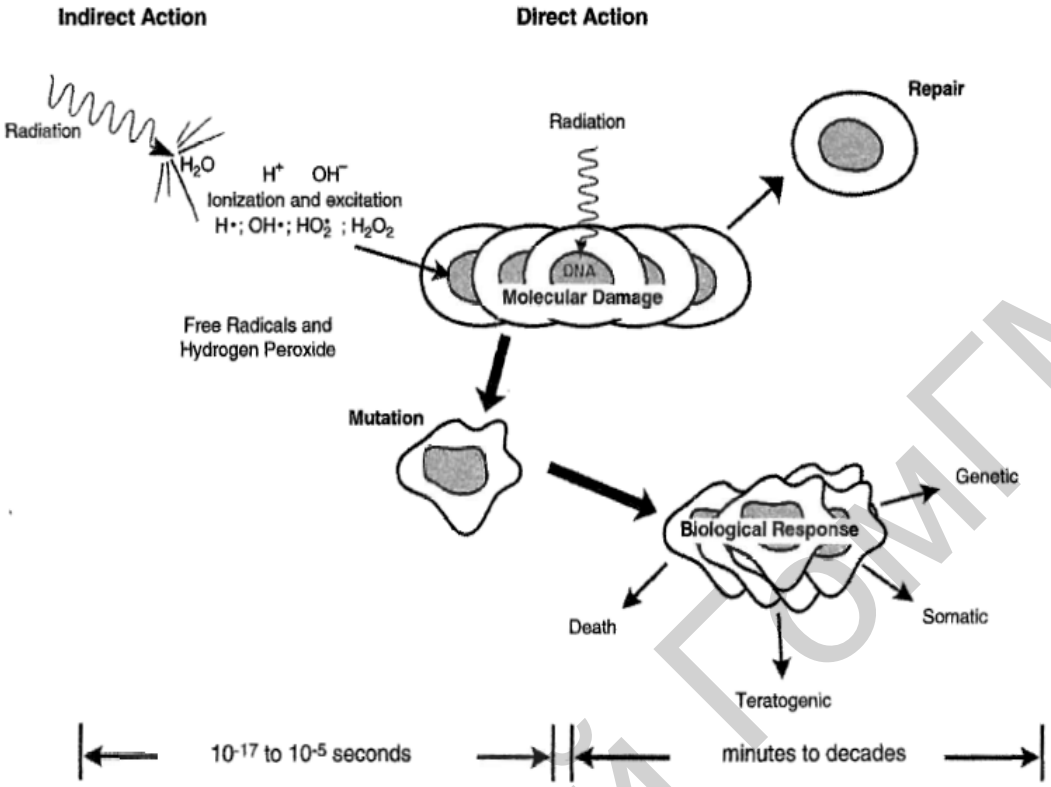

Figure 6.23 — Diagram of variants interaction of ionizing radiation with cells

Radiobiological mechanisms

The biological damage inflicted by irradiation of human cells with ionizing radiation can be divided into 3 consecutive steps:

– A very short initial physical phase (about 10^{-18} s), during which photons interact with orbital electrons, raising them to higher energy levels inside the atoms (excitation), or ejecting some of them from the atoms (ionization). This is the energy deposition phase.

– A chemical phase, again very short (about 10^{-3} s), during which ionized and excited atoms interact, leading either directly or indirectly through the formation of free radicals to the breakage of chemical bonds. Free radicals are highly reactive and can induce chemical changes in biologically important molecules like DNA. Single-strand or double-strand break in DNA appears to be the basic damage leading to biological effects (Figure 6.17).

– A biological phase, much longer (seconds to years), during which the cells react to the inflicted chemical damage. Specific repair enzymes can successfully repair the vast majority of lesions in DNA. A few lesions however may not be repaired, and may therefore lead to cell death. Cell death is not immediate and usually occurs during the next cell division (apoptosis is a minor process in most human cells). However, death due to a lethal lesion may be delayed for a limited number of mitotic divisions (up to 5 or 6). Because the stem cells are the only cells which divide in

normal tissues, the earliest effect observed is a deficit in stem cells. Later, the loss of stem cells will lead to a deficit in differentiated cells, causing the observed clinical reactions.

Radiation therapy works by damaging the DNA of cancerous cells. This DNA damage is caused by one of two types of energy, photon or charged particle. This damage is either direct or indirect ionization of the atoms which make up the DNA chain. Indirect ionization happens as a result of the ionization of water, forming free radicals, notably hydroxyl radicals, which then damage the DNA. It prove to be the most significant technique to cause cell death.

Cancer cells are generally undifferentiated and stem cell-like; they reproduce more than most healthy differentiated cells, and have a diminished ability to repair sub-lethal damage.

One of the major limitations of photon radiation therapy is that the cells of solid tumors become deficient in oxygen. Solid tumors can outgrow their blood supply, causing a low-oxygen state known as hypoxia. Oxygen is a potent radiosensitizer, increasing the effectiveness of a given dose of radiation by forming DNA-damaging free radicals. Tumor cells in a hypoxic environment may be as much as 2 to 3 times more resistant to radiation damage than those in a normal oxygen environment. Much research has been devoted to overcoming hypoxia including the use of high pressure oxygen tanks, blood substitutes that carry increased oxygen, hypoxic cell radiosensitizer drugs such as misonidaole and metronidazole, and hypoxic cytotoxins such as tirapazamine.

Radiation effects on the cell

The hazards of ionizing radiation were recognized soon after the discovery of the x-ray by Roentgen in 1895. A famous example is that of Antoine-Henri Becquerel, the professor of eventual two-time Nobel laureate Marie Curie, one of the discoverers (along with her husband, Pierre) of radium. In 1902, Marie Curie had painstakingly extracted a tenth of a gram of the new metal from large quantities of pitchblend, in which it was contained at a concentration of one part per million. The professor was so proud of his pupil's discovery that he carried a vial containing the first sample of radium ever produced in his vest pocket. Soon he noticed that he had developed a severe burn on the skin of his abdomen underneath the vial. The causative role of the radium in the production of the burn was verified when other researchers intentionally taped pieces of the new metal to their skin, producing similar burns. Experiments on animals by the Curies and others led to the development of therapeutic uses of radium emissions, known at the time as Curie therapy. That the same invisible rays used to diagnose diseases such as cancer could also both cause and cure the disease astonished early x-ray researchers.

Radiation biological effects occur as a result of damage to the cells caused by radiation. This damage takes many forms:

— Cell death.

— Mitotic inhibition (temporary/permanent).
— Chromosome damage/genetic damage leading to mutations.
— Actively dividing cells are particularly sensitive (i.e. bone marrow, lymph glands, gonads).

The nature and degree of cell damage vary according to:
— Radiation dose.
— Dose rate.
— Irradiated volume.
— Type of radiation.

Radiation manifestation in human body

Current knowledge of the risks of ionizing radiation is based on a wide range of epidemiological evidence from plant, animal and cell biology. The most significant body of information comes from the on-going study of those who survived the atom bombs dropped on Hiroshima and Nagasaki in 1945.

The damaging effects of radiation can be divided into two categories: deterministic effects and stochastic effects.

Stochastic effects
— Probability of effects not severity, regarded as a function of dose.
— No dose threshold below which an effect will not theoretically occur.
— Due to modified cell, e. g. somatic cell leading to cancers; reproduction cell leading to hereditary effect.

In stochastic effects, the probability of an effect occurring increases with dose up to a maximum, above which the curve flattens off. At low doses (< 100–200 mGy) effects cannot be easily measured because of the high incidence of cancer in the population and for practical purposes it is assumed that there is no "safe" dose. It is this lack of evidence of a threshold dose that has resulted in the principle of keeping radiation doses as low as reasonably practicable (ALARP). There has, however, been some recent evidence to suggest that there may be some protective effect of radiation at very low doses, but this is a matter of current controversy.

Based heavily on studies of Japanese survivors of atomic bomb attacks, ICRP (International Commission on Radiological Protection) calculated probability coefficients for stochastic effects in the general population are as follows:
— Fatal cancer: 5,0.
— Non-fatal cancer: 1,0.
— Severe hereditary effects: 1,3.

For example, if 100 people are exposed to 1 Sv of radiation, five will theoretically develop a fatal cancer. A dose of 5–6 Sv over a short time period leads to acute radiation sickness and death.

Deterministic effects
— Severity of effects varies with dose.

— Dose threshold may exist below which the effect will not occur.

— Due to cell death, deterministic effects occur when a cell loss is sufficient to impair the organ function (e.g. radiation burns, cataracts and decreased fertility).

Deterministic effects occur at high dose levels, such as those given in radiotherapy treatments and are due to radiation-induced cell death. These effects are characterized by having a threshold dose below which the effect is not observed. The severity of the effect increases with a dose and a dose rate. This may result in the death of the individual, depending on the organs exposed and the dose received. Cataract formation and skin damage are examples of deterministic effects. Normally, in diagnostic procedures, doses are well below the threshold where deterministic effects are observed, but the increasing use of interventional techniques has made exceeding a threshold dose for the skin damage a possibility that cannot be ignored.

Doses lower than about 1Gy generally cause no noticeable acute effects other than slight cellular changes (e.g. measurable chromosome aberrations). There is, however, a small possibility that a cell with noncritically damaged DNA can continue to reproduce and, with the effect of other agents, result in an increased probability of induced cancer or leukaemia. The timing of the appearance of radiation-induced cancers varies, with a mean incidence for leukaemia at about 7 years postirradiation, about 5 years for thyroid and bone cancers and 20 or more years for most other cancers. The time lag in the induction of cancers means that younger subjects are at greater risk. If damage is to the germ cells, genetic effects may occur in future offspring. To date, no hereditary effects have been demonstrated convincingly in humans; however, based on animal experiments, it is concluded that hereditary effects are a possibility. These long-term, low-dose stochastic effects are of a random statistical nature and the probability of occurrence (but not the severity of the effect) is related to the dose.

Based on our current knowledge, no level of exposure to radiation can be described as absolutely safe and no level is uniformly dangerous. Fear of radiation must not be permitted to undermine the great value of radiation in clinical practice. However, safe handling of all levels of radiation is important to prevent or minimize possible biological effects.

Radiation units. Measuring ionizing radiation

The ionizing effects of radiation are measured by units of exposure:

— The coulomb per kilogram (C/kg) is the SI unit of ionizing radiation exposure, and measures the amount of radiation required to create 1 coulomb of charge of each polarity in 1 kilogram of the matter.

— The roentgen (R) is an older traditional unit that is almost out of use, which represented the amount of radiation required to liberate 1 esu of charge of each polarity in 1 cubic centimeter of dry air (Table 6.1).

Table 6.1 — Basic radiation units

Quantity	Conventional	SI unit	Conversions
Exposure	Roentgen (R)	Coulomb/kg of air (C/kg)	1 C/kg = 3876 R 1 R = 258 μCi/kg
Dose	Rad	Gray (Gy)	1 Gy = 100 rad
Dose equivalent	Rem	Sievert (Sv)	1 Sv = 100rem
Activity	Curie (Ci)	Becquerel (Bq)	1 mCi = 37 MBq

However, the amount of the damage done to the matter (especially living tissue) by ionizing radiation is more closely related to the amount of the energy deposited rather than the charge. This is called the absorbed dose.

— The gray (Gy), with units J/kg, is the SI unit of absorbed dose, which represents the amount of radiation required to deposit 1 joule of energy in 1 kilogram of any kind of matter.

— The rad (radioactivity absorbed dose), is the corresponding traditional unit, which is 0,01 J deposited per kg.

A rad is a scientific unit of measure of radiation energy dose. A patient who receives radiation therapy as a treatment for cancer will receive several thousand rads over a very short period of time (weeks or months). For example, modern mammography systems used to take x-ray images of the breast use approximately 0,1 to 0,2 rad dose per x-ray.

Equal doses of different types or energies of radiation cause different amounts of damage to living tissue. For example, 1 Gy of alpha radiation causes about 20 times as much damage as 1 Gy of X-rays. Therefore, the equivalent dose was defined to give an approximate measure of the biological effect of radiation. It is calculated by multiplying the absorbed dose by a weighting factor WR, which is different for each type of radiation (see above Table). This weighting factor is also called the Q (quality factor), or RBE (relative biological effectiveness of the radiation) (Table 6.2).

— The sievert (Sv) is the SI unit of equivalent dose. Although it has the same units as the gray, J/kg, it measures something different. It is the dose of a given type of radiation in Gy that has the same biological effect on a human as 1 Gy of x-rays or gamma radiation.

Smaller quantities are expressed in “millisievert” (one thousandth) or “microsievert” (one millionth) of a sievert. Equivalent dose = weighting factor × absorbed dose. The effect of radiation on a given organism depends on the dose absorbed into the tissues, but also on the type of radiation and the sensitivity of the tissues or organs irradiated. The effect on the tissue will be different, however, depending on whether the particle is energetic or not. Photons generate other effects in the tissues than neutrons or alpha radiation. The absorbed dose is therefore corrected by a weighting factor which allows for the equivalent dose to be obtained. Thus X-, γ- or β-radiation

are similar in their effects and do not need to be corrected (weighting factor equal to 1), while neutrons are assigned a weighting factor between 5 and 20 depending on their level of energy.

Table 6.2 — Weighting factors for calculation of equivalent dose

Type of radiation	Weighting factor
Photons i.e. X-rays and gamma rays	1
Electrons	1
Neutrons	5–20 depending on energy
Protons	5
Alpha particles	20

The highest coefficient is applied to neutrons as their energy is between 100 and 2,000 keV, and reduces again after that. This is explained by the fact that very high energy neutrons pass through tissue so rapidly that they do less damage than if they passed at a lower energy level. Extremely ionizing α-radiation is in turn assigned a weighting factor of 20.

Table 6.3 — Examples of activity radionuclides

1 adult human (100 Bq/kg)	7000 Bq
1 kg of coffee	1000 Bq
Radionuclide for medical diagnosis	70 million Bq
Radionuclide source for medical therapy	100 000 000 million Bq
1 kg uranium	25 million Bq
1 kg low level radioactive waste	1 million Bq
1 kg of granite	1000 Bq

Apart from the normal measures of mass and volume, the amount of radioactive material is given in becquerel (Bq), a measure which enables us to compare the typical radioactivity of some natural and other materials (Table 6.3). A becquerel is one atomic decay per second.

References

1. *Sahani, D. V.* Abdominal imaging / D. V. Sahani, A. E. Samir. 2nd ed. Philadelphia : Elsevier, 2017. 1052 p.

2. *Clarke, C. J. D.* Abdominal X-rays / C. J. D. Clarke, A.E.W. Dux. UK, Oxford : Wiley, 2015. 115 p.

3. Gray's anatomy the anatomical basis of clinical practice / S. Standring [et al.]. 41st ed. London : Elsevier, 2016. 1562 p.

4. Grainger & Allison's diagnostic radiology / A. Adam [et al.]. 6th ed. Philadelphia : Elsevier, 2015. 2214 p.

5. *Herring, W.* Learning radiology. Recognizing the basics / W. Herring. 3rd ed. Philadelphia : Elsevier, 2016. 332 p.

6. *Harisinghani, M. G.* Primer of diagnostic imaging / M. G. Harisinghani, J. W. Chen, R. Weissleder. 6th ed. Philadelphia : Elsevier, 2019. 792 p.

7. *Khandelwal, N.* AIIMC-MAMC-PGI's Comprehensive textbook of diagnostic radiology / N. Khandelwal, V. Chowdhury, A. K. Gupta. New Delhi : Jaypee Brothers medical publishers, 2017. 3400 p.

8. *Penny, S. M.* Examination review for ultrasound. Abdomen & obstetrics and gynecology / S. M. Penny. 2nd ed. Philadelphia : Wolters Kluwer, 2018. 1322 p.

9. *Levy, A. D.* Gastrointestinal imaging / A. D. Levy, K. J. Mortele, B. M. Yeh. New York : Oxford university Press, 2015. 737 p.

10. *Choi, B. I.* Radiology illustrated: gastrointestinal tract, radiology / B. I. Choi. Berlin : Springer, 2015. 602 p.

11. *Hodler, J.* Diseases of the abdomen and pelvis / J. Hodler, R. A. Kubik–Huch, G. K. Schulthess. Cham, Switzerland : Springer, 2018. 264 p.

12. Diagnostic pathology. Gastrointestinal / J. K. Greenson [et al.]. 2nd ed. Philadelphia : Elsevier, 2016. 709 p.

13. *Federle, M. P.* EXPERTddx: Abdomen, pelvis / M. P. Federle, S. P. Raman, M. Tublin. 2nd ed. New York : Elsevier, 2017. 4031 p.

14. *Lamps, L. W.* Diagnostic pathology: hepatobiliary and pancreas / L. W. Lamps, S. Kakar. 2nd ed. London : Elsevier, 2017. 488 p.

15. *Saad, W. E. A.* Portal hypertension / W. E. A. Saad. 3rd ed. New York : Thieme, 2018. 324 p.

16. *Regge, D.* Hepatobiliary and pancreatic cancer / D. Regge, G. Zamboni. Cham, Switzerland : Springer; 2018. 122 p.

17. *Rumack, C. M.* Diagnostic ultrasound / C. M. Rumack, D. Levine. 5th ed. Philadelphia : Elsevier, 2018. 2004 p.

18. Hagen–Ansert, S.L. Textbook of diagnostic sonography / S. L. Hagen–Ansert. 8th ed. Philadelphia : Elsevier, 2018. 1543 p.

19. Coy, D. Body CT : The essentials / D. Coy, E. Lin, J. P. Kanne. New York : McGraw-Hill education, 2015. 279 p.

20. *Westbrook, C.* MRI in practice / C. Westbrook, J. Talbot. 5th ed. UK, Oxford : Wiley, 2019. 387 p.

21. *Yousem, D. M.* Duke review of MRI physics. Case review series / D. M. Yousem. St. Louis, India : Elsevier, 2019. 250 p.

22. *Bennett, P.* Diagnostic imaging. Nuclear medicine / P. Bennett, U. D. Oza. 2nd ed. Philadelphia : Elsevier, 2016. 580 p.

23. *Das, B. K.* Positron emission tomography. A guide for clinicians / B. K. Das. New Delhi, India : Springer, 2015. 192 p.

24. *Soto, J. A.* Emergency radiology / J. A. Soto, B. C. Lucey. 2nd ed. Philadelphia : Elsevier, 2017. 408 p.

25. *Agarwala, R.* Atlas of emergency radiology. Vascular system, chest, abdomen and pelvis, and reproductive system / R. Agarwala. Switzerland : Springer, 2015. 673 p.

26. *Patlas, M.* MDCT and MR imaging of acute abdomen / M. Patlas, D. S. Katz, M. Scaglione. Cham, Switzerland : Springer, 2018. 247 p.

27. *Jankowich, M.* Ultrasound in the intensive care unit / M. Jankowich, E. Gartman. New York : Humana press Springer, 2015. 390 p.

28. *Lumb, P.* Critical care ultrasound / P. Lumb, D. Karakitsos. Philadelphia : Elsevier, 2015. 334 p.

29. Genitourinary radiology / N. R. Dunnick [et al.]. 6th ed. Philadelphia: Wolters Kluwer, 2018. 1802 p.

30. *Zagoria, R. J.* The requisites. Genitourinary radiology / R. J. Zagoria, R. Dyer, C. Brady. 3rd ed. Philadelphia : Elsevier, 2016. 402 p.

31. *Singh, H.* Radiology fundamentals. Introduction to imaging & techno-logy / H. Singh, J. A. Neutze, J. R. Enterline. 5th ed. Switzerland : Springer, 2015. 374 p.

32. *Long, B. W.* MERRILL'S atlas of radiographic positioning & procedures / B. W. Long, J. H. Rollins, B. J. Smith. 13th ed. St. Louis, Missouri : Elsevier, 2016. 571p.

33. *Akata, D.* Diffusion weighted imaging of the genitourinary system / D. Akata, N. Papanikolaou. Cham, Switzerland : Springer, 2018. 178 p.

34. *Fischer, U.* Breast cancer: diagnostic imaging and therapeutic guidance / U. Fischer, F. Baum, S. Luftner–Nagel. Stuttgart, Germany : Thieme, 2018. 239 p.

35. *Hicks, D. G.* Breast / D. G. Hicks, S. C. Lester. 2nd ed. Philadelphia : Elsevier, 2016. 693 p.

36. *Copel, J. A.* Obstetric imaging. Fetal diagnosis and care / J. A. Copel. 2nd ed. Philadelphia : Elsevier, 2018. 721 p.

37. Principles and practice of radiation oncology / E. S. Halperin [et al.]. 7th ed. Philadelphia : Wolters Kluwer, 2019. 2296 p.

38. *Kim, S. H.* Oncologic imaging urology / S. H. Kim, J. Y. Cho. Berlin : Springer, 2017. 260 p.

39. *Aktolun, C.* Nuclear oncology / C. Aktolun, S. J. Goldsmith. Philadelphia : Wolters Kluwer, 2015. 703 p.

40. *Alcázar, J. L.* Ultrasound assessment in gynecologic oncology / J. L. Alcázar. New York : Taylor & Francis Group CRC press, 2018. 81 p.

41. *Knapp, F. F.* Radiopharmaceuticals for therapy / F. F. Knapp, A. Dash. Philadelphia : Springer, 2016. 347 p.

42. *Joiner, M. C.* Basic clinical radiobiology / M. C. Joiner, A. J. Kogel. 5th ed. New York : Taylor & Francis Group CRC press, 2019. 350 p.

43. *Carroll, Q. B.* Radiography in the digital age. Physics, exposure, radiation biology / Q. B. Carroll. 3rd ed. Springfield, Illinois : Charles C Thomas, publisher, 2018. 868 p.

44. *Королюк, И. П.* Лучевая диагностика / И. П. Королюк, Л. Д. Линденбратен. 3-е изд. М. : БИНОМ, 2017. 496 с.

45. *Труфанов, Г. Е.* Лучевая диагностика / Г. Е. Труфанов. М. : ГЭОТАР-Медиа, 2018. 484 с.

Учебное издание

Ермолицкий Николай Михайлович

ЛУЧЕВАЯ ДИАГНОСТИКА
И ЛУЧЕВАЯ ТЕРАПИЯ
(на английском языке)

Учебное пособие

В двух частях

Часть 2
Клиническая радиология и радиотерапия

Редактор ***Т. Ф. Рулинская***
Компьютерная верстка ***Ж. И. Цырыкова***

Подписано в печать 16.05.2022.
Формат 60×84 1/8. Бумага офсетная 80 г/м². Гарнитура «Times New Roman».
Усл. печ. л. 18,14. Уч.-изд. л. 19,83. Тираж 140 экз. Заказ № 251.

Издатель и полиграфическое исполнение:
учреждение образования «Гомельский государственный медицинский университет».
Свидетельство о государственной регистрации издателя,
изготовителя, распространителя печатных изданий № 1/46 от 03.10.2013.
ул. Ланге, 5, 246000, Гомель.